Université de Lille

Doctoral School **Biologie Santé 446**

Laboratoire **Commissariat à l'énergie atomique CEA**

Thesis defended by **Mathilde Champeau**

Defended on **9th December, 2020**

In order to become Doctor from Université de Lille

Academic Field **Chemistry**

Speciality **Biomaterials**

Dissolving microneedles for an optimal transdermal delivery of an active principle used in photodynamic therapy: Development and proof of concept.

Thesis supervised by

Laurent Mortier	Supervisor
Dorothée Jary	Co-Monitor
Séverine Vignoud	Co-Monitor
Serge Mordon	Co-Monitor

Committee members

Referees	Nicole Basset-Seguin	Professor at Hôpital Saint Louis APHP
	Sylvie Begu	Professor at Institut Charles Gerhardt
Examiners	Juergen Siepmann	Professor at Inserm U1008 Controlled Drug Delivery Systems and Biomaterials
	Julie Morell	Senior Researcher at Entreprise Allergan-AbbVie
Supervisors	Laurent Mortier	CHRU Oscar Lambret
	Dorothée Jary	Senior Researcher at CEA-Leti
	Séverine Vignoud	Senior Researcher at CEA-Leti
	Serge Mordon	Professor at Inserm U1189 ONCO-ThAI

Université de Lille

Doctoral School **Biologie Santé 446**

Laboratoire **Commissariat à l'énergie atomique CEA**

Thesis defended by **Mathilde Champeau**

Defended on **9th December, 2020**

In order to become Doctor from Université de Lille

Academic Field **Chemistry**

Speciality **Biomaterials**

Dissolving microneedles for an optimal transdermal delivery of an active principle used in photodynamic therapy: Development and proof of concept.

Thesis supervised by

Laurent Mortier	Supervisor
Dorothée Jary	Co-Monitor
Séverine Vignoud	Co-Monitor
Serge Mordon	Co-Monitor

Committee members

Referees	Nicole Basset-Seguin	Professor at Hôpital Saint Louis APHP
	Sylvie Begu	Professor at Institut Charles Gerhardt
Examiners	Juergen Siepmann	Professor at Inserm U1008 Controlled Drug Delivery Systems and Biomaterials
	Julie Morell	Senior Researcher at Entreprise Allergan-AbbVie
Supervisors	Laurent Mortier	CHRU Oscar Lambret
	Dorothée Jary	Senior Researcher at CEA-Leti
	Séverine Vignoud	Senior Researcher at CEA-Leti
	Serge Mordon	Professor at Inserm U1189 ONCO-ThAI

Keywords: photodynamic therapy, dissolving microneedles, 5-aminolevulinic acid, transdermal drug delivery, skin cancer, hyaluronic acid

Mots clés : thérapie photodynamique, microaiguilles solubles, acide 5-aminolévulinique, délivrance transdermique, cancer de la peau, acide hyaluronique

This thesis has been prepared at the following research units.

Commissariat à l'énergie atomique CEA
17, Avenue des Martyrs
38000 Grenoble
France

☎ (33) 04 38 78 44 00
Web Site http://www.cea.fr/

INSERM Onco Thai U1189
1, avenue Oscar Lambret
59037 LILLE Cedex
France

☎ (33) 03 20 44 67 09
🖷 (33) 03 20 44 67 38
Web Site http://www.oncothai.fr/fr/

A mon papy Mougeot,

&

A ma mamie Dédette

Ita fac, mi Lucili: Vindica te tibi, et tempus, quod adhuc aut auferebatur aut subripiebatur aut excidibat, collige et serva. [...] Omnia, Lucili, aliena sunt, tempus tantum nostrum est.

Epistulae morales ad Lucilium, Seneca

Dissolving microneedles for an optimal transdermal delivery of an active principle used in photodynamic therapy: Development and proof of concept.

Abstract

Non-melanoma skin cancers are on the rise with 2 to 3 million people diagnosed each year and are sometimes treated by local ablation therapy. To avoid this surgery, photodynamic therapy (PDT) appears as an advantageous treatment. Currently used in clinics, PDT consists of applying a cream containing a photosensitive precursor to the damaged skin, which, then metabolizes and under light excitation induces cell death. However, this technique is not fully effective if the skin lesion extends into the deep skin layers. To improve the therapeutic treatment of this type of skin cancer, a patch with dissolving microneedles (MNs) was develop to reach the deep layers of lesions that are difficult to treat. Hyaluronic acid, known for its biocompatibility, solubility and biodegradability, was chosen as the constituent material, and mixed with the 5-aminolevulinic acid (photosensitive precursor, 5-ALA). To ensure the best penetration without causing pain by touching the nerve endings, an optimal "pencil-tip" design was defined with MNs length going from 400 to 750 µm. A simple and robust manufacturing process called solvent casting molding method, has been set up which is an asset for potential industrialization. In absence of realistic skin lesions model, we chose to establish one on rats skin by applying daily UV-B doses. Histology and pharmacokinetic studies validated the presence of precancerous skin lesions and the MN-patch *in vivo* efficiency was therefore tested. After one hour application on the injured rat skin, the MN-patch dissolved and released the 5-ALA that further metabolized to protoporphyrin IX (PpIX). A significant level of PpIX fluorescence was recorded suggesting that after light excitation, a PDT session could be effective. In parallel, to reduce pain felt during PDT treatment, a light device with suitable optical and thermal properties was conceived and coupled to the MN-patch. The idea would be to start the illumination directly after MN-patch application in order to avoid a painful photochemical reaction. This wearable and easy to use system purpose a all-in-one PDT processing which fulfills the criterion of patient compliance, better efficiency and speed of treatment.

Keywords: photodynamic therapy, dissolving microneedles, 5-aminolevulinic acid, transdermal drug delivery, skin cancer, hyaluronic acid

Microaiguilles solubles pour la délivrance transdermique optimale d'un principe actif utilisé en thérapie photodynamique : Mise au point et preuve de concept.

Résumé

Les cancers de la peau de type non mélanome constituent un enjeu sanitaire majeur : l'OMS en dénombre 2 à 3 millions par an. Pour les traiter, il faut parfois recourir à une résection chirurgicale localisée. Pour éviter ce geste, la thérapie photodynamique (PDT) est un traitement alternatif intéressant. Actuellement utilisée en clinique, la PDT consiste à appliquer sur la peau lésée une crème contenant un précurseur photosensible qui après métabolisation et sous excitation lumineuse induit la mort cellulaire. Néanmoins, cette technique atteint ses limites thérapeutiques lorsque la crème ne pénètre pas dans les couches lésées et profondes de la peau. Pour améliorer la délivrance de la PDT, un patch de microaiguilles (MAs) soluble dont la longueur des MAs peut être comprise entre 400 à 750 µm a été développé permettant ainsi d'atteindre l'interface épiderme/derme sans induire de douleur. L'acide hyaluronique, polymère connu pour sa biocompatibilité, solubilité et biodégradabilité, a été choisi comme matériau constitutif du patch et a été mélangé avec l'acide aminolévunique (précurseur photosensible, 5-ALA). Un procédé de fabrication simple et robuste dit de moulage a été mis en place dans une perspective de potentielle industrialisation. Du fait de l'absence d'un modèle réaliste de lésions cutanées, nous avons choisi d'en développer un sur des rats en leur appliquant des doses d'UV-B quotidiennes. Ce modèle a été validé par des études d'histologie et de pharmacocinétique et a permis de tester l'efficacité du patch *in vivo*. Lorsque le patch a été appliqué sur les lésions précancéreuses, il s'est dissous en 1 heure, a libéré le 5-ALA qui s'est ensuite métabolisé en protoporphyrin IX (PpIX). Un taux significatif de fluorescence dû à la PpIX a été recueilli et montre qu'après excitation lumineuse, un traitement PDT pourrait être efficace. Aussi, afin de réduire la douleur ressentie pendant une session PDT, l'illumination commencerait juste après l'application du patch pour éviter l'accumulation de PpIX et *a fortiori* une réaction photochimique douloureuse. De ce fait, un système lumineux dont nous avons contrôlé les propriétés optiques, thermiques et temporelles a été couplé au patch de MAs. Ce système portatif et simple d'utilisation pourrait proposer un traitement PDT tout-en-un qui répond aux critères de rapidité, d'efficacité de traitement et de confort du patient.

Mots clés : thérapie photodynamique, microaiguilles solubles, acide 5-aminolévulinique, délivrance transdermique, cancer de la peau, acide hyaluronique

Remerciements

Avant de lire une thèse qui m'intéresse, j'ai cette petite habitude de lire les remerciements même s'il s'agit d'un.e auteur.e que je ne connais pas. Les remerciements en disent long sur le déroulement et l'ambiance de la thèse. Alors pour celles et ceux qui ont aussi ce petit tic, j'espère par ces nombreuses lignes réussir à vous montrer que ces trois années ont été très enrichissantes tant sur le plan professionnel que personnel.

Je souhaite tout d'abord remercier Séverine VIGNOUD qui m'a donné la chance d'intégrer son laboratoire au DTBS. Merci d'avoir répondu à mes premier mails en novembre 2016, de m'avoir accueillie en stage avant de commencer cette thèse qui m'intéressait depuis le début! Malgré tes responsabilités, tu as toujours réussi à m'accorder du temps, me soutenir moralement et décrypter mes appels au secours. Un grand merci à Dorothée JARY qui est montée dans le bateau de la thèse en cours de navigation. Merci pour l'intérêt que tu as porté à ce projet, pour tous tes conseils, idées, corrections, remarques objectives, pour ton soutien sans faille et toutes les piqures de boost qui m'ont permis de progresser. Je remercie ensuite mon directeur de thèse Monsieur Laurent MORTIER pour nos échanges constants et pour m'avoir accordé sa confiance pour mener à bien ce projet. Merci à Monsieur Serge MORDON, directeur de l'unité Onco-ThAI et expert de la thérapie photodynamique pour m'avoir fait découvrir le monde lumineux.

Mes remerciements vont ensuite à l'ensemble des membres du jury pour avoir accepté d'examiner et d'évaluer mon travail de thèse. Un grand merci à Madame Nicole BASSET-SEGUIN et Madame Sylvie BEGU qui ont suivi mon travail depuis le début grâce aux deux CSIs et qui ont aussi accepté de rapporter mon travail de thèse. Merci aussi à Madame Julie MORELL et Monsieur Juergen SIEPMANN pour l'intérêt qu'ils ont porté à ce sujet de thèse en acceptant notre invitation.

Ces quelques lignes sont aussi l'occasion d'exprimer ma gratitude à toutes les personnes qui ont composé mon environnement professionnel durant ces trois dernières années. La thèse étant menée sur deux laboratoires et rattachée administrativement à la PRTT Hauts de France j'ai eu la chance de rencontrer beaucoup de collègues qui ont contribué au bon déroulement de cette thèse.

Je commence tout d'abord par remercier l'ensemble du laboratoire du L2CB à Grenoble et plus généralement toutes les personnes qui ont croisé mon chemin au DTBS. C'était un bonheur de passer les portes de l'open-space chaque jour pour vous retrouver dans la bonne humeur et la bonne entente. Merci à Véro d'être souriante et toujours là pour les thésard.e.s notamment quand il s'agit de refaire le point sur les bases de la RMN. Merci à Isabelle, qui m'a donné le goût de la recherche après le stage passé à ses côtés. Merci à l'ours Antoine, pour son aide en chimie. Merci à Dom pour sa franchise et sa présence au labo (surtout pendant les bugs UPLC). Merci à Charly d'avoir créer un solarium couplé à une salle d'anesthésie pour que mes petits rats puissent se dorer la pilule sereinement. Merci à Thomas, membre de la ginger team, pour sa bonne humeur H24 et nos premiers échanges lumineux. Merci à Megan pour son aide au texturomètre et ses délicieux cookies. Merci à l'ensemble des thésard.e.s et stagiaires que j'ai rencontré au sein du

laboratoire. Vous êtes devenus bien plus que des collègues ou des partisans de galère. Je pense à Morgane, Clémentine et Claire, toujours au rendez-vous pour une raclette, Paul le voisin aux chaussettes atypiques, Bastien coéquipier de run & bike, Alex qui connait la vraie campagne, Thibault qui dit toujours bonjour, Roxane qui a toujours le sourire, Juliette partenaire de piscine, Maxime, Antoine, Sakthi, Clément, Simon, Michael, Hippolyte, Thibaut toujours présents pour aller manger à la cantine. Et après il y a des dédicaces particulières par exemple pour Rafiki (Raph), curry lover, qui a toujours répondu à toutes mes interrogations et craintes à l'idée de faire des manips *in vivo*. Merci de m'avoir rassurée de nombreuses fois notamment quand mes rats faisaient quelques cabrioles. Une autre dédicace pour mes coéquipiers de paillasse, Anouchka et Bilal avec leur sloggan viral "**it happens" ! Merci pour les discussions scientifiques et surtout pour toutes les autres (et elles furent nombreuses)! Au plaisir de vous retrouver dans notre future entreprise Tessekurle. Et enfin une autre dédicace pour Mélanie, ma co-bureau écolo qui a toujours su me (re)motiver grâce à son sourire communiquant et à de nombreuses conversations de positive-attitude.

Une mention spéciale s'impose aussi pour ma *fashion week team* composée d'Emilie, ma petite perruche, abordée pour la première fois par l'adage bien connu "Les collègues, c'est comme la famille : on ne les choisit pas" et composée de Prisca, ma Prisco, ma coloc chez Cendrillon, mon binôme de thèse, mon soutien permanent. Vous avez été mes deux petits rayons de soleil, toujours là pour rendre un service, aller au lac, au bar, au sport. Vous avez su égayer mes journées et je ne vais pas citer tous les bons moments passés ensemble sinon mes remerciements risqueraient d'être plus volumineux que mon chapitre 4.

Je souhaite ensuite remercier tous les membres de l'unité Onco-ThAI. Merci pour votre accueil, même si je ne venais pas souvent dans le grand Nord vous avez toujours su m'accueillir chaleureusement sous la pluie. Merci à Anne-So, grande statisticienne et passionnée de sports, merci à Greg, pro du Arduino, merci à Pascal pour qui l'impression 3D n'a plus de secret, merci à Fabienne, Laurine et Laura pour les diverses discussions à la pause-repas. Et enfin, merci à Elise et Clément, collègues de thèse à un instant *t*. J'étais ravie de vous rencontrer, merci pour votre aide, votre compassion et compréhension. L'unité est petite mais c'était une chance de vous avoir à mes côtés !

La thèse était en collaboration entre deux laboratoires géographiquement très éloignés (Grenoble-Lille) je remercie la SNCF de m'y avoir conduit avec succès et avec plus ou moins de retard à chaque fois. Plus sérieusement, je remercie Audrey d'avoir géré efficacement mes nombreuses missions et trajets. Merci aussi pour les demandes de remboursements crackers Belin et cire Veet pour mes rats. Je remercie aussi l'ensemble des personnes de la PRTT de Lille qui ont tout fait pour que je me sente à l'aise à chaque fois que je venais sur le campus d'Euratechnologies. Merci à Claire-Noëlle et Olivier qui se sont succédés à la direction du CEA Tech d'avoir été intéressés par le sujet de recherche. Merci à Boris et Pascal pour votre aide et pour m'avoir fait prendre du recul sur mon sujet de thèse.

Je voudrais aussi remercier Monsieur Jean-Jacques FEIGE pour m'avoir autorisée à venir travailler au sein de l'animalerie du BCI-IRIG. Hervé, merci de m'avoir accordé beaucoup de temps pour la rédaction du protocole à l'expérimentation animale. Je partais de rien, tu as su répondre à toutes mes questions et a toujours été présent pour essayer de faire avancer au plus vite toutes les étapes de validation. Charlène, merci de m'avoir rassurée, tu as trouvé les mots et as su me montrer comment manipuler sereinement mon cheptel de rats. Odile, merci pour les formations à l'IVIS et au microscope. Aude et Mariela, votre gentillesse et votre calme m'ont permis de découvrir les joies de l'histologie.

Je remercie l'école doctorale, d'avoir proposé des formations dans lesquelles je me suis épanouie. J'ai en tête par exemple la formation pour *"Ma thèse en 180 secondes"* où j'ai eu la chance de rencontrer Géraldine, formatrice qui m'a coachée pour ce concours oratoire. Je

voudrais aussi remercier Denis BITOUZÈ qui m'a fait découvrir les joies de LaTeX et qui me permet aujourd'hui de rédiger (calmement) dans les normes typographiques ma thèse.

Pour finir, je voudrais remercier les personnes qui en dehors du cadre professionnel ont contribué à mon bien être et mon équilibre. Je remercie les joueur.se.s de basket du mercredi soir, Penne, (camarade de promo à l'A7) et également en thèse, pour nos repas du mercredi midi qui m'ont permis de réaliser qu'on traversait tous des galères à différents moments mais que tout finit par s'arranger. Merci à mes copines du lycée, mes ami.e.s de prépa et mes SA7 gonzs de l'école d'avoir proposé des sorties le week-end qui me permettaient de décrocher de mon sujet.

Merci à ma famille de cœur composée de Tartarins, de Cluisiens et de voisins qui a toujours pris de mes nouvelles et dont j'avais un grand plaisir à retrouver pour les week-end "chasse" et fête de village. Merci à ma petite Mamie Denise d'avoir régulièrement demandé si "mon rapport" avançait bien et si "ma thèse" était bientôt finie, tes sms m'ont souvent fait sourire.

Cet avant-dernier paragraphe est un avant-dernier remerciement mais aussi et surtout des félicitations. Je voudrais les adresser à Ludo pour m'avoir supportée pendant ces trois années de thèse (et aussi pour les années avant!). Merci de m'avoir écoutée râler sans relâche, merci pour ton calme, ta sérénité, ton soutien, ta relecture en période de confinement, ta compréhension, ton humour et ton amour.

Bien évidemment, je voudrais trouver une formule de remerciement à la hauteur du soutien et de l'investissement de mes chers parents... mais ils sont tellement au top que la langue française ne me permettra pas de les remercier dignement et de faire passer toutes les émotions que j'ai traversées avec eux... alors c'est dans eul' jargon berrichon de cheu'nous que j'ai décidé de le faire. On sait pas trop ce que j'ai raguenassé pendant toutes ces années d'études, on sait que j'ai souvent rechigner des gosses, que j'ai été mutin mais vous étiez toujours là pour me tenir le pépin au dessus de la goule quand ça s'abeurnissait et que y'avait un agat d'iau. Je vous ai beurdassé dans tous les coins de France et vous avez toujours été là pour pas me laisser dans la pigouille. Je vous ai bassiné et vous m'avez toujours écoutée. Et mon p'tit gars aujourd'hui si je l'ai fait c'est ben grâce à vous ! Je suis fière des valeurs que vous m'avez transmises et je vous aime tellement... MMM. & PPP. Epipapu !

Acronyms

^{13}C NMR carbon nuclear magnetic resonance. xxvii, 79, 80

^{1}H NMR proton nuclear magnetic resonance. xxvii, 79, 80, 152

5-ALA 5-aminolevulinic acid. xxiii, xxv, xxviii, 2, 9–15, 64, 68–73, 75, 76, 78, 80, 82, 83, 117–125, 148–156, 158, 161, 163, 173–175, 177, 178, 185, 186

ACN acetonitrile. 152

AK actinic keratosis. 1, 3, 5–8, 11, 69, 159, 160

BCC basal cell carcinoma. 1, 3, 5, 7, 8, 14, 156, 160, 161, 177, 178

CMC carboxymethyl cellulose. 71

ELSD Evaporating Light Scattering detector. 153

FTIR Fourier transform infrared spectroscopy. xxvii, 79

HA hyaluronic acid. xxv, xxvii, 1, 2, 75–83, 120, 122, 159, 172, 175, 177, 185

HPLC high pressure liquid chromatography. 78

HYAL 1 hyaluronoglucosaminidase 1. 77

HYAL 2 hyaluronoglucosaminidase 2. 77

LED light-emitting diode. xxviii, 157, 160–162, 165, 166, 168–173, 175, 176, 178

MAL methyl-aminolevulinate. 9, 11–15, 69, 159

MN microneedle. xxvii, xxviii, 1, 2, 4, 64–66, 68–73, 76, 78, 80, 81, 83, 117, 122–125, 149, 151, 152, 154–156, 159, 161–163, 166, 168, 170, 171, 175, 177, 178, 185, 186

MN-patch microneedles patch. xxvii, xxviii, 76, 78, 120, 122, 148, 150, 151, 154–157, 159, 163, 169–172, 175–178

Mw molecular weight. 75, 78, 79, 81, 83, 185

PDMS polydimethylsiloxane. xxviii, 67, 68, 78, 80, 83, 120, 166, 168, 170

PDT photodynamic therapy. xxv, 1–3, 8, 10–15, 64, 68–73, 76, 78, 124, 156–161, 163, 169, 176–178, 185

PEG polythylene glycol. 172

PLA polylactid acid. 71, 172

PLGA polylactid-co-glycolic acid. 71, 172

PpIX protoporphyrin IX. 8–10, 71, 122–124, 148, 149, 156, 158–161, 163, 169, 173–178

PS photosensitizer. 8, 10, 13

PVP polyvinylpyrrolidone. 71

PY 2,5-dipropionic acid. 124, 148

SC *stratum corneum*. 125, 149, 178

SCC squamous cell carcinoma. xxv, 1, 3, 5–8, 13

SEC size exclusion chromatography. 78, 79

ToF-SIMS Time-of-Flight Secondary Ion Mass Spectrometry. 2, 123, 149–152, 154–156

UPLC Ultra Performance Liquid Chromatography. 153

Contents

List of Tables

List of Figures

Introduction

Skin cancer is the most common form of cancer, globally accounting for at least 40 % of cancer cases. Skin cancers include two forms: melanomas and non-melanomas ; and the most common type is the second one that occurs in at least 2–3 million people per year in the world and its incidence is still increasing [158].

Different therapies have been investigated to treat non-melanomas skin cancers such as surgery, cryotherapy or radiotherapy. PDT is another approach that had known a growing interest for the two last decades. PDT presents an acceptable efficiency at long-term follow-up and does not let scars after treatment which is positive since the lesions are usually present on face, hands or neck (sun-exposed areas) [15]. Nowadays, PDT starts to be routinely used in clinics since it is easily performed. Indeed, the principle is quite simple and rest on the combination of three major components that are: photosensitizer, light and oxygen. Therefore, for a conventional treatment in clinics, a cream containing a photosensitive precursor is applied on the lesion for at least three hours and then a precise red light dose is delivered. Afterwards, due to the presence of oxygen, a photochemical reaction occurs which induces cell death [115].

Although this treatment has been efficient on thin skin lesions, for deeper skin tumours, it may be improved. One of the major reason is due to the lack of photosensitive precursor penetration through the skin layers. Tumour cells in deep-seated lesions, such as deep basal cell carcinoma (BCC), are not destroyed because no photochemical reaction occurs due to the photosensitizer absence [41]. On the other hand, this treatment is often painful due to the important number of oxygen species created during light illumination, that are known to stimulate sensory nerve endings [8, 115]. One solution would be to to avoid excessive production of oxygen species by preventing the accumulation of the photosensitizer in the cells and consequently decrease the photochemical reaction burst.

This thesis aims to develop a biomedical device that would allow a better prodrug penetration in deep skin layers and a less painful PDT treatment. The first goal is to design MNs in a disposable patch that would contain the prodrug. When inserted into the skin lesions, the MN tip would reach the bottom of the tumour. The MNs composed of HA, a biocompatible and water-soluble polymer, will be dissolved by the skin and consequently release the prodrug on the whole volume of the skin lesion. The second objective is to couple this MN-patch to a light system that would deliver a low red light dose and starts the illumination just a few minutes after the MN insertion in order to avoid pain usually felt during treatment.

In order to answer this issue, the first chapter provides an overview of the different categories of the non melanoma skin cancers (actinic keratosis (AK), BCC, squamous cell carcinoma (SCC)) and how conventional PDT is performed on these kinds of cancers and the efficiency that is recorded. Since the lack of prodrug penetration results in a treatment efficiency decrease, different methods (chemical of physical) to overcome this issue have been considered and are described in a review. Among the different technologies suggested, the use of MNs appears as a promising approach enabling better drug penetration. Therefore, at the end of this chapter, a

rapid description of the fabrication process and their different types are presented.

The second chapter focuses on the production of the MN-patch in which 5-ALA is loaded. The patch development process is based on an easy one-step solvent casting molding method. The properties of fabricated MNs are characterized in terms of their ability to dissolve, to insert without fracture in the skin and their cytotoxicity. Since the prodrug, the 5-ALA, is included in the needle material (polymer HA), a special care through an analytical follow-up is taken to ensure that there is no interactions between these two products and a good stability of the drug. The results of this chapter are transformed into a publication.

The third chapter describes the *in vivo* experiments that are conducted to test the efficiency of the MN-patch. For this purpose, precancerous skin lesions model are developed on rats by repetitive UV-B illumination. The photosensitizer fluorescence level is recorded after MN-patch application to highlighted if this technology could lead to a succesfull PDT session. These results are part of an article. In order to estimate the prodrug penetration profile, preliminary experiments using innovative technologies (Franz cell apparatus or Time-of-Flight Secondary Ion Mass Spectrometry (ToF-SIMS)) on *ex vivo* skins are also performed.

The final chapter answers the second goal of this thesis which is to couple the MN-patch to a light system less painful in order to propose a proof of concept: PDT all-in-one. The reasons that led to reduce the light dose and the time between release of 5-ALA and illumination are described. The system is then characterized in terms of temperature, light power and uniformity. Finally, a regulatory study has been conducted in order to evaluate the classification of the developed products.

Chapter 1

Literature Review
Improvement of photodynamic therapy efficiency for skin cancers

Outline of the current chapter

Introduction: Literature review

- In this chapter, a focus on the different skin cancers and their localization in the skin layers will be presented.
- Then photodynamic therapy as treatment for non melanoma skin cancers will be reviewed with its principle, some clinical results and their limitations.
- In a review, we showed the different physical or chemical methods that can enhance prodrug penetration and consequently improve photodynamic therapy.
- Among the previous techniques presented, microneedles appear as a new technology that might be able to answer to the lack of prodrug penetration in deep skin lesions.
- Microneedles as devices enabling transdermal drug delivery will be shortly presented with their different forms, advantages and production way.
- Finally, the use of microneedles for photodynamic therapy will be explained with a few examples.

1.1 Medical indication: skin cancers

Skin cancers are the most common malignancy of humans and particularly for Caucasians people with increasing incidence rate [158]. According to the World Health Organization, between 2 and 3 millions of non melanoma skin cancers and 132 000 melanomas are diagnosed each year in the world. According to the Skin Cancer Foundation (Facts and Statistics), more people are diagnosed with skin cancer each year in the U.S. than all other cancers combined.

The etiology might be divided in two categories [6, 48]:

- *Individual people risks*: skin, hair or eyes color (fair), UV sensitivity, skin burns antecedents, numerous moles, family history of skin cancer.
- *Environnemental risks*: previous radiotherapy, phototherapy [16], indoor tanning, UV-radiation exposure.

1.1.1 Different types of skin cancers

According to the previous risks encountered by people, different kinds of skin cancers exist and are divided in two types :

- Non-melanoma skin cancers whose the AK, BCC, squamous cell carcinoma (SCC).

- Melanoma skin cancers

The different localization of skin cancers are depicted in figure 1.1.

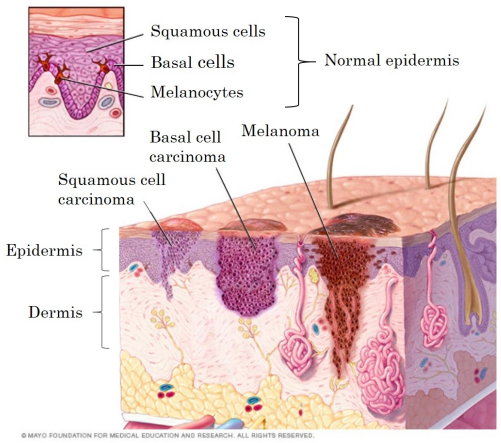

Figure 1.1 – Different types of skin cancer and the localization of their development in the skin.

As depicted in figure 1.1 the non-melanoma skin cancers are localized principally in epidermis and deep epidermis. As for the melanoma skin cancer, it can reach lower dermis and be in contact with blood vessels leading the tumors to spread in the body (metastasis). Melanoma skin cancer affects less people than the non-melanoma skin cancers. An effective treatment for melanoma is still under investigation since this disease is difficult to treat with its potential ability to create metastasis. Non-melanoma skin cancers could be treated thanks to different technologies and one of them will be presented in details in section 1.2 but before a focus on each class of non-melanoma skin cancers will be made.

1.1.2 Non melanoma skin cancers

Non-melanoma skin cancers are divided in three categories : actinic keratosis (AK), squamous cell carcinoma (SCC) and basal cell carcinoma (BCC).

1.1.2.1 Actinic keratosis (AK)

AKs also known as solar keratosis or keratinocytic intraepidermal neoplasia are premalignant tumors that take place in epithelial cells (or keratinocytes) located in epidermis and especially in the *stratum spinosum* (Figure 1.2) [198]. AKs are due to the proliferation of transformed neoplastic keratinocytes. AKs are the most common precancerous lesions among fair-complexioned individuals [138]. A small percentage of AKs may progress to invasive SCC if they are not diagnosed and treated on time [172]. AK could be considered as a SCC at early stage of development [138] but do not extend as deeply as SCC might do [48] . The clinical presentation of an AK is a scaling papule or a red plaque generally on sun exposed zones (head, neck, hands, foot). Diameter could reach 1 to 3 mm or may also become bigger and get several centimeters in size [122]. There are three main grades of AK [184, 212].

- *Grade I*: neo-plastic changes are limited to the lower third of the epidermis. Clinically, AK *grade I* are slightly palpable (better felt than seen). A red pseudonetwork pattern could be observed with a dermatoscope.

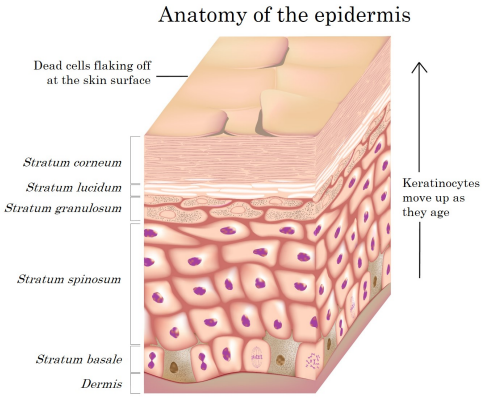

Figure 1.2 – Transversal histological section of epidermis from https://thedc.ca/ourteam/dermatology/.

- *Grade II*: neo-plastic changes are located in the lower two thirds of the epidermis. Clinically, AK *grade II* are moderately thick (easily felt and seen). Dermatoscopy analysis shows background erythema intermingled with keratotic follicular openings.
- *Grade III*: full-thickness atypia is observed. AK *grade III* are very thick and hyperkeratotic (obvious). Observation with dermatoscope shows structureless white-yellow areas.

A fourth grade could be defined as a *grade III* very advanced and presenting vesiculation/erosion in addition [148].

1.1.2.2 Squamous cell carcinoma (SCC)

SCC derives from the keratinocytes of the *stratum spinosum* layer of the epidermis (Figure 1.2). SCCs are principally diagnosed after AKs and are defined as their evolution [21]. Two kinds of SCC are described in the literature:

- *In situ* SCC whose Bowen disease and Erythroplasia of Queyrat belong [5]
- Invasive SCC

If histological examination indicated atypical keratinocytes (hyperkeratosis and parakeratosis) thicker than two-thirds of the full thickness of epidermis, lesions are considered as *in situ* SCC [199, 149]. Invasive SCC is a result of accumulation of mutational and cellular events that lead to invasive growth [168]. Hence invasive SCC can be more biologically aggressive than *in situ* SCC, can recur and has the potential to metastasize which could cause death in particular case [142, 149, 123]. The clinical presentation of a SCC is a sternly demarcated and thick erythematous or peeling red plaques on sun-exposed areas. *In situ* SCCs are difficult to distinguish from AKs because there is no patho-biological difference between them [149, 5]. Moreover, lesions caused by invasive SCC can first appear as erythematous area with crusting and then as a nodule that growth over time and could become ulcerated or necrotic [168, 24]

1.1.2.3 Basal cell carcinoma (BCC)

BCC is one of the most common type of non-melanoma skin cancer (80%) [130] and its incidence is still rising even in younger people (< 40 years old) [131]. Contrary to SCC, BCC is a locally

invasive malignant epidermal skin tumor that grow slowly in the area of origin. BCCs rarely spread to distant parts of the body. BCCs are also keratinocyte tumors that arise from the basal layer of the epidermis called *stratum basale* (Figure 1.2) [16, 47]. BCC has several distinctive varieties [174, 209, 48] :

- Nodular (50-60%) (nBCC)
- Superficial (15%) (sBCC)
- Infiltrative (10-20%) whose morphoeic (5%) (iBCC)

Nodular BCC is most frequently observed on the face. This kind of disease is due to tumor cells growth in rounded masses shown as solid, well-demarcated, lobulated tumor nests of various sizes. This agglomerate may be a central necrosis composed of numerous fibroblasts, mucinous material and hyaluronic acid [130, 144]. Tumor nests of superficial BCC growth is restricted to epidermis or superficial parts of hair follicles. They can be defined as small buds of proliferating basal cells that grow down from the epidermis into the superficial dermis. The most common location of the superficial BCC is the trunk [100, 138]. The third subtype of BCC is the infiltrative one and the most aggressive as it can reach deep dermis and even subcutis [48]. This kind of BCC is difficult to diagnose, however in case of morphoeic BCC, a yellow-white waxy patch with very ill-defined edges could be a proof. When not treated on time, infiltrative BCC could lead to lesions showing ulceration, crusting or fibrosis [209]. Except for superficial BCC, all others lesions thicken cutaneous surface and the diameter of these lesions may range from a few millimeters to several centimeters.

1.2 Non melanoma skin cancer and treatment perspectives

Despite non-melanoma skin cancers are the most common, they can be usually treated by surgical excision, Moh's micrographic surgery or curettage. Recently, non-surgical methods such as cryotherapy, topical chemotherapeutics [35], immunotherapy, chemotherapy, laser treatment and photodynamic therapy have also been developed and are starting to be commonly used [16, 145].

Treatment choice depends on the type of skin lesions, number, size, location of lesions, patient's compliance, general health conditions, and cosmetic outcomes [212]. According to the European Dermatology Forum guidelines on topical photodynamic therapy, this treatment is approved for AK, SCC, superficial and certain thin BCC [115].

1.2.1 Photodynamic therapy

1.2.1.1 Principle

The concept of PDT is a century old and has the advantages to be a selective and localized therapy [62, 46]. This therapy presents an acceptable efficacy at long-term follow-up and do not let scars after treatment which is positive since the lesions are usually present on face, hands or neck (sun-exposed areas) [15]. PDT relies on the combination of three components to induce tumor destruction :

- a photosensitive drug
- a light at a precise power and wavelength
- oxygen

None of these elements is individually toxic, but together they produce a photochemical reaction[1] that generates singlet oxygen which is a highly reactive product causing cells death [2]. Clinical PDT in dermatology consists of the administration of a non-toxic drug, with a cream, known as photosensitizer (PS) to a patient presenting a skin lesion [146]. After an incubation period ($\sim 3\,h$) the lesion is illuminated with a specific wavelength able to stimulate the PS. The excited state of the PS (PS*) is not stable and comes back to its basic state by transferring energy to surrounding oxygen that will become an active singlet oxygen $O^{\bullet}$. This free radical will oxidize all tissues constituents in its close environment and destroy cells, therefore the effect will be localized [15].

1.2.1.2 Parameters

- **Photosensitizer (PS)**

PS should respect characteristics such as being non-toxic, water soluble, chemically and physically stable, selective for neoplastic tissues with the shortest time interval between administration and maximal accumulation. PS should also be eliminated by the body in a short time period in order to avoid unwanted photoreactions [146, 17]. Historically, hematoporphyrin and hematoporphyrin derivatives (HpD) were the first PSs to be studied in details [44]. However these compounds presented a photosensitivity for a long period of time (8 weeks), so patients had to avoid sunlight which was very constraining. Moreover, tumour-localizing properties of this PS were not as pronounced as first thought [25]. These deficiencies and the fact that this product was orally administered make its use difficult for dermatology. Therefore, a new approach has been investigated consisting in the development of endogenous photosensitizers. Endogenous PS are synthetized in the body from nonphotosensitizing precursors. Precursor's chemical conversion is established by metabolic pathways. The major endogenous PSs (protoporphyrin IX (PpIX), uroporphyrin, coproporphyrin) are products of heme cycle (Figure 1.3) [81]. Therefore, this second generation of PS is very selective and present a modest absorption on the range $600-700\,nm$ that allows them to be activated until several millimeters in biological tissues (See next paragraph 1.2.1.2) [45].

Actually, the 5-aminolevulinic acid (5-ALA) and the methyl-aminolevulinate (MAL) are the most widely used molecules as precursor drugs for PpIX production by the heme-synthesis. 5-ALA or MAL could be administrated as a cream which is interesting for topical application and especially skin treatments in dermatology. They are selective and have the possibility to be accumulated in tumours cells because individual steps of the heme cycle are disordered [2] and increased the production of various intermediate leading to a PpIX accumulation [17, 81]. 5-ALA is commercially available under the pharmaceuticals products Alacare®, Alafast®, Levulan®, Ameluz® and MAL is commercially available with the Metvixia® cream.

[1] This reaction will be more discussed in the introduction of section 1.3.

[2] The heme cycle disorder leads to a high concentration in porphobilinogen deaminase and a low concentration in ferrochelatase but this cycle perturbation will be more detailed in 1.3.

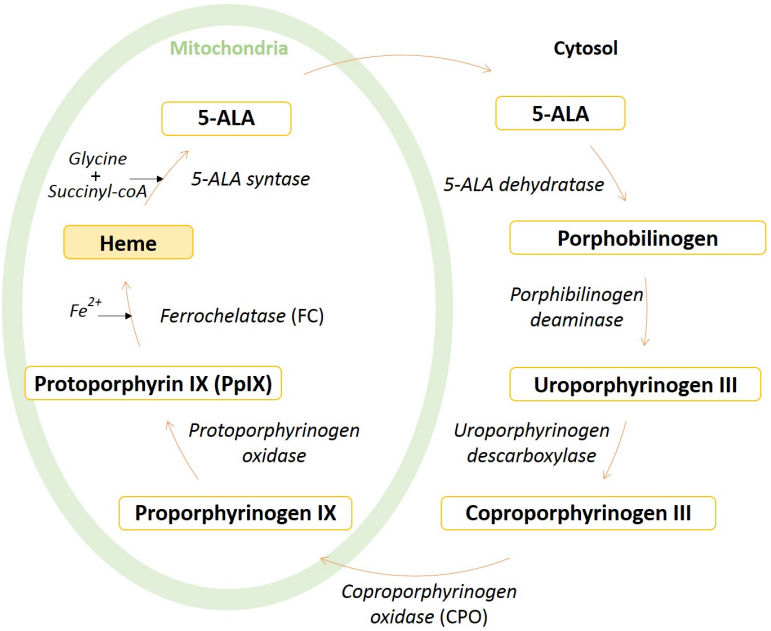

Figure 1.3 – Heme cycle.

- **Light**

Light at a precise wavelength is used to stimulate the PS. The choice of light source is mainly based on PS absorption but also according to its cost, and its size [2]. Light source needs especially to present spectral characteristics that match with the absorption wavelength range of the PS in order to generate enough singulet oxygen to produce a cytotoxic effect. In dermatology (and others specialities) light should reach all the injured tissue. The interaction of light with tissue is governed by three basic processes that can occur when a photon of light reaches the skin: reflection, scattering, and absorption. In case of PDT, absorption phenomenon is privileged [17]. The higher wavelength is, the deeper light penetrates tissues as presented on figure 1.4 [164]. Blue light (400 nm) has relatively low penetration in tissue (only absorbed in the superficial epidermis of skin) whereas red light (600 – 700 nm) penetrates more deeply [7]. A smart compromise has to be found between a minimal light absorption by tissues and a maximal light absorption by the PS.

For skin cancer treatment, 5-ALA which then produces PpIX is often used and a light set at 630 nm is advantageous to activate PpIX. This wavelength is in the red light, allowing penetration in deep tissues and corresponds to the last excitation peak of PpIX (Figure 1.5) [19, 72]. The fluence rate and exposure time also affect PDT response and need to be controlled. Nowadays, research is conducted with the aim of reducing light exposure time, irradiance and fluence rate in order to improve patient compliance [188, 189]. Similarly, light fractionation significantly increases the efficiency of PDT which allows skin re-oxygenation between two exposures [191].

- **Singlet oxygen and cells death**

Photochemical reaction needs oxygen to occur and to destroy malignant cells. The lifetime of singlet oxygen $O^{\bullet}$ is very short (approximately 10 – 320 ns), so its diffusion is only limited to cell's organelles (Distance of diffusion : 10 – 50 nm) [45]. Thus, photodynamic damage will occur

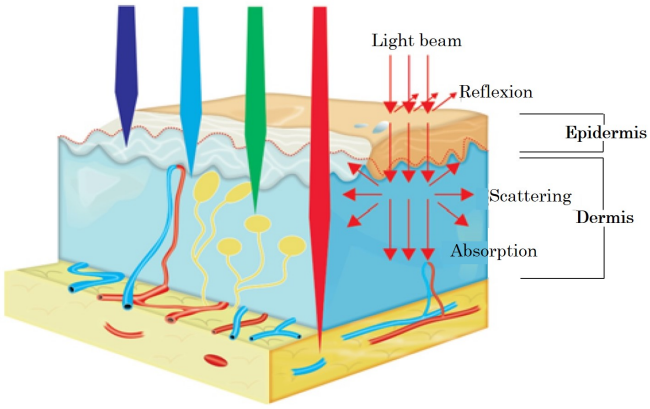

Figure 1.4 – Penetration of light in skin [164].

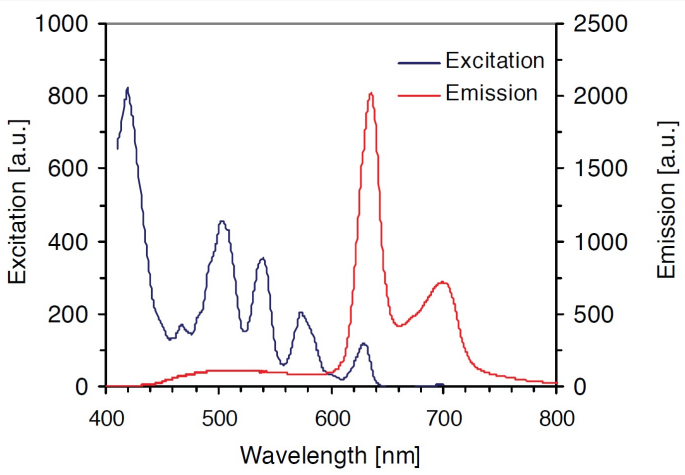

Figure 1.5 – Excitation and emission spectra of PpIX [52].

very close to the intracellular location of the PS [51, 109]. Two main mechanisms of tumoral cell death can occur thanks to singlet oxygen: apoptosis and necrosis [45, 163].

- Apoptosis defines the programmed cell death. When cells are subjected to aggression altering their integrity, they develop defense and immune responses but in case of abnormal activity, cells stop their cellular division. When damages are too important, a *"cellular suicide"* is engaged [160, 151].

- Necrosis defines the non-programmed cell death. It happens accidentality when cells are mistreated (burning, string compressions), they burst and their cytoplasm content is released provoking an inflammatory response [101].

Singlet oxygen is mainly responsible for cytotoxicity induced by PDT. Nevertheless, due to the large proportion of oxygen consumed by the photochemical reaction, other mechanisms can occur and kill surrounding cells. Photo-oxidative stress can lead to ischemia (restriction in blood

supply to tissues) or vascular response can induce vasoconstriction (narrowing of the blood vessels) that will also damage or kill cells [90].

1.2.2 Efficiency of PDT on non melanoma skin cancers

1.2.2.1 Treatment of AKs with PDT

Topical photodynamic therapy employing 5-ALA and MAL as endogenous precursor has been widely used to treat actinic keratosis and shows quite good clinical outcomes on many patients as presented in table 1.1. Moreover, in 2019, a group of 13 European practitioners (Morton et al.) decided to evaluate the average efficiency of conventional PDT[3] on AKs. Therefore, the authors chose 6 multicentric, randomized, double-blind studies from 2004 to 2012 which represent more than 1500 patients enrolled. Then the authors reported the clearance rates 3 months after the treatments between **81 and 92%** for thin and moderate thickness non-hyperkeratotic AKs localized on the face and scalp [115]. Since the last 5 years, to improve PDT outcomes, the tendency is to perform a lesion pretreatment or to combine PDT with other treatments such as cryotherapy or chemotherapy [115].

AK grade	Patients number	Photosensitizer	Method	Light	Clearance rate	Ref.
I to III	181	5-ALA 20 % (w/vol)	Drug is applied twice to each lesion.	$\lambda = 417\,nm$ (Blue) Intensity = $10\,mW/cm^2$	75 % at 8 weeks 89 % at 12 weeks	Piacquadio et al. 2004 [138]
I to III	202	MAL 16 % (w/w) : Metvix cream ©	Incubation time : 3 h.	$\lambda = 570 - 670\,nm$ (Red) Intensity = 70-$200\,mW/cm^2$ Dose = $75\,J/cm^2$	75 % at 3 months	Szeimiesa et al. 2002 [172]
I to IV	42	Metvix cream ©	Previous curettage of the lesion then application of the cream under occlusion for 3 h.	$\lambda = 570 - 670\,nm$ (Red) Intensity = 50-$200\,mW/cm^2$ Dose = $75\,J/cm^2$	89 % at 3 months	Pariser et al. 2003 [131]
Unspecified	30	Metvix cream ©	MAL application and occlusion for 3 h.	Daylight	79 % at 3 months	Wiegell et al. 2012 [202]

Table 1.1 – Photodynamic therapy on AK : protocols and clinical results.

[3] Conventional PDT involves application of a topically applied photosensitizing agent, an incubation time of approximately 3 hours and an illumination typically by a narrowband red LED light source.

1.2.2.2 Treatment of SCCs with PDT

Topical PDT employing 5-ALA or MAL as PS has also been used to treat SCCs. Methods and results are presented in table 1.2. Most of the studies involving PDT on SCC required lesion preparation (abrasion or curettage) or two cycles of MAL-PDT [115] which was also evidenced in the following short table 1.2. Overall, the clearance rates stay satisfactory and make PDT highly recommended for this medical indication. Nevertheless, it has been evidenced that the lesion size might also impact the clearance rate. Indeed 82% of lesions up to 14 mm were cleared after a 12 months follow-up whereas when the lesion size increased up to 30 mm or even 100 mm the clearance rate dropped to 55 % [119]. This is a major drawback since SCCs could potentially metastasize if not treated on time [35, 213]. Besides, PDT is currently not indicated for treating invasive SCC for reasons indicated hereinbefore [219, 115].

SCC type	Patients number	Photosensitizer	Method	Light	Clearance rate	Ref.
In situ	87	MAL 16 % (w/w) Metvix cream ©	Lesions surface were prepared by debridement with a curette. Cream was applied to the lesion for 3 h. Treatment was repeated once after 1 week for a complete treatment cycle.	λ = 570 – 670 nm (Non coherent red light) Dose = 75 J/cm^2	93 % at 3 months and 80 % at 12 months	Morton et al. 2006 [120]
Bowen's disease (*In situ*)	85	5-ALA cream prepared at 20 %	Prior to the first treatment hyperkeratosis and crusts were gently removed with a curette. Cream was applied for 3 h and covered with a plastic film.	λ = 630 nm Dose = 100 J/cm^2 Intensity = 100 mW/cm^2	78.6 % at 6–12 weeks	Westers-Attema et al. 2015 [199]
Bowen's disease (Large lesions d > 20 mm)	40 lesions	5-ALA in oil in water 20 % (w/w)	A previous abrasion on the lesion was carried. Cream was applied for 4 h under occlusive tissue.	λ = 630 nm Dose = 100 J/cm^2	78 % at 12 months	Morton 2001 [118]
In situ	55 and 112 lesions	Metvix cream ©	Cream was applied for 3 h prior to illumination. 7 days later: a second MAL-PDT session was performed.	λ = 635 nm Dose = 37 J/cm^2	73 % at 3 months and 56 % at 2 years.	Calzavara-Pinton et al. 2008 [21]

Table 1.2 – Photodynamic therapy on SCCs : protocols and clinical results.

1.2.2.3 Treatment of BCCs with PDT

PDT can be considered for recurrent and multiple BCCs, especially for those which are bad candidates for surgery due to co-morbid systemic disease or critical cosmetic location of the lesions [88]. A few clinical studies on BCCs are presented in table 1.3. No results on infiltrative BCCs were presented in the following table because numerous studies have excluded them from their experiments when choosing patients [31, 66]. Moreover when PDT was tried on morpheic BCCs, there was no clearance [162], so we decided to focus on the other BCCs categories. However, PDT is a recommended treatment for BCCs since superficial BCCs respond well with a clearance rate between **79 and 100 %** whereas for thicker or nodular BCCs the clearance rate is decreased [4, 9] which is also displayed in table 1.3. The poor penetration of the prodrug in deep skin layers could explain the lower efficiency observed for nodular BCCs [135]. Indeed, Ahmadi et al. applied the cream (5-ALA at 20% w/w) with a thickness currently used in clinics and found that only 36.8 % of the total dose was released during the 4 h application period (*Experiments were performed with Franz cell apparatus*) [4]. To reach sufficient prodrug concentration in depth allowing a biologic rationale for a clinical PDT, Peng et al. estimated that an application of MAL (1 mm thick layer and 1 cm outside the lesion) at 160 mg g^{-1} for 3 h induced the highest ratio of porphyrin fluorescence in tumor depth [135]. To sum up, conventional PDT can not be used for all BCCs and if so, a previous lesion preparation should be ensured or several PDT sessions should take place [115].

Table 1.3 – Photodynamic therapy on BCC : protocols and clinical results.

BCC type	Patients number	Photosensitizer	Method	Light	Clearance rate	Ref.
Superficial	92	MAL	Lesion was debrided using a curette. Cream (1 mm thick) was applied and the lesion was covered with an adhesive occlusive dressing for 3 hours. Two PDT sessions with an interval of 1 week between each session were performed.	$\lambda = 570 - 670$ nm Dose = 75 J/cm^2 Intensity = 100 mW/cm^2	93 % at 3 months	Vinciullo et al. 2005 [194]
Nodular	36				82 % at 3 months	
Nodular	168 lesions	MAL prepared at 16 % (w/w)	Lesion was debulked, then cream was applied for 3 to 24 hours and covered by a semipermeable film.	$\lambda = 570 - 670$ nm Dose = 75 J/cm^2 Intensity = 100-180 mW/cm^2	At a mean period of 35 months 86 % for thick nBCC 93 % for thin nBCC	Soler et al. 2001 [162]
Superficial	323	5-ALA prepared at 20 % concentration in a cream base (Neribas)	Excessive scaling was removed by curettage. Then 5-ALA cream was applied and covered with a semipermeable dressing and aluminium foil for 3.5 h.	Two light fractions λ = 635 nm with 2 hours interval. First dose : 20 J/cm^2 for 4.23 min Second dose : 80 J/cm^2 for 18.8 min	77 % at 48 months	Kessels et al. 2016 [82]

Superficial	87 with 128 lesions	MAL 16 % (w/w) Metvix cream ©	Scales and crusts were removed. A layer of about 1 mm thick of cream was applied on the lesion and covered with an occlusive dressing for 3 hours. One cycle of two treatment sessions 7 days apart [4] was applied.	$\lambda = 630$ nm Dose = 37 J/cm^2 for 7-10 min	92 % at 3 months 90 % at 3 months	Szeimies et al. 2008 [171]

1.2.2.4 Assessment and perspectives

As presented in the previous sections and in the tables 1.1, 1.3 and 1.2, PDT can be used on most of the non melanoma skin cancer types and quite good clinical results were observed. To obtain these satisfactory clinical results, especially for thicker skin lesions, skin preparation prior to drug application on the lesions was necessary and consists often of a curettage or a debulking. A long prodrug incubation with a highly prodrug dose is also mandatory to allow efficient prodrug depth penetration [18, 54, 115, 161]. These supplementary steps added to conventional PDT make this treatment extended in time, painful and tedious. To overcome the pain during the treatment, an anesthetic cream may be applied, ice or cold water could be vaporized on the treated area [8] or the irradiation could also be decreased [189, 192]. Moreover to enhance prodrug penetration and reduce treatment time, different solutions have been considered and will be presented in the next section 1.3 with a recently review published in *Photochemistry and Photobiology* and entitled: **"Photodynamic therapy for skin cancers: How to enhance drug penetration?"**.

1.3 Methods to improve drug penetration

[4] If sBCC lesions showed non-clearance 3 months later they could be retreated with a second cycle of two MAL-PDT sessions 7 days apart.

Photodynamic therapy for skin cancer: how to enhance drug penetration?

Mathilde Champeau[a,b,*], Séverine Vignoud[a], Laurent Mortier[b], Serge Mordon[b]

[a] *CEA, LETI-DTBS, 17 rue des Martyrs, Grenoble Cedex, France*
[b] *Univ. Lille, Inserm, CHU Lille, U1189 - ONCO-THAI - Image Assisted Laser Therapy for Oncology, F-59000 Lille, France*

Abstract

Photodynamic therapy (PDT) induced by protoporphyrin IX (PpIX) has been widely used in dermatological practices such as treatment of skin cancers. Clearance rate depends on different factors such as light irradiation, skin oxygenation and drug penetration. The poor penetration of 5-aminolevulinic acid (5-ALA) with topical application is limited and restrains the production of PpIX which could restrict PDT outcomes. This review will focus on techniques already used to enhance drug penetration in human skin, and will present their results, advantages, and drawbacks. Chemical and physical pretreatments will be discussed. Chemical pre-treatments comprise of drug formulation modification, use of agents that modify the heme cycle, enhance PpIX formation, and the combination of differentiation-promoting agent prior to PDT. On the other hand, physical pretreatments affect the skin barrier by creating holes in the skin or by removing *stratum corneum*. To promote drug penetration, iontophoresis and temperature modulation are interesting alternative methods. Cellular mechanisms enrolled during chemical or physical pretreatments have been investigated in order to understand how 5-ALA penetrates the skin, why it is preferentially metabolized in PpIX in tumour cells, and how it could be accumulated in deeper skin layers. The objective of this review is to compare clinical trials that use innovative technology to conventional PDT treatment. Most of these pretreatments present good or even better clinical outcomes than usual PDT.

Keywords: photodynamic therapy, drug penetration, skin pretreatment, skin cancer, 5-aminolevulinic acid

2010 MSC: 00-01, 99-00

*Corresponding author
Email address: mathilde.champeau@cea.fr (Mathilde Champeau)

1. Introduction

Protoporphyrin IX-induced PDT has been widely used in dermatological practice such as treatment of skin cancers [1] .

Historically, treatments using light appeared during antiquity and were used by the Egyptians, Indians, Greeks and Chinese to treat skin diseases. Therapy using an exogenous substance reacting with sun's photons was observed during the 15^{th} century BC in India. At the end of the 19^{th} century, interaction between light and molecules was considered for medical treatment. The concept of PDT was first introduced by Van Tappeiner who mentioned the necessity of oxygen to obtain a chemical reaction over a century ago [2]. When PDT depends on the combination of three components to induce tumour destruction: a photosensitive drug, light, and oxygen (Figure 1). None of these elements is individually toxic, but together they produce a photochemical reaction that generates singlet oxygen which is a highly reactive product causing cell death [3]. Figure 2 displays the different energy states and the different pathways leading to fluorescence and other photochemical process. First the photosensitizer (PS) at its ground and singlet state absorbs a photon and moves to its excited energy state. Because of the internal conversion the PS energy decreases and reaches the lower allowed transition of its excited state. Inter-system conversion causes this singlet state to become a triplet state. The singlet state relaxation produces fluorescence, and the triplet produces phosphorescence. A molecule with high triplet energy quantum yield can initiate chemical reactions (type I) that produce free radicals, and then could react with oxygen to form singlet oxygen. Singlet oxygen is a reactive oxygen species that is reponsible for degradation of several cell components, and induce cell death by type II chemical reactions [4].

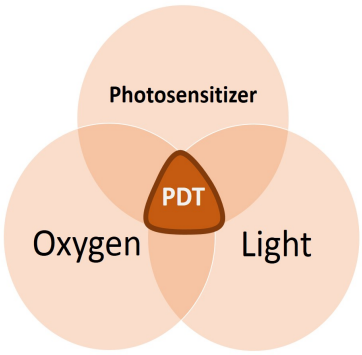

Figure 1: Synergy between three parameters produces PDT.

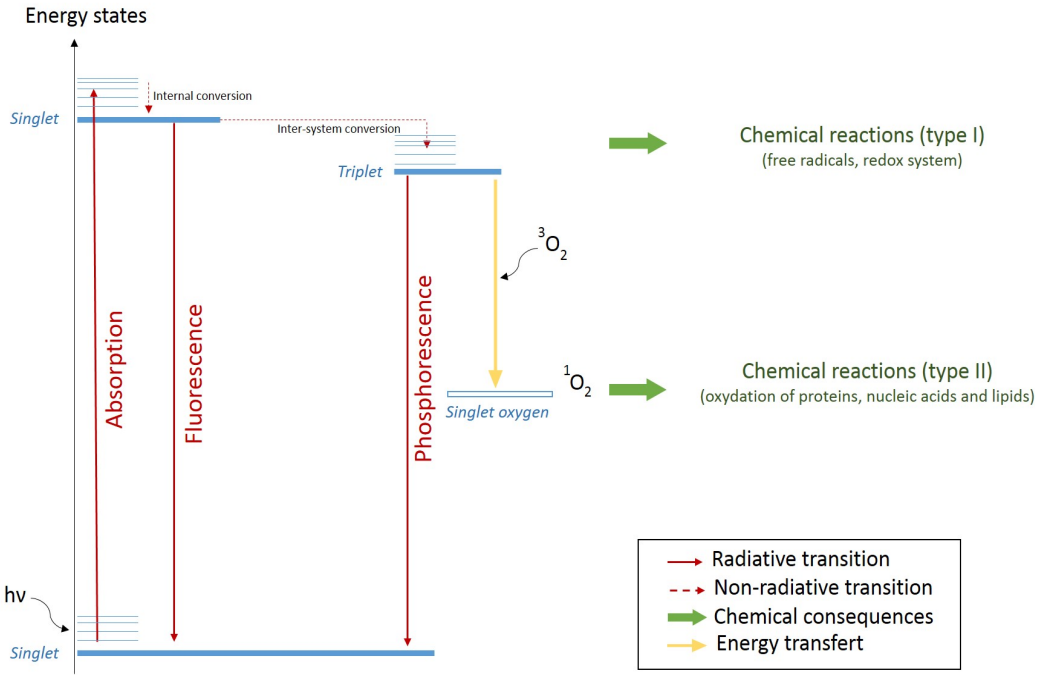

Figure 2: Jablonski diagram representing the different processes leading to singlet oxygen production responsible for cell death.

PDT treatment in dermatology consists of the administration of a non-toxic drug known as a photosensitizer (PS) to a patient presenting a lesion, which is frequently, but not always cancerous [5].

Photosensitizers should have characteristics such like being non-toxic, water soluble, having a chemical and physical stability, being selective for neoplastic tissues with the quickest time interval between administration and maximal accumulation, and able to be eliminated by the body in a short time in order to avoid photoreactions [5]. Historically, hematoporphyrin and hematoporphyrin derivative (HpD) were the first PSs to be studied in detail [6]. However these compounds present photosensitivity after a long time (8 weeks), so patients had to avoid sunlight which was very constraining. Moreover, tumour-localizing properties of these PSs were not as pronounced as first thought [7]. These deficiencies and the fact that these products were orally administered made their use difficult for dermatology. So a new kind of PS has been developed: endogenous photosensitizers. Endogenous PS are synthetized in the body from nonphotosensitizing precursors (also called prodrugs). A precursor's chemical conversion is established by metabolic pathways and particularly by the heme cycle.

Nowadays in the field of dermatology, topical application of 5-aminolevulinic acid (5-ALA) (a non-photosensitizing precursor) is used to induce *in situ* synthesis of endogenous PS according to the heme cycle [8]. Figure 3 displays the heme cycle where 5-ALA is the first metabolite in the heme biosynthesis pathway in humans. 5-ALA -when not voluntary added- is originallly produced by glycine and succinyl coenzyme A, and then migrates to the cytosol. From there, porphobilinogen is formed due to the condensation of two molecules of 5-ALA. Four molecules of porphobilinogen are connected together, and after porphibilinogen deaminase they form the cyclic uroporphyrinogen III. Decarboxylation of uroporphyrinogen leads to coproporphyrinogen III which then generates within mitochondria proporphyrinogen IX after coproporphyrinogen oxidase (CPO) acts upon coproporphyrinogen III. This last molecule is further oxidized to form PpIX. PpIX is subsequently chelated with iron to form heme [9]. 5-ALA is also valuable for PDT because it has the possibility to be preferentially accumulated in tumour cells. This fact could be explained by a change in mitochondrial function (lack of energy), alteration in porphyrin transporters, or a perturbation in heme biosynthetic enzyme in tumour cells. Indeed individual steps of the heme cycle are delayed by an high concentration of porphobilinogen deaminase and low concentration of ferrochelatase (FC). Moreover the enzyme responsible for converting protoporphyrin IX (PpIX) in heme has been found in reduced levels in a variety of tumour tissues including liver, bladder, colorectal, esophageal, gastric, and rectal [9]. This deregulation causes the accumulation of various intermediate products leading to PpIX accumulation [8]. This accumulation has been also shown in different skin lesions (psoriatic plaques, actinic keratosis, and basal cell carcinoma) where PpIX fluorescence was at higher levels as compared to healthy skin. [10, 11]

For most clinical trials [12–15], 5-ALA was administrated at a high dose ($\approx$ 80 mg) as a cream on the lesion to promote PpIX accumulation [16]. After an incubation period[1], lesions were illuminated with a special wavelength (usually 635 nm) appropriate for tissue transmission and able to stimulate the PS [1, 3]. Stimulated PS (PS*) follow the process presented in figure 2 and PDT occurs.

PDT efficiency depends on several parameters such as light dosimetry, fluence rate, time between PS administration and irradiation (also called *incubation period)*, exposure time, rate of oxygen, kinetic distribution of PS in tissues, PS selectivity, and concentration [3, 18, 19]. PDT

[1]Incubation time is usually 3 h in conventional PDT treatment. This period is not the perfect one to obtain the best accumulation of PpIX in cells [17] but is the most suitable for hospital practice.

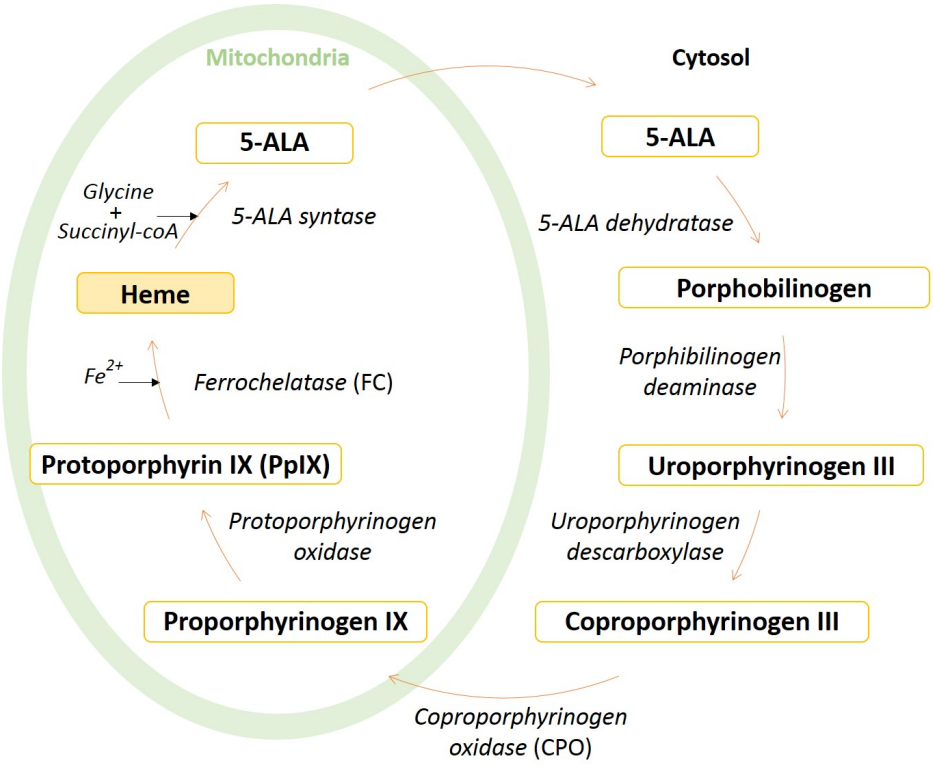

Figure 3: Heme cycle.

optimization is difficult because all parameters are correlated. Production and distribution of PS remains the most important parameters since thereafter photodynamic therapy (PDT) result on it. Photosensitizer formation and epidermal penetration depth represent basic predictors of drug efficacy in dermatological PDT [20]. Concentration, distribution, aggregation, and accumulation of PS modifies the photobleaching[2] kinetic [20].

Despite progress concerning few parameters, PDT is currently limited by poor tissue penetration of the porphyrin precursor 5-aminolevulinic acid. This review will focus on one of the three important parameters needed for PDT. Lack of 5-ALA penetration through the skin is due to molecule hydrophilicity that prevents it to cross the *stratum corneum* (SC) [21]. The aim of this review is to present the chemical and physical methods to increase drug penetration before PDT. To increase penetration of 5-ALA into deep epidermal regions different adaptations to standard PDT treatment have been considered. Proposals have been made concerning chemical

[2]Photobleaching is defined as a drug photodegradation and should be avoided in PDT treatment.

modification of the drug precursor that could lead to a better penetration. Others strategies have been developed to control the heme cycle by adding special agents in order to promote PpIX accumulation. Modification of the skin surface has been researched by physical pretreatment such as creating holes, changing the temperature, or a voltage shocks have been proposed [22].

2. Chemical methods

Althought 5-ALA has been widely use for PDT treatment, the preparation is quite difficult because of its properties. 5-ALA-stability within solution or topical formulation is low because of 5-ALA dimerization to 2,5-pyrazinedipropionic acid (PY) which makes its formulation quite challenging.

Extrinsic parameters. To overcome 5-ALA-degradation, pH range, concentration and appropiate temperature should be well controlled [23]. According to Elfsson et al. [24], stability of 5-ALA was maintained at low pH. Solutions of 5-ALA in buffer ($0.060\,\mathrm{mol\,L^{-1}}$) were investigated at 50 °C. At $pH = 2.53$ no degradation was observed for 37 days whereas at $pH = 4.81$ and $pH = 7.42$ after respectively 257 h and 3 h half of the 5-ALA compound was degraded [24]. Similarly, De Blois et al. [25] showed a decrease of 5-ALA-degradation when pH values were lower. A solution of 5-ALA at 0.1% was investigated at 21 °C. These solutions were stable for 128 days at $pH \leq 6$ whereas at $pH \geq 7$, 5-ALA content declined below 90% within a few days (≈ 10 days) [25]. Nevertheless, for some applications it is sometimes necessary to work with a physiological pH ($pH \approx 7$). So it was recommended to decrease the 5-ALA concentration to increase its stability according to a kinetic equation proposed by Elfsson et al. [24] [24]. De Blois et al. [25] had proven that a solution of 5-ALA at $pH = 5$ at 0.5% could be stable for 178 days whereas solutions with initial concentrations of 2, 5 and 10% had an 5-ALA content which dropped below 90% respectively after 150, 94, and 29 days [25]. Finally to overcome 5-ALA degradation temperature should be controlled too, because an increase of temperature enhanced 5-ALA degradation which followed Arrhenius law [25].

Intrinsic parameters. Once a stable formulation is developed, there is still the problem of poor penetration of 5-ALA through the skin. This fact is accounted for by the physicochemical properties of 5-ALA. The drug is highly hydrophilic with an octanol:water partition coefficient at -1.5 ($\log P$) which does not match with the lipophilic character of the skin surface. Therefore, no interaction between the skin and the prodrug that could initiate 5-ALA penetration occurs. Moreover, this drug has a zwitterionic nature which means that at any pH the molecule is charged

and it is wellknown that charged molecules do not cross the *stratum corneum* (SC) easily because they could interact with components from skin [26, 27]. Although 5-ALA has a low molecular weight ($131\,\mathrm{g\,mol^{-1}}$) penetration through the *stratum corneum* is limited to a maximum depth of 1 mm and is nonhomogenous [28]. To overcome these limitations different strategies have been developed such as using others prodrugs instead of 5-ALA, or making new drug delivery system to ensure 5-ALA penetration into the skin.

2.1. Use of different prodrugs

Because of 5-ALA properties and in order to enhance drug penetration through the stratum corneum, other prodrugs with longer carbon chains, more lipophilic, have been developed [29, 30]. Chemical structures of these prodrugs are presented in figure 4 and their use in clinical trials on human patients is presented in table 1.

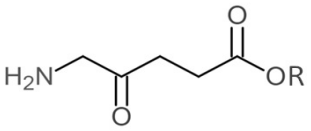

Carbonyl group -R	Name
-H	5-ALA
CH_3	MAL
CH_3	Ethyl-ALA
CH_3	Propyl-ALA
CH_3	Butyl-ALA
CH_3	Hexyl-ALA
CH_3	Octyl-ALA

Figure 4: Chemical structure of the different prodrugs used for enhancing drug penetration and PDT outcomes.

Methyl-5-aminolevulinate (MAL) is currently used in clinic similarly to 5-ALA [36]. Due to its methyl group, methyl-5-aminolevulinate (MAL) is more lipophilic and has better selectivity for tissue. MAL-PDT could be more effective than 5-ALA-PDT in the case of deep lesions (squamous cell carcinoma (SCC)) [37]. Overall 5-ALA-PDT and MAL-PDT are both successful dermatologic therapies with high clearance rates[3] from 75% to 80% [32, 36]. In order to increase the penetration of drug through the *stratum corneum*, ethyl-ALA, propyl-ALA, butyl-ALA have

[3]Clerance rate is defined in this review as the disapperance of skin lesions.

Table 1: Prodrugs used for enhancing photodynamic therapy.

Type of lesions	Prodrugs	Method	Efficacy	Ref.
Superficial basal cell carcinoma (sBCC) and Bowen disease (BD) on 40 human patients	MAL	Application of 5-ALA (20 %) or MAL (16 %) cream on lesions after surface preparation.	No significant difference was found between 5-ALA or MAL. PpIX fluorescence induced in lesions of sBCC and BD was similar. Secondly, patients pain was not different with one or another prodrug.	[31]
Extensive actinic keratosis (AK) on 16 human patients	MAL	Visible layer of 5-ALA cream (20 %) or MAL cream (20 %) was applied on lesions.	Both 5-ALA-PDT and MAL-PDT result in a significant reduction in scalp AK. 5-ALA-PDT was more painful than MAL-PDT in the treatment of extensive scalp AK.	[32]
Healthy excised human stratum corneum	Butyl-ALA	*Ex vivo* Franz cell. Butyl-ALA (10 %) in 4 different cream formulation, 5-ALA (10 %) in 5 different cream formulation.	Permeation coefficient of butyl-ALA in SC was higher than 5-ALA, not dependant on cream formulation.	[33, 34]
Actinic keratosis (AK) Grade I, II, III on human patients (200 lesions)	Hexyl-ALA	Daylight PDT study compared 0.2 % hexyl-ALA and 16 % MAL on the treatment of AK.	Hexyl-ALA was less effective for grade II-III AKs compared to MAL. For grade I AKs clearance was equal.	[35]

been produced. These prodrugs improved PpIX penetration after topical application to skin *in vivo* [30], but their formulation (esterification) required numerous chemical steps [33, 38, 39]. Similarly, hexyl-ALA and octyl-ALA have been developed and tested *in vitro* [29] and *in vivo* [35]. These two prodrugs have great penetration and could be utilized in smaller concentrations than 5-ALA or MAL [35]. Nevertheless, these prodrugs are too lipophilic, and can be accumulated in the SC which compromises their biological action [40]. So 5-ALA and MAL remain the most used drugs . To enhance their penetration through the SC new vehicles or drug delivery systems have been developed.

2.2. Skin penetration of 5-ALA with different vehicles

Due to the difficulties encountered with long carbon chain prodrugs 5-ALA and MAL remain the two most used PSs for PDT on skin cancers, despite their limited penetration through the skin. Therefore, new vehicles for drug administration have been developed in order to enhance drug permeation and promote improved PpIX formation.

Topical delivery is considered to be the delivery route of choice, and is the most adequate for skin cancer since it localizes the photosensitizer to the site of application and avoids skin photosensitivity everywhere in the body [36]. So different vehicles such as creams[4], gels[5], patch systems, lotions, liposomes, nanoparticles, powders and microemulsions have been developed to be applied on skin lesions to overcome the penetration issue [43, 44]. Each formulation was developed in an environment favorizing 5-ALA stability.

2.2.1. Cream formulations

5-ALA has been clinically used as a cream formulation. Lipophilic cream can enhance drug affinity with skin and increase the penetration of 5-ALA. The most employed formulation consists of 5-ALA at 20% w/v in acid solution with 48% ethanol, water, laureth-4, isopropyl alcohol, and polyethylene glycol [36, 44]. This composition is FDA-approved and commercialized as Levulan® Kerastick ™ in the U.S. This product has been principally used in the U.S [45]. In Europe, a similar cream composed of 16% w/w MAL in a solution containing different excipients such as cetostearyl alcohol, peanut oil, glycerol, methylparaben, propylparaben, and water is

[4] A cream is a semi-solid emulsion of oil in water or water in oil. A cream tends to be more viscous than a gel and therefore need a shear stress more important to ensure penetration through the skin[41, 42].

[5] A gel is a thermodynamically stable solid-liquid biphasic system consisting of a continuous three dimensionale interpenetrating network, one solid and the second liquid.

mainly used. This formulation is employed as frequently as the one composed of 5-ALA, and is commercialized by Galderma under the trademark Metvix®. Although crossing the SC is not fully overcome, Levulan® and Metvix® have been widely used and has acceptable clearance rates and cosmetic outcomes. However, some side effects such as burning, stinging, itching, erythema, or even oedema have been detected during light exposure and could become more intense after few minutes of light exposure [46, 47].

2.2.2. Gel formulations

In order to avoid side effects during 5-ALA-PDT and MAL-PDT, some gel formulations containing the drug have also been developed. To enhance the physical stability of a cream for the treatment of AKs, Risaliti et al. [43] developed three galenic gel formulations (named Natrosol, Sepigel and Carbopol) each containing 10% w/w of 5-ALA. In terms of viscosity, microbiological stability and storage stability, the Sepigel formulation composed of 10% of 5-ALA, 87% of water and 3% of polyacrylamide, isoparaffin and laureth-7 displayed the best results for skin cancer treatment. Comparison between this gel and a lipophilic cream used in the study on 15 patients proved that Sepigel caused less unpleasant effects than a cream during coating and during irradiation. This formulation also has the advantage to be better absorbed by the skin [43]. This improved penetration was also observed in the other gel formulations. One was prepared by mixing surfactant, water, cetylstearyl-2-ethylhexanoate, and 1.5% (w/w) of 5-ALA and displayed excellent skin permeation [48]. Another gel composed of isopropyl alcohol, dimethyl isosorbide, medium chain triglycerides, water, Pluronic F 127, and 10% w/w of 5-ALA presented better permeation coefficient through human *stratum corneum* than German Pharmacopoeia creams [49]. On the other hand, a 5-ALA nanoemulsion gel was compared to a MAL cream on pig skin. A nanoemulsion of 5-ALA penetrated deeper skin layers and produced higher fluorescence signals (5 fold) than MAL cream [50]. Since 5-ALA stability was increased due to the presence of the nanoemulsion, this formulation was used for AK treatment on 122 patients to test the efficacy and safety of this product. At the end of the study (12 weeks), lesions complete clearance rate was 81% with the nanoemulsion gel, whereas it was 22% with the placebo treatment. This study proved that the nanoemulsion gel was well suited for PDT of AK with high efficacy despite the low 5-ALA concentration (10%) [51]. Another study with 630 enrolled patients proved the efficacy of the 5-ALA nanoemulsion by comparing it with the MAL cream. At a long follow-up (12 months), the proportion of patients fully cleared was, respectively, 47% for the 5-ALA nanoemulsion and 36% for the MAL treatment [52]. Since these results, the

5-ALA nanoemulsion formulation has been FDA-approved and put on the market as Ameluz® in 2016. The efficacy was established on AKs, and is under clinical investigation on 186 patients suffering from superficial basal cell carcinoma (BCC) (NCT03573401). To facilitate gel use, they can also be integrated into patches.

2.2.3. Patches

Patches are small, soft and adhesive devices that contain a drug which could be delivered when applied onto the surface of the skin. Patches containing 5-ALA were developed to facilitate classical PDT that consisted of applying a cream on neoplastic lesions and keeping them under occlusion. The patch is able to adhere to the skin, allow to deliver a precise 5-ALA dose, and blocking the lesion due to a backing layer. A schematic representation is presented in Figure 5 [53].

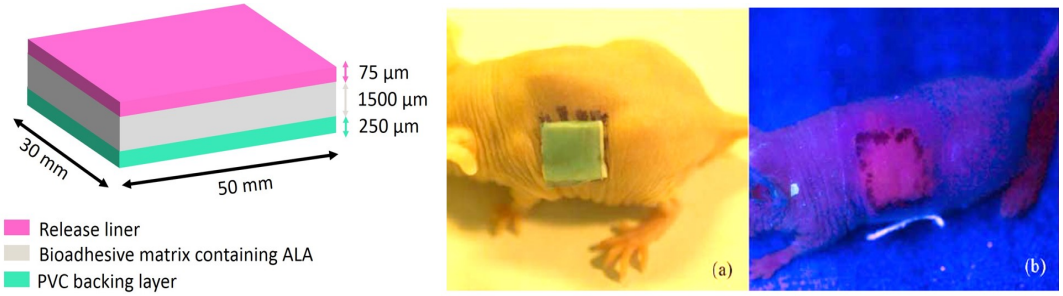

Figure 5: Patch formulation and its *in vivo* use on nude mouse. PpIX fluorescence was observed 4 h after patch removal [53].

Different compositions were developed. For instance, a solution was first prepared by mixing cetylsteryl-2-ethylhexanoate, water, surfactant, and 1.5% w/w of 5-ALA. Then it was mixed with a carrageenan hydrogel and freeze-dried to form a homogenous aerogel (film). Permeation of 5-ALA was investigated by using porcine abdominal skin in Franz diffusion cells. After 48 h, diffusion was improved with the patch than with a hydroxyethylcellulose gel containing 1.5% w/w of 5-ALA . Nevertheless, a degradation of 5-ALA was detected in the patch after 14 days which make its use impossible after a long term storage [48].

A second example is a square, self-adhesive patch (PD P 506 A ®) containing 8 mg of 5-ALA for 4 cm^2 tested on 25 patients during a clinical phase I study. The aim of the study was to evaluate PpIX fluorescence corresponding to patch application duration and the 5-ALA pharmacokinetics. Maximum fluorescence was observed after 4 hours of patch application, and was more intense in AK lesions than in normal skin. Pharmacokinetics study revealed a small

increase of 5-ALA in the blood, but normal values returned rapidly after patch removal. These experiments had proven that use of patches for skin cancer was safe and tolerable [54]. This same patch was clinically used on 218 patients suffering from AKs. Efficacy rate on a lesion was superior to 82% when 3 to 8 patches were applied per patient. The use of this patch was favorable because it was easy to handle, apply (no skin preparation was necessary), and induced very good efficacy and cosmetic results compared to placebo-PDT or cryosurgery [55]. Because of these satisfactory clinical outcomes, this patch was then commercialized as Alacare®. Alacare®-PDT has the potential to become the first-line treatment in the therapy of AK. However, in case of thick lesions and without a skin surface pretreatment, this therapy might be less efficient. Also the patch area is quite small ($32\,cm^2$) which limits its use for large skin lesions. [56]

2.2.4. Drug delivery systems

Micro or nanocarriers are commonly used as drug delivery systems since they can penetrate through small capillaries and are taken up by cells, which allows efficient drug accumulation in certain locations. Their use in topical formulation for 5-ALA delivery is very attractive since they might easily cross the SC. Some of these different vehicles (liposomes, nanoparticles, micelles, nanofibers, patches) are presented in figure 6.

Liposomes. Liposomes are spherical vesicles with a diameter from 70 nm to few micrometers. Liposomes are formed by one or more lipid concentric bimolecular layers often made of phospholipids and present an aqueous core (Figure 6a) [41]. Liposomes have been used *in vitro* and *ex vivo* in topical photodynamic therapy [60]. This drug delivery system has the advantage to encapsulate lipophilic molecules within the lipid bilayers or hydrophilic drugs such as 5-ALA within the aqueous core. Dragicevic-Curic and Fahr [61] reviewed the use of different types of liposomes for encapsulating 5-ALA for topical PDT [61]. In most presented studies, liposomes promote higher 5-ALA penetration into skin than free 5-ALA. Phospholipids present on the particule surface could interact with the SC and act as penetration enhancers. This accumulation of 5-ALA in the skin enhanced PpIX formation which should lead to better PDT efficacy and enable topical PDT of deep skin lesions [61, 62]. Liposomes are extensively used as controlled and targeted drug delivery systems which allow to use a low concentration of 5-ALA [63]. Compared to free 5-ALA, liposomes can reduce drug absorption into systemic circulation, limit its cytotoxicity, the risk of photosensitivity after the treatment, and could possibly avoid pain and side effects (itching, burning) induced by the use of an high 5-ALA concentration [61]. To our knowledge, except for a study on tumour mouse models [60] and a study on patients suffering

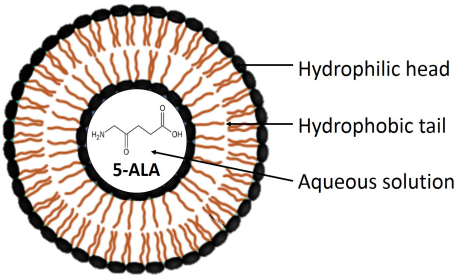

(a) Scheme of a liposome encapsulating 5-ALA.

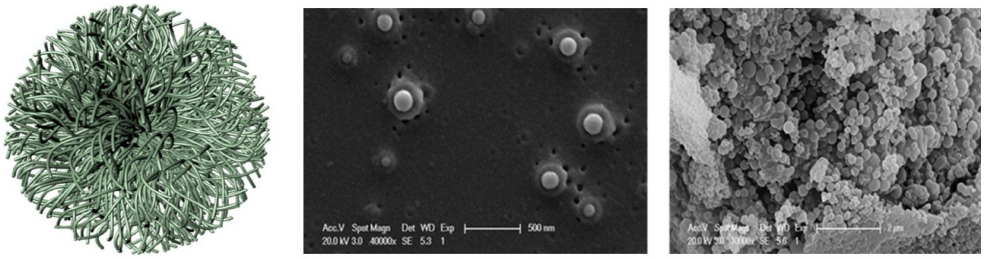

(b) Scheme of polymeric PLGA nanoparticles loaded with 5-ALA [57] and scanning electron microscope (SEM) observations of nanoparticles [58].

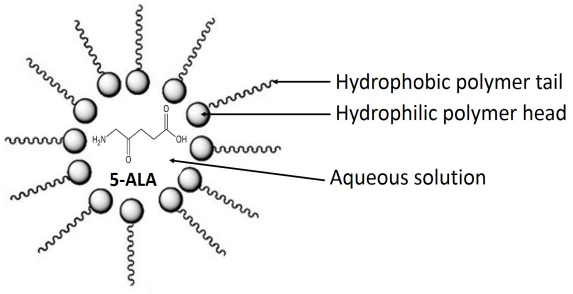

(c) Scheme of a 5-ALA loaded micelle.

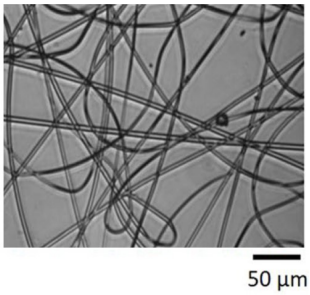

(d) SEM observations of electrospun nanofibers from 25% w/w PMVEMA-ES solutions in ethanol combined with 5-ALA (16,7 % w/w) [59].

Figure 6: Representation of the different vehicles used for topical delivery of 5-ALA.

from acne [64, 65], no *in vivo* studies on patients suffering from skin cancer have been conducted.

Polymer nanoparticles. Nanoparticles are colloidal systems with a diameter between 10 nm and 1000 nm. They are generally composed of biodegradable polymers or lipids and are able to entrap drugs by adsorption or encapsulation [41]. A new 5-ALA delivery approach using poly(lactic-co-glycolic acid) (PLGA) nanoparticles has been investigated (Figure 6b). Due to their size the drug have the ability to go through the skin pores and penetrate more easily the epidermis [62]. An *in vitro* experiment on human epidermoid squamous cells carcinoma revealed that 5-ALA

loaded in nanoparticles induced more PpIX fluorescence and a higher photocytotoxicity than free 5-ALA at the same concentration (0.1 mM) [58]. PLGA nanoparticles provided a promising 5-ALA delivery strategy for topical PDT on SCC but *in vivo* investigations should be pursued.

Polymeric micelles. Polymeric micelles are composed of a core and a shell formed by the self-assembly of block copolymers. They have a spherical shape with a particle diameter from 10 nm to 100 nm. Their composition and size enhance their permeation through the skin. Polymeric micelles are starting to be used to encapsulate 5-ALA (Figure 6c). Tong et al. [66] chose to study the interaction between α-cyclodextrin and a poly(ethylene glycol) (PEG) conjugated to form a pseudopolyrotaxane for entrapping 5-ALA. The produced micelles were stable in a physiological environment, were able to release 5-ALA, and enhanced cellular uptake. Therefore, a PpIX accumulation was observed and a higher photodynamic cytotoxicity than free 5-ALA [66]. Such prodrug micelles may provide new opportunities for the development of 5-ALA-based photodynamic cancer therapy and further investigation on *in vivo* systems might be interesting.

Nanofibers. Nanofibers can be generated from different polymers, and hence have different physical properties. Nanofibers possess extremely high specific surface area that can be usefull for drug delivery due to their nanoscale diameter. The method most commonly used to produced nanofibers is electrospinning. This technique consists of applying a high electric force to a polymer solution to form charged threads. Electrospun nanofibers with 5-ALA (Figure 6d) were first synthetized with poly(methyl vinyl ether-alt-maleic acid) (PMVEMA) and poly(methyl vinyl ether-alt-maleic ethyl monoester) (PMVEMA-ES), and 5-ALA was incorporated within these nanofibers. The prodrug was stable in this conformation. Franz cells were used to evaluate the kinetic release of 5-ALA, and showed that nanofibers loaded with 5-ALA were able to deliver the drug and served as a substrate for the production of PpIX [59].

A combination of 5-ALA and micro or nanocarriers might provide an interesting strategy to enhance clinical outcomes with PDT, but in some drug delivery systems *in vivo* investigations are necessary to conclude their safety and therapeutic efficacy [61].

2.3. Agents that control heme cycle and promote PpIX accumulation

Some prodrugs pass through the *stratum corneum*, but sometimes the amount is not sufficient to produce enough PpIX for PDT treatment. Other strategies have been developed to control the heme cycle in order to ensure enough PpIX production. To make sure that PpIX will accumulate in cells it is important that PpIX does not convert in to heme (Figure 3). An iron-chelating agent

can be used to inhibit the conversion of PpIX to heme by removing Fe^{2+} from the cellular system which will result in a temporary increased accumulation of PpIX (3-5 fold) [67](Figure 3).

The adding of iron chelators like desferrioxamine (DFO) or hydroxypyridinone (HPO) can act on heme cycle and increase amount on PpIX in cells. DFO and HPO are ligands able to bind with iron as central metal atom to form a coordination complex. The binding involves donation of electrons. DFO and CP94 complex are presented in figure 7 [68]. Other strategies for iron chelating are reported in table 2 [69].

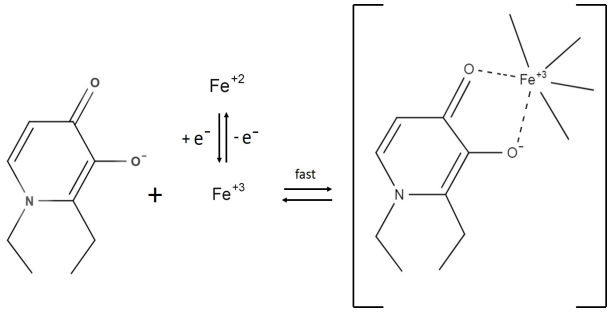

(a) CP94 and its iron-complex

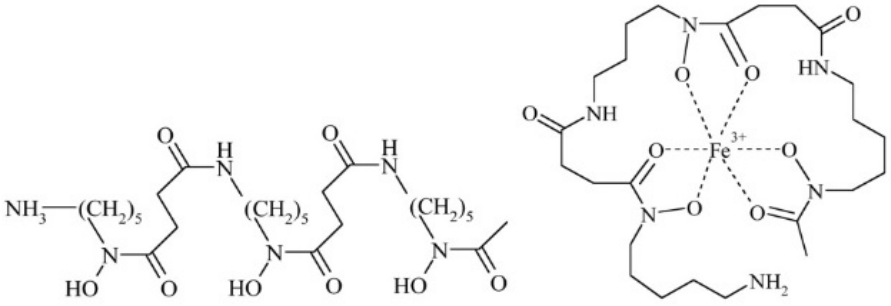

(b) DFO and its iron-complex

Figure 7: Representation of iron-complex involved to promote PpIX accumulation.

The hydroxypyridinone iron chelator CP94 (1,2-diethyl-3-hydroxypyridin-4-one hydrochloride) has been used *in vivo* with human cells [67] or on patients [73]. Comparison studies between CP94+MAL-PDT and MAL-PDT highlighted that use of an iron chelator was useful to obtain PpIX accumulation and caused a better clearance rate as presented in table 2 [71]. DFO was also used, but Curnow et al. have recently reported that CP94 was a more efficient enhancer of PpIX-induced PDT *in vitro* than DFO [1].

It is also important to note that iron has other functions than converting PpIX in heme. Iron is necessary for a number of important cellular functions such as DNA synthesis. Decreasing iron

Table 2: Iron chelators used for enhancing photodynamic therapy.

Type of lesions	Prodrugs	Method	Efficacy	Ref.
Human epidermoid squamous carcinoma cells	CP94	Comparison of MAL-PDT ($500\,\mu molL^{-1}$) and MAL+CP94-PDT ($500\,\mu molL^{-1} + 150\,\mu molL^{-1}$).	Addition of CP94 increased PpIX accumulation. Necrosis increased with MAL+CP94.	[67]
Nodular BCC (nBCC) on 36 human patients	CP94	Topical formulation of 5-ALA (20%) was mixed with an increasing concentration of CP94 (from 0% to 40%) before PDT treatment.	40 % CP94 resulted in significantly greater clearance rates in nBCC than with 5-ALA (20%) alone. There was also no apparent increase in pain during irradiation.	[70]
nBCC on 12 human patients	CP94	Topical formulation of MAL (Metvix® 16%) was mixed with an increasing concentration of CP94 (from O% to 40%) before PDT treatment.	Combining CP94 with MAL is a safe and effective way of increasing the efficacy of MAL-PDT.	[71]
49 patients with superficial or nBCC, BD or AK.	DFO	Topical formulation of 20 % 5-ALA and 3 % DFO.	DFO increased the selectivity of the 5-ALA-induced porphyrin synthesis in neoplastic. Clearance rates were interesting: sBCC (88 %), nBCC (32 %), AK (81 %) and BD (30 %).	[72]

concentration in the cell due to iron-chelators results in antiproliferative effects via inhibition of DNA synthesis. 1,2-diethyl-3-hydroxypyridin-4-one (CP94) can particularly induce these effects due to faster access into intracellular iron pools [71]. Even if CP94 has a proven good efficacy in treatment of skin cancer with PDT, to our knowledge there has been no more clinical trial on patients since 2008.

2.4. Chemical enhancers for PpIX accumulation

Instead of influencing the heme cycle, some chemical products such as methotrexate (MTX), 5-fluorouracil (5-FU), and tazarotene (TZ) act directly on the cell process as will be presented in the further paragraphs. They are called differentiation-promoting agents[6]. They can improve PDT due to their selectivity by preferentially enhancing PpIX accumulation in a variety of preneoplastic and neoplastic epithelial cancer cells while causing very little damage to non-cancerous cells. [74].

MTX is an antifolate which inhibits cell proliferation and triggers cellular differentiation. Presence of MTX activates the first apoptosis signal (FAS) which is a receptor on the surface of the cells that leads to programmed cell death [75]. MTX can be used as an oral pretreatment before ALA-PDT as presented in table 3, and it results in the improvement of cell death [76]. Moreover, pretreatment with MTX is selective since the presence of MTX stimulates mitochondrial CPO activity. CPO is particularly present in malignant cells, and its stimulation leads to a hyperproduction of PpIX (Figure 3) [77]. Even if a low dose of methotrexate renders PDT more effective, MTX is a toxic chemical compound with a lot of side effects and contraindications [78]. PDT has to be easy, patient-friendly treatment and use of this chemical enhancer is not fully in agreement with this.

Vitamin D is a differentiation-promoting hormone with six different forms (including cholecalciferol which is present in food, and calcitriol which plays a role in PDT.) The goal of vitamin D in the body is to maintain a normal range of calcium and phosphorus in fluids. Calcitriol is the most potent and active hormonal form of vitamin D that maintains calcium homeostasis by its actions in bones, kidneys, intestines, and parathyroid glands. Calcitriol and its receptor are also present in a wide variety of cells and tissues, including cancer cells. Its goal is to regulate cellular proliferation and differentiation. Concentration of calcitriol in the body is very important

[6]Differentiation-promoting agents stimulate genes, body functions and lead to cellular differentiation. Cancer cells present a less differentiated phenotype and tend to proliferate. Increasing cell differentiation can decrease significantly their proliferative ability.

Table 3: Combination of a differentiation-promoting agent with PDT.

Type of lesions	Prodrugs	Method	Efficacy	Ref.
Skin carcinoma cells *in vitro* and *in vivo*. Cultured human cells, normal keratinocytes, and *in vivo* skin tumour models.	MTX	Preincubation with methotrexate for 72 h then incubation with ALA for 4 h.	Intracellular PpIX was increased (2 to 4 fold) in carcinoma cells versus normal keratinocytes. Photodynamic treatment was enhanced by the combined therapy compared with PDT alone. *In vivo*, methotrexate preconditioning enhanced PpIX accumulation in cultures of keratinocytes, skin tumours in mice and human squamous cell tumours implanted in mice.	[76]
Basal cell carcinoma (BCC) and squamous cell carcinoma on mice.	Natural vitamin D (cholecalciferol)	Mice were fed for 10 days with vitamin D or vitamin was applied topically on mice.	Oral Vitamin D improved PpIX accumulation in SCC. Topical application of active vitamin D enhanced PpIX accumulation in BCC in mice.	[79]
Human SCC cell line implanted in a subcutaneous tumour model in nude mice.	Vitamin D (calcitriol)	Systemic calcitriol (0.5 µg/kg to 10 µg/kg daily) was given for 3 days.	Systemically administered vitamin D enhanced PpIX levels in subcutaneous tumours in mice by decreasing FC levels and increasing cell differentiation.	[80]
Actinic keratosis.	5-FU	Patients applied 5-FU cream once daily for 6 days, prior to the PDT treatment visit (Application of MAL for 3 hours then illumination).	PpIX accumulation was higher when the lesions were pretreated with 5-FU. Clinical response measured at 3 months after PDT was better after 5-FU pretreatment.	[81]
24 patients with AKs on the hands.	5-FU	Lesions were pretreated for seven days twice daily with 5-FU before daylight-PDT.	Response rate was higher for the combination of 5-FU and daylight-PDT (63 %) than for daylight-PDT alone (52 %).	[82]

since at a concentration smaller than nanomolar, it promotes cell proliferation whereas at higher concentrations it inhibits proliferation. Also, whatever the concentration, cell differentiation still occurs [83]. Anand et al. [84] showed that coproporphyrinogen oxidase and ferrochelatase were increased and decreased respectively after vitamin D pretreatment (oral administration) which promoted formation of PpIX and inhibited its transformation into heme (Figure 3). Calcitriol pretreatment caused a marked increase in PpIX accumulation in the tumour site. Yet, pretreatment with vitamin D induced a small increase (2-fold) in tumour necrotic factor (TNF) and after PDT-irradiation TNF levels were highly elevated (70 fold above baseline). High TNF levels promoted an activation of the extrinsic apoptotic pathway, and enhanced 5-ALA-PDT-mediated cell death. In addition, markers of cellular differentiation and proliferation were increased (4-6 folds) in tumours compared to normal skin. Tumours cell proliferation might be more susceptible to PDT in the presence of vitamin D [85], but it could be a problem if some cells are not destroyed by the 5-ALA-PDT-treatment and continue to proliferate after [83]. Nevertheless, some studies have been conducted on cell cultures [86, 87] and principally on small animals. They are presented in table 3. Despite some disadvantages such as hyper proliferation or hypercalcemia, some clinical trials are under investigation in order to establish whether oral Vitamin D/5-ALA-PDT is an interested innovative combination therapy for 50 patients with BCC skin cancer. (NCT03483441 or NCT03467789)

Contrary to MTX, 5-fluorouracil (5-FU) is FDA-approved and can be used topically. 5-FU is a drug developed in the 1960s and has been widely used alone especially for dermatology and skin cancer as a neoadjuvant[7] cream [74, 88]. Logically, 5-FU can be used in PDT. 5-FU is able to rapidly enter the cell and is converted to several active metabolites. One metabolite is a thymidylate synthase inhibitor that interrupts the synthesis of pyrimidine thymidine, which is a nucleoside required for DNA replication [89]. Lack of pyrimidine thymidine causes growth arrest and apoptosis. In addition, upregulation of coproporphyrinogen oxidase and downregulation of ferrochelatase were observed and lead to PpIX accumulation [88]. Combination of 5-FU with PDT has been extensively studied and is an effective method to improve clearance rate as presented with some examples in table 3. 5-FU seems to be a good candidate and its combination with PDT improve treatment outcome. Contrary to MTX and calcitriol, 5-FU does not present huge disadvantages except that sometimes severe inflammatory and erosive reactions can appear

[7] 5-FU is used as a neoadjuvant in order to reduce tumour size (dermabrasion effect) before treatment that could be surgery, radiotherapy or photodynamic therapy.

[90].

Retinoid prodrugs are also used prior to PDT. Tazarotene (TZ) is part of the acetylenic class of retinoids and is known to be converted by deesterification in cognate carboxylic acid that is its active form. Then it is able to disrupt gene expression, modify cell differentiation, and modulate cell proliferation or hyperplasia [91]. TZ on human BCC cells has shown an activation of caspases[8] due to reactive oxygen species. In parallel, a decrease of anti-apoptosis proteins and cell cycle arrest have also been detected. These observations contributed to apoptosis of human BCC cells [92]. Use of TZ alone on 109 patients suffering of sBCC or nBCC was effective with regression of tumour size (up to 50 %) which was possibly due to antiproliferative and proaptotic actions [93]. So TZ has a metabolic effect and a dermabrasion effect too. These previous clinical studies show favorable clinical outcomes and the production of reactive oxygen species lead researchers to believe that TZ administration prior to PDT might enhance lesion clearance rate. Galitzer [94] conducted a clinical study on 10 patients with at least 4 AK lesions. The pretreatment consisted of applying TZ gel 0.1 % twice daily on lesions one week before 5-ALA-PDT. Eight weeks after 5-ALA-PDT treatment, more subjects (8 vs. 3) achieved higher clearance rate (lesion count reduction $\geq 50\%$) in the TZ pretreatment than in the control group. These results suggest a slight tendancy toward enhancement of 5-ALA-PDT outcome when lesions were pretreated with TZ [94]. Oral retinoid delivery prior to PDT has been investigated as well. A daily dose of 0.5 mg/kg of etretinate during 2 months led to thinner and less keratotic tumours that allowed a better 5-ALA penetration and a potential increase of PpIX [95]. As the other alternatives proposed for pretreatments, tazarotene has also side-effects and may increase erythema, dry skin, burning, craking of skin, or itchiness [91].

3. Physical methods

Physical pretreatments of the skin help the penetration of the photosentizing agent and then promote better outcomes for treatment of skin cancers with PDT. Several techniques will be presented and each affects the skin barrier differently. Holes can be created with a laser or microneedles, or SC removal can take place with curettage or microdermabrasion. Temperature modification or application of a voltage gradient on the skin can also increase skin permeability and enhance drug penetration [22].

[8] Caspases are enzymes responsible of apoptosis and necrosis.

3.1. Skin puncture

Ablative fractional laser (AFL). This technique affects the skin barrier as presented in figure 8a. The laser beam strikes the skin surface and creates vertical, ablated channels by vaporizing a small column of tissue. [96]. The depth of the microchannels created can be controlled by changing the laser energy. When the energy was between 32 mJ and 380 mJ, microchannels depth was between 300 µm and 2100 µm (Figure 8b) [97].

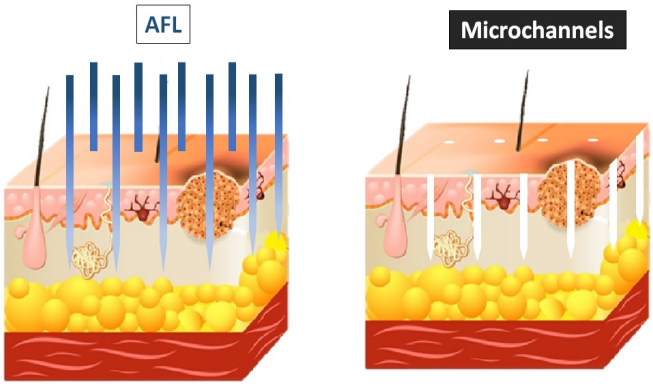

(a) Skin was pulverized and microchannels were created where AFL was applied.

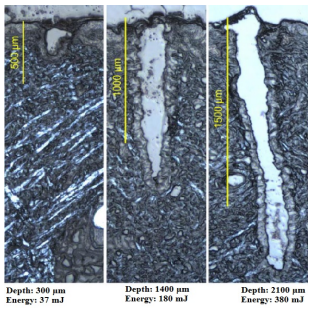

(b) The depth of microchannels created with ablative fractional laser (AFL) depends on laser energy. Vertical section of frozen biopsies [97].

Figure 8: Principle and results of AFL on skin tissues.

Lasers with wavelenght in the far infrared spectrum are particularly used since they are strongly absorbed by tissue water (human skin is composed of 70 % by water) [98–100]. Their use started around 2007 [101] and three groups of AFL are currently used: CO_2-laser (10 600 nm), Er:YAG-laser (Erbium yttrium aluminium garnet, 2940 nm), and Er:YSSG-laser (Yttrium scandium gallium garnet, 2790 nm).

The creation of vertical micropores facilitates the photosensitizing agent uptake and may improve PDT efficacy [102]. Moreover, modification of the skin barrier increases drug delivery and then could decrease the incubation time and gives similar treatment efficacy as compared to conventional PDT [103]. Because drug penetration is enhanced, PpIX fluorescence is more intense and is more homogeneous in deeper skin regions[103]. The fluorescence intensities could be controlled by choosing an adequate laser density [104]. The combination of skin pretreatment with AFL followed by PDT has been studied in clinical trial and some results are presented in table 4.

Althought AFL seems to be a reliable and effective method, it remains an ablative method and is aggresive. Therefore it presents a high risk of potential skin damage with scarring, discoloration and skin infection [101]. In addition, the device is large and costly which make its use quite restrictive and not allowed in all medical facilities.

Microneedles (MNs). Needles and especially microneedles represent a unique technological approach to enhance drug permeation through the *stratum corneum*. In fact, it is not necessary to use needles with large dimensions because drugs to deliver have micro size [105]. Microneedle (MN) have been developed with lengths inferior to 900 µm which could limit pain because they do not penetrate in deep vascular and nervous regions [106]. Due to their micro size MN cannot be seen by patients and reduce needle phobia [107]. The small length improves patient compliance and safety because length is adequate enough to successfully reach the dermal layers without inducing bleeding and touching active immune cells. Design of MNs with special materials can have strong mechanical properties to enable disruption and penetration through the *stratum corneum*. Moreover they can exist in a few shapes: tetrahedron [108], pyramidal, conical [109], beveled tip, or tapered cone [110] which promote different insertion pathways and permeation in the skin [111]. So hydrophilic or high molecular weight drugs can be diffused in skin tissues [112]. There are four types of MNs : solid, coated, hollow and dissolving MNs [113, 114] and they can be assembled as a roller (Figure 9a) [115] or as low cost patches (Schema 9b). These noninvasive transdermal patches can be used easily by anyone [111] and make skin pretreatment rapid.

Solid MNs have been commonly used for skin pretreatment before conventional PDT. They improve the cutaneous delivery of 5-ALA or MAL [106], and could reduce incubation time about 20 min [117]. Some clinical studies are presented in table 4. 5-ALA-coated MNs have also been studied on mouse skin tumour model. An higher formation of PpIX ($\times 3.2$) and PpIX in deeper

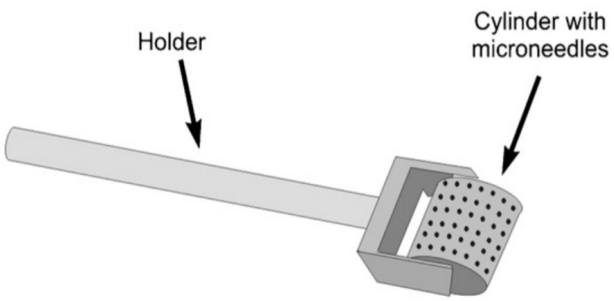

(a) Schematic presentation of a Dermaroller® [116]

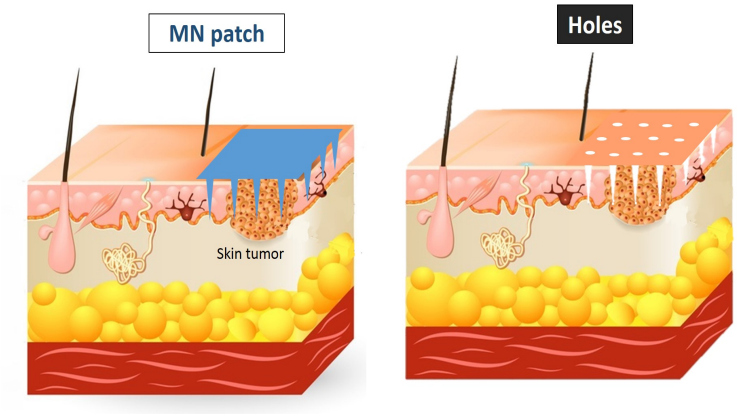

(b) Microneedles patch is applied on skin thanks to finger pressure then is removed and creates holes in the skin.

Figure 9: Microneedles systems to create holes in the skin.

skin regions (480 µm vs 150 µm) were observed with coated MNs compared to topical application [16]. To our knowledge hollow MNs and dissolvable MNs have not been part of clinical or preclinical studies yet.

MNs promote good PDT-outcome for actinic keratosis and have also good cosmetic outcome since they create small holes that stimulate collagen and elastin production [118, 119]. They also up regulate the expression of genes which promote extracellular matrix production and remodeling [28, 120]. Although MN have displayed promising results (Table 4), their use for the treatment of basal cell carcinoma (BCC) or squamous cell carcinoma (SCC) have not been investigated yet.

Table 4: Clinical trials with skin pretreatments creating holes before PDT.

Type of lesions	Physical pretreatment	Method	Efficacy	Ref.
AKs on the face (20 patients).	CO_2-laser	Comparaison between no skin pretreatment and pretreatment with CO_2-laser. Each arm was followed with 15 min or 30 min ALA incubation (20% Levulan® cream).	Clearance rates at 8 weeks after ALA PDT and 30 minutes incubation were 90 % with CO_2-laser and 71 % without CO_2-laser. Same tendancy was observed after 15-minutes incubation (86 % vs 69 %).	[121]
Facial nBCC (32 patients).	CO_2-laser	Tumours were debulked and patients were randomized to either AFL-PDT or PDT. CO_2-laser treatment was applied at 5 % density which corresponds to producing channels with an ablation depth up to 1000 µm and spaced 410 µm apart. MAL (16% Metvix® cream) was applied for 3 h and then lesions were illuminated.	Clearance rates at 3 months were 100 % for AFL-PDT and 88 % for PDT. Long-term efficacy (1 year) was similar after PDT and AFL-PDT with a trend for a favourable short-term cure rate after AFL-PDT.	[122]
Thin nBCC (39 patients).	Er:YAG	Randomized comparison between AFL-PDT and conventional MAL-PDT with 16% Metvix® cream.	Clearance rates at 3 months were 84 % for AFL-PDT and 50 % for MAL-PDT. AFL-PDT and MAL-PDT did not differ significantly with respect to cosmetic outcomes or safety.	[123]
Grade I and II AKs (10 patients).	Stainless steel MN roller (1500 µm)	MAL-PDT (gentle curettage, 16% Metvix® cream ($\approx$ 1 g), incubation time, light) or MN-PDT (16% Metvix® cream ($\approx$ 1 g), MN roller passing 7 or 8 times, incubation time, light).	Clearance rate was 88.3%, with no difference between the two arms. Loss of side-effects and good cosmetics outcomes were noted in case of MN-PDT. Pain was more pronounced with MN-PDT than conventional PDT.	[124]
Grade II AKs (33 patients).	Steel MN roller (200 µm)	Two pretreatments: microneedle roller or sham roller administration prior to 5-ALA application (20% Levulan® cream). Two incubation times : 10 min or 20 min .	AK clearance rate was better with MN pretreatment after 20 min incubation (74 % vs 58 % with sham roller). For the 10 min incubation time, clearance rate was not significantly different between the two pretreatments.	[115]

3.2. Stratum corneum removal

Removal of *stratum corneum* (SC) can be done by abrasion, curettage, debulking, or tape stripping. In each technique the objective is to disrupt or reduce thickness of the SC by removing hyperkeratosis layers. [69, 125]

Curettage. It consists of using a sharp curette ring to remove hard keratotic tissue. To minimize the possibility of recurrences, the practician needs to remove 5 mm of the surrounding tissue with normal appearance [125]. This technique has been recommended for skin preparation since it delineates well the tumour [126], it is effective, acceptable, and quite inexpensive [127]. This gentle removal is often used for superficial basal cell carcinoma (sBCC) treatment and consists of scraping crust and scale [128]. Curettage increased PpIX fluorescence [129] and according to Soler et al. [130] MAL-PDT with prior curettage was a promising method for the treatment of BCC with a clearance rate of 91 % for sBCC (131 lesions treated), 93 % for thin nBCC (82 lesions) and 86 % for thick nBCC (86 lesions treated). Cosmetic outcomes were excellent (i.e lesion area not visible) and recurrence rate after ALA-PDT with prior curettage was low which make it a good skin pretreatment method [126, 130]. Nevertheless some authors report that curettage may damage surrounding healthy tissue and cause pain for patients [126, 129].

Abrasion. This technique also called microabrasion uses a pad made of aluminium oxide crystals [127, 131]. When a pressure is exerted, it will remove hyperkeratosis layers, crusts and the *stratum corneum* (SC) in order to improve transdermal skin delivery of 5-ALA or MAL cream [125]. This technique has proved to enhance absorption of 5-ALA. The method could avoid the use of high drug concentration, and reduce incubation times from hours to minutes. Those evolutions may enhance the efficacy of PDT [132].

Debulking. It is a surgical act used when the lesions are large. It consists of reducing as much as possible the bulk of the tumour. This technique is often used for thicker lesions such as nBCC [125]. After this partial removal it is necessary to treat the edge with PDT. Three weeks before 5-ALA-PDT, Thissen et al. [133] had chosen to debulk nBCCs (24) on 23 patients. 92 % of the nBCC showed a complete response on clinical and histopathological examination with excellent cosmetic outcomes and no serious side effects. nBCC are difficult to treat with only PDT since either photosensitizer or light cannot penetrate deep enough. Debulking could be used prior to PDT to enhance clinical response [133].

Tape stripping. It can be used for the treatment of AK on the lips and in the preparation of large skin areas. Tape is applied onto the skin lesions and is then pulled off sharply which can reduce uniformaly SC by 30 % [125, 134]. This technique does not require effort, is inexpensive, safe, and minimally invasive.

3.3. Other methods

Temperature. Hyperthermia consists of elevating temperature in a body region. Contrary to the previous physical techniques presented in this review, this method is known to be slightly invasive and without large side effects [135]. Historically (5000 years ago) this technique was used to treat diseases or to cauterize tumours by using a metal heated stick. With the evolution of medicine and emergence of precise surgery, radiotherapy, chemotherapy, *etc.* this technique was put aside [136]. Nowadays hyperthermia is experiencing a resurgence and is used as a complement to standard cancer treatments, and is particularly combined with PDT for skin cancer treatment.

Increase of a temperature to a body area can lead to cell alteration. Protein and DNA synthesis can be disrupted or inactivated. The cell membrane can be destabilized which causes a burst release of chemicals in the intracellular structures. Inhibition of cell proliferation could occur which inactivates the development of cancer cells [135, 136].

Elevating temperature may also enhance PDT. First, an increase of temperature led to an improved penetration of 5-ALA in mice skin [137]. Secondly, conversion of 5-ALA to PpIX was higher when the skin was heated during 5-ALA incubation. Increase of PpIX level was detected when temperature was elevated. After 4 hours, the fluorescence ratio (between the mean of PpIX fluorescence and autofluorescence) was equal to 1, 2, 7 when the temperature was respectively 26 °C, 28.6 °C, and 40.8 °C. Like many metabolic pathways in the body and according to the Arrhenius law, the conversion of ALA is modulated by temperature [137, 138]. This large amount of PpIX led to an elevation of the photobleaching rate in human cells during light exposure [139]. Thirdly, 5-ALA uptake in cells was better when the skin was warmed due to a disruption is the cell membrane [140, 141]. Finally, increasing temperature led to the vasodilation of skin vessels which increased the amount of oxygen in the skin. Photodynamic therapy (PDT) generates singlet oxygen to kill cancerous cells. The more oxygen, the higher chances of inducing cell death. An increase of apoptotic cell death was observed due to an increased of superoxide singulet oxygen during a thermal PDT on *in vitro* human skin fibroblasts [142].

All the above reasons cause an increase in PDT efficiency when combined with thermal treatment as long as the temperature is well controlled to prevent damage to surrounding tissues

[140]. Willey et al. tried thermal-PDT on 18 patients suffering of AK on the extremities (head, fingers, toes). Warming the skin during 5-ALA incubation was well tolerated, did not create side effects, improved PDT efficacy even at one year follow-up with a medium clearance rate of 90 % [138, 143].

While highly increased temperature treatments have been effective other studies have indicated that temperatures greater than 10 °C can be used effectively in PDT [144, 145]. This necessity has been showed during daylight PDT treatment which consists in not using a laser with a special wavelength that could be costly or painfull but rather using the sunlight which allows to excitate PpIX continuously [146]. Daylight MAL-PDT (Metvix® cream) is starting to be used for actinic keratosis and displays good clearance rate after three months, 77 % when sun-exposed 244 min (30 patients) [147] or 77 % when sun-exposed 150 min (120 patients) [148]. Daylight MAL-PDT is a convenient and effective treatment but presents some disadvantages since its arrangement is dependant on weather and especially on temperature. This treatment could be difficult to perform in northern countries [149] contrary to southern countries [150].

Iontophoresis. Iontophoresis is a method to improve transdermal drug delivery and is based on the use of a voltage gradient applied to an electrolytic formulation, using a positive (anode) and a negative (cathode) electrode on the skin (Figure 10) [151]. This technique is known to facilitate the transport of ionic species. In addition, drugs transport should be well controlled since drugs should cross the SC, and reach the viable epidermis in the desired amounts but not enter into the circulatory system. [152]

Two mechanisms are involved for 5-ALA penetration and are dependent on pH. At physiological pH ($pH \approx 7$) 5-ALA is a zwitterion and its transport into skin layers is due to electroosmosis. At acidic $pH = 4$, the acidic groups of 5-ALA are ionized and the transport is linked to electromigration because 5-ALA has greater cationic character [152, 153].

Iontophoresis on skin excised from porcine ears showed that 5-ALA was delivered in higher concentrations (6 fold) than with a conventional topical application [153, 154]. This technique should also reduce the incubation time before PDT treatment. Therapeutic levels of PpIX in *ex vivo* human *stratum corneum* were achieved faster with the use of iontophoresis than without [152]. After 10 min iontophoresis with a 2 % 5-ALA solution, an amount of 0.065 µmol/cm^2 was transported across the SC whereas the same amount was obtained by passive topical diffusion after 6.5 h with a 20 % 5-ALA solution [155].

Clinical trials on human patients with the comparaison of iontophoresis and no pretreatment

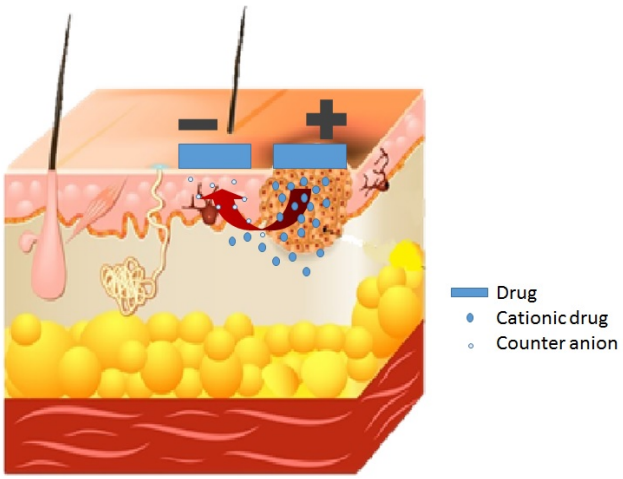

Figure 10: Transport of ionic drug through the skin thanks to iontophoresis.

prior to 5-ALA-PDT were not extensively investigated on skin cancers. One study was conducted by Omi et al. [156] on 5 patients suffering from solar keratosis lesions and Bowen disease showed a PpIX production after delivery of 5-ALA by iontophoresis. One or two weeks after PDT treatment, histological examinations confirmed the complete dissaperance of tumour cells [156]. Although iontophoresis-PDT is not usually compared to conventional PDT, this is a technique that could be combined with PDT. For example, iontophoresis-assisted AFL prior to PDT on 41 patients suffering of AK has been compared to AFL-PDT. Group A received iontophoresis-assisted AFL-PDT with a two hour incubation time. Group B and group C received AFL-PDT two or three hours incubation time, respectively. After 12 months, complete response rate was evaluated to be 83%, 66%, and 86% for group A, group B and group C, respectively. These results proved that the adding of iontophoresis in the clinical protocol is effective and reduces the incubation time by one hour [157].

Iontophoresis's advantages are numerous. This is a non-invasive technique that keeps the skin intact, controls and targets drug delivery. These points and the previous investigations should motivate researchers to use this technique in clinical trials more frequently. However, special attention should be taken to ensure drug accumulation in the tumour without entering the systemic circulation which can cause side effects. [152]

4. Conclusion

Skin cancers are the most common malignancy of humans and particularly for caucasians with an increasing incidence rate. According to the World Health Organization, between 2 and 3 million cases of non melanoma skin cancers are diagnosed each year in the world. PDT appears to be a safe treatment, simple to set up, efficient, and favorable cosmetic outcomes which could make PDT a routine technique widely used in the world. Unfortunately, a lack of 5-ALA penetration through the skin has been observed during the treatment and reduces PDT benefits. Throughout the last decade, it has been proven with the above mentioned studies that drug chemical modification or skin pretreatment may optimize the efficacy of PDT by allowing better drug penetration and better PpIX metabolisation. Despite of the presented studies not having been conducted in large randomized clinical trials, the results up till now are promising. These new perspectives may allow better patient compliance by reducing drug incubation period and better clearance rates.

Among all these techniques some of them seem to be very promising since they present good efficiency with encouraging risk-benefit balance and they can be easily implemented. For instance, the application of TZ cream prior to PDT could be performed by the patient itself. Adjusting the temperature may also be easily performed during PDT treatment and does not present adverse side effects. The use of microneedles to create holes in the SC could be done rapidly prior to PDT, it is painless and allow sa more rapid and efficient treatment. In the future, it would be also interesting to combine different pretreatments (like pairing iontophoresis-assisted AFL prior to PDT as presented in the above results) to evaluate if there is synergy between them. It would be also possible to create heated microneedles that could deliver 5-ALA or a dermoabrasive and dissolvable patch containing an iron chelator and the prodrug. A lot of pretreatment combinations may be imagined, but to be routinely used in hospitals clinician standardized PDT protocols are needed. These new and future protocols should be largely and randomly tested to evaluate which is the most safe, effective, easily to perform, and less costly. Bibliometric analysis and clinical trials still under investigation show an increasing interest of researchers to improve conventional PDT for skin cancers and in the next years the previous difficulties encountered may disappear and be replaced by a better, complete, and simple PDT protocol that could be standardized and used all over the world.

Acknowledgements

This project is supported by the European Union – European Regional Development Fund. LETI/DTBS is supported by the French National Research Agency in the framework of the "Investissement d'avenir" program Glyco@Alps (ANR-15-IDEX-02) and Arcane Labex (ANR-12-LABX-003).

References

[1] A. Curnow, M. Aj, Enhancing Protoporphyrin IX induced Photodynamic Therapy with a Topical Iron Chelating Agent in a Normal Skin Model, Journal of Heavy Metal Toxicity and Diseases 1 (2016). doi:10.21767/2473-6457.100002.

[2] M. D. Daniell, J. S. Hill, A history of photodynamic therapy, Australian and New Zealand Journal of Surgery 61 (1991) 340–348.

[3] P. Agostinis, K. Berg, K. A. Cengel, T. H. Foster, A. W. Girotti, S. O. Gollnick, S. M. Hahn, M. R. Hamblin, A. Juzeniene, D. Kessel, M. Korbelik, J. Moan, P. Mroz, D. Nowis, J. Piette, B. C. Wilson, J. Golab, Photodynamic therapy of cancer: An update, CA: A Cancer Journal for Clinicians 61 (2011) 250–281. doi:10.3322/caac.20114.

[4] N. Basset-Seguin, La photothérapie dynamique en dermatologie: Place actuelle et perspectives, in: Annales de Dermatologie et de Vénéréologie, volume 133, Elsevier Masson, 2006, pp. 421–423.

[5] C. Robertson, D. H. Evans, H. Abrahamse, Photodynamic therapy (PDT): A short review on cellular mechanisms and cancer research applications for PDT, Journal of Photochemistry and Photobiology B: Biology 96 (2009) 1–8. doi:10.1016/j.jphotobiol.2009.04.001.

[6] T. J. Dougherty, Photosensitizers: Therapy and detection of malignant tumors, Photochemistry and Photobiology 45 (1987) 879–889.

[7] A. P. Castano, T. N. Demidova, M. R. Hamblin, Mechanisms in photodynamic therapy: Part one—photosensitizers, photochemistry and cellular localization, Photodiagnosis and Photodynamic Therapy 1 (2004) 279–293. doi:10.1016/S1572-1000(05)00007-4.

[8] J. C. Kennedy, S. L. Marcus, R. H. Pottier, Photodynamic therapy (PDT) and photodiagnosis (PD) using endogenous photosensitization induced by 5-aminolevulinic acid (ALA): Mechanisms and clinical results, Journal of clinical laser medicine & surgery 14 (1996) 289–304.

[9] X. Yang, P. Palasuberniam, D. Kraus, B. Chen, Aminolevulinic Acid-Based Tumor Detection and Therapy: Molecular Mechanisms and Strategies for Enhancement, International Journal of Molecular Sciences 16 (2015) 25865–25880. doi:10.3390/ijms161025865.

[10] A. L. Golub, E. G. Dickson, J. C. Kennedy, S. L. Marcus, Y. Park, R. H. Pottier, The monitoring of ALA-induced protoporphyrin IX accumulation and clearance in patients with skin lesions by in vivo surface-detected fluorescence spectroscopy, Lasers in medical science 14 (1999) 112–122.

[11] T. Smits, C. A. Robles, P. E. van Erp, P. C. van de Kerkhof, M.-J. P. Gerritsen, Correlation between macroscopic fluorescence and protoporphyrin IX content in psoriasis and actinic keratosis following application of aminolevulinic acid, Journal of investigative dermatology 125 (2005) 833–839.

[12] A. Westers-Attema, B. G. Lohman, F. van den Heijkant, P. J. Nelemans, V. J. Winnepenninckx, N. W. Kelleners-Smeets, K. Mosterd, Photodynamic Therapy in Bowen's Disease: Influence of Histological Features and Clinical Characteristics on Its Success, Dermatology 230 (2015) 55–61. doi:10.1159/000366500.

[13] M. Ericson, C. Sandberg, B. Stenquist, F. Gudmundson, M. Karlsson, A.-M. Ros, A. Rosen, O. Larko, A.-M. Wennberg, I. Rosdahl, Photodynamic therapy of actinic keratosis at varying fluence rates: Assessment of photobleaching, pain and primary clinical outcome, British Journal of Dermatology 151 (2004) 1204–1212. doi:10.1111/j.1365-2133.2004.06211.x.

[14] C. Sandberg, B. Stenquist, I. Rosdahl, A.-M. Ros, I. Synnerstad, M. Karlsson, F. Gudmundson, M. B. Ericson, O. Larkö, A.-M. Wennberg, Important factors for pain during photodynamic therapy for actinic keratosis, Acta dermato-venereologica 86 (2006) 404–408.

[15] R.-M. Szeimies, P. Calzavara-Pinton, S. Karrer, B. Ortel, M. Landthaler, Topical photodynamic therapy in dermatology, Journal of Photochemistry and Photobiology B: Biology 36 (1996) 213–219.

[16] A. K. Jain, C. H. Lee, H. S. Gill, 5-Aminolevulinic acid coated microneedles for photodynamic therapy of skin tumors, Journal of Controlled Release 239 (2016) 72–81. doi:10.1016/j.jconrel.2016.08.015.

[17] A. Juzeniene, P. Juzenas, L.-W. Ma, V. Iani, J. Moan, Topical application of 5-aminolaevulinic acid, methyl 5-aminolaevulinate and hexyl 5-aminolaevulinate on normal human skin, British Journal of Dermatology 155 (2006) 791–799. doi:10.1111/j.1365-2133.2006.07484.x.

[18] S. Berrahmoune, N. Fotinos, L. Bezdetnaya, N. Lange, J. C. Guedenet, F. Guillemin, M. A. D'Hallewin, Analysis of differential PDT effect in rat bladder tumor models according to concentrations of intravesical hexyl-aminolevulinate, Photochemical & Photobiological Sciences 7 (2008) 1018. doi:10.1039/b804921a.

[19] L. Brancaleon, S. W. Magennis, I. D. Samuel, E. Namdas, A. Lesar, H. Moseley, Characterization of the photoproducts of protoporphyrin IX bound to human serum albumin and immunoglobulin G, Biophysical Chemistry 109 (2004) 351–360. doi:10.1016/j.bpc.2003.12.008.

[20] L. Schmitz, B. Novak, A.-K. Hoeh, H. Luebbert, T. Dirschka, Epidermal penetration and protoporphyrin IX formation of two different 5-aminolevulinic acid formulations in ex vivo human skin, Photodiagnosis and Photodynamic Therapy 14 (2016) 40–46. doi:10.1016/j.pdpdt.2015.11.004.

[21] R. F. Donnelly, D. I. Morrow, P. A. McCarron, A. D. Woolfson, A. Morrissey, P. Juzenas, A. Juzeniene, V. Iani, H. O. McCarthy, J. Moan, Microneedle-mediated intradermal delivery of 5-aminolevulinic acid: Potential for enhanced topical photodynamic therapy, Journal of Controlled Release 129 (2008) 154–162. doi:10.1016/j.jconrel.2008.05.002.

[22] C. Bay, C. M. Lerche, B. Ferrick, P. A. Philipsen, K. Togsverd-Bo, M. Haedersdal, Comparison of Physical Pretreatment Regimens to Enhance Protoporphyrin IX Uptake in Photodynamic Therapy: A Randomized Clinical Trial, JAMA Dermatology 153 (2017) 270. doi:10.1001/jamadermatol.2016.5268.

[23] A. Bunke, O. Zerbe, H. Schmid, G. Burmeister, H. P. Merkle, B. Gander, Degradation mechanism and stability of 5-aminolevulinic acid, Journal of pharmaceutical sciences 89 (2000) 1335–1341.

[24] B. Elfsson, I. Wallin, S. Eksborg, K. Rudaeus, A. M. Ros, H. Ehrsson, Stability of 5-aminolevulinic acid in aqueous solution, European journal of pharmaceutical sciences 7 (1999) 87–91.

[25] A. W. De Blois, R. J. E. Grouls, E. W. Ackerman, W. J. A. Wijdeven, Development of a stable solution of 5-aminolaevulinic acid for intracutaneous injection in photodynamic therapy, Lasers in medical science 17 (2002) 208–215.

[26] M. R. Prausnitz, V. G. Bose, R. Langer, J. C. Weaver, Electroporation of mammalian skin: A mechanism to enhance transdermal drug delivery, Proceedings of the National Academy of Sciences 90 (1993) 10504–10508.

[27] B. W. Barry, Novel mechanisms and devices to enable successful transdermal drug delivery, European journal of pharmaceutical sciences 14 (2001) 101–114.

[28] M.-C. Kearney, S. Brown, M. T. McCrudden, A. J. Brady, R. F. Donnelly, Potential of microneedles in enhancing delivery of photosensitising agents for photodynamic therapy, Photodiagnosis and Photodynamic Therapy 11 (2014) 459–466. doi:10.1016/j.pdpdt.2014.09.003.

[29] F. S. De Rosa, A. C. Tedesco, R. F. V. Lopez, M. B. R. Pierre, N. Lange, J. M. Marchetti, J. C. G. Rotta, M. V. L. B. Bentley, In vitro skin permeation and retention of 5-aminolevulinic acid ester derivatives for photodynamic therapy, Journal of controlled release 89 (2003) 261–269.

[30] R. Lopez, Photodynamic therapy of skin cancer: Controlled drug delivery of 5-ALA and its esters, Advanced Drug Delivery Reviews 56 (2004) 77–94. doi:10.1016/j.addr.2003.09.002.

[31] R. M. Valentine, S. H. Ibbotson, C. T. A. Brown, K. Wood, H. Moseley, A Quantitative Comparison of 5-Aminolaevulinic Acid- and Methyl Aminolevulinate-Induced Fluorescence, Photobleaching and Pain During Photodynamic Therapy: Photochemistry and Photobiology, Photochemistry and Photobiology 87 (2011) 242–249. doi:10.1111/j.1751-1097.2010.00829.x.

[32] F. Moloney, P. Collins, Randomized, double-blind, prospective study to compare topical 5-aminolaevulinic acid methylester with topical 5-aminolaevulinic acid photodynamic ther-

apy for extensive scalp actinic keratosis, British Journal of Dermatology 157 (2007) 87–91. doi:10.1111/j.1365-2133.2007.07946.x.

[33] A. Winkler, C. Mullergoymann, The influence of topical formulations on the permeation of 5-aminolevulinic acid and its -butyl ester through excised human stratum corneum, European Journal of Pharmaceutics and Biopharmaceutics 60 (2005) 427–437. doi:10.1016/j.ejpb.2005.01.014.

[34] A. Winkler, C. C. Müller-Goymann, Comparative permeation studies for 5-aminolevulinic acid and its n-butyl ester through stratum corneum and artificial skin constructs, European journal of pharmaceutics and biopharmaceutics 53 (2002) 281–287.

[35] N. Neittaanmaki-Perttu, M. Gronroos, T. Karppinen, T. Tani, E. Snellman, Hexyl-5-aminolaevulinate 0.2% vs. methyl-5-aminolaevulinate 16% daylight photodynamic therapy for treatment of actinic keratoses: Results of a randomized double-blinded pilot trial, British Journal of Dermatology 174 (2016) 427–429. doi:10.1111/bjd.13924.

[36] M. H. Gold, Therapeutic and Aesthetic Uses of Photodynamic Therapy Part five of a five-part series: ALA–PDT and MAL–PDT What Makes Them Different, The Journal of clinical and aesthetic dermatology 2 (2009) 44.

[37] J. Lin, M. T. Wan, Current evidence and applications of photodynamic therapy in dermatology, Clinical, Cosmetic and Investigational Dermatology (2014) 145. doi:10.2147/CCID.S35334.

[38] G. F. Gola, G. M. Di Venosa, D. A. Sáenz, G. H. Calvo, G. M. Cabrera, A. G. Casas, J. A. Ramírez, Synthesis of chemically diverse esters of 5-aminolevulinic acid for photodynamic therapy via the multicomponent Passerini reaction, RSC Advances 6 (2016) 89492–89498. doi:10.1039/C6RA15832C.

[39] W. Zhu, Y.-H. Gao, C.-H. Song, Z.-B. Lu, T. Namulinda, Y.-P. Han, Y.-J. Yan, L.-X. Wang, Z.-L. Chen, Synthesis and evaluation of new 5-aminolevulinic acid derivatives as prodrugs of protoporphyrin for photodynamic therapy, Photochemical & Photobiological Sciences 16 (2017) 1623–1630. doi:10.1039/C7PP00203C.

[40] J. Kloek, G. M. Beijersbergen van Henegouwen, Prodrugs of 5-Aminolevullinic Acid for Photodynamic Therapy, Photochemistry and photobiology 64 (1996) 994–1000.

[41] M.-A. Bolzinger, S. Briançon, Y. CHEVALIER, P. François, Formulation des systèmes pâteux ou préparations semi-solides (2015).

[42] L. Buhse, R. Kolinski, B. Westenberger, A. Wokovich, J. Spencer, C. W. Chen, S. Turujman, M. Gautam-Basak, G. J. Kang, A. Kibbe, B. Heintzelman, E. Wolfgang, Topical drug classification, International Journal of Pharmaceutics 295 (2005) 101–112. doi:10.1016/j.ijpharm.2005.01.032.

[43] L. Risaliti, V. Piazzini, M. G. Di Marzo, L. Brunetti, R. Cecchi, P. Lencioni, A. R. Bilia, M. C. Bergonzi, Topical formulations of delta-aminolevulinic acid for the treatment of actinic keratosis: Characterization and efficacy evaluation, European Journal of Pharmaceutical Sciences 115 (2018) 345–351. doi:10.1016/j.ejps.2018.01.045.

[44] R. F. Donnelly, P. A. McCarron, A. D. Woolfson, Drug Delivery of Aminolevulinic Acid from Topical Formulations Intended for Photodynamic Therapy, Photochemistry and Photobiology (2005) 750–767.

[45] E. Jeffes, Levulan ® : The first approved topical photosensitizer for the treatment of actinic keratosis, Journal of Dermatological Treatment 13 (2002) s19–s23. doi:10.1080/095466302317414663.

[46] C. A. Morton, Methyl aminolevulinate (Metvix®) photodynamic therapy-practical pearls, Journal of dermatological treatment 14 (2003) 23–26.

[47] K. Lang, K. W. Schulte, T. Ruzicka, Aminolevulinic acid (Levulan®) in photodynamic therapy of actinic keratoses, Clinical Trials 432 (2001) 18.

[48] C. Valenta, B. Auner, I. Loibl, Skin permeation and stability studies of 5-aminolevulinic acid in a new gel and patch preparation, Journal of Controlled Release 107 (2005) 495–501. doi:10.1016/j.jconrel.2005.07.006.

[49] N. Grüning, C. C. Müller-Goymann, Physicochemical Characterisation of a Novel Thermogelling Formulation for Percutaneous Penetration of 5-Aminolevulinic Acid, Journal of Pharmaceutical Sciences 97 (2008) 2311–2323. doi:10.1002/jps.21157.

[50] T. Maisch, F. Santarelli, S. Schreml, P. Babilas, R.-M. Szeimies, Fluorescence induction of protoporphyrin IX by a new 5-aminolevulinic acid nanoemulsion used for photodynamic therapy in a full-thickness ex vivo skin model: Letter to the Editor, Experimental Dermatology 19 (2009) e302–e305. doi:10.1111/j.1600-0625.2009.01001.x.

[51] R.-M. Szeimies, P. Radny, M. Sebastian, F. Borrosch, T. Dirschka, G. Krähn-Senftleben, K. Reich, G. Pabst, D. Voss, M. Foguet, R. Gahlmann, H. Lübbert, U. Reinhold, Photodynamic therapy with BF-200 ALA for the treatment of actinic keratosis: Results of a prospective, randomized, double-blind, placebo-controlled phase III study: PDT with BF-200 ALA for actinic keratosis, British Journal of Dermatology 163 (2010) 386–394. doi:10.1111/j.1365-2133.2010.09873.x.

[52] T. Dirschka, P. Radny, R. Dominicus, H. Mensing, H. Brüning, L. Jenne, L. Karl, M. Sebastian, C. Oster-Schmidt, W. Klövekorn, Long-term (6 and 12 months) follow-up of two prospective, randomized, controlled phase III trials of photodynamic therapy with BF-200 ALA and methyl aminolaevulinate for the treatment of actinic keratosis, British Journal of Dermatology 168 (2013) 825–836.

[53] P. A. McCarron, R. F. Donnelly, A. Zawislak, A. D. Woolfson, Design and evaluation of a water-soluble bioadhesive patch formulation for cutaneous delivery of 5-aminolevulinic acid to superficial neoplastic lesions, European Journal of Pharmaceutical Sciences 27 (2006) 268–279. doi:10.1016/j.ejps.2005.10.009.

[54] J.-D. Fauteck, G. Ackermann, M. Birkel, M. Breuer, A. C. E. Moor, A. Ebeling, C. Ortland, Fluorescence characteristics and pharmacokinetic properties of a novel self-adhesive 5-ALA patch for photodynamic therapy of actinic keratoses, Archives of Dermatological Research 300 (2008) 53–60. doi:10.1007/s00403-007-0787-0.

[55] A. Hauschild, E. Stockfleth, G. Popp, F. Borrosch, H. Brüning, R. Dominicus, H. Mensing, U. Reinhold, K. Reich, A. Moor, M. Stocker, C. Ortland, M. Brunnert, R.-M. Szeimies, Optimization of photodynamic therapy with a novel self-adhesive 5-aminolaevulinic acid patch: Results of two randomized controlled phase III studies, British Journal of Dermatology 160 (2009) 1066–1074. doi:10.1111/j.1365-2133.2009.09040.x.

[56] F. Kuonen, O. Gaide, Nouvelle lumière sur la thérapie photodynamique cutanée, Revue médical suisse 10 (2014) 754–759.

[57] M. Sechi, V. Sanna, N. Pala, Targeted therapy using nanotechnology: Focus on cancer, International Journal of Nanomedicine (2014) 467. doi:10.2147/IJN.S36654.

[58] L. Shi, X. Wang, F. Zhao, H. Luan, Q. Tu, Z. Huang, H. Wang, H. Wang, In vitro evalua-

tion of 5-aminolevulinic acid (ALA) loaded PLGA nanoparticles, International Journal of Nanomedicine (2013) 2669. doi:10.2147/IJN.S45821.

[59] A. Mira, C. R. Mateo, R. Mallavia, A. Falco, Poly(methyl vinyl ether-alt-maleic acid) and ethyl monoester as building polymers for drug-loadable electrospun nanofibers, Scientific Reports 7 (2017). doi:10.1038/s41598-017-17542-4.

[60] M.-W. Lin, Y.-B. Huang, C.-L. Chen, P.-C. Wu, C.-Y. Chou, P.-C. Wu, S.-Y. Hung, A Formulation Study of 5-Aminolevulinic Encapsulated in DPPC Liposomes in Melanoma Treatment, International Journal of Medical Sciences 13 (2016) 483–489. doi:10.7150/ijms.15411.

[61] N. Dragicevic-Curic, A. Fahr, Liposomes in topical photodynamic therapy, Expert Opinion on Drug Delivery 9 (2012) 1015–1032. doi:10.1517/17425247.2012.697894.

[62] M. Schneider, F. Stracke, S. Hansen, U. F. Schaefer, Nanoparticles and their interactions with the dermal barrier, Dermato-endocrinology 1 (2009) 197–206.

[63] A. J. Plaunt, K. M. Harmatys, K. A. Hendrie, A. J. Musso, B. D. Smith, Chemically triggered release of 5-aminolevulinic acid from liposomes, RSC Adv. 4 (2014) 57983–57990. doi:10.1039/C4RA10340H.

[64] J. An, J.-E. Kim, D.-H. Lee, B. Y. Kim, 0.5% Liposome-encapsulated 5-aminolevulinic acid (ALA) photodynamic therapy for acne treatment, Journal ofJournal of Cosmetic and Laser Therapy, Cosmetic and Laser Therapy, 13 (2011) 28–32. doi:doi:10.3109/14764172.2011.552613.

[65] J. de Leeuw, N. van der Beek, P. Bjerring, H. Martino Neumann, Photodynamic therapy of acne vulgaris using 5-aminolevulinic acid 0.5% liposomal spray and intense pulsed light in combination with topical keratolytic agents, Journal of the European Academy of Dermatology and Venereology 24 (2010) 460–469. doi:10.1111/j.1468-3083.2009.03447.x.

[66] H. Tong, Y. Wang, H. Li, Q. Jin, J. Ji, Dual pH-responsive 5-aminolevulinic acid pseudopolyrotaxane prodrug micelles for enhanced photodynamic therapy, Chemical Communications 52 (2016) 3966–3969. doi:10.1039/C6CC00450D.

[67] Y. Dogra, D. C. Ferguson, N. J. Dodd, G. R. Smerdon, A. Curnow, P. G. Winyard, The hydroxypyridinone iron chelator CP94 increases methyl-aminolevulinate-based photody-

namic cell killing by increasing the generation of reactive oxygen species, Redox Biology 9 (2016) 90–99. doi:10.1016/j.redox.2016.07.002.

[68] D. S. Kalinowski, The Evolution of Iron Chelators for the Treatment of Iron Overload Disease and Cancer, Pharmacological Reviews 57 (2005) 547–583. doi:10.1124/pr.57.4.2.

[69] M. Gerritsen, T. Smits, M. Kleinpenning, P. van de Kerkhof, P. van Erp, Pretreatment to Enhance Protoporphyrin IX Accumulation in Photodynamic Therapy, Dermatology 218 (2009) 193–202. doi:10.1159/000183753.

[70] S. Campbell, C. Morton, R. Alyahya, S. Horton, A. Pye, A. Curnow, Clinical investigation of the novel iron-chelating agent, CP94, to enhance topical photodynamic therapy of nodular basal cell carcinoma, British Journal of Dermatology 159 (2008) 387–393. doi:10.1111/j.1365-2133.2008.08668.x.

[71] A. Pye, S. Campbell, A. Curnow, Enhancement of methyl-aminolevulinate photodynamic therapy by iron chelation with CP94: An in vitro investigation and clinical dose-escalating safety study for the treatment of nodular basal cell carcinoma, Journal of Cancer Research and Clinical Oncology 134 (2008) 841–849. doi:10.1007/s00432-008-0358-6.

[72] S. Fijan, H. Honigsmann, B. Ortel, Photodynamic therapy of epithelial skin tumours using delta-aminolaevulinic acid and desferrioxamine, British Journal of Dermatology 133 (1995) 282–288.

[73] C. Morton, S. Campbell, D. Gould, A. Curnow, Topical photodynamic therapy with the iron chelator, CP94, for nodular basal cell carcinoma., Journal of the American Academy of Dermatology 50 (2004) P120.

[74] E. V. Maytin, S. Anand, C. Wilson, K. Iyer, 5-Fluorouracil as an enhancer of aminolevulinate-based photodynamic therapy for skin cancer: New use for a venerable agent?, 2011, p. 78860K. doi:10.1117/12.874188.

[75] M. Nihal, J. Wu, G. S. Wood, Methotrexate inhibits the viability of human melanoma cell lines and enhances Fas/Fas-ligand expression, apoptosis and response to interferon-alpha: Rationale for its use in combination therapy, Archives of Biochemistry and Biophysics 563 (2014) 101–107. doi:10.1016/j.abb.2014.04.019.

[76] S. Anand, G. Honari, T. Hasan, P. Elson, E. V. Maytin, Low-Dose Methotrexate Enhances Aminolevulinate-Based Photodynamic Therapy in Skin Carcinoma Cells In vitro

and In vivo, Clinical Cancer Research 15 (2009) 3333–3343. doi:10.1158/1078-0432.CCR-08-3054.

[77] I. Postiglione, A. Chiaviello, G. Palumbo, Enhancing Photodynamyc Therapy Efficacy by Combination Therapy: Dated, Current and Oncoming Strategies, Cancers 3 (2011) 2597–2629. doi:10.3390/cancers3022597.

[78] S. Shen, T. O'Brien, L. M. Yap, H. M. Prince, C. J. McCormack, The use of methotrexate in dermatology: A review: Methotrexate in dermatology, Australasian Journal of Dermatology 53 (2012) 1–18. doi:10.1111/j.1440-0960.2011.00839.x.

[79] E. V. Maytin, S. Anand, K. Rollakanti, Clinical potential for vitamin D as a neoadjuvant for photodynamic therapy of nonmelanoma skin cancer, 2015, p. 93080H. doi:10.1117/12.2077234.

[80] E. V. Maytin, S. Anand, N. Atanaskova, C. Wilson, Vitamin D as a potential enhancer of aminolevulinate-based photodynamic therapy for nonmelanoma skin cancer, in: Optical Methods for Tumor Treatment and Detection: Mechanisms and Techniques in Photodynamic Therapy XIX, volume 7551, International Society for Optics and Photonics, 2010, p. 755105.

[81] E. V. Maytin, S. Anand, Combination photodynamic therapy using 5-fluorouracil and aminolevulinate enhances tumor-selective production of protoporphyrin IX and improves treatment efficacy of squamous skin cancers and precancers, 2016, p. 96940E. doi:10.1117/12.2218138.

[82] C. Nissen, I. Heerfordt, S. Wiegell, C. Mikkelsen, H. Wulf, Pretreatment with 5-Fluorouracil Cream Enhances the Efficacy of Daylight-mediated Photodynamic Therapy for Actinic Keratosis, Acta Dermato Venereologica 97 (2017) 617–621. doi:10.2340/00015555-2612.

[83] S. Anand, C. Wilson, T. Hasan, E. V. Maytin, Vitamin D3 Enhances the Apoptotic Response of Epithelial Tumors to Aminolevulinate-Based Photodynamic Therapy, Cancer Research 71 (2011) 6040–6050. doi:10.1158/0008-5472.CAN-11-0805.

[84] S. Anand, K. R. Rollakanti, R. L. Horst, T. Hasan, E. V. Maytin, Combination of Oral Vitamin D3 with Photodynamic Therapy Enhances Tumor Cell Death in a Murine Model of

Cutaneous Squamous Cell Carcinoma, Photochemistry and Photobiology (2014) n/a–n/a. doi:10.1111/php.12286.

[85] L. Wyld, O. Smith, J. Lawry, M. W. R. Reed, N. J. Brown, Cell cycle phase influences tumour cell sensitivity to aminolaevulinic acid-induced photodynamic therapy in vitro, British journal of cancer 78 (1998) 50.

[86] N. Sato, B. W. Moore, S. Keevey, J. A. Drazba, T. Hasan, E. V. Maytin, Vitamin D enhances ALA-induced protoporphyrin IX production and photodynamic cell death in 3-D organotypic cultures of keratinocytes, Journal of Investigative Dermatology 127 (2007) 925–934.

[87] E. Cicarma, M. Tuorkey, A. Juzeniene, L.-W. Ma, J. Moan, Calcitriol treatment improves methyl aminolaevulinate-based photodynamic therapy in human squamous cell carcinoma A431 cells, British Journal of Dermatology 161 (2009) 413–418. doi:10.1111/j.1365-2133.2009.09180.x.

[88] S. Anand, K. R. Rollakanti, N. Brankov, D. E. Brash, T. Hasan, E. V. Maytin, Fluorouracil Enhances Photodynamic Therapy of Squamous Cell Carcinoma via a p53-Independent Mechanism that Increases Protoporphyrin IX levels and Tumor Cell Death, Molecular Cancer Therapeutics 16 (2017) 1092–1101. doi:10.1158/1535-7163.MCT-16-0608.

[89] D. B. Longley, D. P. Harkin, P. G. Johnston, 5-Fluorouracil: Mechanisms of action and clinical strategies, Nature Reviews Cancer 3 (2003) 330–338. doi:10.1038/nrc1074.

[90] C. Berking, A. Hauschild, O. Kölbl, G. Mast, R. Gutzmer, Basal Cell Carcinoma-Treatments for the Commonest Skin Cancer, Deutsches Aerzteblatt Online (2014). doi:10.3238/arztebl.2014.0389.

[91] J. Lanoue, G. Goldenberg, Basal cell carcinoma: A comprehensive review of existing and emerging nonsurgical therapies, The Journal of clinical and aesthetic dermatology 9 (2016) 26.

[92] C.-S. Wu, G.-S. Chen, P.-Y. Lin, I.-H. Pan, S.-T. Wang, S. H. Lin, H.-S. Yu, C.-C. Lin, Tazarotene Induces Apoptosis in Human Basal Cell Carcinoma via Activation of Caspase-8/t-Bid and the Reactive Oxygen Species-Dependent Mitochondrial Pathway, DNA and Cell Biology 33 (2014) 652–666. doi:10.1089/dna.2014.2366.

[93] L. Bianchi, A. Orlandi, E. Campione, C. Angeloni, A. Costanzo, L. Spagnoli, S. Chimenti, Topical treatment of basal cell carcinoma with tazarotene: A clinicopathological study on a large series of cases, British Journal of Dermatology 151 (2004) 148–156. doi:10.1111/j.1365-2133.2004.06044.x.

[94] B. I. Galitzer, Effect of retinoid pretreatment on outcomes of patients treated by photodynamic therapy for actinic keratosis of the hand and forearm, J Drugs Dermatol 10 (2011) 1124–32.

[95] M.-H. Lin, J. Y.-Y. Lee, C.-Y. Ou, T.-W. Wong, Sequential systemic retinoid and photodynamic therapy for multiple keratotic pigmented nodular basal cell carcinomas on the scalp, The Journal of Dermatology 36 (2009) 518–521. doi:10.1111/j.1346-8138.2009.00692.x.

[96] S. Prakash, S. Kumar, Fabrication of microchannels: A review, Proceedings of the Institution of Mechanical Engineers, Part B: Journal of Engineering Manufacture 229 (2015) 1273–1288. doi:10.1177/0954405414535581.

[97] C. S. Haak, W. A. Farinelli, J. Tam, A. G. Doukas, R. R. Anderson, M. Haedersdal, Fractional laser-assisted delivery of methyl aminolevulinate: Impact of laser channel depth and incubation time, Lasers in Surgery and Medicine 44 (2012) 787–795. doi:10.1002/lsm.22102.

[98] M. Haedersdal, F. H. Sakamoto, W. A. Farinelli, A. G. Doukas, J. Tam, R. R. Anderson, Pretreatment with ablative fractional laser changes kinetics and biodistribution of topical 5-aminolevulinic acid (ALA) and methyl aminolevulinate (MAL): PRETREATMENT WITH AFXL CHANGES OF ALA AND MAL, Lasers in Surgery and Medicine 46 (2014) 462–469. doi:10.1002/lsm.22259.

[99] T. Omi, K. Numano, The role of the CO2 laser and fractional CO2 laser in dermatology, Laser therapy 23 (2014) 49–60.

[100] E. H. Taudorf, C. S. Haak, A. M. Erlendsson, P. A. Philipsen, R. R. Anderson, U. Paasch, M. Haedersdal, Fractional ablative erbium YAG laser: Histological characterization of relationships between laser settings and micropore dimensions: FRACTIONAL ABLATIVE ERBIUM YAG LASER, Lasers in Surgery and Medicine 46 (2014) 281–289. doi:10.1002/lsm.22228.

[101] J. Preissig, K. Hamilton, R. Markus, Current Laser Resurfacing Technologies: A Review that Delves Beneath the Surface, Seminars in Plastic Surgery 26 (2012) 109–116. doi:10.1055/s-0032-1329413.

[102] K. Togsverd-Bo, C. Haak, D. Thaysen-Petersen, H. Wulf, R. Anderson, M. Haedesdal, Intensified photodynamic therapy of actinic keratoses with fractional CO2 laser: A randomized clinical trial: Intensified PDT of AK with fractional CO2 laser, British Journal of Dermatology 166 (2012) 1262–1269. doi:10.1111/j.1365-2133.2012.10893.x.

[103] H. S. Song, S.-E. Jung, Y. H. Jang, H. Y. Kang, E.-S. Lee, Y. C. Kim, Fractional carbon dioxide laser-assisted photodynamic therapy for patients with actinic keratosis, Photodermatology, Photoimmunology & Photomedicine 31 (2015) 296–301. doi:10.1111/phpp.12184.

[104] C. Haak, K. Christiansen, A. Erlendsson, E. Taudorf, D. Thaysen-Petersen, H. Wulf, M. Haedersdal, Ablative fractional laser enhances MAL-induced PpIX accumulation: Impact of laser channel density, incubation time and drug concentration, Journal of Photochemistry and Photobiology B: Biology 159 (2016) 42–48. doi:10.1016/j.jphotobiol.2016.03.021.

[105] D. V. McAllister, P. M. Wang, S. P. Davis, J.-H. Park, P. J. Canatella, M. G. Allen, M. R. Prausnitz, Microfabricated needles for transdermal delivery of macromolecules and nanoparticles: Fabrication methods and transport studies, Proceedings of the National Academy of Sciences 100 (2003) 13755–13760.

[106] P. Mikolajewska, R. F. Donnelly, M. J. Garland, D. I. J. Morrow, T. R. R. Singh, V. Iani, J. Moan, A. Juzeniene, Microneedle Pre-treatment of Human Skin Improves 5-Aminolevulininc Acid (ALA)- and 5-Aminolevulinic Acid Methyl Ester (MAL)-Induced PpIX Production for Topical Photodynamic Therapy Without Increase in Pain or Erythema, Pharmaceutical Research 27 (2010) 2213–2220. doi:10.1007/s11095-010-0227-2.

[107] H. S. Gill, D. D. Denson, B. A. Burris, M. R. Prausnitz, Effect of Microneedle Design on Pain in Human Volunteers:, The Clinical Journal of Pain 24 (2008) 585–594. doi:10.1097/AJP.0b013e31816778f9.

[108] T. Miyano, Y. Tobinaga, T. Kanno, Y. Matsuzaki, H. Takeda, M. Wakui, K. Hanada, Sugar

micro needles as transdermic drug delivery system, Biomedical Microdevices 7 (2005) 185–188.

[109] J. W. Lee, J.-H. Park, M. R. Prausnitz, Dissolving microneedles for transdermal drug delivery, Biomaterials 29 (2008) 2113–2124. doi:10.1016/j.biomaterials.2007.12.048.

[110] J.-H. Park, M. G. Allen, M. R. Prausnitz, Polymer Microneedles for Controlled-Release Drug Delivery, Pharmaceutical Research 23 (2006) 1008–1019. doi:10.1007/s11095-006-0028-9.

[111] A. L. Teo, C. Shearwood, K. C. Ng, J. Lu, S. Moochhala, Transdermal microneedles for drug delivery applications, Materials Science and Engineering: B 132 (2006) 151–154. doi:10.1016/j.mseb.2006.02.008.

[112] M. R. Prausnitz, R. Langer, Transdermal drug delivery, Nature Biotechnology 26 (2008) 1261–1268. doi:10.1038/nbt.1504.

[113] Y.-C. Kim, J.-H. Park, M. R. Prausnitz, Microneedles for drug and vaccine delivery, Advanced Drug Delivery Reviews 64 (2012) 1547–1568. doi:10.1016/j.addr.2012.04.005.

[114] M. R. Prausnitz, Microneedles for transdermal drug delivery, Advanced Drug Delivery Reviews 56 (2004) 581–587. doi:10.1016/j.addr.2003.10.023.

[115] T. A. Petukhova, L. A. Hassoun, N. Foolad, M. Barath, R. K. Sivamani, Effect of Expedited Microneedle-Assisted Photodynamic Therapy for Field Treatment of Actinic Keratoses: A Randomized Clinical Trial, JAMA Dermatology 153 (2017) 637. doi:10.1001/jamadermatol.2017.0849.

[116] M. Badran, J. Kuntsche, A. Fahr, Skin penetration enhancement by a microneedle device (Dermaroller®) in vitro: Dependency on needle size and applied formulation, European Journal of Pharmaceutical Sciences 36 (2009) 511–523. doi:10.1016/j.ejps.2008.12.008.

[117] H. Lev-Tov, L. Larsen, R. Zackria, H. Chahal, D. Eisen, R. Sivamani, Microneedle-assisted incubation during aminolaevulinic acid photodynamic therapy of actinic keratoses: A randomized controlled evaluator-blind trial, British Journal of Dermatology 176 (2017) 543–545. doi:10.1111/bjd.15116.

[118] M. T. Clementoni, M. B-Roscher, G. S. Munavalli, Photodynamic photorejuvenation of the face with a combination of microneedling, red light, and broadband pulsed light, Lasers in Surgery and Medicine 42 (2010) 150–159. doi:10.1002/lsm.20905.

[119] A. G. Harris, C. Naidoo, D. F. Murrell, Skin needling as a treatment for acne scarring: An up-to-date review of the literature, International Journal of Women's Dermatology 1 (2015) 77–81. doi:10.1016/j.ijwd.2015.03.004.

[120] S. P. Sullivan, D. G. Koutsonanos, M. del Pilar Martin, J. W. Lee, V. Zarnitsyn, S.-O. Choi, N. Murthy, R. W. Compans, I. Skountzou, M. R. Prausnitz, Dissolving polymer microneedle patches for influenza vaccination, Nature Medicine 16 (2010) 915–920. doi:10.1038/nm.2182.

[121] M. Alexiades, Randomized, Controlled Trial of Fractional Carbon Dioxide Laser Resurfacing Followed by Ultrashort Incubation Aminolevulinic Acid Blue Light Photodynamic Therapy for Actinic Keratosis:, Dermatologic Surgery 43 (2017) 1053–1064. doi:10.1097/DSS.0000000000001117.

[122] C. Haak, K. Togsverd-Bo, D. Thaysen-Petersen, H. Wulf, U. Paasch, R. Anderson, M. Haedersdal, Fractional laser-mediated photodynamic therapy of high-risk basal cell carcinomas - a randomized clinical trial, British Journal of Dermatology 172 (2015) 215–222. doi:10.1111/bjd.13166.

[123] S. Choi, K. Kim, K. Song, Er:YAG ablative fractional laser-primed photodynamic therapy with methyl aminolevulinate as an alternative treatment option for patients with thin nodular basal cell carcinoma: 12-month follow-up results of a randomized, prospective, comparative trial, Journal of the European Academy of Dermatology and Venereology 30 (2016) 783–788. doi:10.1111/jdv.13453.

[124] L. Torezan, Y. Chaves, A. Niwa, J. A. Sanches, C. Festa-Neto, R.-M. Szeimies, A Pilot Split-Face Study Comparing Conventional Methyl Aminolevulinate-Photodynamic Therapy (PDT) With Microneedling-Assisted PDT on Actinically Damaged Skin:, Dermatologic Surgery 39 (2013) 1197–1201. doi:10.1111/dsu.12233.

[125] E. Christensen, T. Warloe, S. Kroon, J. Funk, P. Helsing, A. Soler, H. Stang, Vatne, C. Mørk, Guidelines for practical use of MAL-PDT in non-melanoma skin cancer, Journal

of the European Academy of Dermatology and Venereology 24 (2010) 505–512. doi:10.1111/j.1468-3083.2009.03430.x.

[126] E. Dika, P. A. Fanti, A. Ismaili, C. Misciali, S. Vaccari, A. Barisani, A. Patrizi, Basal cell carcinoma margin delineation: Is curettage useful? A surgical and histological study, Journal of Dermatological Treatment 24 (2013) 238–242. doi:10.3109/09546634.2012.756572.

[127] J.-A. See, S. Shumack, D. F. Murrell, D. M. Rubel, P. Fernández-Peñas, R. Salmon, D. Hewitt, P. Foley, L. Spelman, Consensus recommendations on the use of daylight photodynamic therapy with methyl aminolevulinate cream for actinic keratoses in Australia: Daylight PDT consensus recommendations, Australasian Journal of Dermatology 57 (2016) 167–174. doi:10.1111/ajd.12354.

[128] M. C. Fargnoli, K. Peris, Photodynamic therapy for basal cell carcinoma, Future Oncology 11 (2015) 2991–2996. doi:10.2217/fon.15.208.

[129] C. V. Nissen, S. R. Wiegell, P. A. Philipsen, H. C. Wulf, Short-term chemical pretreatment cannot replace curettage in photodynamic therapy, Photodermatology, Photoimmunology & Photomedicine 32 (2016) 146–152. doi:10.1111/phpp.12236.

[130] A. M. Soler, T. Warloe, A. Berner, Giercksky, KE, A follow-up study of recurrence and cosmesis in completely responding superficial and nodular basal cell carcinomas treated with methyl 5-aminolaevulinate-based photodynamic therapy alone and with prior curettage, British Journal of Dermatology 145 (2001) 467–471.

[131] J.-Y. Fang, W.-R. Lee, S.-C. Shen, Y.-P. Fang, C.-H. Hu, Enhancement of topical 5-aminolaevulinic acid delivery by erbium:YAG laser and microdermabrasion: A comparison with iontophoresis and electroporation, British Journal of Dermatology 151 (2004) 132–140. doi:10.1111/j.1365-2133.2004.06051.x.

[132] D. J. Karimipour, G. Karimipour, J. S. Orringer, Microdermabrasion: An Evidence-Based Review:, Plastic and Reconstructive Surgery 125 (2010) 372–377. doi:10.1097/PRS.0b013e3181c2a583.

[133] M. Thissen, C. A. Schroeter, H. A. M. Neumann, Photodynamic therapy with delta-aminolaevulinic acid for nodular basal cell carcinomas using a prior debulking technique, British Journal of Dermatology 142 (2000) 338–339.

[134] H. Dickel, A. Goulioumis, T. Gambichler, J. Fluhr, J. Kamphowe, P. Altmeyer, O. Kuss, Standardized Tape Stripping: A Practical and Reproducible Protocol to Uniformly Reduce the Stratum Corneum, Skin Pharmacology and Physiology 23 (2010) 259–265. doi:10.1159/000314700.

[135] K. Takahashi, T. Hasegawa, T. Ishii, A. Suzuki, M. Nakajima, K. Uno, I. Yasuda, A. Kishi, K. Sadamoto, F. Abe, Antitumor effect of combination of hyperthermotherapy and 5-aminolevulinic acid (ALA), Anticancer research 33 (2013) 2861–2866.

[136] A. Bettaieb, P. K., D. A., Hyperthermia: Cancer Treatment and Beyond, in: L. Rangel (Ed.), Cancer Treatment - Conventional and Innovative Approaches, InTech, 2013, pp. 257–282. doi:10.5772/55795.

[137] J. T. Van den Akker, K. Boot, D. I. Vernon, S. B. Brown, L. Groenendijk, G. C. van Rhoon, H. J. Sterenborg, Effect of elevating the skin temperature during topical ALA application on in vitro ALA penetration through mouse skin and in vivo PpIX production in human skin, Photochemical & Photobiological Sciences 3 (2004) 263–267.

[138] A. Willey, R. R. Anderson, F. H. Sakamoto, Temperature-Modulated Photodynamic Therapy for the Treatment of Actinic Keratosis on the Extremities: A Pilot Study, Dermatologic Surgery 40 (2014) 1094–1102. doi:10.1097/01.DSS.0000452662.69539.57.

[139] A. Juzeniene, P. Juzenas, I. Bronshtein, A. Vorobey, J. Moan, The influence of temperature on photodynamic cell killing in vitro with 5-aminolevulinic acid, Journal of Photochemistry and Photobiology B: Biology 84 (2006) 161–166. doi:10.1016/j.jphotobiol.2006.02.009.

[140] J. Yang, A. C.-H. Chen, Q. Wu, S. Jiang, X. Liu, L. Xiong, Y. Xia, The influence of temperature on 5-aminolevulinic acid-based photodynamic reaction in keratinocytes in vitro, Photodermatology, photoimmunology & photomedicine 26 (2010) 83–88.

[141] S. Mordon, A commentary on the role of skin temperature on the effectiveness of ALA-PDT in Dermatology, Photodiagnosis and Photodynamic Therapy 11 (2014) 416–419. doi:10.1016/j.pdpdt.2014.05.004.

[142] A. Mamalis, E. Koo, G. Sckisel, D. Siegel, J. Jagdeo, Temperature-dependent impact of thermal aminolaevulinic acid photodynamic therapy on apoptosis and reactive oxygen

species generation in human dermal fibroblasts, British Journal of Dermatology 175 (2016) 512–519. doi:10.1111/bjd.14509.

[143] A. Willey, R. R. Anderson, F. H. Sakamoto, Temperature-Modulated Photodynamic Therapy for the Treatment of Actinic Keratosis on the Extremities: A One-Year Follow-up Study, Dermatologic Surgery 41 (2015) 1290–1295. doi:10.1097/DSS.0000000000000512.

[144] C. Morton, H. Wulf, R. Szeimies, Y. Gilaberte, N. Basset-Seguin, E. Sotiriou, S. Piaserico, R. Hunger, S. Baharlou, A. Sidoroff, L. R. Braathen, Practical approach to the use of daylight photodynamic therapy with topical methyl aminolevulinate for actinic keratosis: A European consensus, Journal of the European Academy of Dermatology and Venereology 29 (2015) 1718–1723. doi:10.1111/jdv.12974.

[145] H. C. Wulf, Photodynamic therapy in daylight for actinic keratoses, JAMA dermatology 152 (2016) 631–632.

[146] S. R. Wiegell, M. Haedersdal, P. A. Philipsen, P. Eriksen, C. D. Enk, H. C. Wulf, Continuous activation of PpIX by daylight is as effective as and less painful than conventional photodynamic therapy for actinic keratoses; a randomized, controlled, single-blinded study, British Journal of Dermatology 158 (2008) 740–746.

[147] S. Wiegell, M. Haedersdal, P. Eriksen, H. Wulf, Photodynamic therapy of actinic keratoses with 8% and 16% methyl aminolaevulinate and home-based daylight exposure: A double-blinded randomized clinical trial, British Journal of Dermatology 160 (2009) 1308–1314. doi:10.1111/j.1365-2133.2009.09119.x.

[148] S. Wiegell, S. Fabricius, I. Stender, B. Berne, S. Kroon, B. Andersen, C. Mørk, C. Sandberg, G. Jemec, M. Mogensen, K. Brocks, P. Philipsen, J. Heydenreich, M. Haedersdal, H. Wulf, A randomized, multicentre study of directed daylight exposure times of $1\frac{1}{2}$ vs. $2\frac{1}{2}$ h in daylight-mediated photodynamic therapy with methyl aminolaevulinate in patients with multiple thin actinic keratoses of the face and scalp: Daylight-mediated PDT of thin actinic keratoses, British Journal of Dermatology 164 (2011) 1083–1090. doi:10.1111/j.1365-2133.2011.10209.x.

[149] S. Wiegell, S. Fabricius, M. Gniadecka, I. Stender, B. Berne, S. Kroon, B. Andersen, C. Mørk, C. Sandberg, K. Ibler, G. Jemec, K. Brocks, P. Philipsen, J. Heydenreich, M. Haedersdal, H. Wulf, Daylight-mediated photodynamic therapy of moderate to thick

actinic keratoses of the face and scalp: A randomized multicentre study: Daylight-mediated PDT of moderate to thick actinic keratoses, British Journal of Dermatology 166 (2012) 1327–1332. doi:10.1111/j.1365-2133.2012.10833.x.

[150] B. Grinblat, G. Galimberti, G. Pantoja, G. Sanclemente, M. Lopez, D. Alcala, L. Torezan, D. Kerob, T. Pascual, E. Chouela, Feasibility of daylight-mediated photodynamic therapy for actinic keratosis throughout the year in Central and South America: A meteorological study, International journal of dermatology 55 (2016).

[151] C. N. Lemos, J. G. de Souza, P. S. Simão, R. F. V. Lopez, Iontophoresis Improved Growth Reduction of Invasive Squamous Cell Carcinoma in Topical Photodynamic Therapy, PLOS ONE 11 (2016) e0145922. doi:10.1371/journal.pone.0145922.

[152] T. Gratieri, Y. N. Kalia, Topical Iontophoresis for Targeted Local Drug Delivery to the Eye and Skin, in: A. J. Domb, W. Khan (Eds.), Focal Controlled Drug Delivery, Springer US, Boston, MA, 2014, pp. 263–284. doi:10.1007/978-1-4614-9434-8_12.

[153] R. F. Lopez, M. V. L. Bentley, M. B. Delgado-Charro, R. H. Guy, Iontophoretic delivery of 5-aminolevulinic acid (ALA): Effect of pH, Pharmaceutical research 18 (2001) 311–315.

[154] J. D. Byrne, J. J. Yeh, J. M. DeSimone, Use of iontophoresis for the treatment of cancer, Journal of Controlled Release (2018). doi:10.1016/j.jconrel.2018.06.020.

[155] H. Boddé, P. Roemelé, W. Star, Quantification of Topically Delivered 5-Aminolevulinic Acid by Iontophoresis Across Ex Vivo Human Stratum Corneum, Photochemistry and Photobiology 4 (2002) 418–423.

[156] T. Omi, M. Akimoto, M. Miyazaki, S. Kawana, Iontophoresis-enhanced cutaneous absorption of 5-aminolevulinic acid shortens the incubation period in photodynamic therapy, Laser therapy 18 (2009) 143–149.

[157] S.-H. Choi, T.-H. Kim, K.-H. Song, Efficacy of iontophoresis-assisted ablative fractional laser photodynamic therapy with short incubation time for the treatment of actinic keratosis: 12-month follow-up results of a prospective, randomised, comparative trial, Photodiagnosis and Photodynamic Therapy 18 (2017) 105–110. doi:10.1016/j.pdpdt.2017.01.184.

1.4 Transdermal drug delivery with microneedles

As presented in the paragraph "*Microneedles*" of the previous review 1.3, microneedles appear to be a physical method able to enhance 5-ALA drug penetration and reduce incubation time. It has briefly exposed that many designs and shapes have been proposed. The importance of the design, as well of the production method, will be more detailed in the next section. Finally, the four different kinds of MN (solid, coated, hollow and dissolvable) will be reviewed and few of their new current application in PDT will be mentioned.

1.4.1 Microneedles design

MNs are an exciting technology to enable transdermal drug delivery and their design is essential to fulfil this mission and is depending on two main criteria:

- MNs should penetrate the *stratum corneum* to access viable epidermis without breaking, requiring an optimized design for mechanical properties. (*Mechanical aspect*)
- MNs have been developed as a non-invasive micro-device, therefore they should be painless for the patients and not cause high tissue damages when inserted. (*Medical aspect*)

To answer these previous points, geometry parameters of microneedles have been thinking carefully. An optimized design involves to choose the appropriate microneedles height, width, thickness, tip angle, base diameter, shape and density (number) according to the kind of application.

1.4.1.1 Mechanical aspect

Two main key features must be taken into account for MN conception: efficient skin penetration and risk of needles breaking. In order to fulfil these criteria, MN shape must be optimised for providing sufficient mechanical properties [38].

- **Fracture force**

The non breaking ability of MN during compression is directly linked to their shapes. It has been demonstrated that contrary to square or rectangular MN, circular MN with the same contact area can withstand more intense forces (stress and bending force) [1]. Height is also an important criterion to take into account for MN development since the longer they are, the more they break [38, 1]. Similarly, when the base diameter increases, the fracture force also increases indicating that MNs are more resistant to rupture. Therefore, thin and long MNs are fragile resulting in an increased risk of fracture in skin tissue. On the other hand, fracture force is also controlled by inherent properties of materials and especially its Young modulus. The higher it is, the more MNs could resist to stress and strain [38, 1]. Tip diameter do not drastically impact fracture force [38] but for polymeric MN it can weaken material structure stimulating fracture and potentially impacting microneedle insertion [89].

- **Insertion force**

Insertion force is directly linked with the microneedle tip and especially with the microneedle surface area applied on the skin [37]. According to Davis calculations, the larger the MN interfacial contact area, the higher the insertion force needs to be [38]. MNs are always assembled together as an array and it has been shown that the insertion force was dependent on the interspacing between microneedles. Penetration percentage is more important when spacing

between MN increases [89]. Similarly, when the base diameter increases, the insertion force increases too. In [89], Kochhar et al. proved that a MN-array made of MNs with respectively a base diameter and a spacing of 300 µm and 1800 µm or 400 µm and 2400 µm had optimal characteristics to penetrate the skin. If the spacing was shorter, about 150 µm, on a same array, density/number of microneedles will be more important and will form a "bed of nails" and prevent MN penetration [89, 128]. Patterning of MN on the array is also a factor to keep in mind when designed. Indeed, square or rectangular patches have been presented as better for drug permeability in the skin than triangular or diamond patch [140, 141].

1.4.1.2 Medical aspect

MNs have been created particularly to limit pain which imply an optimal geometry to gently penetrate the skin. It is well known that dermis is a nervous region with a lot of receptors, so increasing microneedle height involves that they can touch those sensitive zones and create pain. It has been proved that 30 % of patients do not complain when MN with length inferior to 700 µm are inserted [58]. Likewise when 150 µm long MNs were applied they were characterized as painless by the patients [79]. Number of MNs on an array has also been presented as a factor affecting the level of pain [73]. Pain increases when the number of MNs on a same array also increases [186]. Finally, microneedle tip should be sharp enough to prevent the subject from suffering [58, 186]. Nevertheless, it is necessary to keep in mind that larger microneedles are stronger and can also deliver more drug [58].

To conclude, optimization of a microneedle device is constrained by different parameters. Among all of them, to obtain a good microneedle design that minimizes pain, provides sufficient mechanical properties for allowing insertion in the skin without breaking, we can retain few parameters as essentials. As presented hereinabove, a circular shape, a low density of MN on an array and a small MN height are preferred to combine good mechanical insertion and patient compliance.

On the other hand, to find the balance between all the parameters, biomimetic research has recently developed painless needle based on the mosquito's proboscis [170] or on the honeybee stinger structures [98]. Indeed, these insects can cleverly pierce human skin without any mechanical failure and without pain thanks to ingenious mechanisms, microstructures and intelligent insertion modes [103]. A lot of design might be designed but the different ways of production should be adapted. Technologies able to produce microneedles will be presented in the next section 1.4.2.

1.4.2 Microneedles processing

Numerous types of microneedles for transdermal drug delivery have been developed with different materials hence different ways of production have been investigated. The MN fabrication process depends on the needle material (silicon, metal or polymer) and the desired geometry [86]. The most common techniques used will be presented hereinafter.

1.4.2.1 Laser-cutting

Laser cutting is a technology that uses a laser to cut materials and particularly metals. This process is automated as the shape of the MN is modelled with a software, in a file that can be read by the laser cutting machine. Sufficient high beam intensity is directed on the material, which

then could melt, burn or vaporize away [78]. The laser beam traces the desired shape of the needle and then thin stainless steel sheet is cut in the plane of the sheet using an infrared laser [104]. Laser cutting has the advantage to produce a high-quality surface finishing. Microneedles obtained with this process can then be electro-polished [56].

1.4.2.2 Micromachining

Micromachining also called subtractive manufacturing is another technology that enables to cut a piece of raw material (often metal) into a desired final design by a controlled material-removal process. There are different methods of machining but most of them are carried by computer numerical control to monitor the mills, lathes, planers etc [156]. This method has several advantages such as producing repetitive, uniform and reusable array of MN. Moreover, this technique is considered as simple, fast and cost-effective [176, 152].

1.4.2.3 Photolithography

Photolithography process patterns some parts of a thin film or the bulk of a substrate. This technology uses light to transfer a geometric pattern from a photomask to a light-sensitive chemical photoresist on the substrate. A series of chemical treatments then either engraves the exposure pattern into, or enables deposition of a new material in the desired pattern upon the material underneath the photo resist. This method is principally used for non-degradable polymers such as photolithographic epoxy or optically curable polymers SU-8 that has been extensively used to develop microneedles [86]. SU-8 microneedles pillar array structures were thus created using a conventional UV mask and contact printing method. SU-8 is basically a negative photoresist material that allows the fabrication of a MN array, meaning that it can be crosslinked by light exposure, making it insoluble in specific solvent which dissolves the non-exposed resin. Briefly, SU-8 was spin coated on the wafer and pretreatments such as pre exposure, baking and vacuuming at different temperatures and pressures were carried out. Then, a mask with a geometric pattern is deposited on the wafer and UV light exposure ($< 400\,\text{nm}$) is performed and only crosslinked materials not masked which allow to obtain MNs. Finally the solid MNs were washed and cleaned using oxygen plasma [26]. Hollow microneedles or tapered can also be designed using photolithography techniques and depending on the photomask used [83].

1.4.2.4 Wet or dry-etching of silicon

Micro and nanotechnology usually implicated for silicone electronics are expanding to other application fields and are now used to developed MNs. Indeed MNs have been developed by combining few processes usually suitable for semi electronics [186]. These devices can be designed by using a series of photolithography, thin-film deposition, wet or dry-etching, reactive ion etching techniques using single-crystal Si. These technologies consist in attacking or protecting the silicon wafer in order to create special affinities between chemicals. According to the masks used or the pre-treatments different kind of microneedles geometries can be obtained. Nevertheless, the production process for silicon microneedles requires expensive micro fabrication [74, 197, 205, 206].

1.4.2.5 Molding method or solvent casting molding method

A fabrication process was developed based on casting a viscous solution in a mold. This fabrication process is an economical manner suitable for scale-up to mass production [94] and is

only divided in three important steps that are presented in figure 1.6.

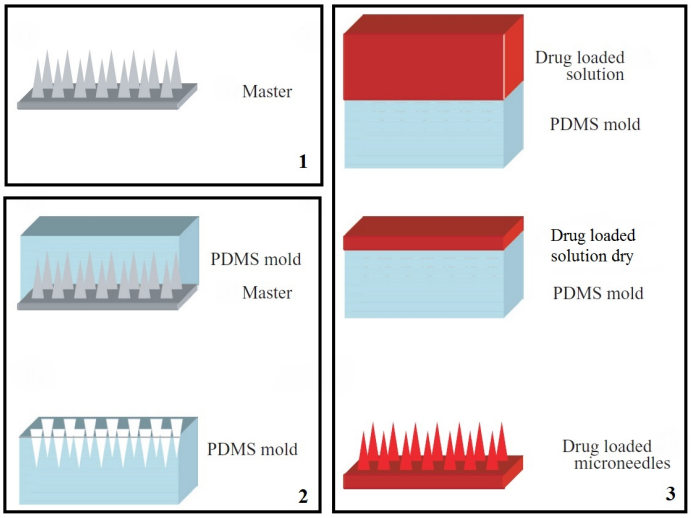

Figure 1.6 – Microneedles obtained by shape-molding process [182].
1-Master structure. 2-Fabrication of PDMS mold. 3-Casting of the (drug loaded) solution in the mold.

- **Master structure**

Silicon, metal [182] or SU-8 microneedles [55] are produced by previous methods described and serve as master structure also called male microneedle master-mold. Photolithography or micromachining are usually used to produce master structure. This master structure produced can be used several times to make molds [133].

- **Female mold**

A female mold is made with another polymer. PDMS is often used because it is chemically inert, non-hygroscopic, inexpensive, with low surface energy and good thermal stability [132]. Moreover PDMS has poor adhesion and flexibility properties, improving the ability to coat microstructures and facilitating separation of microstructures from MN [94]. Thanks to its mechanical durable properties [132], PDMS female mold can be used several times. Experimentally PDMS mold could be created by pouring PDMS over the master structure and cured by placing in an oven for a specific time period. The temperature range may be large (between 40 °C – 80 °C) and the drying period may be comprised between 2 h – 12 h [195, 75]. The cured PDMS mold was then peeled off from the master [75].

- **Casting**

A matrix -usually polymeric- is used to fill the female mold. Polymer hydrogel is prepared at low viscosity [85] because high viscosity showed difficulties in drying out and MN produced had weak mechanical properties creating distortion during skin insertion [94]. Hydrogels could be poured on a female mold and centrifuged to fill the microneedle mold cavities and then dried. The centrifugation continuously compressed the mold contents which minimized void formation

during drying [186]. Polymeric matrix could also be injected through microchannel and filling of the female mold is ensured by microinjection [153].

To conclude, different manufacturing methods were investigated to produce microneedles. The way of production determines consequently the kind of MN. For example, laser-cutting is not suited for producing dissolving MNs or solvent casting molding method for producing hollow MNs. Moreover, MN processing such as laser-cutting, micromachining or photolithography does not allow to integrate a drug directly in the MN whereas by solvent casting molding method, a drug can be easily inserted during the casting step.

1.4.3 Different kinds of MNs

There are four different types of microneedle-based drug delivery for skin application [55, 86, 139] which are displayed in figure 1.7:

- Solid microneedles for skin pretreatments (starting to be used clinically to enhance 5-ALA penetration prior to PDT)
- Drug-coated microneedles
- Hollow microneedles
- Dissolving microneedles

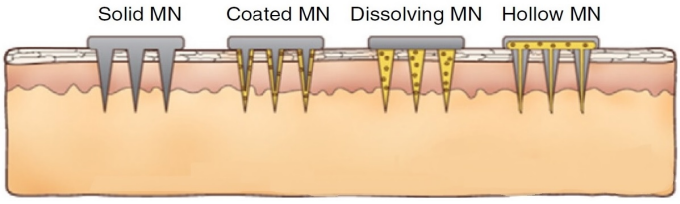

(a) Microneedles are applied to the skin.

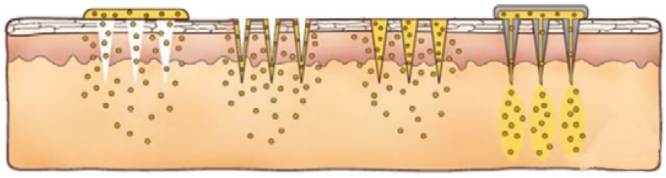

(b) Drug is delivered in the skin.

.

Figure 1.7 – Methods of drug delivery to the skin using different kind of microneedles [86]

1.4.3.1 Solid microneedles for skin pretreatments

Sharp solid microneedles can be used for skin pretreatment. They are inserted in the skin and then removed leaving micrometric pores in the skin surface. The holes thus created allow to insert drugs with formulation such as cream, gel, lotion or patch. Indeed the drug delivery

system can be applied to the skin surface and drug could slowly diffuse through the micropores. This method of inserting, removing MN and applying drug formulation has been called “poke and patch” [186]. This passive diffusion is controlled by microchannels created and in particular by their pore size, number and also by the drug concentration in the formulation [68]. This kind of microneedles is made with materials providing sufficient mechanical strength. In fact, these microneedles could be inserted and removed a few times. Materials used can be silicon, metal (titanium, stainless steel) and less often ceramic (alumina) [20] or polymer (SU-8) [105]. Solid microneedles were widely used over the two last decades for different applications such as the transdermal delivery of insulin [104, 216], or calcein [63] or even Anthrax vaccine (based on recombinant Bacillus anthracis protective antigen) [107, 208]. Solid MNs are especially used for skin pretreatments before PDT treatment to allow better 5-ALA or MAL penetration as it has been shown in the review in section 1.3 with the recent studies (2013 and 2017) lead in [180] by Torezan et al., and in [137], by Petukhova et al. Overall, when solid MN were used prior to PDT, the authors underlined the loss of side-effects of their patients and good cosmetics outcomes [180], higher AK clearance rate [137] or even a reduced incubation time with equivalent clinical results [97].

The previous studies and the fact that the “poke and patch” method is technically very simple have made this pretreatment promising for PDT and in 2020, there have been 5 clinical trials investigating the efficacy of MN for skin cancers (especially AKs). Solids microneedles are an exciting technique but micro-pores created by the “poke” step need to stay open in order to allow penetration of the drug which could also lead to skin infections. Moreover the drug amount diffused through the skin is not precisely known which could be a restriction [186, 68].

1.4.3.2 Coated microneedles

Solid microneedles can be used not only for piercing the skin layers but also as drug vehicles. Indeed, they can be covered by a thin layer of drug on their surface to bring it into the skin. Coated microneedles are often fabricated from silicon or metal, cleaned and then covered with a drug. The appropriate coating solution is often a mixture of a surfactant, a viscosity enhancer and prepared in an aqueous or organic solvent and needs to be optimised regarding the active molecule and the MN material. Solid MNs were then sprayed or dipped in this coating solution thanks to a dip coating-device. In most cases, dip coating is performed just once into the coating solution [57, 55]. Layer properties depend on surface tension and viscosity of the formulation [183]. Coated MNs can be inserted in the skin and the drug is rapidly released into the skin [214]. Contrary to solid MNs, this kind of MNs allow a simple one-step application process and can administrate a precise dose [183].

Despite being attractive for different applications, such as the transdermal delivery of desmopressin [36], or vaccine for H3N2 virus [92], or even lidocaine delivery [214] all the experiments remain at the preclinical stage. For PDT application, 5-ALA coated on microneedles was only investigated once by Jain, Lee, and Gill and their test on mice showed promising results for PDT since 1.75 mg of 5-ALA suppressed the growth of mouse skin tumor by 57 % [71]. Amount of drug coated and presumed released is very well known contrary to the previous "poke and patch" method. Nevertheless, because layer coated is thin (≈100 nm) the drug volume released may be insufficient for therapeutic activity and could limit some of their applications[5] [186].

[5] For example, the conventional PDT treatment using the prodrug in a Metvixia® cream advise to administrate ≈ 80 mg

1.4.3.3 Hollow microneedles

This type of microneedle is similar to hypodermic needles except that with their micron size they are painless. Hollow MNs penetrate the *stratum corneum*, and the drug is then injected thanks to an internal channel in the MN which allow to diffuse the drug into the viable epidermis and reach deeper dermal skin or blood [167]. The drug delivery is dependent on the flow rate applied. Therefore, the injection is controlled by pressure which depends on the combination of hollow MN array and injection applicator (syringe, pump). This design set-up is essential because pressure is the key element to either deliver rapid bolus injection, slow injection or varied delivery rate. The pressure applied needs to be measured precisely because mechanical strength of the needle depends on it [186, 68]. To design successful hollow microneedles, the materials often used are: silicon, glass, metal and polymer [86]. Processing are chosen according to the materials chosen and photolithography [136, 111], etching [53] and laser micromachining [193] are frequently considered for manufacturing.

Hollow microneedles have been already clinically used for example for the transdermal delivery of methyl nicotinate for muscle soreness in healthy patients [159] or intradermal influenza vaccine in healthy adults [59]. Hollow microneedles allow to deliver higher amount of drug than coated MN and their investigations in clinics have started, but to our knowledge they were never used for PDT.

1.4.3.4 Dissolving microneedles

Dissolving microneedles have a drug encapsulated in their matrix that is biocompatible, biodegradable and mechanically robust. When inserted in the tissue, they are dissolved by body fluids and could deliver drug with a precise kinetic profile according to the matrix chosen [94]. In fact, they enable controlled delivery as a bolus or sustained release. Materials used as matrix are often polymer, polysaccharides [94], sugar [108] or bio-sourced components. To achieve a bolus drug release, dissolving MNs are made of polymer such as PVP [169] or CMC [94, 95] that allow a rapid dissolution (< 5 min or < 20 min respectively). Moreover, the drug can be loaded essentially in the needle or even in the needle tip to be rapidly released [94]. On the other hand to achieve a slower drug release, PLA, PLGA may be used since they biodegraded in a few days [133, 125]. In addition, the drug could be loaded in the support of the MNs or may be first encapsulated either within CMC or PLGA microparticles which could be then loaded in microneedles [133, 94]. To produce dissolving MNs, solvent casting molding method is preferentially used and Lee, Park, and Prausnitz defined a few requirements as important factors to produce reliable dissolving MNs [94]:

- Sufficient mechanical strength for insertion into the skin
- Gentle fabrication to avoid damaging sensitive drugs (i.e avoiding process with photopolymerization or elevated temperature or organic solvent [186, 68])
- Controlled release for bolus or sustained drug delivery (i.e choosing a relevant polymer)
- Rapid dissolution of MN made of safe materials (i.e studying materials biocompatibility)

Dissolving microneedles were used for different clinical applications such as vaccination for influenza [64], or transdermal delivery of triamcinolone for the treatment of keloids (skin disease) [173] or even for cosmetic assessment [84]. The interest of dissolving MNs for PDT application starting in 2009, with Donnelly et al. who developed carbohydrate MN arrays loaded with 5-ALA. Drug release experiments revealed than less than 0.05 % of the total drug loaded was released across a model silicone membrane. Moreover, the research team showed the inherent

difficulties in the processing and storage of carbohydrate based dissolving MN with 5-ALA [43]. In 2020, Requena, Donnelly et al. changed the processing and produced 5-ALA loaded in Gantrez AN-139 MNs, started their first preclinical study on xerographic tumour mice and showed that dissolving MNs delivered, with the same incubation time, a similar amount of PpIX compared to the cream containing 5-ALA at a concentration of 20 %. In parallel, in 2018, Zhao et al. prepared tip-loaded fast-dissolving microneedles made of sodium hyaluronate (HA) and containing 5-ALA. They demonstrated *in vivo*, on subcutaneous mouse tumor model, that PDT efficacy of 5-ALA-loaded hyaluronic acid microneedles was much better than 5-ALA injection in spite of relatively lower 5-ALA dose (0.61 mg vs. 1.65 mg). The subcutaneous tumor inhibition rate was up to 97 % which made the use of dissolving microneedles promising for future PDT clinical trials. At the end of 2019, Zhu et al. also used hyaluronic acid as the biodegradable matrix to load 5-ALA and evidenced remarkable tumor elimination on subcutaneous tumor mice [217]. To our knowledge, only these three teams are working on the potential use of loading 5-ALA in dissolving MNs for PDT. However, in [61], Hamdam, Donnelly et al. produced Gantrez® S-97 dissolving microneedles containing Redaporfin™ which is a preformed near-IR photosensitizer that could be used for PDT.

In conclusion, as shown in Figure 1.8a, photodynamic therapy for skin cancers is of interest to many research teams, since over the last two decades the number of papers published increased. The use of MN to improve drug delivery prior to PDT is also knowing a growing interest as displayed in figure 1.8b. Solid MNs have been extensively used for PDT. Recently, newer dissolving MN, due to their advantages such as being easy to handle in one step without sharp or biohazardous waste, are starting to be used in preclinical studies.

Summary: Literature review

- Skin cancers affect more and more the population, consequently efficient treatments are required.
- PDT is a possible treatment for non melanoma skin cancer but the poor penetration of the prodrug through the skin limit its efficiency in case of thick skin lesions.
- Different methods (chemical or physical) were purposed to enhance PDT treatment.
- Among the previous techniques presented, microneedles appear as a new technology that might be promising to enhance prodrug penetration in deep skin lesions.
- MNs are an innovative technology already used in different applications and were able to deliver numerous drugs. Solid MNs started to be used prior to PDT as a roller to create holes but the microchannels created can quickly become clogged and stop the penetration of the cream containing the 5-ALA.
- Dissolving microneedles made with a polymer could be a solution to this problem since they have sufficient mechanical strength to puncture the *stratum corneum*, could maintain open skin holes and release the drug in depth during their dissolution.

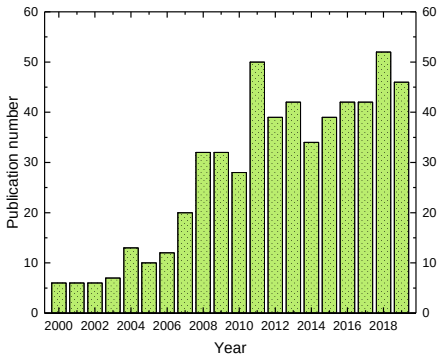

(a) Number of publications found from 2000 to 2019 with keywords "photodynamic therapy" and "skin cancer" on Web of Science.

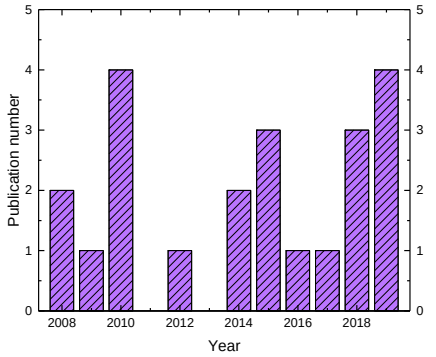

(b) Number of publications found from 2008 to 2019 with keywords "photodynamic therapy" and "microneedle" in the field of "dermatology" on Web of Science.

Figure 1.8 – Number of publications found in the last decades on photodynamic therapy for dermatology and the use of MN in this application.

Chapter 2

Dissolving microneedles containing 5-ALA
Enhancement of prodrug penetration in depth

Outline of the current chapter

Introduction

- The aim of this chapter is to propose a solution with dissolving MNs to enhance 5-ALA penetration in deep skin lesions.
- HA, due to its biocompatibility and previous reported uses in biomedical fields, has been chosen as the dissolvable and biodegradable material for producing the MNs.
- In an article, we will show that an easy one-step solvent casting molding method allowed to produce reproducible and robust MNs containing the 5-ALA prodrug.
- Furthermore, particular care has been taken to ensure 5-ALA stability in the patch, interactions between HA and 5-ALA have therefore been carefully studied and 5-ALA environment was precisely controlled.
- Supplementary data concerning extended results (*not presented in the article*), sterilization of the microneedles patch, cytotoxicity at high MN-patch concentrations, or stability in long-term follow-up are available.

2.1 Polymer choice: hyaluronic acid

To produce dissolving MNs able to be used in PDT, functional and technical specifications were needed. Since 5-ALA will be embedded in the MN-patch, the materials constituting the MN-patch should be soluble to release the prodrug, biocompatible and biodegradable to avoid cytotoxic effects after application on skin. Moreover, the materials should be easy to process without addition of organic solvent or use of high temperature to ensure 5-ALA stability and no skin irritation. Therefore, we naturally turned to a natural polysaccharide with those intrinsic properties: hyaluronic acid.

2.1.1 Biocompatible

HA is a high molecular weight biopolysacharide, naturally occurring in human body, which has important biological functions since mostly found in connective tissues, synovial fluid, vitreous fluid of the eye or even umbilical cords. This biopolymer is naturally synthesized by hyaluronan synthases (integral membrane proteins) which alternate addition of glucuronic acid and N-acetylglucosamine to the growing chain (figure 2.1). These different characteristics make HA a polymer with good biocompatibility, highly non-antigenic and non-immunogenic effects [126]. Consequently, for the last three decades HA has been widely used as a component for artificial matrices and in bioengineering for tissue scaffolding or reparation [126, 154].

2.1.2 Biodegradation mechanisms involved

Since HA is already synthesized and present in human body, with a high turnover, logically our body also planned a degradation process. As described by Lyu and Untereker in [102] or by Saltzman and Kyriakides in [150] when a polymer is implanted different reactions can lead to the polymer degradation and the three most common mechanisms are the following:

- Enzymatic degradation due to defense system activation

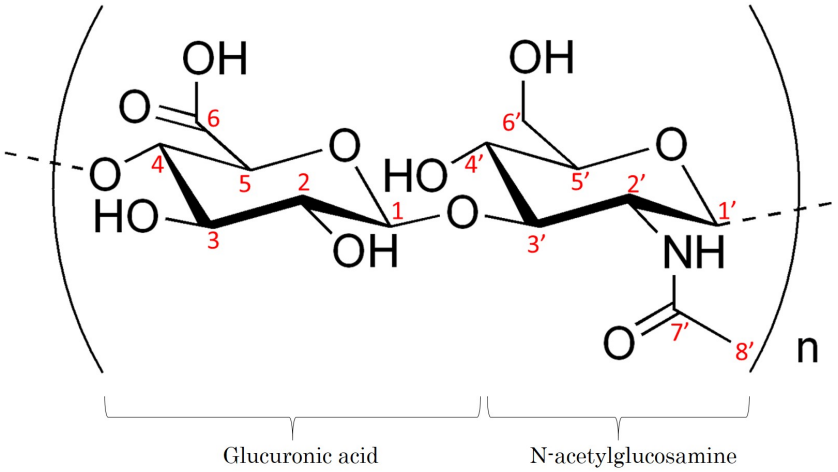

Figure 2.1 – Chemical structure of hyaluronic acid.

- Oxidation reaction due to oxidants produced because of the foreign materials presence in the body
- Hydrolysis reaction with water present in human tissues

The catabolism of HA can be described as a depolymerization process because of glycosidic bond cleavage leading to smaller molecule chains. HA degradation process has been well studied in literature and is principally due to enzymatic pathway but hydrolysis and oxidation could also be mechanisms that degrade HA [165, 166].

2.1.2.0.1 Enzymatic degradation Hyaluronidases are enzymes well known in HA degradation and two categories are essential: hyaluronoglucosaminidase 1 (HYAL 1) and hyaluronoglucosaminidase 2 (HYAL 2). HYAL 1 cleaves high molecular weight HA (> 1 MDa) in smaller molecular chain of about 20 kDa. Then hyaluronoglucosaminidase 2 (HYAL 2) will carry those fragments and convert them in tetrasaccharides and other enzymes will carry these smaller polymers and convert them in monosacharrides. Those different products of enzymatic degradation are naturally present in the human body, so will join the natural elimination process consisting in a degradation metabolism in liver, kidney or lymph node thanks to endothelial cells [39, 50, 49].

2.1.2.0.2 Oxidation degradation Even if hyaluronic acid is a natural bio-component, the insertion of a biomaterial based on HA could be sometimes considered as a foreign body material by the immune system and a slight inflammatory response could happen. Consequently, free radical depolymerization is launched and macrophages intertwined with endothelial cells to eliminate hyaluronan [50].

2.1.2.0.3 Hydrolysis degradation This mechanism of HA degradation is the last one to occur and is based on the hydrolysis of glycoside bonds and leading to the formation of smaller chains. This reaction is highly depending on on the hydrophilicity of the polymer which is also linked to its chemical structure and its available hydrophilic group [39, 179].

2.1.3 Easy to process

This last decade, HA has been widely used for producing dissolving microneedles especially with the solvent casting molding method as presented in several studies [157, 99]. HA is a biopolymer soluble in water, therefore its formulation prior to casting is very simple and in most of the studies it only consisted in mixing the polymer and the drug with water before filling the PDMS mold [218, 110, 87]. The dissolution time of HA-based MN depends on the HA Mw and higher Mw led to longer application time of MN-patch for a complete dissolution of MNs into the skin [96].

To conclude, hyaluronic acid is a good candidate since it fulfills all the specifications for producing dissolving MNs (biocompatible, soluble and biodegradable). Moreover, this biopolymer is also well known for its capability of skin regeneration so it is an added value to also improve cosmetic outcomes after PDT treatment.

2.2 Preliminary tests and characterisations

2.2.1 Physico-chemical characterisations

2.2.1.1 Determination of the HA molecular weight

To determine precisely the HA molecular weight, size exclusion chromatography (SEC) has been used. It was realized with a high pressure liquid chromatography (HPLC) equipped with a SEC column (TOSOH TSK gel SuperMultipore PW-M). In our lab (LETI/DTBS, Grenoble), two HA were previously purchased from Contipro, one with a low Mw and one with a high Mw, respectively expected at 5.0×10^4-8.0×10^4 g mol^{-1} and 2.5×10^5-4.5×10^5 g mol^{-1} and abusively called "low" HA and "high" HA. A solution S was composed of 0.1 mol L^{-1} of $NaNO_3$ and 0.1 mol L^{-1} PB (phosphate buffer without salt) at $pH7$. The "low" and "high" HA samples were solubilized in solution S to obtain final concentrations respectively at 5 mg mL^{-1} and 1 mg mL^{-1}. A sample volume of 100 µL was injected in the column and the mobile phase (solution S) has a flow of 0.6 mL min^{-1}. After the column separation, the sample is analysed by UV-visible and with multi-angle light scattering analysis (MALS, Wiatt Dawn Helios) associated with a differential refractometer (dRI, Wyatt OptiLab). Then the software Astra 6.1 was used for data treatment to obtain the number average molar mass (Mn), the average molar mass (also called molecular weight Mw) and the polydispersity index (PDI).

Reference HA	Mn (g mol^{-1})	Mw (g mol^{-1})	PDI
"low"	$(4.40 \pm 0.02) \times 10^4$	$(5.50 \pm 0.04) \times 10^4$	1.24 ± 0.03
"high"	$(2.05 \pm 0.02) \times 10^5$	$(2.43 \pm 0.01) \times 10^5$	1.19 ± 0.01

Table 2.1 – Average molar masses and polydispersity index of the "low" and "high" HA.

The average molar masses calculated by SEC-MALS are displayed in table 2.1, for the "low" sample the Mw value is indeed in the value range given by the supplier but our characterization is more precise. For the "high" sample the Mw value is a little bit below the one provided by the supplier that is why a precise characterisation of the HA molecular weight by SEC is essential.

2.2.1.2 Chemical structure

In order to confirm the chemical structure of HA, FTIR, ^{1}H NMR and ^{13}C NMR experiments were performed. Methods will be explained in section 2.3.

With the FTIR result displayed in figure 2.2, we found out the presence of HA characteristic bands that were congruent with the previous literature [40, 22, 143]. Indeed, the band at 3260 cm^{-1} was attributed to the vibration of OH and the stretching of NH. The bands at 2855 cm^{-1} and 1600 cm^{-1} corresponded to the vibration of CH_2 and the amide carbonyl groups respectively. The band at 1400 cm^{-1} was assigned to the stretching of COOH. Lastly, the absorption bands at 1028 cm^{-1} and 597 cm^{-1} were attributed to the linkage stretching of the C−OH and the C−O−C.

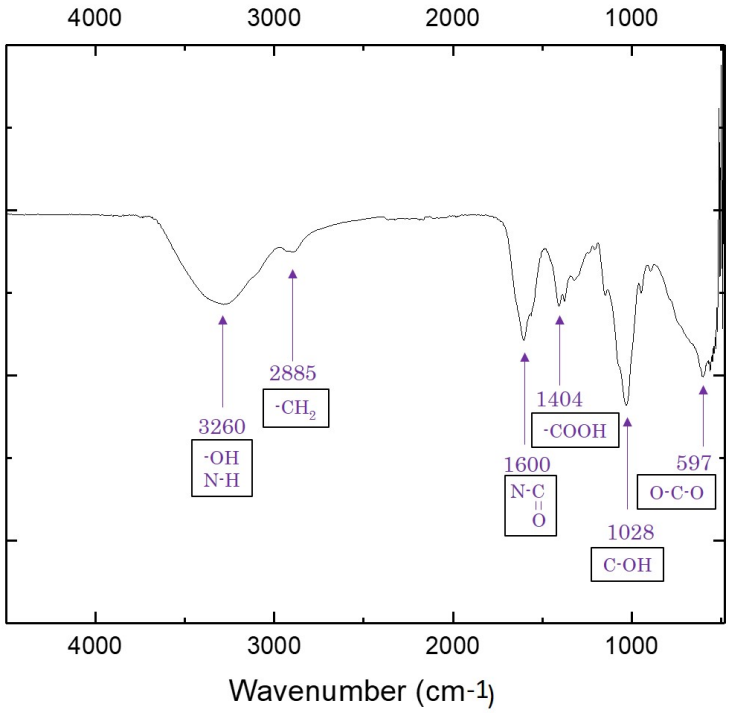

Figure 2.2 – FTIR spectrum of HA representing its characteristic peaks.

Figure 2.3.A displayed the results obtained by ^{1}H NMR, with a single peak well defined at 1.95 ppm, which is characteristic of the CH_3 from the N-acetyl group. The other chemical shifts less defined from 3.0 to 4.0 ppm are due to glucosidic hydrogen and between 4.40 and 4.55 ppm the signals came from the anomeric hydrogen. Overall the ^{1}H NMR spectrum is very close to those obtained in literature [210, 211].

To conclude on the HA chemical structure, a ^{13}C NMR experiment was performed and results are displayed in figure 2.3.B. As depicted by the table in 2.3.C all the peaks observed were assigned to the carbons found in the HA and matched with literature [124, 69]. These results also highlighted the absence of impurities since no other peaks even at a low intensity were

noticeable.

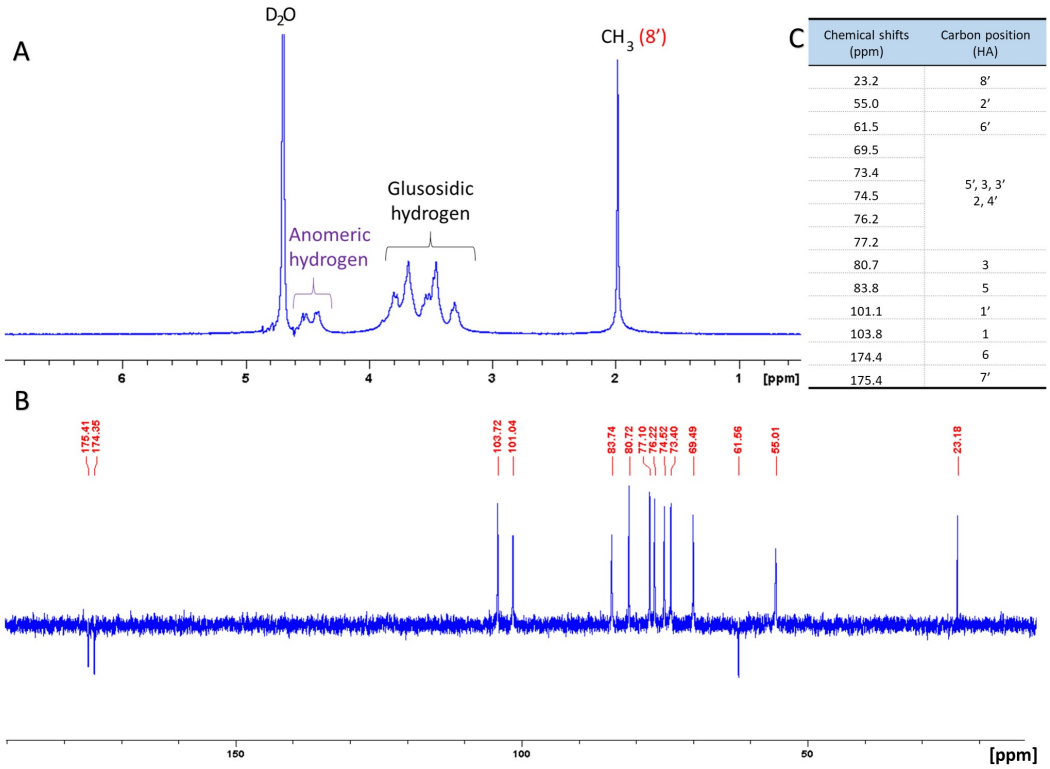

Chemical shifts (ppm)	Carbon position (HA)
23.2	8′
55.0	2′
61.5	6′
69.5	
73.4	
74.5	5′, 3, 3′ 2, 4′
76.2	
77.2	
80.7	3
83.8	5
101.1	1′
103.8	1
174.4	6
175.4	7′

Figure 2.3 – A: ^{1}H NMR spectrum of HA. B: ^{13}C NMR spectrum of HA. C: Summary of the ^{13}C chemical shifts according to the chemical structure of HA in figure 2.1.

2.2.2 Different shapes of HA-based microneedles

In order to show that HA is an easy polymer to process, different PDMS molds with different shapes were tried and the MNs morphologies were observed under a digital microscope. *The methods will be explained in section* 2.3. Figure 2.4 displayed the different obtained results . Overall, the obtained morphology was satisfying and congruent with the dimensions and shapes designed which confirms that HA is a polymer appropriate for MN production.

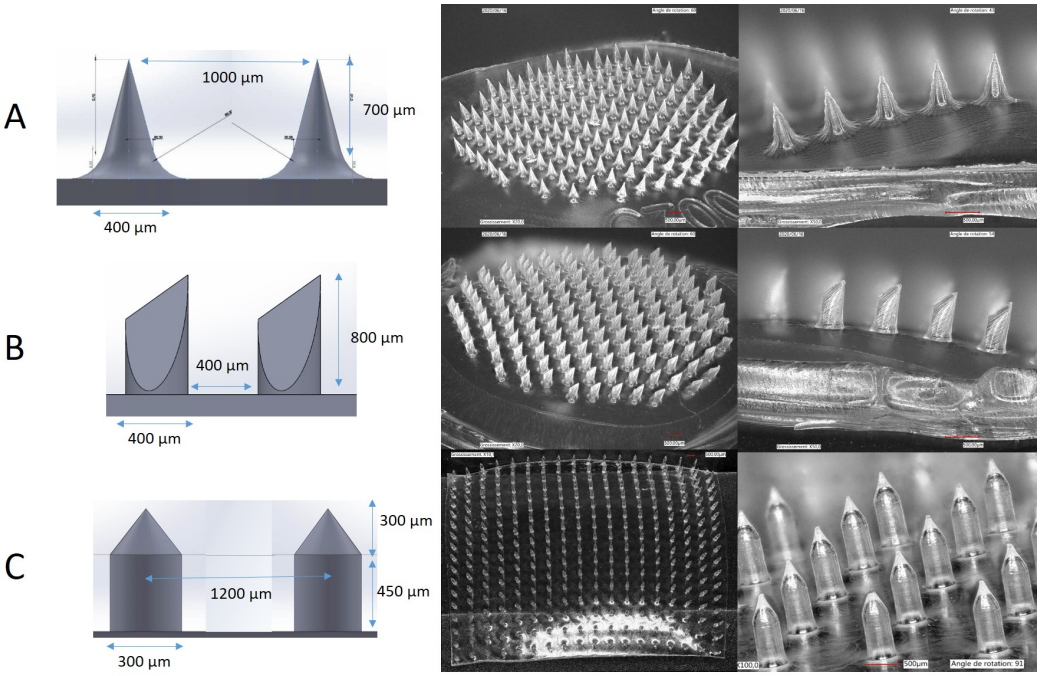

Figure 2.4 – Different shapes of HA-based microneedles (HA concentration : 5% w/w). A: Conical microneedles included in a circle shaped patch (MN number : 163. Patch surface: 2.54 cm^2). B: Beveled microneedles included on a circle shaped patch (MN number: 138 . Patch surface: 2.54 cm^2). C: "Pencil-tip" shape microneedles included on a squared shaped patch (MN number: 400. Patch surface: $20 \times 20 cm^2$).

2.2.3 Dissolution rate according to the Mw and the concentration

In order to evaluate approximately the polymer dissolution expected during skin insertion we performed a preliminary test with a phantom skin. According to Chen et al. in [27], a phantom skin was prepared by mixing 24 g of gelatin (Fluka, Millipore) and 1 g of agar (Fluka, Millipore) in 100 mL of deionized water. The mixture was microwave heated for 30 s and poured into a Petri dish of 15 cm diameter and dried at room temperature ($\approx 20\,°C$) overnight. Then the patches were inserted into the phantom skin and removed after different time periods to evaluate the dissolution rate. The patches were further observed under digital microscope to evaluate the dissolution by looking at the loss in MN height. The results are displayed in figures 2.5a and 2.5b.

Molecular weight	Concentration (%)	Microneedles height (µm)	Microscopy images		
			t = 0 s	t = 15 s	t = 30 s
Low	5	400	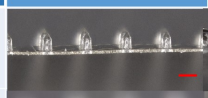	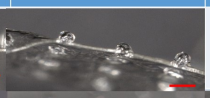	Full dissolution
	10	400		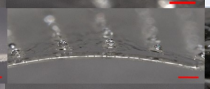	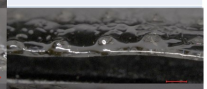
	15	400			
	20	400	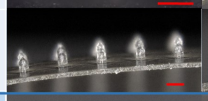	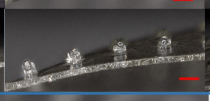	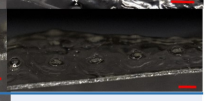
	5	750	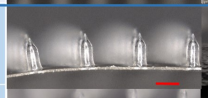	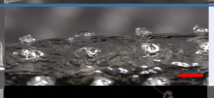	Full dissolution
	10	750			
	15	750			
	20	750		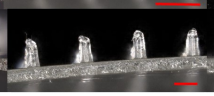	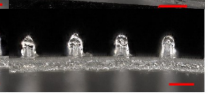

(a) Representative microscopic images of low HA ($(5.50 \pm 0.04) \times 10^4$ g mol^{-1}) at different concentrations : 5 %, 10 %, 15 %, and 20 % (w/v) before application on the skin phantom (0 s) and after 15 s or 30 s dissolution in phantom skin. Two MN heights were also investigated.

Molecular weight	Concentration (%)	Microneedles height (µm)	Microscopy images		
			t = 0 s	t = 15 s	t = 30 s
High	5	750	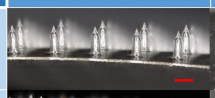		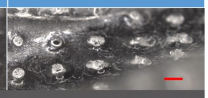
	10	750			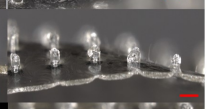
	15	750		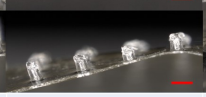	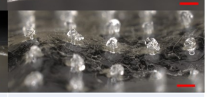
	20	750	Solution too viscous to produce microneedles		

(b) Representative microscopic images of high HA ($(2.43 \pm 0.01) \times 10^5$ g mol^{-1}) at different concentrations : 5 %, 10 %, 15 %, and 20 % (w/v) before application on the skin phantom (0 s) and after 15 s or 30 s dissolution in phantom skin. Only the dissolution of MNs with a height of 750 µm were evaluated.

.

Figure 2.5 – HA molecular weight and concentration: Effects on dissolution time of microneedles in a phantom skin.

Since the phantom skins were prepared in water, HA-based MN dissolved very rapidly during insertion assay. This skin reproduction does not mimic precisely the dissolution kinetics that could occur in human skin as the water content is much higher in the phantom skin. Nevertheless, it was observed that when the concentration was increased the dissolution rate became slower. Similarly and by comparing figures 2.5a and 2.5b when the Mw was higher the dissolution was less rapid which has been already described in [96] by Leone et al. Moreover, by observing figure 2.5a, a tendency towards a more rapid dissolution when the MN height is lower was also highlighted.

Besides, for high Mw with a concentration up to 10 % the processing was difficult since the solution was highly viscous and could dry before the pouring in the PDMS mold. A progressive adding of the HA in deionized water and a strong mixing overnight were sometimes necessary to obtain a uniform solution ready to cast in PDMS molds. Despite these precautions, it has not been possible to prepare microneedles with the high HA at 20 % (w/v) because the solution was highly viscous and almost dried when we tried to fulfill the PDMS mold.

These preliminary results and the common concentration used in the literature (see table 2.2) lead us to further work with the low Mw measured at $(5.50 \pm 0.04) \times 10^4\,\mathrm{g\,mol^{-1}}$ and at a concentration of 5 % (w/v) to ensure a fast dissolution and consequently a rapid 5-ALA release into the skin.

Mw (kDa)	Concentration (% (w/w))	Type of skin	Dissolution time (min)	Ref.
< 150	4.9	*Ex vivo* human skin	10	[110]
1220	18.4	Human subjects	60	[30]
Between 1900 and 3200	3	*Ex vivo* porcine skin	8 min to dissolve 43 % of the MN array	[134]
10	30	*In vivo* mice	5 min to dissolve all MN tips	[217]
10	50	*In vivo* mice	6 min to dissolve 80 % of the MN array	[215]

Table 2.2 – Microneedles produced with different HA at various concentrations and their dissolution rate.

These preliminary tests showed that HA would be a perfect candidate to produce MNs and to deliver 5-ALA into the skin. Therefore, the second step is to produce HA-based microneedles in which 5-ALA would be embedded. This work development has been detailed in a recent article published in the *International Journal of Pharmaceutics* where the methods to produce, characterize and evaluate the potential efficacy of the MN-patch were described.

2.3 Article: A facile fabrication of dissolving microneedles containing 5-ALA.

A facile fabrication of dissolving microneedles containing 5-aminolevulinic acid.

Mathilde Champeau[a,b,*], Dorothée Jary[a], Laurent Mortier[b], Serge Mordon[b], Séverine Vignoud[a]

[a] *CEA, LETI-DTBS, 17 rue des Martyrs, Grenoble Cedex, France*
[b] *Univ. Lille, Inserm, CHU Lille, U1189 - ONCO-THAI - Assisted Laser Therapy and Immunotherapy for Oncology, F-59000 Lille, France*

Abstract

Photodynamic therapy induced by protoporphyrin IX (PpIX) is widely used to treat precancerous skin lesions. The penetration depth of the prodrug 5-aminolevulinic acid (5-ALA) using topical application is currently limited, which hampers the production of PpIX in deep seated lesions. To enhance 5-ALA delivery in deep skin layers, a soluble microneedles patch (MN-patch) containing 5-ALA has been successfully developed by using a fast solvent casting molding method which could be easily up-scaled. The shape, number and height of the needles have been designed according to the medical application and the mechanical strain necessary for skin insertion. Hyaluronic acid (HA) has been chosen as the needle materials due to its biocompatibility, fast solubility and biodegradation and was mixed with 5-ALA prior to casting. HA-based MN-patch containing 5-ALA have exhibited mechanical properties enabling a good insertion into the skin without significant damages to MN. Interactions between HA and 5-ALA were evaluated by Fourier transform infrared spectroscopy (FTIR) and carbon nuclear magnetic resonance (^{13}C NMR), stability of 5-ALA in the MN-patch was monitored by proton nuclear magnetic resonance (^{1}H NMR) and exhibited a good stability over 5 months after manufacturing. Dissolution rate of the whole patch was completed in 1 hour in *ex vivo* rat skin without cytotoxicity. Overall, the MN-patch can be a promising technique to enhance 5-ALA penetration and produce PpIX in deeper skin lesions.

Keywords: 5-aminolevulinic acid, hyaluronic acid, dissolving microneedles, solvent casting molding method, photodynamic therapy

*Corresponding author
Email address: mathilde.champeau@cea.fr (Mathilde Champeau)

Glossary

^{13}C NMR carbon nuclear magnetic resonance. 1, 7, 8, 13, 14

^{1}H NMR proton nuclear magnetic resonance. 1, 7, 10, 14

5-ALA 5-aminolevulinic acid. 1–4, 6–17, 21–24

FTIR Fourier transform infrared spectroscopy. 1, 7, 12

HA hyaluronic acid. 1, 3, 4, 6, 7, 9–15, 21, 22

MN microneedle. 2–4, 6, 7, 17

MN_l little microneedle. 4, 5, 9, 16–22, 24

MN_t tall microneedle. 4, 5, 9, 11, 17, 19–22, 24

MN-patch microneedles patch. 1, 4, 9, 11, 21, 23

PDMS polydimethylsiloxane. 4–6

PDT photodynamic therapy. 1–4, 12, 15, 24

PpIX protoporphyrin IX. 1, 2, 24

PY 2,5-pyrazinedipropionic acid. 4, 7, 8, 12, 14, 15, 22–24

RT room temperature. 3

SC *stratum corneum*. 2, 16, 24

TGA thermogravimetric analysis. 6, 11, 15

1. Introduction

Transdermal drug delivery, usually ensured by using creams, lotion or patches, offers several important advantages over traditional drug delivery methods (oral administration or injection). It indeed enables to control the amount of drug delivered at local areas, which allows to administrate lower doses [1]. A targeted drug administration also decreases undesirable side effects and increases therapeutic benefits [2]. Moreover the non-invasive nature of transdermal drug delivery allows to improve patient acceptability and compliance [3]. This way of administration is commonly used for the treatment of skin cancers by photodynamic therapy (PDT) by using creams. PDT is a treatment relying on a combination of three parameters: drug content, oxygenation rate and light irradiation intensity. 5-aminolevulinic acid (5-ALA) is widely used as a PpIX photosensitive precursor and topically applied on the skin lesions. Light irradiation at PpIX exciting wavelength combined with the presence of oxygen promotes photochemical reaction leading to cell death. Treatment efficiency is linked to different factors including drug penetration. However, drug penetration is often hampered by the *stratum corneum* (SC), which is the outer first layer of epidermis that provides a barrier to external environment and difficult to penetrate for many drugs [3]. Moreover, the physicochemical properties of 5-ALA such as its hydrophilicity or zwitterionic nature also limit its penetration, which prevents access to deep skin layers [4, 5]. These limitations make PDT unsuitable for basal cell carcinoma (superficial, nodular or infiltrative) and invasive squamous cell carcinoma that have tumor cells in deep epidermis or dermis [6, 7]. To overcome this lack of drug penetration, different (chemical or physical) strategies have been suggested [5], among which the use of microneedles (MNs) appears to be a promising technique [8–10].

MNs are assembled together to form an array or patch that enables to bypass the SC by creating holes in it, resulting in enhanced transdermal drug delivery through the created microchannels [11]. MNs have been developed with a height inferior to 900 µm in order to limit pain. Indeed, this height criterion improves patient compliance and safety since MN cannot penetrate deep vascular and nervous regions. At the same time, this height is adequate to successfully reach the dermal layers without inducing bleeding and touching active immune cells. Due to their microsize, MN cannot be seen by patients, which reduces needle phobia [12]. Although MN dimensions are in the microscale, their design with adequate materials confers them strong mechanical properties to pierce the SC, which allows the diffusion in skin tissues of hydrophilic or high molecular weight drugs [13].

Different types of MN-mediated drug delivery have been developed. Solid MNs can be inserted in the skin and then removed letting micron-scale pores in the skin surface, followed by drug formulation application. This passive diffusion of drugs requires a two-step application process, which is prone to errors in the delivered dose [14]. It also can be dangerous for the patient itself since materials used to produce solid MNs such as silicon have dubious biocompatibility and can break, which could lead to complications [15, 16]. To avoid the two-step application, drugs have been coated on solid MNs. Nevertheless, the drugs were rapidly delivered in small quantity ($\leq 2\,\mathrm{mg}$) [11, 17, 18] and the risk of broken materials was still present. Hollow MNs are another type of MN whose principle is based on hypodermic needles. Such MNs could avoid the two-step process and deliver a large drug amount but due to their micro size they may become blocked by compressed dermal tissue when inserted into the skin [11].

Recently, dissolving MNs have been attracting attention for drug delivery since they allow to get rid of the aforementioned issues. The principle is that a drug is encapsulated in the needle matrix that is biocompatible, soluble and mechanically robust. When inserted in the skin, this matrix is dissolved by body fluids and delivers the drug with a controlled kinetic profile depending on the chosen matrix. Materials used as matrix are often polymers, such as carbohydrates [19, 20] or other bio-sourced components [16]. Polymers such as polyvinylpyrrolidone [21] or carboxymethylcellulose [20, 22] allow a rapid dissolution ($\leq 5\,\mathrm{min}$ or $\leq 20\,\mathrm{min}$, respectively) whereas polylactic acid or poly(lactic-co-glycolic acid) are biodegraded in a few days [23, 24]. Because the drug is embedded in the polymer matrix, the fabrication process must be soft to ensure drug stability and avoid as much as possible the use of organic solvents.

Hyaluronic acid (HA) is a polysaccharide that can be shape-molded and stored at room temperature (RT). HA is a component naturally present in the human body, widely distributed in body tissues, intracellular fluids and well excreted by different organs ; it is a polymer fully biocompatible and already used in many medical fields [25]. Moreover, this is a water soluble polymer that can be dissolved after skin contact in a few minutes ($\leq 10\,\mathrm{min}$) [26, 27]. These characteristics make it a good candidate to produce dissolving MNs to transport 5-ALA.

In the present study, we aimed at exploring the processing and the properties of HA-MN with 5-ALA embedded in the polymer matrix. 5-ALA was embedded only in one easy step, in the whole patch including the basis without MN. The aim was to deliver 5-ALA from the top of the skin to the deeper skin lesions to allow PDT treatment on the whole damaged skin volume. Since 5-ALA and HA were mixed together, interactions between the polymer and the drug was carefully studied and 5-ALA stability was investigated for different time periods. Furthermore,

microneedles shape was designed as a "pencil-tip" to confer them strong mechanical properties to penetrate the cutaneous lesions. As all basal cell carcinomas do not extend to the same depth, different heights of needles were processed and characterized. Moreover MN-patch could be loaded with large different amounts of 5-ALA which offer different dosages. The characteristics of the MN-patch (compression, insertion tests, dissolution rate) have been conducted to evaluate whether this strategy is a promising approach to enhance PDT outcomes on deep skin cancers.

2. Materials and methods

2.1. Chemicals

5-ALA hydrochloride salt (GMP grade) was purchased from Biosynth Chemistry & Biology. Polydimethylsiloxane (PDMS) (Sylgard , Dow Corning), potassium phtalate monobasic (KHP, TraceCERT®), Dulbecco's modified eagle medium (DMEM), penicillin streptomycin solution (Pen Strep) and the cell proliferation reagent WST-1 were obtained from Sigma-Aldrich Chemical Co. HA with a molecular weight (MW) of $(5.50 \pm 0.04) \times 10^4\,\mathrm{g\,mol^{-1}}$ was purchased from Contipro France. 2,5-pyrazinedipropionic acid (PY) was purchased from Carbosynth Product. All other chemicals were of analytical reagent grade.

2.2. Fabrication of HA microneedles patches

Soluble HA microneedles were fabricated by solvent casting molding method. This technique consists of using an aluminium master structure to obtain a PDMS mold from which dissolvable polymer microneedle replicates are formed. The overall steps of the preparation of dissolving microneedles are displayed in scheme 1.

- **Aluminum master structure**

  An array of 20×20 MN was machined on an aluminium surface of $25 \times 25\,\mathrm{mm^2}$. MN design is similar to a pencil-tip: a conical tip sits on top of a cylinder body. Two types of MN were designed: a tall one (MN_t) and a little one (MN_l). For the tall microneedle patch, the height was 750 µm ($height_{tip} = 300$ µm and $height_{body} = 450$ µm), the base diameter was 300 µm and each MN was tip-spaced with 1200 µm. For the little microneedle patch, the height was 400 µm ($height_{tip} = 150$ µm and $height_{body} = 250$ µm), base diameter was 300 µm and each MN was tip-spaced with 1200 µm.

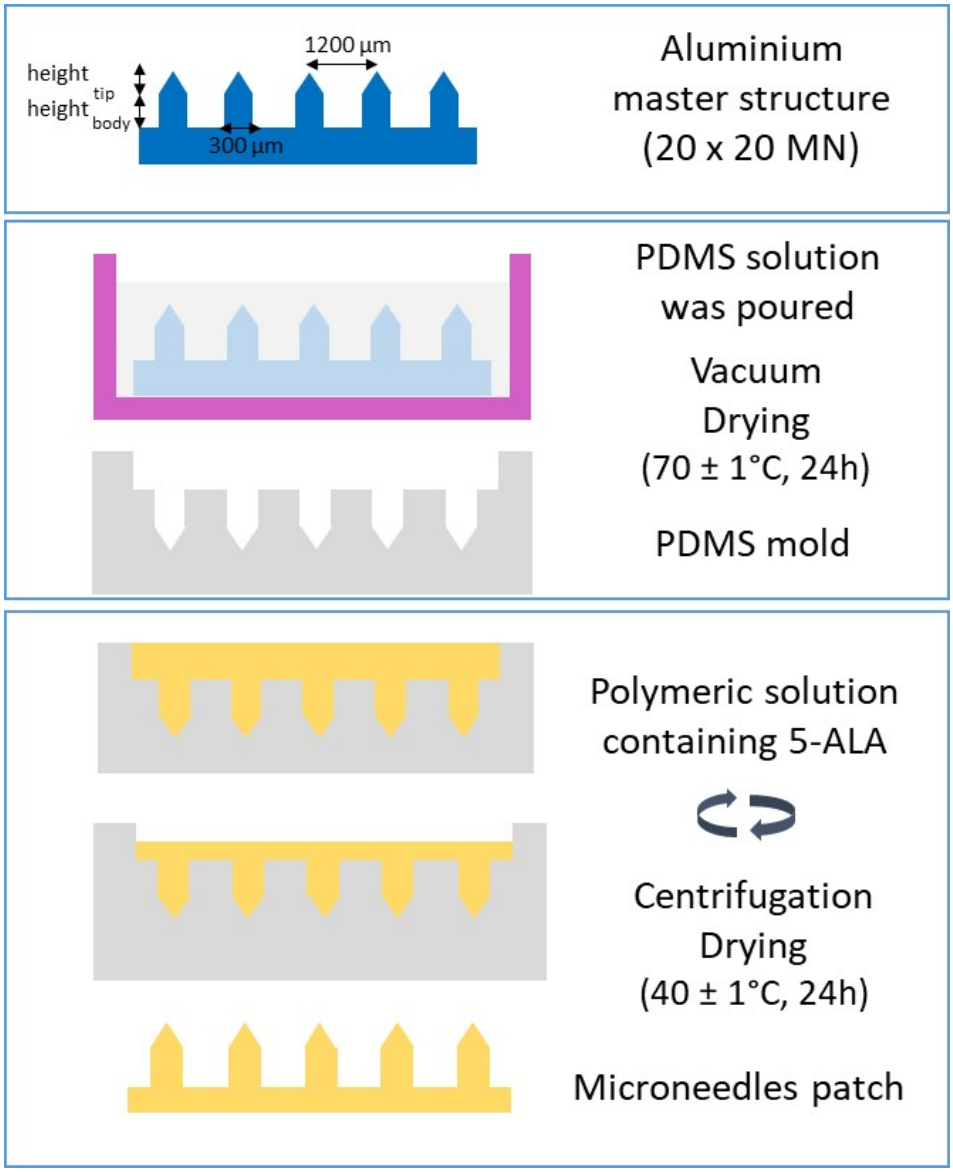

Scheme 1: Preparation of the MN-patch by solvent casting molding method. Three major steps are essential: aluminium master structure design, fabrication of PDMS mold and casting of the solution in the mold. Two heights were designed for the aluminium master structure: a tall one MN_t at 750 µm and a little one MN_l at 400 µm.

- **PDMS mold**

  A PDMS solution (10% reticulated) was poured on the master structure tipped up, then vacuum was applied and PDMS was dried at (70 ± 1) °C for 24 h.

- **Molding of HA microneedles**

  A HA solution ($50\,mg\,mL^{-1}$) was prepared by vigorous mixing in distilled water and different amounts of 5-ALA were added to the solution leading to final concentrations of 0, 10 or $50\,mg\,mL^{-1}$. 200 µL of HCl at $0.03\,mol\,L^{-1}$ were added to the solution in order to be at *pH* of 5 and ensure 5-ALA stability. A solution amount of 2.0 mL was casted in the PDMS mold. The mold was centrifugated at 21 °C and 4000 rpm for 35 min to ensure a complete filling of the cavities. Then it was placed in an oven at (40 ± 1) °C for 24 h, after which the HA microneedle patch was gently removed from the mold. Each patch is expected to contain 100 mg of HA and 0 mg (MN-0), 20 mg (MN-20) or 100 mg (MN-100) of 5-ALA.

2.3. Characterization of 5-ALA-MN-patch

2.3.1. Microscopic analysis of HA microneedle arrays

A digital microscope (VHX 8000, Keyence) was used to observe the morphology (height, tip diameter, width of base) of microneedle patch under normal light. Microneedles heights were analyzed with the ImageJ software.

2.3.2. Mechanical properties

To determine the loss in height of MN when compressed at a precise force, a texturometer (TA.XT Plus, Stable micro systems, UK) was used. The MN array was placed on the metal platflorm and an axial compression force was applied with the probe. The MN array was pressed at a rate of $0.5\,mm\,s^{-1}$ with a force ranging from 0 N per needle to 0.5 N per needle for 10 s. Pre-test and post-test speed were of $5\,mm\,s^{-1}$, and the trigger force was set at 0.01 N. The patch was then observed under digital microscope and measurements were performed with the ImageJ software.

2.3.3. Water content in the microneedle patch

To evaluate the residual water content in the microneedle patch, thermogravimetric analysis (TGA) was performed at a heating rate of 5 °C/min on a TGA Q5000 from TA Instruments and TA universal analysis was the software used.

2.4. Drug stability in the MN patch

2.4.1. Chemical stability of 5-ALA by quantitative proton nuclear magnetic resonance (^1H NMR)

To evaluate the amount of 5-ALA in the MN-patch, potassium phthalate monobasic (KHP) was added as an internal standard. A solution of KHP was prepared at $10\,mg\,mL^{-1}$ in D_2O.

For analysis, a small amount of the MN-patch (approximately 10 mg) was dissolved in 650 µL of D_2O and 50 µL of the KHP solution was added. Then proton nuclear magnetic resonance spectra were recorded using a Bruker Spectrospin spectrometer operating at 300 MHz and 295 K. The TopSpin software was used to analyze the spectra. The content of 5-ALA was calculated using one of the signals of the internal KHP standard and one of the signals of the analyte as presented in equation 1, where x represents the analyte 5-ALA, NH_{KHP} is the number of protons of KHP (2), NH_x is the number of protons of 5-ALA (2), m_{KHP} is the weighted amount of standard material potassium phthalate monobasic, Mw_x is the molar weight of 5-ALA (131.13 g mol^{-1}), Mw_{KHP} is the molar weight of KHP (204.22 g mol^{-1}), A_x is the integral between 4.0 and 4.15 ppm and A_{KHP} is the integral between 7.45 and 7.6 ppm.

$$m_x = \frac{NH_{\mathrm{KHP}} \times m_{\mathrm{KHP}} \times Mw_x \times A_x}{NH_x \times Mw_{\mathrm{KHP}} \times A_{\mathrm{KHP}}} \tag{1}$$

The same equation 1 was also used to quantify the amount of the degradation product of 5-ALA, which is 2,5-pyrazinedipropionic acid (PY). When the analyte is PY, NH_x is equal to 2, Mw_x is 224.21 g mol^{-1} and A_x is the integral between 8.35 and 8.45 ppm.

The weight percentages of 5-ALA and PY were then obtained according to equations 2 and 3, respectively, where m_{5-ALA} and m_{PY} are calculated by equation 1 and m_{tot} corresponds to the mass of the MN-patch (either MN-20 or MN-100) used for the analysis.

$$w_{5-ALA} = \frac{m_{5-ALA}}{m_{tot}} \tag{2}$$

$$w_{PY} = \frac{m_{PY}}{m_{tot}} \tag{3}$$

2.4.2. Interactions between drug and polymer followed by FTIR and ^{13}C NMR

Molecular interactions between 5-ALA and HA in the MN-patch were studied with ATR-FTIR. FTIR spectra of the MN patch were performed using a spectrometer IRAffinity-1, MIracle-10 from Shimadzu in the wave number range from 500 to 5000 cm^{-1} with a resolution of 4 cm^{-1}. Samples were directly placed on the crystal surface and scanned 32 times per analysis.

To determine the chemical structure of hyaluronic acid, analysis of the ^{13}C nucleus present in the compound was studied by ^{13}C NMR spectroscopy. Approximately ten milligrams of HA was dissolved in 700 µL of D_2O. A DEPT-Q (Distorsionless enhancement by polarization transfer including the detection of quaternary nuclei) sequence was performed to complete carbon

assignments using a Bruker Spectrospin spectrometer operating at 75 MHz, 355 K and using a 5 mm QNP probe.

2.5. Penetration and dissolution of the microneedles patch

2.5.1. Skin model

As an alternative to biological tissue, a modeling clay (Plastiline ®, composed of kaolin, sulfur and glycerine) was spread to obtain a thickness of 2 cm and used as a skin model regarding mechanical properties. Microneedle patches (MN-0, MN-20 and MN-100) were inserted in this phantom skin by thumb pressure that is estimated to be at 0.17 N/needle (measurement performed with the texturometer) and then was removed. The skin model was observed with a digital microscope to evaluate the penetration profile and depth.

2.5.2. Ex vivo rat skin

Ex vivo rat skin was streched and fixed with pins on a polystyrene plate. MN-patches were inserted in the *ex vivo* rat skin by thumb pressure. The pressure was kept constant for 10 sec. Then the MN-patch was kept inserted in the skin for a precise amount of time (from 5 min to 45 min) with the help of an occlusive tape (Tegaderm™, 3M). After MN-patch removal, the skin was observed in top view and then it was embedded in tissue freezing medium (TFM, M-M FRANCE). As for the MN-patch, it was kept in a dry Petri dish until microscope analysis was carried out to quantify the dissolution kinetics.

2.6. Drug release measurements

Petri dishes (surface: 9.6 cm^2) were filled with 750 µL of water acidified with HCl to obtain a pH of 5. Therefore, a thin water layer (< 1 mm) was present in all the Petri dishes. Then MN-patches loaded with 5-ALA, either MN-20 or MN-100, were placed needles down into the Petri dishes and slightly agitated at 75 rpm. At predetermined time points, the solution was collected for analysis and replaced by a same volume of fresh water at $pH5$. The amount of solution removed was freeze dried for 72 h and then dispersed in D_2O for quantifying released 5-ALA by ^{1}H NMR according to the previous equations hereinbelow. The experiments were conducted in triplicate.

2.7. In vitro cytotoxicity study

The cytotoxicity of MN-patches as well as individual products, 5-ALA, 5-ALA-free patches (MN-0) and product of 5-ALA biodegradation (PY), was assessed. To this end, the patches

or pure chemicals were dissolved in cell culture media. After 24 h of preincubation of the cells (NIH3T3 murine fibroblats cells, $4 \times 10^3 cells/well$) in DMEM containing 10 % of new born calf serum and 1 % of Pen Strep, the medium was replaced by one containing the different tested products followed by a new incubation of 24 h at 37 °C. The WST-1 reagent was then added. After 2 h at 37 °C, absorbance at 450 nm was recorded using a microplate reader (Infinite M1000, Tecan). The absorbance was linked to the metabolic activity of cell mitochondria and the density of living cells (DLC) was calculated as mentioned in equation 4, where AS, APC and ANC respectively represent the absorbances of the sample, the positive control and the negative control, the negative control being cells growing in the culture media without any added product and the positive control being cells growing in the cell culture media containing H_2O_2 at 0.01 mol L^{-1}.

$$DLC = \frac{AS - APC}{ANC - APC} \times 100 \tag{4}$$

3. Results and discussion

3.1. Microneedle preparation and characterizations

Tall microneedle (MN_t) and little microneedle (MN_l) were successfully produced with expected dimensions using the solvent casting molding method as displayed in figure 1. The heights of the MN_t and MN_l microneedles were respectively 749 ± 6 µm and 390 ± 7 µm and the base diameter was 285 ± 10 µm which corresponds well to the original master structure dimensions. The slight difference in microneedle height (respectively 0.13 % and 2.5 % for MN_t and MN_l) and diameter (5 %) might be explained by the retraction of the HA matrix during the drying process. Mönkäre et al. also reported a height reduction of 6.6 % when they developed immunoglobulinG-loaded hyaluronan-based dissolving microneedles by solvent casting molding method and they explained it by the shrinking of the HA during drying process [27]. Similarly Zhao et al. fabricated 5-ALA-loaded dissolving microneedles made of HA and attribute the 9.3 % reduction in height to water evaporation during drying process [28] which could consequently induce polymer shrinkage.

Drug distribution was expected to be homogeneous as the solution containing 5-ALA and HA was homogeneous before pouring. Indeed, a uniform pale yellow color could be observed from the tip to the base of the MN-patch containing 5-ALA (Figure 1, right). However, crystallization or precipitation of 5-ALA could have taken place during drying, leading to inhomogeneous drug

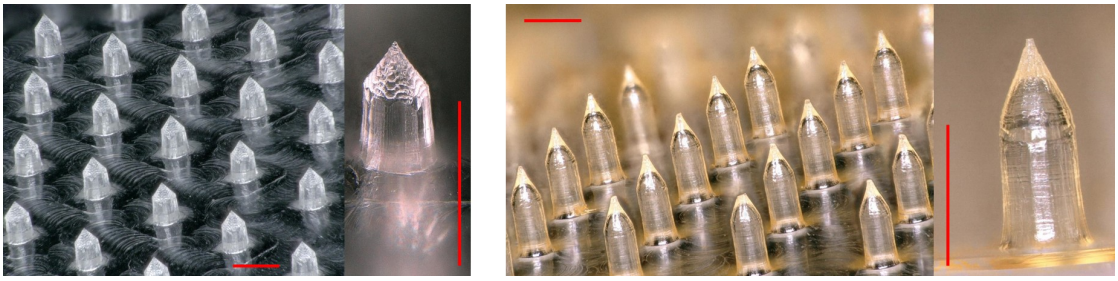

Figure 1: Digital microscopy images of MN-patch fabricated by solvent casting molding method. (Left: MN_l-*0*, right: MN_t-*20*.) Scale bars represent 500 µm.

distribution. Consequently analysis of 9 different parts of the patch was performed in order to quantify drug content in each part. Each piece was analyzed by ^{1}H NMR (Figure 2) and the percentage of 5-ALA was calculated according to ^{1}H NMR equations (Eq 1 and Eq 2).

The theoretical values for the 5-ALA relative weight percentage, considering only dry matters, are respectively equal to 17 %(w/w) and 50 %(w/w) for MN-20 and MN-100. Taking into account the residual water, a lower 5-ALA absolute weight percentage is expected. Indeed, the results presented in figure 3 show that the absolute percentage of 5-ALA was of 10.0 %(w/w) and 31.2 %(w/w) for MN-20 and MN-100, with low intra and inter patches standard deviations ($< 2\%$ (w/w)) demonstrating the homogeneous distribution of the drug. For the MN-20 patch, the content in water was evaluated at 14 %(w/w) by TGA corresponding to a drop of the 5-ALA weight percentage from 17 %(w/w) to 14 %(w/w), which is in good agreement with the obtained value of 10.0 %(w/w) taking into account all the experimental errors.

The process investigated in this study allows to produce reproducible MN-patches with precise amount of drug homogeneously distributed in the whole patch. Moreover, the amount of 5-ALA loaded in the MN-patch was a thousand times more important than previous studies lead by Zhao et al. or Zhu et al. since both authors only added 5-ALA in the tips of the HA-microneedles and not in the whole needle [28, 29]. Therefore they were forced to process the microneedles in several steps whereas performing a unique easy solvent casting method as presented in section 2.2 simplifies the process which would be an important asset for industrialization. Even when the active component is mixed with the polymer solution, several steps may be involved. It was the case for Mönkäre et al. that applied vacuum prior to centrifugation to produce IgG-loaded hyaluronan-based dissolving microneedles[27]. For the MN-patches developed in this study, centrifugation was sufficient to ensure the complete filling of all microneedle tips as the poured solution at a low HA concentration (50 mg mL^{-1}) had a moderate viscosity with a shear

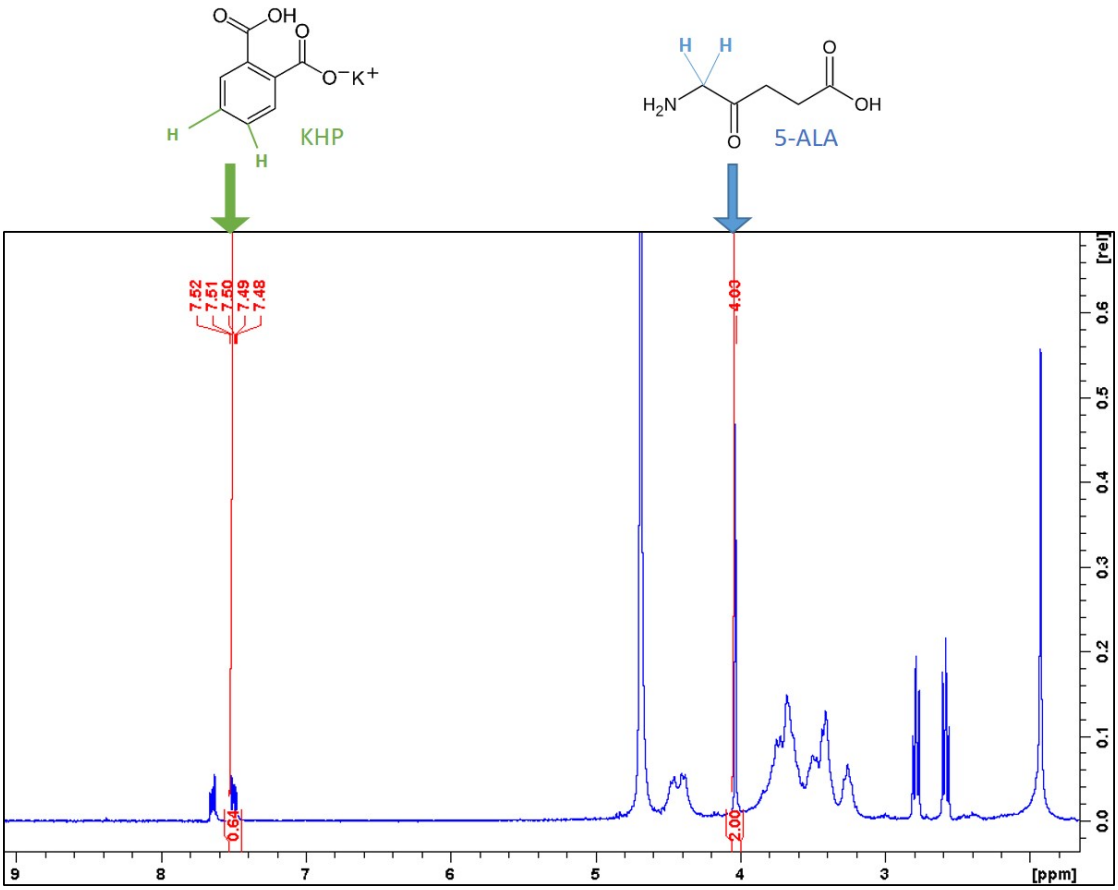

Figure 2: ^{1}H NMR spectrum of a piece of MN-20. The integration value of the singlet of 5-ALA at 4.04 ppm was for 2 protons and the integration value of the multiplet of KHP between 7.4 and 7.5 ppm was for 0.64 protons. The others peaks between 2 and 6 ppm are characteristics either of 5-ALA or HA.

viscosity measured at 0.05 Pa s (shear rate: 50 s^{-1}).

3.2. 5-ALA stability in the MN-patch

To ensure a long drug stability, special care was taken by controlling the temperature, the pH and the 5-ALA concentration because these three parameters are considered to be the most influencing for respecting 5-ALA stability [5]. Indeed, 5-ALA is known to be unstable and dimerize in PY, constituting the major degradation product. This is usually a problematic aspect in the design of drug delivery systems intended for photodynamic therapy [30].

According to previous studies led by De Blois et al., the risk of 5-ALA to dimerize is reduced when the temperature is decreased to 21 °C [31]. The authors modelled the degradation rate of 5-ALA as a second order reaction kinetics and an Arrhenius plot allowed to determine the half

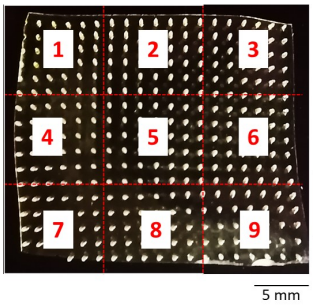

		MN-20				MN-100			
		Sample 1 (n=9)	Sample 2 (n=9)	Sample 3 (n=9)	All samples (n=27)	Sample 1 (n=9)	Sample 2 (n=9)	Sample 3 (n=9)	All samples (n=27)
Weight percentage (% w/w)	Mean	10.4	9.6	10.0	10.0	30.3	30.8	32.8	31.2
	SD	0.4	0.8	0.9	0.8	1.5	1.7	1.1	1.8

Figure 3: A: photograph of the MN_t-20 patch, the dotted lines represent the different parts of the patch to evaluate the percentage of 5-ALA in each samples numeroted from 1 to 9. B: table summarizing the weight percentages of 5-ALA in the MN-20 and MN-100 patches. Experiments were repeated three times. Results are presented as mean value ± standard deviation.

time[1] of 5-ALA at different temperatures for a solution at $7.6 \times 10^{-3}\,\mathrm{mol\,L^{-1}}$ and pH 5. At the beginning of the solvent casting molding process, 5-ALA is contained in a polymeric solution and poured in the PDMS mold. At the initial 5-ALA concentration of $7.6 \times 10^{-2}\,\mathrm{mol\,L^{-1}}$ for MN-20 and $0.38\,\mathrm{mol\,L^{-1}}$ for MN-100, by extending the De Blois et al. model, the half times were estimated at 40 days and 8 days for MN-20 and MN-100. During the drying process, for example after 85 % of water evaporation, the concentrations will be more elevated and were estimated for MN-20 and MN-100 at $0.51\,\mathrm{mol\,L^{-1}}$ and $2.55\,\mathrm{mol\,L^{-1}}$ which lead to predicted half lifes respectively equal to 6 days and 28 hours. Since the drying step was set at 40 °C for 24 hours, 5-ALA should stay stable in MN-20 but a slight degradation might occur in MN-100.

The second parameter that has been adjusted in order to optimize 5-ALA bioavaibility, was the pH, as it is known that 5-ALA is degraded at pH higher than 5 [32]. Since human skin pH is estimated on average at 5 [33], pH 5 has been defined as the optimal value for 5-ALA MN-patch preparation that should not induce skin disorders or irritation when the MN-patch will dissolve [34]. This pH value was adjusted by addition of HCl, with a final concentration of $3\,\mathrm{mmol\,L^{-1}}$.

The third parameter to adjust is the 5-ALA concentration that is required to be kept as low as possible to ensure its stability [35]. Nevertheless, due to the final application in PDT requiring high doses of drug [2], two high contents of 5-ALA in MN-patches were evaluated (20 mg to 100 mg per patch).

First, the presence of 5-ALA in the MN-patch prepared with a pH solution at 5 and a drying

[1] Half-life can be defined as the time where the 5-ALA concentration reduced to half of its original value.
[2] The conventional PDT treatment using the prodrug in a Metvixia® cream advise to administrate ≈ 80 mg.

temperature of 40 °C was confirmed by FTIR. Figure 4 shows the IR spectra of MN-20 and MN-100 compared with those of HA and 5-ALA alone. On the four spectra, the bands observed between 3200-3600, 2850-3000 and 1550-1650 cm^{-1} were assigned to vibration of OH, CH_2 and primary NH_2 respectively. The bands at 1730 cm^{-1} and at 1600 cm^{-1} correspond respectively to the carbonyl groups of 5-ALA and the amid group of HA [36, 37]. These two bands appear in MN-20 spectra and are more intense in the MN-100 sample which evidenced the presence of the two compounds in the final material. The band relative to primary amino group is also present in the MN-20 and MN-100 spectra, which confirms the presence of 5-ALA in the patch. MN-20 and MN-100 spectra do not present new large peaks which might suggest that there is no covalent bonds between 5-ALA and HA. Nevertheless, this spectra cannot show that no chemical reaction occurred between the HA polymer and the 5-ALA prodrug. Even if unexpected, since the MN-patch preparation was performed at low temperature (40 °C) without the presence of a coupling agent [38], a reaction between the HA carboxyl group might occur with the amino group present on the 5-ALA to form an amido compound. Infrared spectroscopy correlation table indicates that the characteristic absorption peaks of the amido-group are between 3050-3500 cm^{-1} (2 large bands), 1630-1710 cm^{-1} for respectively the vibration of N-H and C=O. Therefore these bands are potentially covered by the HA signal and results of figure 4 cannot strictly confirm that no covalent groups were created.

To further verify that HA was not modified because of 5-ALA, ^{13}C NMR was performed. As presented in figure 5, all the characteristic peaks of HA were present in the HA that has been in contact with 5-ALA and correspond to the one reported in literature [39, 40]. Some slight shifts (inferior to 1 ppm) may be observed but they have been previously described as conformational rearrangements due to hydrogen bonds [41, 42]. Except at 28 ppm where a low intensity peak was observed due to an impurity, no other peaks were detectable. Consequently, this experiment demonstrate that no covalent bonding was created between 5-ALA and HA. Furthermore the filtrate of the MN-patch isolated with 10 kDa Amicon® Ultra Centrifugal Filters was analysed by ^1H NMR and only evidenced the presence of 5-ALA with a spectrum similar to pure 5-ALA.

Once no interaction between 5-ALA and HA was proven, the 5-ALA stability was studied. Initially, 5-ALA and PY were separately dissolved in D_2O and figure 6 summarizes the data derived from their ^1H NMR analysis. The chemical shifts presented were close to those reported in the literature [30, 32, 43]. PY spectrum shows a singlet signal for the aromatic proton (a) at 8.4 ppm and two triplet signals at 3.1 and 2.8 ppm characterising CH_2 groups (b and c) from the propionic acid chains. 5-ALA spectrum shows a singlet signal for the CH_2 (x) groups at 4.1

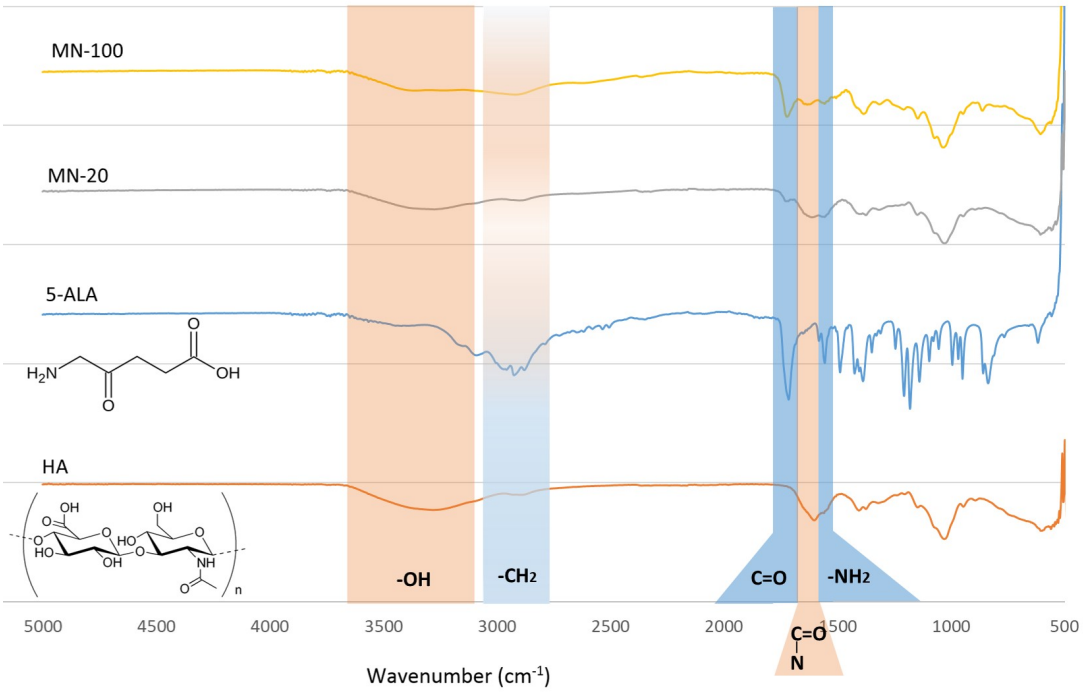

Figure 4: IR spectra of 5-ALA, HA and the microneedle patches MN-20 and MN-100. Blue strips correspond to 5-ALA signature bands and orange strips to HA signature bands.

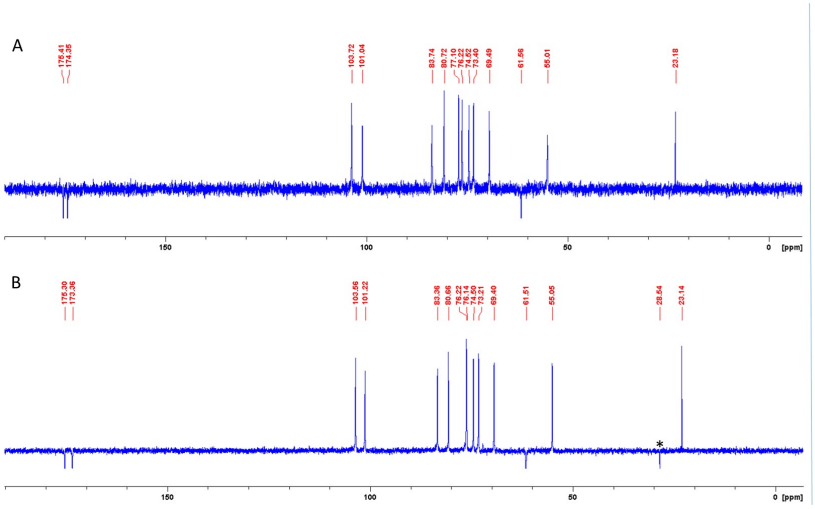

Chemical shifts (ppm)	Carbon position (HA)
23.2	8′
55.0	2′
61.5	6′
69.5	5′, 3, 3′ 2, 4′
73.4	
74.5	
76.2	
77.2	
80.7	3
83.8	5
101.1	1′
103.8	1
174.4	6
175.4	7′

Figure 5: A: ^{13}C NMR spectrum of MN-0 (HA only). B: HA from MN-20 was isolated with 10 kDa Amicon® Ultra Centrifugal Filters, analyzed by ^{13}C NMR and compared to the one above. C / CH_2 are down and CH / CH_3 are up on the spectrum. C: Structure of HA and summary of the ^{13}C chemical shifts (parts per million).

ppm and two other triplet signals at 2.8 and 2.6 ppm characterizing CH_2 groups (y and z) from the carboxylic acid chain. When 5-ALA and PY are mixed together and analyzed by ^{1}H NMR the PY triplet signals (b and c) and the 5-ALA triplet signals (y and z) overlap. Only the two singlet signals for the aromatic protons (a) at 8.4 ppm and for the CH_2 (x) groups at 4.1 ppm were still well defined and will be used to quantify the weight percentage of 5-ALA and PY (see equations 1, 2 and 3). No other peaks appears when HA and 5-ALA were mixed together.

Carbon position (PY)	Chemical shifts (ppm)	Multiplet
a	8.4	Single
b	3.1	Triple
c	2.8	Triple

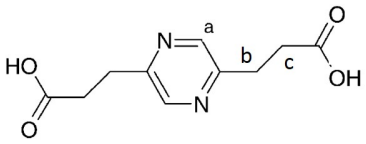

Carbon position (5-ALA)	Chemical shifts (ppm)	Multiplet
x	4.1	Single
y	2.8	Triple
z	2.6	Triple

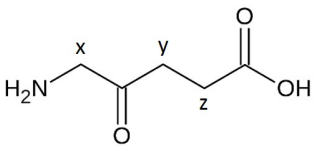

Figure 6: Structure of 2,5-pyrazinedipropionic acid and 5-aminolevulinic acid and summary of ^{1}H chemical shifts (parts per million)

Figure 7 displays the stability of 5-ALA in the MN-20 patch when stored in hermetic box, containing a desiccant bag, without air at 20 °C and sheltered from light. The weight percentage of 5-ALA evolved from about 10 %(w/w) to 7 %(w/w) in 145 days. This evolution seems not significant and may be partially due to a slight increase in water content in the MN-20 patch. Indeed TGA experiments showed that the water content was 15 %(w/w) after 145 days whereas it was 14 %(w/w) at day 1. The adsorption of H_2O molecules on the microneedles patch may increase the global mass of the patch (m_{tot}) and could affect the absolute weight percentage of 5-ALA according to equation 2 which could explain a 1 % slight decrease. Overall, this mean value of 7 %(w/w) stays in a satisfactory experimental range and evidences a very good stability of 5-ALA in the MN-20 patch over 5 months.

On the other hand, there was no degradation of 5-ALA in PY higher than 1 %(w/w) until the 145^{th} day. A very limited degradation below 1% during this period is considered as a very encouraging result. Further optimization of storing conditions could be undertaken in order to decrease this degradation level. Indeed, PY is a compound with unknown toxicity and scant information concerning its effect during PDT is available. Its presence should then be kept to

a minimum [44] by avoiding 5-ALA degradation, which should guarantee a safe and successful PDT treatment [30].

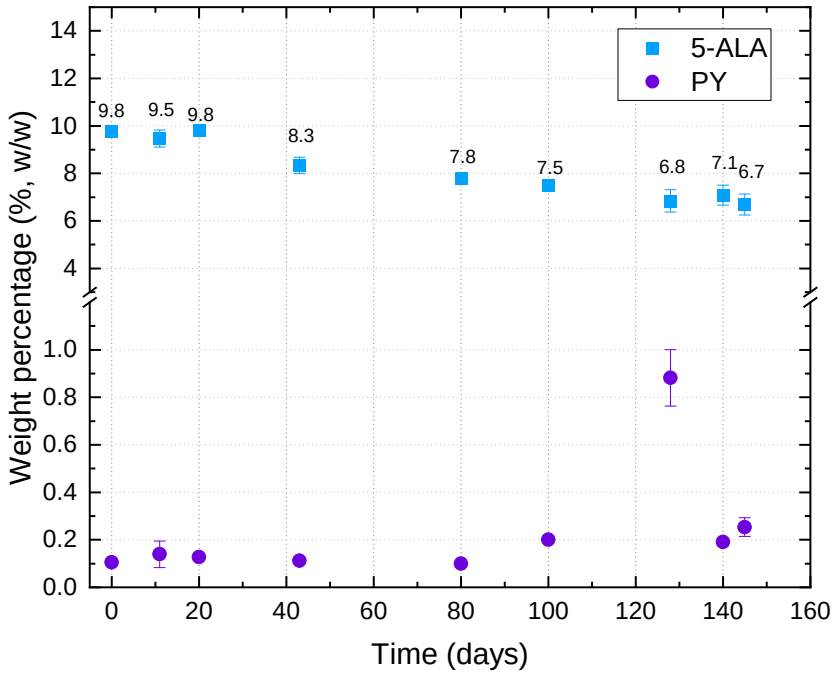

Figure 7: Stability of 5-ALA in the MN-20 patch. Analyses were performed in triplicate. Results are presented as mean value ± standard deviation.

Although, all the parameters responsible of 5-ALA stability were not optimized as much as possible, the stability results (figure 7) were satisfactory since they were higher than those expected regarding previous results reported in the literature [30–32].

3.3. MN-patch mechanical properties: compression and insertion

3.3.1. Morphology and compression mechanical properties

Prior to biological validations by inserting the patch in skin models or animals skin, it was necessary to control whether the MN-patch had sufficient mechanical properties to pierce the *stratum corneum* without microneedles fracture, bending or height reduction.

Mechanical compression tests were performed to evaluate the MN-patch mechanical strength and results for the MN_l are displayed in figure 8. There was no significant deformation or fracture

when the compression force applied was below 0.5 N/needle. The loading at 20 or 100 mg in the MN_l-patch did not affect the mechanical behaviour. A slight height reduction (about 50 µm) could be observed for the MN_l-*0*, MN_l-*20* or MN_l-*100* when the force compression applied was equal to 0.5 N/needle. It represents a loss in height of 12.5 %. Almost the same behaviour was observed for the MN_t-*0* and MN_t-*20* (*results not shown*) since the loss in height do not exceed 7 % even at 0.5 N/needle. For the MN_t-*100* at 0.3N/needle and 0.5 N/needle, the loss in height were higher and reached 17 % and 53 %. Nevertheless, the insertion force in the skin was measured with the texturometer and estimated at 0.17 N/needle which insure that insertion could occur without microneedle bending or breaking. The performances of all our needles except MN_t-*100* were comparable or even better than the previous reported one indicating a height reduction of ALA-loaded HA microneedle patch (initial height: 900 µm) of almost 200 µm for a compression force applied of 0.5 N/needle, which corresponds to a loss in height of 22 % [28]. Furthermore, the important height reduction observed for the MN_t-*100* might be explained by Zhu et al. work, indicating that the decrease of polymer interactions is due to 5-ALA small molecules that insert between the polymer chains. Consequently, the Young's modulus is decreased and the microneedle become more deformable [29].

In order to gather all required properties for the intended application, the shape of microneedle has been designed in order to reach sufficient mechanical strength for skin insertion, and optimal height for therapeutic indication. To this end, the morphology of the MN-patch developed here consists in a "pencil-tip" shape (Figure 1) that presents an aspect ratio for the MN_t and MN_l respectively equal to 5:2 and 4:3 that should be sufficient to pierce and facilitate insertion in the skin [20, 45]. Indeed, the aspect ratio recommended for clinical use by Gittard et al. was 2:1 as it exhibits high mechanical strength and no difficulty for penetration. Nevertheless, this value is only an arbitrary recommendation since they also showed that other aspect ratio such as 3:1 could be efficient too. The most important conclusion of their study showed that when the aspect ratio increased it was associated with lower failure force [45]. Secondly and still to ensure efficient mechanical properties, the base was cylindrical with a diameter fixed at 300 µm. It has been demonstrated that contrary to square or rectangular MN, circular MN can withstand higher forces (stress and bending force) [46]. Thirdly, for the intended application of skin cancer, it is necessary to reach the lower epidermis or the upper dermis without inducing pain or high tissue damages. Thus, depending on the state of the lesions, a low microneedle height of 400 µm or a high one of 750 µm would be the most appropriate. Moreover, these chosen heights are inferior to 900 µm which has been identified as a high value inducing breaking of the

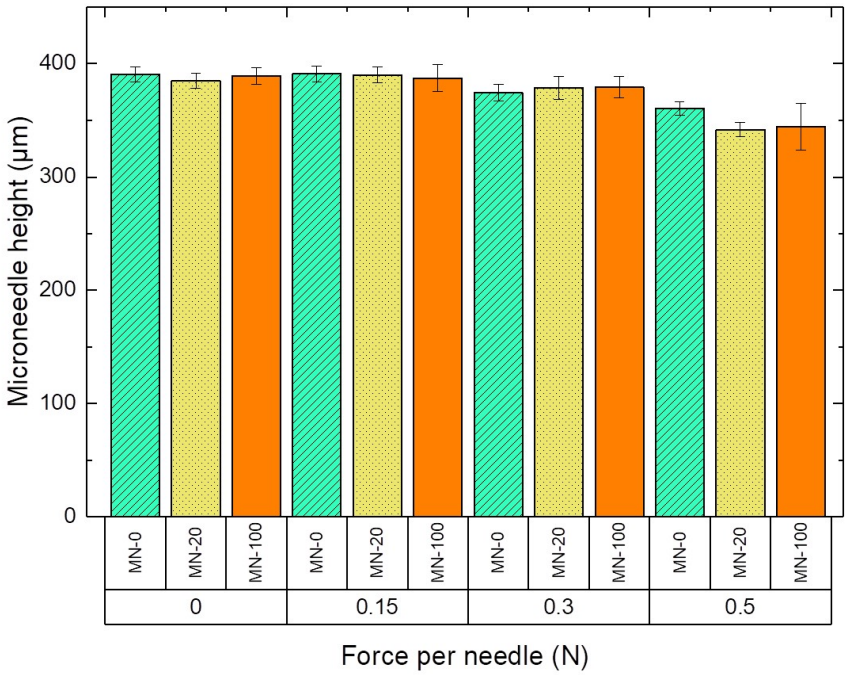

Figure 8: Mechanical behaviour of MN_l after compression at different forces. Analyses were performed on three different patches with at least 10 height measurements on different microneedles from each patch. Results are presented as mean value ± standard deviation.

MNs [46, 47].

3.3.2. Insertion tests in ex vivo skin and a skin model

Since mechanical strength of microneedles was measured as high enough compared to theoretical skin hardness, it was necessary to further examine their insertion ability. The MN-patch was applied to hair shaved *ex vivo* rat skin and removed. Subsequently, microholes were created on top of the skin and a penetration profile might be observed in cross section. Nevertheless, figure 9 shows that the insertion depth in *ex vivo* rat skin was quite low (less than 20 µm) which was far shorter than the microneedles height (750 µm). The main reason of this observation is due to the tissue embedding process with freezing medium which can deeply modify cutaneous

structures by shrinking.

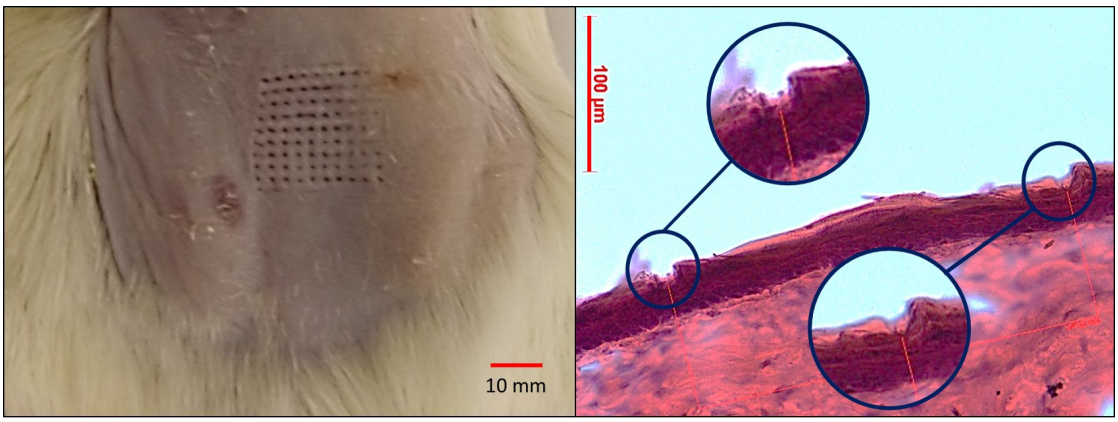

Figure 9: Left: top view observation of rat skin after MN-patch removal. Right: cross section of cryoconserved rat skin after hematoxylin/eosin coloration. The blue circles show the penetration profile of microneedle in the skin.

It was thus necessary to find a skin phantom model with similar mechanical properties and easy to cut without a prior embedding process in order to assess the puncture ability of our device. Classically, gelatin based gels are used but as it is prepared in water, HA-based MN dissolved very rapidly during insertion assay. In order to overcome this difficulty, a Plastiline® material made of oils, mineral waxes and fillers has been chosen with a Young's modulus measured at 10 kPa very close from the skin's one. Therefore it was possible to observe the microchannels created after insertion.

After microneedles insertion, a slice of the skin phantom was manually cut under a binocular magnifier with a scalpel following a ruler. The cross-section observation suggests that the insertion depth was about 374 ± 10 µm and 594 ± 61 µm for respectively MN_l and MN_t as presented in figure 10. Larrañeta et al. worked on another alternative that consists in assembling multiple layers of Parafilm™. Authors then inserted the microneedles and evaluated the percentage of holes created in each Parafilm™layer [48]. As Plastiline®, Parafilm™method allows to develop a rapid microneedle quality control. Similarly, Enfield et al. chose a Blu-Tack® material which is a pressure-sensitive clay-like adhesive known for its low elasticity and soft pliable consistency [49]. The microneedle array with a needle height of 280 µm was inserted into this artificial material and the micropores created were observed under optical coherence tomography system. The depth penetration measured on Blu-Tack® material and forearm skin were respectively 254 ± 7 µm and 179 ± 14 µm [49]. Overall, materials mimicking tissue (Plastiline ®, Parafilm™or Blu-Tack®)

appeared to be good alternatives to biological tissue for MN insertion studies however the depth penetration might be overvalued as shown by Enfield et al. [49].

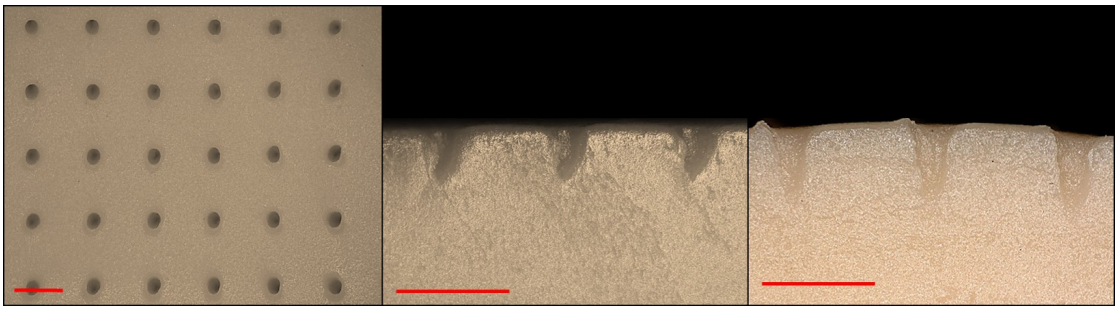

Figure 10: Left: top view observation of phantom skin after MN-patch removal. Middle: cross section of phantom skin after MN_l removal. Right: cross section of phantom skin after MN_t removal. Experiments repeated 5 times. Scale bars represent 1000 µm.

On the other hand, top view observation on *ex vivo* rat skin (figure 9, left) and on the membrane model (figure 10, left) evidenced that microneedles had perfored the skin barrier since microholes were observed. The interval between them was equal to 1200 µm which corresponds well to the original spacing on master structure. Pore diameters created were measured on the Plastiline membrane model at 269 ± 10 µm which is close to the microneedle base diameter set up at 300 µm.

In addition, the spacing between the microneedles has been demonstrated as a parameter influencing the insertion force required to make the microneedles penetrate through the skin. Indeed, Olatunji et al. developed Gantrez® microneedles and showed that the insertion forces required for 330 µm tip-spaced MNs (16 MNs/array) and 900 µm tip-spaced MNs (4 MNs/array) were respectively equal to 0.030 N/needle and 0.028 N/needle (insertion speed of $0.5\,\mathrm{N\,mm^{-1}}$) [50]. Another study led by Kochhar et al. established that penetration percentage was more important when spacing between MNs tips increased. For instance, they revealed that microneedles (microneedle array: $1.44\,\mathrm{cm^2}$) with a base diameter set at 300 µm and a tip-interspacing of 1800 µm had optimal characteristics to penetrate the skin with 64 % penetration [51]. A large spacing also avoids to form a "bed of nails" described by the same authors as a too high density of microneedles that reduce penetration and efficiency of microneedle penetration [51]. Moreover a high density of microneedles is also restrictive as demonstrated by Gill et al. who showed that a 10-fold increase in the number of microneedles is two-fold more painful [12]. In this study, in agreement with these previous research works, the spacing between microneedle tips was set

at 1200 µm with 400 MNs/array. Such parameters enable easy manual MN-patch insertion as presented in figures 9 and 10, would be sufficient for high dose delivery while avoiding crowding, and should ensure a minimal pain.

3.4. Dissolution rate of the MN-patch after insertion in ex vivo rat skin, release kinetics of 5-ALA and MN-patch biocompatibility

HA has been widely used the last decade as a component of artificial matrices and in bioengineering for tissue scaffolding or skin reparation. HA is known to be a highly water-soluble polysaccharide. Consequently when the HA-based MN-patch will be applied on the skin, which is approximately composed of 70 % of water, it is firstly expected that the MN-patch dissolves and releases 5-ALA [52]. When the whole patch will be dissolved into the skin, HA will be further biodegraded since this polymer is already present in the human body and naturally degraded. In fact, the catabolism of HA has been widely described in the literature as a depolymerization process due to the enzymatic cleavage of glycosidic linkages leading to smaller molecule chains. These smaller molecules are naturally present in the human body and will join the natural elimination process consisting in a degradation metabolism in liver or lymph nodes thanks to endothelial cells. The half-life of HA was estimated between 1 and several days. Then the remainder enters in the bloodstream and is eliminated with a half-life between 2 and 5 min [53–55]. Therefore, HA is a good candidate to be dissolved by the skin, leading to 5-ALA release, and be furthermore rapidly biodegraded by a natural enzymatic pathway.

Kinetics of MN-patch dissolution was estimated by removing the patch from the *ex vivo* skin at different times and results are displayed in figure 11. At 10 min, there was no obvious dissolution for the MN_l whereas MN_t dissolution was initiated. This fact could be explained by the MN_t size that can reach deeper skin layer and particularly the lower dermis which is more hydrated and could enhance HA dissolution. A significant dissolution for both patches (MN_l or MN_t) occurred after 45 min. After 60 min, the disintegration of the patch base was noticeable. These experiments showed that when the MN-patch will be applied on the skin, a first drug release at 45 minutes time scale will take place due to microscale needles fast dissolution. Then a second slower drug release at 60 minutes time scale will occur due to the MN-patch base disintegration and could constitute a drug reservoir.

However, the dissolution was not homogenous. Indeed, MN-patch surface is quite large ($25 \times 25\,\mathrm{mm}^2$) and it is conceivable that the entire patch do not receive homogenous force which lead to partial microneedle penetration and inhomogenous dissolution. Different studies have

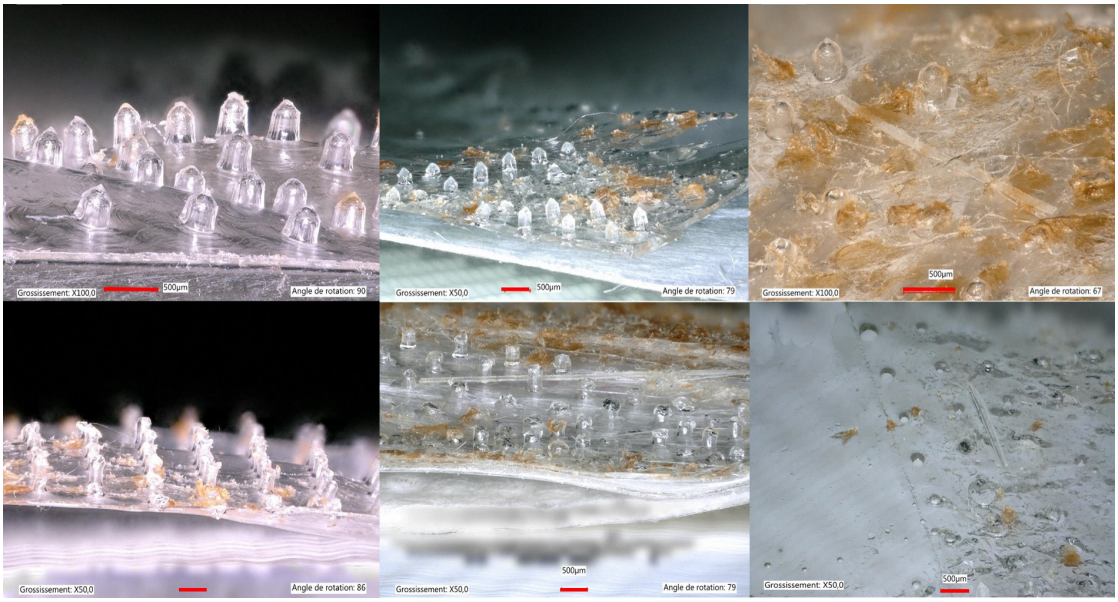

Figure 11: Microscopic images of microneedle patches after their application to *ex vivo* rat skin. Upper line corresponds to MN_l and lower line to MN_t. From left to right: 10, 45 and 60 min. Scale bars represent 500 µm.

been conducted to developed microneedle applicator, nevertheless they are rigid and are not suitable to be applied on body curves[56]. Ripolin et al. conducted a study where they hold a pressure for 45 s and then use a strong adhesive to fix the microneedle patch into the skin. They proved a successful insertion but there was no microscopical images of the microneedle disintegration [57]. Overall, adhesive bandages may be an effective solution to ensure microneedle insertions and keeping them into the skin. Nevertheless, if the lesion is located on the nose a bandage may be unsuitable to maintain a pressure on the MN-patch and a thumb pressure may be more easier to perform. Therefore, the force that 8 people exerted spontaneously with their thumb, for 10 seconds using the texturometer was measured. We have observed that when the indication was "apply a pressure on the whole patch that could allow its insertion in the skin" the force was measured at 24.5 ± 7.5 N which represent 0.34 N/needle and is higher than the one needed for good needles insertion in the skin.

In the other hand, the dissolution rate can be controllable by the initial polymer solution i.e HA concentration and/or HA molecular mass. Indeed, a lower HA concentration will result in a faster dissolution. Similarly an upper HA molecular mass will lead to a lower dissolution due to stronger entanglement between polymeric chains (*Preliminary experiments were realized on gelatin phantom skin and are not presented here*). In fact, Leone et al. have also described

these properties and they mentioned that a balance may be found between dissolution rate and mechanical properties since a lower molecular (4.9 kDa) mass may dissolve faster than upper one at 4.9 kDa but microneedles appeared less robust [58].

This first evaluation of MN-patch dissolution rate was comforting with the end-use application desired. Nevertheless, on *ex vivo* rat skin, it was not possible to evaluate the amount of 5-ALA released at predetermined time points because a long extraction protocol would have been necessary and might have degraded the 5-ALA. Therefore, an *in vitro* drug release experiment was set up in an attempt to mimic the dissolution rate observed in *ex vivo* rat skin. Indeed, after 80 min, macroscopic observation highlighted that the patch was almost completely dissolved as it was after 60 min in *ex vivo* rat skin. As displayed in figure 12, the amount of 5-ALA released was respectively equal to 77 % and 88 % for MN-20 and MN-100. Therefore, it may be assumed that these quantities may also be released during *ex vivo* or *in vivo* experiments which could be a sufficient quantity to perform a PDT treatment in a reasonable time-frame. The 5-ALA release kinetics of MN-100 appears to be slightly faster than that of the MN-20 patch. Indeed, drug delivery is governed by diffusion through the polymer (Fick's law) and by the polymer dissolution (due to convection) [59]. Considering that MN-100 contains more 5-ALA, the prodrug diffusion through the microneedles might be more intense and explain this larger 5-ALA percentage released. Overall, the ability of the patch to deliver 5-ALA in a short time period ($< 1h30$) is impressive compared to previous studies [60–62]. For example in 2006, McCarron et al. showed that a bioadhesive patch made of poly(methyl vinyl ether-co-maleic anhydride) and tripropyleneglycol methyl ether and containing either 19 mg cm^{-2} or 50 mg cm^{-2} of 5-ALA only released 57 % in 6 hours [63]. However, the *in vitro* measurements that the authors investigated were conducted with a Franz diffusion cell and they only dosed the amount that cross all the skin phantom. We may assume that 5-ALA was still contained in the skin itself. Although 5-ALA is a key parameter at the origin of PpIX production, instead of dosing this prodrug precursor, it would also be interesting to evaluate the amount of PpIX itself by testing the patches *in vivo* on skin lesions in order to evaluate PpIX accumulation in the different skin layers [61].

Since dissolution was effective on *ex vivo* rat skin, and release of 5-ALA was effective, it is now important to control its cytotoxicity with a view to future use of this device *in vivo*. To evaluate the biocompatibility of the MN-20 and MN-100 patches, a WST-1 cytotoxicity assay was performed and results are presented in figure 13.

The density of living cells cultured in medium which were in contact with MN-0 was com-

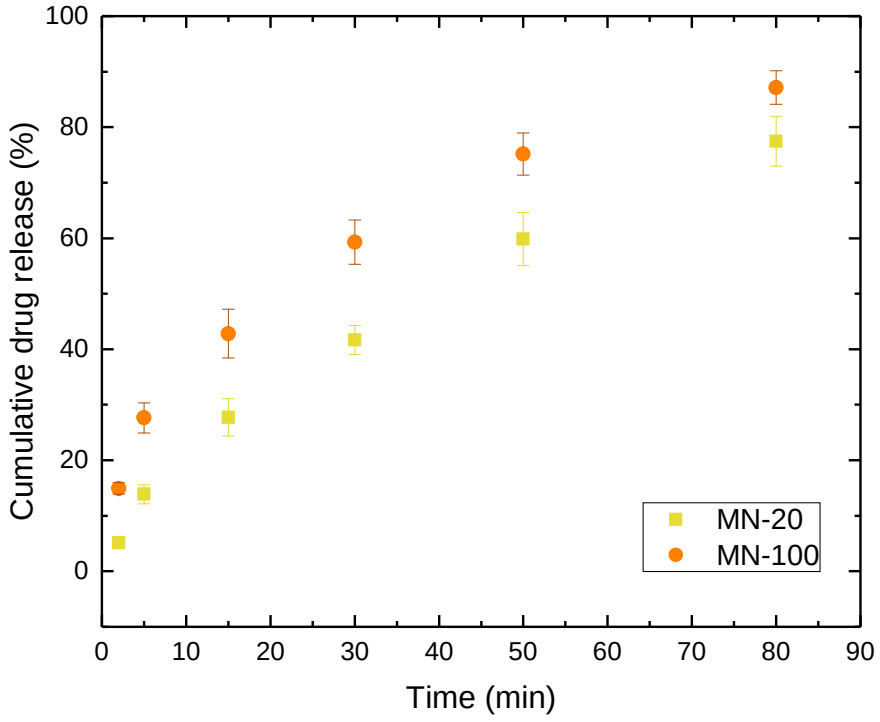

Figure 12: Cumulative amount of released 5-ALA in water at $pH5$ from MN-20 and MN-100 patches during 80 min.

parable to the negative control indicating that MN-0 was not cytotoxic. It was expected since MN-0 was only composed of HA and this polymer is well known for its biocompatibility as a naturally occuring biopolymer. For example, in a 70 kg-human body roughly 15 g of HA is present and 50 % is concentrated in the skin [64]. Developing HA based microneedles was relevant and cytotoxicity experiments approved it.

Furthermore the density of the living cells cultured in medium which were in contact with MN-20 and MN-100 were also comparable to the negative control no matter the concentration. As the MN-p contained 5-ALA and PY, different conditions with these two molecules were also tested and results are displayed in figure 14. As presented in section 3.1, the weight percentages of 5-ALA in the MN-20 and MN-100 were respectively equal to 10.0 %(w/w) and 31.2 %(w/w). Therefore, when the cytotoxicity of the patch was tested at the higher concentration (40 µg mL^{-1}), the 5-ALA concentration was at most equal to 4.0 µg mL^{-1} or 12.5 µg mL^{-1}

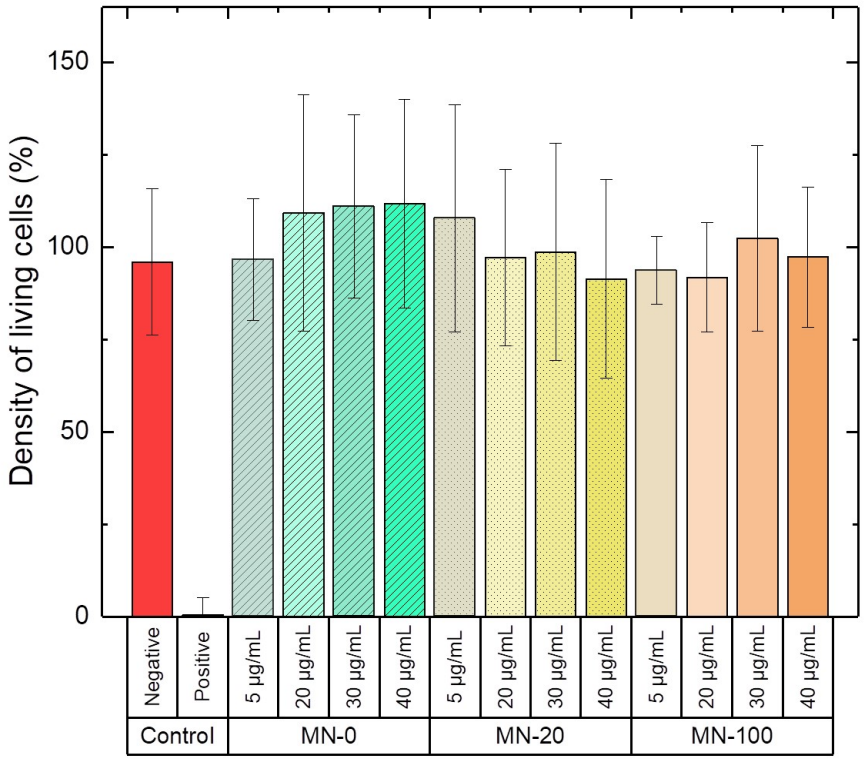

Figure 13: Density of living NIH3T3 fibroblasts after 24 h incubation with MN-0, MN-20, or MN-100. Negative control corresponds to cells incubated in medium only. Positive control corresponds to cells incubated in medium containing H_2O_2.

and these concentrations appeared to be non cytotoxic for the cells (figure 14, left) which was comparable to the results obtained in the litterature by Li et al., Dan et al. [65, 66]. Moreover, the density of living cells after contact with PY remains about 100 % which was comforting as a 1 % degradation of 5-ALA in PY was observed in MN-patch.

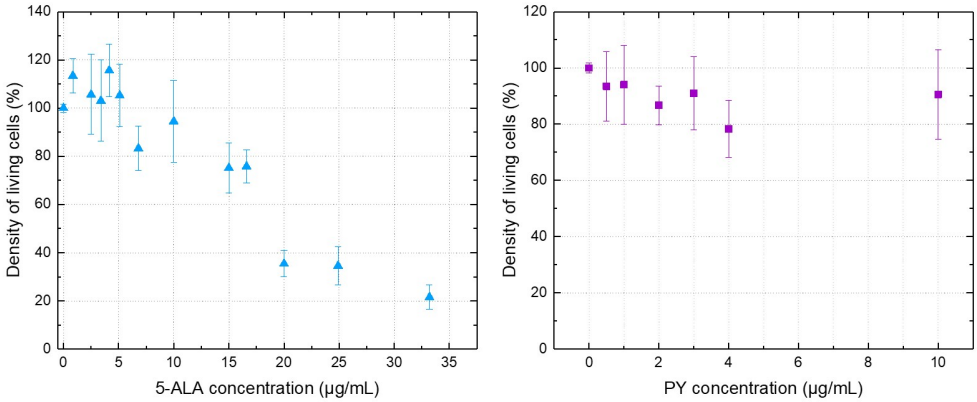

Figure 14: Density of living NIH3T3 fibroblasts after 24 h incubation with 5-ALA or PY.

4. Conclusion

Microneedle patches were fabricated by a single step of solvent casting molding method. The manufacture way very easy, low cost and relevant which would allow a facile translation of this technology. Two heights were developed: 400 µm and 750 µm. Each microneedle patch could contain 20 mg or 100 mg of 5-ALA consequently a single application is sufficient to deliver the amount required for PDT treatment. 5-ALA stability was followed to ensure that there was no dimerization in PY and exhibited a very good stability in the MN-patch even 5 months after manufacturing. Mechanical compression tests were performed and the different kinds of MN-patches do not present a significant deformation when the force applied was not superior to 0.3 N/needle. These results suggested that MN-patch had efficient strength to pierce the *stratum corneum*. Indeed, *ex vivo* rat skin was well perforated due to microneedle application since micropores were created. A clear penetration profile was distinguishable on phantom skin with depth penetration of 374 ± 10 µm and 594 ± 61 µm for respectively MN_l and MN_t. Dissolution rate was estimated on *ex vivo* rat skin demonstrating that the microneedles were dissolved within 45 min and the support started to dissolve after 60 min.

According to the previous results, MN-patches might be a promising technique to enhance 5-ALA penetration and produce PpIX in deeper skin lesions. In the very near future, *in vivo* tests on rats suffering from precancerous skin lesions will be carried out to show microneedle possible benefit during PDT treatment.

Acknowledgments

This project is supported by the European Union – European Regional Development Fund. LETI/DTBS is supported by the French National Research Agency in the framework of the "Investissement d'avenir" program Glyco@Alps (ANR-15-IDEX-02) and Arcane Labex (ANR-12-LABX-003). The authors would also like to thank Manuel Alessio for the design of the aluminium microneedle master structure. Mathilde Menneteau is also acknowledged for her help with cytotoxicity experiments. The authors are grateful to Nicolas Duraffourg for assistance with the NMR analysis.

References

[1] J. Escobar-Chavez, R. Diaz-Torres, I. M. Rodriguez-Cruz, Dominguez-Delgado, Sampere-Morales, Angeles-Anguiano, Melgoza-Contreras, Nanocarriers for transdermal drug delivery, Research and Reports in Transdermal Drug Delivery (2012) 3. doi:10.2147/RRTD.S32621.

[2] S. F. Taveira, R. F. V. Lopez, Topical administration of anticancer drugs for skin cancer treatment, in: Skin Cancers-Risk Factors, Prevention and Therapy, InTech, 2011.

[3] R. Lutton, J. Moore, E. Larrañeta, S. Ligett, R. F. Donnelly, Microneedle characterisation: The need for universal acceptance criteria and GMP specifications when moving towards commercialisation, Drug Delivery and Translational Research 5 (2015) 313–331. doi:10.1007/s13346-015-0237-z.

[4] M.-C. Kearney, S. Brown, M. T. McCrudden, A. J. Brady, R. F. Donnelly, Potential of microneedles in enhancing delivery of photosensitising agents for photodynamic therapy, Photodiagnosis and Photodynamic Therapy 11 (2014) 459–466. doi:10.1016/j.pdpdt.2014.09.003.

[5] M. Champeau, S. Vignoud, L. Mortier, S. Mordon, Photodynamic therapy for skin cancer: How to enhance drug penetration?, Journal of Photochemistry and Photobiology B: Biology 197 (2019) 111544. doi:10.1016/j.jphotobiol.2019.111544.

[6] R. F. Donnelly, D. I. J. Morrow, M. T. C. McCrudden, A. Z. Alkilani, E. M. Vicente-Pérez, C. O'Mahony, P. González-Vázquez, P. A. McCarron, A. D. Woolfson, Hydrogel-Forming and Dissolving Microneedles for Enhanced Delivery of Photosensitizers and Precursors, Photochemistry and Photobiology 90 (2014) 641–647. doi:10.1111/php.12209.

[7] J. Lin, M. T. Wan, Current evidence and applications of photodynamic therapy in dermatology, Clinical, Cosmetic and Investigational Dermatology (2014) 145. doi:10.2147/CCID.S35334.

[8] R. F. Donnelly, D. I. Morrow, P. A. McCarron, A. D. Woolfson, A. Morrissey, P. Juzenas, A. Juzeniene, V. Iani, H. O. McCarthy, J. Moan, Microneedle-mediated intradermal delivery of 5-aminolevulinic acid: Potential for enhanced topical photodynamic therapy, Journal of Controlled Release 129 (2008) 154–162. doi:10.1016/j.jconrel.2008.05.002.

[9] R. F. Donnelly, D. I. Morrow, P. A. McCarron, A. David Woolfson, A. Morrissey, P. Juzenas, A. Juzeniene, V. Iani, H. O. McCarthy, J. Moan, Microneedle arrays permit enhanced intradermal delivery of a preformed photosensitizer, Photochemistry and photobiology 85 (2009) 195–204.

[10] J. W. Lee, K. H. Yoo, B. J. Kim, M. N. Kim, Photodynamic therapy with methyl 5-aminolevulinate acid combined with microneedle treatment in patients with extensive alopecia areata: Correspondence, Clinical and Experimental Dermatology 35 (2009) 548–549. doi:10.1111/j.1365-2230.2009.03695.x.

[11] R. F. Donnelly, D. I. Morrow, T. R. Singh, K. Migalska, P. A. McCarron, C. O'Mahony, A. D. Woolfson, Processing difficulties and instability of carbohydrate microneedle arrays, Drug Development and Industrial Pharmacy 35 (2009) 1242–1254. doi:10.1080/03639040902882280.

[12] H. S. Gill, D. D. Denson, B. A. Burris, M. R. Prausnitz, Effect of Microneedle Design on Pain in Human Volunteers:, The Clinical Journal of Pain 24 (2008) 585–594. doi:10.1097/AJP.0b013e31816778f9.

[13] M. R. Prausnitz, R. Langer, Transdermal drug delivery, Nature Biotechnology 26 (2008) 1261–1268. doi:10.1038/nbt.1504.

[14] F. S. Iliescu, D. Dumitrescu-Ionescu, M. Petrescu, C. Iliescu, A review on transdermal drug delivery using microneedles: Current research and perspective, Ann. Acad. Rom. Sci 7 (2014) 7–34.

[15] R. F. Donnelly, D. I. J. Morrow, M. T. C. McCrudden, A. Z. Alkilani, E. M. Vicente-Pérez, C. O'Mahony, P. González-Vázquez, P. A. McCarron, A. D. Woolfson, Hydrogel-Forming

and Dissolving Microneedles for Enhanced Delivery of Photosensitizers and Precursors, Photochemistry and Photobiology 90 (2014) 641–647. doi:10.1111/php.12209.

[16] S. Liu, M.-n. Jin, Y.-s. Quan, F. Kamiyama, K. Kusamori, H. Katsumi, T. Sakane, A. Yamamoto, Transdermal delivery of relatively high molecular weight drugs using novel self-dissolving microneedle arrays fabricated from hyaluronic acid and their characteristics and safety after application to the skin, European Journal of Pharmaceutics and Biopharmaceutics 86 (2014) 267–276. doi:10.1016/j.ejpb.2013.10.001.

[17] M. Cormier, B. Johnson, M. Ameri, K. Nyam, L. Libiran, D. D. Zhang, P. Daddona, Transdermal delivery of desmopressin using a coated microneedle array patch system, Journal of Controlled Release 97 (2004) 503–511. doi:10.1016/j.jconrel.2004.04.003.

[18] A. K. Jain, C. H. Lee, H. S. Gill, 5-Aminolevulinic acid coated microneedles for photodynamic therapy of skin tumors, Journal of Controlled Release 239 (2016) 72–81. doi:10.1016/j.jconrel.2016.08.015.

[19] T. Miyano, Y. Tobinaga, T. Kanno, Y. Matsuzaki, H. Takeda, M. Wakui, K. Hanada, Sugar micro needles as transdermic drug delivery system, Biomedical Microdevices 7 (2005) 185–188.

[20] J. W. Lee, J.-H. Park, M. R. Prausnitz, Dissolving microneedles for transdermal drug delivery, Biomaterials 29 (2008) 2113–2124. doi:10.1016/j.biomaterials.2007.12.048.

[21] S. P. Sullivan, D. G. Koutsonanos, M. del Pilar Martin, J. W. Lee, V. Zarnitsyn, S.-O. Choi, N. Murthy, R. W. Compans, I. Skountzou, M. R. Prausnitz, Dissolving polymer microneedle patches for influenza vaccination, Nature Medicine 16 (2010) 915–920. doi:10.1038/nm.2182.

[22] J. W. Lee, S.-O. Choi, E. I. Felner, M. R. Prausnitz, Dissolving Microneedle Patch for Transdermal Delivery of Human Growth Hormone, Small 7 (2011) 531–539. doi:10.1002/smll.201001091.

[23] J.-H. Park, M. G. Allen, M. R. Prausnitz, Polymer Microneedles for Controlled-Release Drug Delivery, Pharmaceutical Research 23 (2006) 1008–1019. doi:10.1007/s11095-006-0028-9.

[24] A. Nayak, D. B. Das, Potential of biodegradable microneedles as a transdermal delivery vehicle for lidocaine, Biotechnology Letters 35 (2013) 1351–1363. doi:10.1007/s10529-013-1217-3.

[25] J. Necas, L. Bartosikova, P. Brauner, J. Kolar, Hyaluronic acid (hyaluronan): A review, Veterinární Medicína 53 (2008) 397–411. doi:10.17221/1930-VETMED.

[26] Z. Zhu, H. Luo, W. Lu, H. Luan, Y. Wu, J. Luo, Y. Wang, J. Pi, C. Y. Lim, H. Wang, Rapidly Dissolvable Microneedle Patches for Transdermal Delivery of Exenatide, Pharmaceutical Research 31 (2014) 3348–3360. doi:10.1007/s11095-014-1424-1.

[27] J. Mönkäre, M. Reza Nejadnik, K. Baccouche, S. Romeijn, W. Jiskoot, J. A. Bouwstra, IgG-loaded hyaluronan-based dissolving microneedles for intradermal protein delivery, Journal of Controlled Release 218 (2015) 53–62. doi:10.1016/j.jconrel.2015.10.002.

[28] X. Zhao, X. Li, P. Zhang, J. Du, Y. Wang, Tip-loaded fast-dissolving microneedle patches for photodynamic therapy of subcutaneous tumor, Journal of Controlled Release 286 (2018) 201–209. doi:10.1016/j.jconrel.2018.07.038.

[29] J. Zhu, L. Dong, H. Du, J. Mao, Y. Xie, H. Wang, J. Lan, Y. Lou, Y. Fu, J. Wen, B. Jiang, Y. Li, J. Zhu, J. Tao, 5-Aminolevulinic Acid-Loaded Hyaluronic Acid Dissolving Microneedles for Effective Photodynamic Therapy of Superficial Tumors with Enhanced Long-Term Stability, Advanced Healthcare Materials 8 (2019) 1900896. doi:10.1002/adhm.201900896.

[30] P. A. McCarron, R. F. Donnelly, A. D. Woolfson, G. P. Andrews, Analysis of pyrazine 2,5-dipropionic acid in 5-aminolevulinic acid-loaded urological and topical delivery vehicles: Methodology and assay validation, Journal of Pharmaceutical and Biomedical Analysis 36 (2005) 1099–1105. doi:10.1016/j.jpba.2004.09.004.

[31] A. W. De Blois, R. J. E. Grouls, E. W. Ackerman, W. J. A. Wijdeven, Development of a stable solution of 5-aminolaevulinic acid for intracutaneous injection in photodynamic therapy, Lasers in medical science 17 (2002) 208–215.

[32] A. Bunke, O. Zerbe, H. Schmid, G. Burmeister, H. P. Merkle, B. Gander, Degradation mechanism and stability of 5-aminolevulinic acid, Journal of pharmaceutical sciences 89 (2000) 1335–1341.

[33] H. Lambers, S. Piessens, A. Bloem, H. Pronk, P. Finkel, Natural skin surface pH is on average below 5, which is beneficial for its resident flora, International Journal of Cosmetic Science 28 (2006) 359–370. doi:10.1111/j.1467-2494.2006.00344.x.

[34] L. Baranda, R. Gonzalez-Amaro, B. Torres-Alvarez, C. Alvarez, V. Ramirez, Correlation between pH and irritant effect of cleansers marketed for dry skin, International Journal of Dermatology 41 (2002) 494–499. doi:10.1046/j.1365-4362.2002.01555.x.

[35] B. Elfsson, I. Wallin, S. Eksborg, K. Rudaeus, A. M. Ros, H. Ehrsson, Stability of 5-aminolevulinic acid in aqueous solution, European journal of pharmaceutical sciences 7 (1999) 87–91.

[36] J. Chen, Q. Peng, H.-J. Jodl, Infrared spectral comparison of 5-aminolevulinic acid and its hexyl ester, Spectrochimica Acta Part A: Molecular and Biomolecular Spectroscopy 59 (2003) 2571–2576. doi:10.1016/S1386-1425(03)00011-8.

[37] K. J. Reddy, K. T. Karunakaran, Purification and characterization of hyaluronic acid produced by Streptococcus zooepidemicus strain 3523-7, Journal of BioScience and Biotechnology (2013) 7.

[38] P. Bulpitt, D. Aeschlimann, New strategy for chemical modification of hyaluronic acid: Preparation of functionalized derivatives and their use in the formation of novel biocompatible hydrogels (1998) 18.

[39] M. A. Napier, N. M. Hadler, Effect of calcium on structure and function of a hyaluronic acid matrix: Carbon-13 nuclear magnetic resonance analysis and the diffusional behavior of small solutes, Proceedings of the National Academy of Sciences 75 (1978) 2261–2265. doi:10.1073/pnas.75.5.2261.

[40] N. Izawa, T. Hanamizu, R. Iizuka, T. Sone, H. Mizukoshi, K. Kimura, K. Chiba, Streptococcus thermophilus produces exopolysaccharides including hyaluronic acid, Journal of Bioscience and Bioengineering 107 (2009) 119–123. doi:10.1016/j.jbiosc.2008.11.007.

[41] B. J. Kvam, M. Atzori, R. Toffanin, S. Paoletti, F. Biviano, 1H- and 13C-NMR studies of solutions of hyaluronic acid esters and salts in methyl sulfoxide: Comparison of hydrogen-bond patterns and conformational behaviour, Carbohydrate Research 230 (1992) 1–13. doi:10.1016/S0008-6215(00)90509-3.

[42] M. K. Cowman, D. M. Hittner, J. Feder-Davis, C-NMR Studies of Hyaluronan: Conformational Sensitivity to Varied Environments, Macromolecules 29 (1996) 2894–2902. doi:10.1021/ma951701x.

[43] E. K. Jaffe, J. S. Rajagopalan, Nuclear magnetic resonance studies of 5-aminolevulinate demonstrate multiple forms in aqueous solution, Bioorganic Chemistry 18 (1990) 381–394. doi:10.1016/0045-2068(90)90022-W.

[44] R. F. Donnelly, P. A. McCarron, D. A. Woolfson, Derivatives of 5-aminolevulinic acid for photodynamic therapy, Perspectives in medicinal chemistry 1 (2007) 1177391X0700100005.

[45] S. D. Gittard, B. Chen, H. Xu, A. Ovsianikov, B. N. Chichkov, N. A. Monteiro-Riviere, R. J. Narayan, The effects of geometry on skin penetration and failure of polymer microneedles, Journal of Adhesion Science and Technology 27 (2013) 227–243. doi:10.1080/01694243.2012.705101.

[46] P. Aggarwal, C. Johnston, Geometrical effects in mechanical characterizing of microneedle for biomedical applications, Sensors and Actuators B: Chemical 102 (2004) 226–234. doi:10.1016/j.snb.2004.04.024.

[47] S. P. Davis, B. J. Landis, Z. H. Adams, M. G. Allen, M. R. Prausnitz, Insertion of microneedles into skin: Measurement and prediction of insertion force and needle fracture force, Journal of Biomechanics 37 (2004) 1155–1163. doi:10.1016/j.jbiomech.2003.12.010.

[48] E. Larrañeta, J. Moore, E. M. Vicente-Pérez, P. González-Vázquez, R. Lutton, A. D. Woolfson, R. F. Donnelly, A proposed model membrane and test method for microneedle insertion studies, International Journal of Pharmaceutics 472 (2014) 65–73. doi:10.1016/j.ijpharm.2014.05.042.

[49] J. Enfield, M.-L. O'Connell, K. Lawlor, E. Jonathan, C. O'Mahony, M. Leahy, In-vivo dynamic characterization of microneedle skin penetration using optical coherence tomography, Journal of Biomedical Optics 15 (2010) 046001. doi:10.1117/1.3463002.

[50] O. Olatunji, D. B. Das, M. J. Garland, L. Belaid, R. F. Donnelly, Influence of Array Interspacing on the Force Required for Successful Microneedle Skin Penetration: Theoretical and Practical Approaches, Journal of Pharmaceutical Sciences 102 (2013) 1209–1221. doi:10.1002/jps.23439.

[51] J. S. Kochhar, T. C. Quek, W. J. Soon, J. Choi, S. Zou, L. Kang, Effect of Microneedle Geometry and Supporting Substrate on Microneedle Array Penetration into Skin, Journal of Pharmaceutical Sciences 102 (2013) 4100–4108. doi:10.1002/jps.23724.

2.4 Supplementary informations

2.4.1 Complementary information

2.4.1.1 Stability

When the article was submitted 6 months ago, the stability of 5-ALA was studied up to 150 days and a non-significant slight decrease of less than 3 % in 5-ALA percentage over the time period was observed. 125 days later i.e. after 275 days of storage the 5-ALA weight percentage dropped to $5.6 \pm 0.4\%(w/w)$ and the amount of PY reached $0.7 \pm 0.6\%(w/w)$ which represent a decrease in 5-ALA amount of approximately 4.4 %. In order to increase the patch stability, the storage may be optimized for example by loading the receptacle with argon before vacuum. This has been already realized by a team working on another MN-patch in our lab and it appears more efficient than the conditions we used.

Besides, the stability of MN-100 has also been studied but stopped rapidly. Indeed, even if $27.1 \pm 0.3\%(w/w)$ of 5-ALA was still present in the patch after 127 days[1], the patch appeared flask after 10 days (figure 2.6). This is probably due to the increase of water content in the patch that leads to chain relaxations and to an unusable patch. Besides, a change of patch colour is observed which is probably due to PY presence. Another hypothesis would be to explain this colour change by the polymer oxidation or the polymer physical aging which is frequently observed when there are chain relaxations [200].

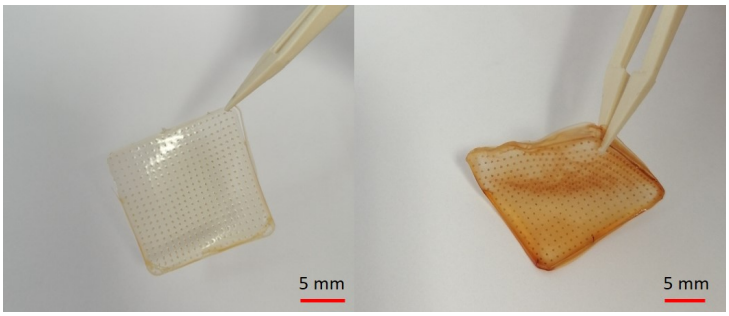

Figure 2.6 – Left: MN-100 after 1 day of storage. Right: The same MN-100 patch after 12 days and with the same storage conditions.

2.4.1.2 Mechanical behaviour of MN-100

Figure 2.7 displayed the mechanical compression tests performed on MN_t. This graph has been described in section 3.3.1 in the article. To sum up, a slight height reduction was observed on MN_t-0 and MN_t-20 with a loss in height inferior to 7 % even at the highest compression force of 0.5 N/needle. Nevertheless, for the MN_t-100 at 0.3 N/needle and 0.5 N/needle the loss in height were higher and reached 17 % and 53 % which has been previously described by a decrease in polymer chain interactions due to the presence of the prodrug 5-ALA.

The stability in terms of prodrug presence has been investigated and showed that MN-20 patch could be used even after 5 months of storage contrary to MN-100 patch that looked macroscopically degraded. Nevertheless, further investigations should be done on the mechanical

[1] Initial 5-ALA weight percentage in MN-100 patch was measured at 30 % (w/w).

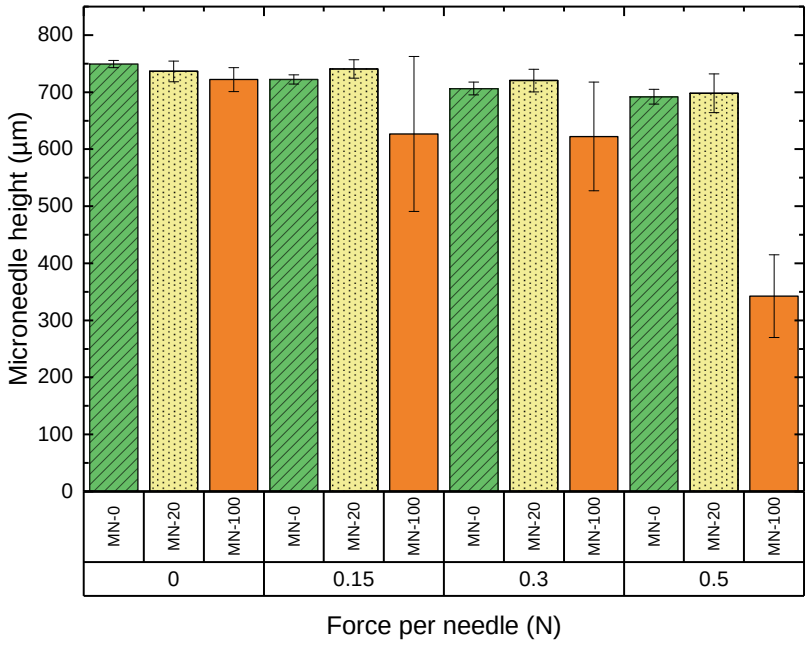

Figure 2.7 – Mechanical behaviour of MN_t after compression at different forces. Analyses were performed on three different patches with at least 10 height measurements on different microneedles from each patch. Results are presented as mean ± standard deviation.

properties evolution of the MN-20 patch. Indeed, the compression tests were only realized on "fresh" patches and it would be interesting to check if their insertion ability and fracture toughness are still congruent with the further use on skin lesions.

2.4.1.3 Cytotoxicity

The cytotoxicity has been previously studied for MN-patches concentration up to 40 µg mL^{-1}. By following the same method, higher concentrations for MN-0, MN-20 and MN-100 were tested and the results are presented in figure 2.8. Even at the highest concentration of 400 µg mL^{-1}, the patches were not toxic for the cells although a slight decrease in viability may be observed for the MN-100. These results were surprising especially for MN-20 and MN-100 that contained respectively 10 % (w/w) and 30 % (w/w) of 5-ALA. Indeed, in the condition of 400 µg mL^{-1} it was expected to have 40 µg mL^{-1} and 120 µg mL^{-1} of 5-ALA which are concentrations supposed to alter cells viability as previously shown in figure 14 in the article. As this result was confusing, we measured again the toxicity of 5-ALA and this time the IC50[2] was evaluated at 220 µg mL^{-1}

[2]IC50 is the half maximal inhibitory concentration. It consists of measuring the potency of a substance to inhibit a specific biological or biochemical function.

whereas it has been previously estimated at 21.6 µg mL^{-1}. It is hard to compare our results with others teams because each research group used different cell line, different cell number and all these details may impact the results. Nevertheless, we compare these last values to Chu et al. who worked with nasopharyngeal carcinoma (NPC/CNE2) at 3×10^4 cells/well and that displayed no cytotoxicity of 5-ALA even at 131 µg mL^{-1} which stay in the order of magnitude of our last results [32]. Likewise, Osaki et al. studied cytotoxicity of 5-ALA with KLN205 lung cancer cells at 1×10^4 cells/well and demonstrated that even with a 5-ALA concentration at 655 µg mL^{-1} no cytotoxicity on the cell was observed [129]. To conclude, it is possible that at the time at which we performed the first cytotoxicity assay (Figure 14 in the article, IC50 at 21.6 µg mL^{-1}) , the cell line or the WST-1 reagent used might have been old and revise the cell viability downwards. Although, 5-ALA cytotoxicity is highly variable, what is comforting is that the MN-patches are not toxic at 24 h on NIH3T3 fibroblast cells.

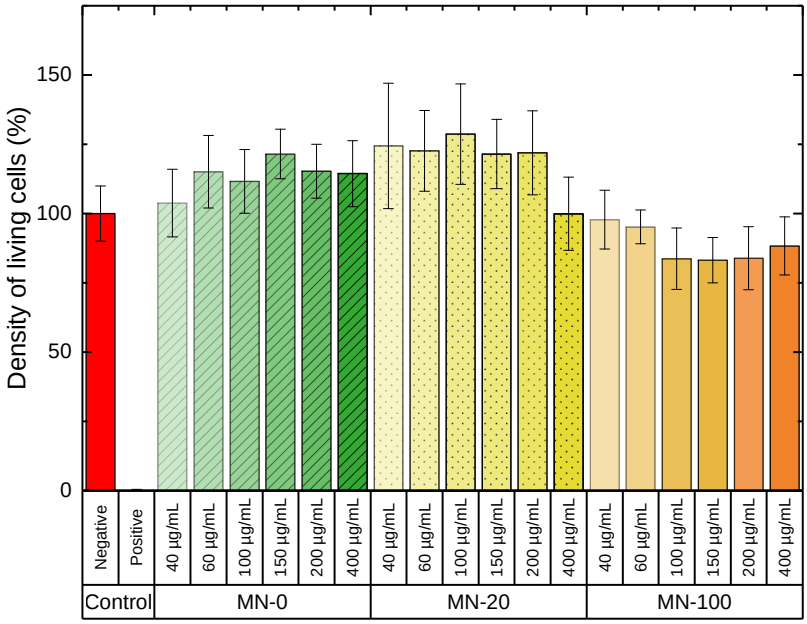

Figure 2.8 – Density of living NIH3T3 fibroblasts after 24 h incubation with MN-0, MN-20 or MN-100.

2.4.2 Sterilization

Due to the promising results highlighted in the aforementioned article (section 2.3), it was then required to produce a sterile MN-patch to test the technology *in vivo*. Consequently, 5-ALA solution was prepared either at 10 mg mL^{-1} to produce MN-20 or at 50 mg mL^{-1} to produce MN-100 and filtered on Acrodisc® syringe filter with Supor® membrane at 0.2 µm. An amount

of 100 mg of HA was dissolved in deionized water (in approximately 50 mL) and strongly mixed before being filtered on Acrodisc® syringe filter with Supor® membrane at 0.45 µm and re-filtrated on 0.2 µm. The filtrate was placed in previously autoclaved Eppendorf tubes and lyophilized for 72 hours. The PDMS molds were also autoclaved and the polymeric solution composed of 5-ALA and HA was cast as usual and dried in the oven. To ensure no contamination, a lid was placed on top of the PDMS mold.

According to the European Pharmacopoeia a filtration on 0.2 µm is sufficient to remove all the bacteria but further investigations are required. Following the European Pharmacopoeia, the MN-patch (prepared with sterilized compounds) was dissolved in 9 mL of Tryptone Soja Bouillon (TSB), which is a general medium for the growth of a wide variety of microorganisms, agitated at 70 rpm in a oven at 30 °C for at least 30 days. As a positive control, Escherichia coli (ATCC® 11775™) at 100 CFU in TSB was used. The negative control consisted of TSB alone. The two control groups were prepared in the same time as the MN-patch sample and agitated and heated in the same conditions.

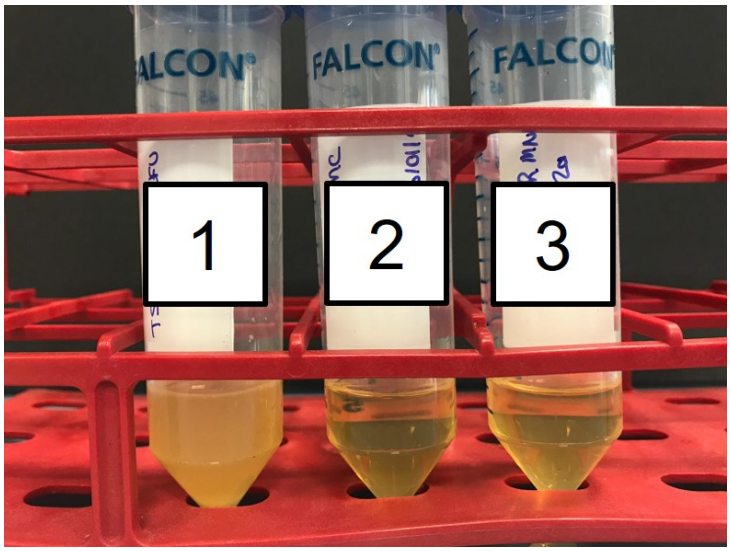

Figure 2.9 – Sterilization test after 57 days.
Tube 1: positive control. Tube 2: negative control. Tube 3: Sample containing MN-patch.

As presented in figure 2.9, the positive control culture medium blurred due to the presence of bacteria whereas the optical density of the negative control was lower. The optical density of the tube number 3 is comparable to the negative control which indicates that the filtration was effective and allow to sterilize the patch. Although this eye observation is considered as sufficient by the European Pharmacopoeia, a more precise evaluation was realized by measuring the optical density of the samples. Briefly, 1 mL of each sample was analysed with a UV spectrophotometer (Varian Cary 300 UV-Vis) from 400 nm to 800 nm. TSB alone was set as the blank sample and defined the baseline. The absorbance measurements were recorded at different time periods. The wavelength chosen for the sterilisation monitoring was set at 600 nm because known to minimize absorbance by media components (such as TSB) while maximizing turbidity measurement. This wavelength is often used for the measurement of optical density in bacterial cultures [60]. The results are presented in figure 2.10 and confirmed that either MN-0, MN-20 or MN-100 were produced in sterilized conditions. Admittedly, a slight OD increase for the MN-20 or MN-100

patches may be observed after 20 days that is not due to bacteria in the medium (too low absorbance) but it could be hypothesise that 5-ALA has started to degrade due to the experiment conditions (temperature set at 37 °C and pH at approximately 7). As previously presented, the degradation products is a porphyrin derivative that might mildly absorb at the wavelength chosen.

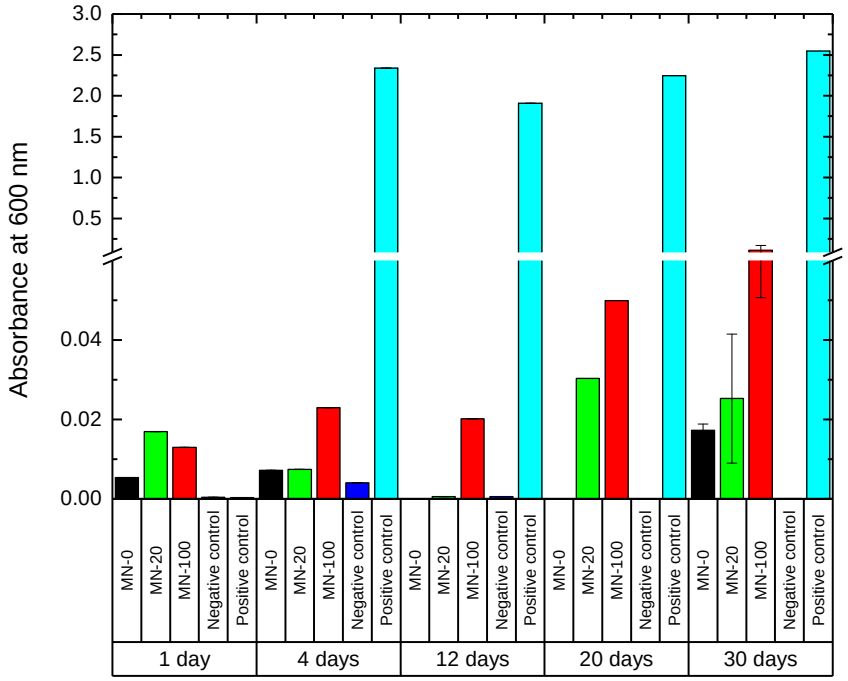

Figure 2.10 – Optical density control of MN-0, MN-20 and MN-100. Positive control corresponds to a solution containing bacteria (100 CFU) and negative control corresponds to TSB alone.

Conclusion

- The choice of HA as the material used to produce dissolving microneedles in which 5-ALA has been embedded was described. Indeed, its high biocompatibility and dissolution rate make HA a good candidate.
- Preliminary tests were performed to choose HA Mw and its concentration. A "low" Mw at $(5.50 \pm 0.04) \times 10^4\,g\,mol^{-1}$ and concentrated at 5 % (w/w) appeared to be a good compromise to obtain a patch exhibiting a fast dissolution.
- As presented in the article, with the solvent casting molding method, two microneedle heights have been developed: 750 µm and 400 µm since not all skin precancerous lesions extend to the same depth. Similarly, two amounts of 5-ALA were loaded in the MN-patch: 20 mg or 100 mg.
- Finally, in this article it was demonstrated that due to the "pencil-tip" shape, the MN exhibited mechanical properties enabling a good insertion into the skin. Moreover, dissolution was efficient and no cytotoxic effects were identified.
- Stability of 5-ALA in the MN-patch (either MN-20 or MN-100) has been assessed as satisfying over 5 months after manufacturing but their mechanical properties over the time should also be reported.
- Due to the promising results, sterile MN-patches were successfully prepared and could be tested *in vivo* to assess their efficiency to produce PpIX.

Chapter 3

Preclinical studies
Production of PpIX on an *in vivo* skin lesions model and prodrug penetration profile on *ex vivo* skin

Outline of the current chapter

Introduction

- In chapter 2, the release of 5-ALA in deep skin layers by the MN-patch was highlighted in the perspective of the targeted biological applications.
- Even if 5-ALA could be easily released without degradation, *in vivo* tests were absolutely required to evaluate its metabolization to PpIX, which is a key element to carry out PDT. Therefore, an experimental procedure has been written in order to use animals for scientific purpose.
- To obtain PpIX in conditions usually encountered in dermatological practice, precancerous lesions were induced on rats by using UV-B illumination. To validate the model, pharmacokinetics and histological studies were performed and detailed in the first part of the article.
- Once the model of skin lesions on rat was established, the $MN_t - 20$ patch (containing 10 % w/w of 5-ALA) was tested and the amount of fluorescence due to PpIX was measured.
- Supplementary data based on additional results, which are not presented in the article, concerning depth of PpIX fluorescence in the samples, measurement of 2,5-dipropionic acid (PY) fluorescence or even usage of a new bandage are available.
- To better establish the prodrug penetration in depth, two methods were developed on *ex vivo* skins and and have provided promising prospects.

3.1 Application for authorization of a scientific project using animals

The purpose of this form is to gather information enabling the ethics committee of the user establishment where the project using animals for scientific purposes will be carried out to ethically evaluate the project and the Ministry of Higher Education and Research to authorize the project following the ethical evaluation. This form is composed of:

- a non-technical summary available by all on the Ministry's website in which the Three R rules (Replace, Reduce and Refine) are developed
- a project's description in which the experimental procedures are explained
- the choice, relevance of the strain and the animal number

In order to answer the **Three R rules** in the application form, it was explained that the study of 5-ALA delivery through the skin and then its metabolization in PpIX on tumour cells cannot be done on a cellular model or by computer simulation. That is why an *in vivo* model was required and at this time, the animal model could not be **replaced**. The number of rats has been determined by establishing an experimental plan (Yates' algorithm) in order to **reduce** it as much as possible, while not compromising the validity of the statistical tests that will be carried out. Lately, to ensure **refinement** it was mentioned that the state of health of the animals will be monitored throughout the experiment. Indeed, the rats were anesthetized during all the experimental procedures. Qualified personnel monitored the state of health of

the animals regularly throughout the experiments, particularly in the injured skin area. This allowed immediate and appropriate intervention at the slightest sign of suffering. The animals were housed in groups in a cage enriched with play accessories and nesting materials.

The whole application form is available under the APAFIS number 18456-2019011414199848v2 and has been approved by the Ministry on January 14th, 2019.

3.2 Why the rat model has been chosen?

According to two recent reviews led by Todo and Jung et al. and as presented in table 3.1 it was clear that the hairless rat would perfectly fit the skin layers reported for human. Indeed, this model has been commonly used in cosmetics, dermatological, pharmacological and toxicology research. The structure of its different skin layers are very close from those of human and would have been perfect to study the MN insertion, its dissolution and estimate the amount of 5-ALA release in deep skin layers. Firstly, our choice was oriented on a strain available at Janvier Labs that was the SPRAGUE DAWLEY® Hairless Rat. Nevertheless, at the time we needed it, the model was no longer available as a breathable strain but only as a cryoconserved one and the revitalization would have taken more than 6 months. Therefore, we looked for another hairless rat but a large overview in all the animal laboratories suppliers showed than only immunodeficient strains existed. Breeding immunodeficient rats is constraining and was not possible in our animal house. For reasons of time, we looked for other species. The pig was commonly used for drug permeation research but this is a large mammal. Moreover, as the application (APAFIS) was already approved for rodents we decided to chose rat (with hair) instead of mice since the rat skin stay close enough to the human one as seen in table 3.1. Having chosen rat with hairs will add a shaving step before inducing skin lesions or MN-patch application as will be presented in the next section.

Species	*Stratum corneum* (SC) (µm)	Epidermis (µm)	Whole skin (mm)
Human (healthy)	17.2 ± 0.6	45.3 ± 5.6	2.5 ± 0.6
Hairless rat	15.4 ± 3.3	28.3 ± 5.3	0.9 ± 0.1
Pig ear	10	50	1.3
Pig back	26	66	3.6
Rat	18	32	2.9
Mouse	6.9 ± 1.6	21 ± 8	0.8 ± 0.1

Table 3.1 – Comparison of skin thickness among species adapted from [178, 76]

3.3 Article: Introduction of a model of skin lesions on rats and testing of dissolving MNs containing 5-ALA

Introduction of a model of skin lesions on rats and testing of dissolving microneedles containing 5-aminolevulinic acid

Mathilde Champeau[a,b,*], Dorothée Jary[a], Anne-Sophie Vignion-Dewalle[b], Serge Mordon[b], Elisabeth Martin de Lassalle[c], Séverine Vignoud[a], Laurent Mortier[b]

[a] *CEA, LETI-DTBS, 17 rue des Martyrs, Grenoble Cedex, France*
[b] *Univ. Lille, Inserm, CHU Lille, U1189 - ONCO-THAI - Assisted Laser Therapy and Immunotherapy for Oncology, F-59000 Lille, France*
[c] *Pathology institute, Pole of Biology, Pathology and Genetics of the CHRU (University Hospital Research Center), 59000 Lille, France*

Abstract

Topical photodynamic therapy (PDT) is widely used to treat non melanoma skin cancers. It consists of topically applying on the skin lesions a cream containing a prodrug (5-aminolevulinic acid (5-ALA) or methyl aminolevulinate (MAL)) that is then metabolized to the photosensitizer protoporphyrin IX (PpIX). Light irradiation at PpIX excitation wavelength combined with oxygen then lead to a photochemical reaction inducing cell death. Nevertheless, this conventional PDT treatment is currently restricted to superficial skin lesions since the penetration depth of the prodrug is limited and hampers the production of PpIX in deep seated lesions. To overcome this problem, dissolving microneedles (MNs) included in a square flexible patch were developed. This easy-to-handle MN-patch is composed of 5-ALA mixed with hyaluronic acid (HA) and has the ability to dissolve after skin application. To evaluate the efficiency of this MN-patch *in vivo*, a skin lesion model has been developed on rats by applying UV-B illuminations. After 40 UV-B illuminations, histological and pharmacokinetic controls confirmed that the rats presented skin lesions. Once the rat skin lesion model has been validated, it was demonstrated that the MNs penetrated into the skin and fully dissolved in one hour on most of the rats. After one hour, the fluorescence images showed that the MN-patch produced a consequent and homogeneous level of PpIX. Overall, the dissolving MN-patch is a recent technology that has interesting features and several preclinical investigations should be led to compare its efficiency to that of the conventional treatment for PDT of non melanoma skin cancers.

Keywords: skin lesions, animal model, photodynamic therapy, dissolving microneedles, 5-aminolevulinic acid

*Corresponding author
Email address: mathilde.champeau@cea.fr (Mathilde Champeau)

Glossary

5-ALA 5-aminolevulinic acid. 1–3, 5, 7, 14, 16

AK actinic keratosis. 2, 10

BCC basal cell carcinoma. 2

HA hyaluronic acid. 1, 3, 5, 14

MAL methyl aminolevulinate. 1–3, 6, 8

MED minimal erythema dose. 6

MN microneedle. 1–3, 5, 12–14, 16

MN-patch microneedles patch. 3, 5, 7, 12–16

PDMS polydimethylsiloxane. 5

PDT photodynamic therapy. 1–4, 8, 13, 14, 16

PpIX protoporphyrin IX. 1–4, 6–8, 11, 13, 14, 16

SC *stratum corneum*. 2, 3

1. Introduction

5-ALA and MAL are photensensitizer drug precursors used for PDT in dermatology and often delivered topically. These prodrugs tend to accumulate and metabolize in PpIX preferentially in neoplastic cells since the haem biosynthetic pathway is disrupted [1]. Briefly, PDT rests on the synergy between three parameters : a *photosensitizer* (PpIX) which is activated by *light* at its excitation wavelength and when combined with the *presence of oxygen* promotes highly cytotoxic singlet oxygen leading to cells death [2].

Conventional PDT treatment for non melanoma skin cancer consists of topically applying on the lesions either Metvix® cream containing 16 % of MAL or Levulan Kerastick® cream containing 20 % of 5-ALA. Metvix® and Levulan Kerastick® are respectively used in Europe

and the United States [2]. Topical PDT is well established for the treatment of actinic keratosis (AK), superficial basal cell carcinoma (BCC) or Bowen's disease. However, the clearance rate after PDT treatment on deep seated lesions such as nodular BCC, thick superficial BCC or highly graded AK is less efficient than for thin superficial lesions [3]. This slight resistance reported for thick lesions is due to the poor penetration of the prodrugs in the skin [4, 5]. Therefore, several techniques (chemical or physical) were designed to enhance drug penetration through the skin [6].

One of the physical strategy is the use of MNs. When applied on the skin and thanks to their robustness, MNs allow to bypass the *stratum corneum* (SC) and create microchannels whose depth depends on microneedle height. MNs can be assembled together as a patch or as a roller and are easy to handle, low cost and painless. The use of MN rollers associated with PDT has been widely studied and showed that the penetration of 5-ALA was significantly increased leading to better PDT outcomes [7, 8]. Nevertheless, this passive diffusion required a two-step application process and the delivered prodrug dose is not precisely known [9]. Moreover, among different types of MNs developed within the scientific community, solid MNs often made of silicon can certainly promote passive diffusion but can also be dangerous for the patient since silicon is known to be a non-biodegradable material and can lead to infections when residues are present under skin [10].

To overcome the aforementioned problems, dissolving MNs have been attracting attention for prodrug delivery. The use of a dissolving microneedles patch (MN-patch) is easy since it consists only of applying it on the skin in one step, moreover the delivered prodrug amount is precisely controlled and there is no risk of cytotoxicity. Indeed, the prodrug is encapsulated in a MN-patch matrix that is chosen as biocompatible, dissolvable and biodegradable. This matrix is dissolved by body fluids when the MN-patch is inserted in the skin. Recently, dissolving MN-patch containing 5-ALA made of different polymers such as poly(methylvinylether/maelic acid) [10], galactose [11], Gantrez AN-139 (copolymer of methyl vinyl ether and maleic anhydride) [12] or HA were proposed [13, 14]. Among these studies, the efficiency of the dissolving MNs were not often evaluated in preclinical study and when *in vivo* experiments were performed, MNs were always tested on subcutaneous mouse tumour model that are not realistic [13]. Moreover, the mouse skin is really thin compared to the human skin and the ability of the microneedles to pierce the SC can not be well evaluated on this mouse model [15, 16]. Indeed, the major advantage of 5-ALA MNs is to enhance prodrug penetration in depth compared to the usual cream. If the skin is thin, the puncture behaviour, the mechanical strength of MNs and therefore the usefulness of

MNs would not been highlighted. Besides, a thin skin such as the mouse one might allow a good cream penetration whereas this is known to be limited and accumulate preferentially in the SC in most of the clinical PDT treatments.

To assess the relevance of MNs and especially to highlight their ability to perforate the SC, the rat skin known to be more representative of the human skin than the mice one was chosen in this study. Nevertheless and to our knowledge, no skin lesions model exist on rats. Therefore, the main purpose of this study was to develop a model of skin lesions on rats by using daily UV-B illumination. In a first instance, a small sample of rats received from 30 to 70 UV-B illuminations in order to see from how many exposures skin lesions started to develop. For this purpose, a pharmacokinetics study was performed and consisted of applying the commercial Metvix® cream on rat skin having been exposed to different numbers of UV-B illuminations. Then, the PpIX fluorescence resulted from the metabolization of MAL in neoplastic cells was recorded and directly related to the skin lesion induction. In parallel, a histological analysis was established to microscopically validate the presence of tumour cells in the rat skin biopsy. In a second instance, to evaluate the suitability of the model for studying PDT, a larger sample of rats -having received the predetermined number of UV-B exposures- was included in another pharmacokinetics study. The second goal of this study was to test dissolving MN-patch containing 5-ALA on this rat model. To this end, the insertion and dissolution abilities of the MN-patch were observed. Then the level of PpIX produced was recorded by measuring the fluorescence in top view after two different application times. A successful outcome of this work might lead to enhance PDT outcomes on deeper skin lesions.

2. Materials and methods

2.1. Experimental animal studies

Experimental animal studies were established by respecting the 3R rules (reduce, refine, replace) and approved by the ethical committee number 44. After the final authorization by the Minister of Higher Education, Research and Innovation, the project was referenced as APAFIS#19456-2019011414199848v2.

Five weeks aged female rats of Wistar Han IGS strain (Charles River Laboratory) were used in the study. The rats were fed *ad libitum* and had free access to water all the time. The room was maintained at 22 ± 1°C with artificial light from 6:00 AM to 8:00 PM. To provide animal welfare, previous limit points were established. A loss in weight superior to 15 %, a behaviour

change or a necrosis on the UV-illuminated area were considered as experimental endpoint. If one of them was reached, the animal was ethically euthanised by CO_2 inhalation or lethal dose of pentobarbital (Exagon®).

2.2. UV-B illumination procedure

UV-B illumination is well known to cause pre-malignant cutaneous lesions. Indeed, UV-B causes direct DNA damage and mutations [17, 18]. If there is a mutation in the portion corresponding to the p53 gene (tumour supressor gene) then its antiproliferative and pro-apoptotic capacities are dysfunctional and lead to the creation of a cluster of tumour cells [19, 20]. Therefore, we chose this kind of light illumination.

During the illumination period, hair removal was regularly performed (around 1 time per week). The dorsal skin (5×5 cm^2) of the rats was shaved and hairs were removed with wax (Veet, Spawax). After depilation, no exposure to UV-B light was carried out during 24 h to avoid a large skin injury. The rats were anaesthetized in pairs with isoflurane gas (Iso-vet®) with an induction at 5 % and an upholding at 2.5 %. Then the two rats were inserted into the exposure chamber. Exposure chamber (UV-crosslinker, CL1000M, Thermofisher) was set up to deliver UV-B light (centered at 316 nm) and its power was controlled with a radiometer (UVP Ultra Violet Product) and fixed at 0.43 mW/cm^2. The exposure times varied according to the objectives as below described.

2.3. Fluorescence spectroscopy

Top view PpIX fluorescence level was monitored by using an IVIS system (Illumina, PerkinElmer) set up with excitation and emission filters respectively at 430 ± 50 nm and 615 ± 40 nm. Fluorescence data were then treated with the ImageJ software.

2.4. Preparation of the MN-patch

MN-patches were produced by solvent casting molding method as described elsewhere [21]. Briefly and as summarized in figure 1, an array of 20×20 MNs was machined on an aluminium surface of 25×25 mm. MN design is similar to a "pencil-tip". The full height was 750 µm ($height_{tip}$ = 300 µm and $height_{body}$ = 450 µm), base diameter was 300 µm and each MN was tip-spaced with 1200 µm. Secondly, a female polydimethylsiloxane (PDMS) mold was created with the previous design. Thirdly, HA solution ($M_w = (5.50 \pm 0.04) \times 10^4$ g mol^{-1}, Contipro, France) was prepared at 50 mg mL^{-1} by mixing well with distilled water and 10 mg mL^{-1} of 5-ALA (GMP grade, Biosynth Chemistry & Biology) were added and mixed again. HCl at

$0.03\,\mathrm{mol\,L^{-1}}$ was added to the solution in order to be at $pH = 5$. A solution amount of 2.0 mL was cooled in the PDMS mold. The system was centrifuged at $21 \pm 1°\mathrm{C}$ and 4000 rpm for 35 min. Then it was placed in the oven at $40 \pm 1°\mathrm{C}$ for 24 h. Finally, MN-patch was removed from the mold and placed on a sticky occlusive film (Tegaderm, 3M).

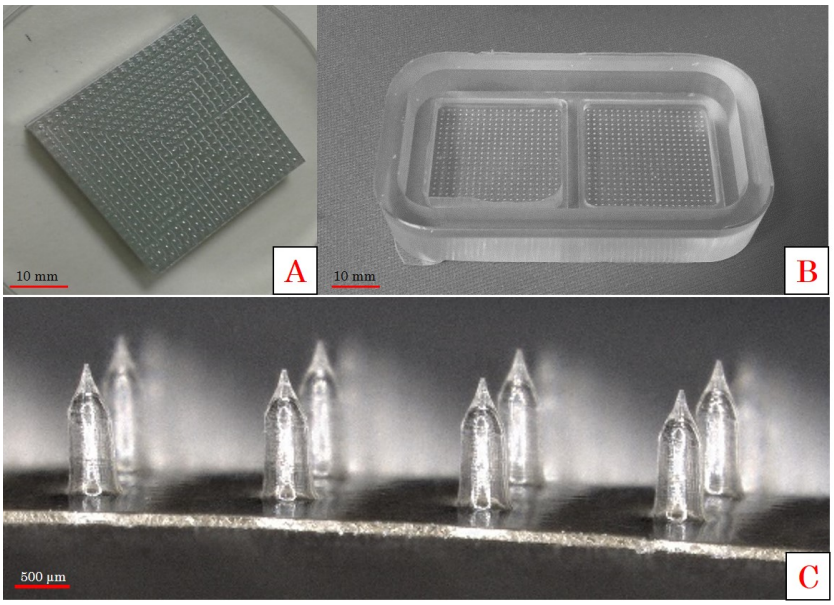

Figure 1: A: Aluminium master structure. B: Double female polydimethylsiloxane (PDMS) mold. C: Digital microscopy image of microneedles patch (MN-patch) fabricated by solvent casting molding method.

2.5. Minimal erythema dose testing

The minimal erythema dose (MED) is defined as the dose ($\mathrm{mJ\,cm^{-2}}$) of UV-B radiation producing a minimal erythema (sunburn, redness caused by the engorgement of capillaries) 24 hours after UV-B exposure and depends on the type of skin, the age and the previous skin irritation [22, 23]. The MED testing is essential to determine an appropriate UV-B dose for research purposes and to exclude under- or over-dosing.

On two female Wistar rats (5 weeks old), the MED was determined visually by using 6 incremental UV-B exposures from $96\,\mathrm{mJ/cm^2}$ to $593\,\mathrm{mJ/cm^2}$ ($96\,\mathrm{mJ/cm^2}$, $192\,\mathrm{mJ/cm^2}$, $288\,\mathrm{mJ/cm^2}$, $362\,\mathrm{mJ/cm^2}$, $456\,\mathrm{mJ/cm^2}$ and $593\,\mathrm{mJ/cm^2}$). These doses were achieved by using variable exposure times during a unique UV-B illumination.

2.6. Induction and validation of the presence of skin lesions

2.6.1. Chronic UV-B exposure to induce skin lesions

The aim of this procedure was to see from how many UV-B exposures skin lesions started to appear. To this end, 15 female Wistar Han IGS rats were divided into five groups of three animals each. The first group was exposed 30 times to UV-B at 90 % of the MED (once per day ; 5 days per week). Each following group was exposed 40, 50, 60 or 70 times with the same UV-B dose, respectively.

2.6.2. Pharmacokinetics validation

To evaluate the induction of skin lesions by UV-B illuminations, a pharmacokinetics procedure was established. 24 hours after the last UV-B exposure, animals were anaesthetized with isoflurane gas. Metvix® cream (methyl aminolevulinate, $168\,\mathrm{mg\,g^{-1}}$) was applied for 1 hour to the dorsal UV-B exposed skin (after 30, 40, 50, 60 or 70 illuminations (IL)) and was also applied to an area never exposed to UV-B to serve as normal skin controls for each rat. The fluorescence level obtained due to the metabolization of MAL to PpIX in tumour cells was reported with the IVIS (Illumina, PerkinElmer) apparatus as mentioned in section 2.3.

2.6.3. Histological study

Biopsies of the skin exposed to UV-B and normal skin were realized after animal sacrifice. The biopsy was fixed in paraformaldehyde at 4 % (overnight at $4 \pm 1°\mathrm{C}$) and then dehydrated with different baths of ethanol and xylene. Last, the skin biopsy was embedded in paraffin (Paraplast®, Leica). Tissue sections (10 µm thick) were cut, deparaffinized and stained with hematoxylin/eosin. The slides were further observed with a microscope (Axioplan 2, ZEISS).

2.7. Testing of the developed rat skin lesions model

Once the number of UV-B exposure necessary to induce skin lesions was determined, it was applied on a larger rat sample in order to validate the rat skin lesions model. Therefore a total of 40 rats was involved in this experiment and divided in two equal groups as presented in figure 2a. The cream was applied on an area of $25 \times 25\,\mathrm{mm}$ with the finger and kept under an occlusive film (Tegaderm, 3M) for either 30 minutes or 60 minutes (Group 1 or Group 2). Then PpIX fluorescence level was recorded as previously described with the IVIS system.

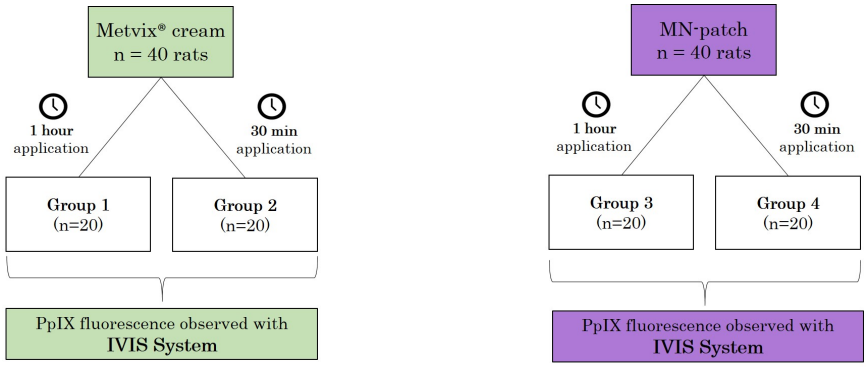

(a) *In vivo* experimental study design involving the cream application.

(b) *In vivo* experimental study design involving the MN-patch application.

Figure 2: Summary of the *in vivo* experimental studies design. (PpIX : protoporphyrin IX; MN-patch : microneedles patch)

2.8. MN-patch application

The MN-patch containing 20 mg of 5-ALA was inserted in the injured skin by applying a sufficient force. A sticking plaster was added and hooked to the anaesthetia table to ensure a constant pressure on the MN-patch. The MN-patch was inserted in a total of 40 rats for either 30 minutes or 60 minutes as presented in figure 2b. Kinetics of MN-patch dissolution was estimated by removing the patch from the skin after either 30 minutes or 60 minutes (Group 3 or Group 4). Then the MN-patches were removed and observed under normal light with a digital microscope (VHX 8000, Keyence) to evaluate the morphology after insertion.

2.9. Statistical analysis

A statistical analysis of differences in fluorescence between groups having received 0, 30, 40, 50, 60 or 70 UV-B illuminations was performed using the Kruskal–Wallis test. A Mann-Whitney test on non-matched data was used to compare the fluorescence levels obtained with the two application times (30 min vs. 60 min). All tests used a two-sided alpha level of significance of 0.05. All the analyses were completed using XLSTAT software.

3. Results and discussion

3.1. Evaluation of the MED

This test was performed on two female Wistar rats (5 weeks old) and the MED was evaluated between 96 mJ/cm^2 and 192 mJ/cm^2. Then the mean was set at 144 mJ/cm^2. To our knowledge,

no MED testing on 5 weeks old female Wistar rat was performed so this value was compared to the ones obtained for other species and sex. From this comparison, the MED we obtained it was congruent with previous results where the MED were respectively equal to $103.5\,\mathrm{mJ/cm^2}$, $170\,\mathrm{mJ/cm^2}$ and $200\,\mathrm{mJ/cm^2}$ for female HWY/Slc hairless rats [24], male rat Sprague Dawley [25] and male Wistar rats [26].

3.2. Induction of skin lesions on rats and validation of the animal model

3.2.1. Induction of skin lesions

The fluorescence level resulting from the metabolism of MAL to PpIX in tumour cells was expressed as a function of the number of UV-B illuminations (IL) received by the animal. The data are displayed in figure 3. By only considering the mean value (empty square in figure 3), a maximum of fluorescence was reached after 50 IL and then the fluorescence level tended to decrease. Because the maximum of fluorescence was obtained at 50 IL and as the fluorescence is mainly due to the presence of tumour cells [6], it may be supposed that the maximum of tumour cells induced by UV-B exposure was attained. To explain the fluorescence decrease observed at 60 IL and 70 IL, the rat skin appearance over time after UV-B illuminations displayed in figure 4 can be argued. Indeed, it is noticeable that some crusts appeared after 50 UV-B illuminations and became more severe at 60 and 70 UV-B illuminations. These crusts might have decreased the penetration and metabolization of MAL to PpIX leading to underestimated fluorescence levels at 60 IL and 70 IL. In conventional PDT it is recommended to remove crusts and scales prior to treatment to enhance drug penetration and PpIX accumulation in the skin [27]. However in our case, crusts removal would have induced bleeding (which is unethical) and potential interferences with fluorescence level measurement and was therefore not applied.

The statistical analysis demonstrated a significant difference in fluorescence level between the groups (0, 30, 40, 50, 60 and 70 illuminations) ($p - value = 0.003$) but no pairwise significant differences were detected *post hoc* (probably due to the small sample sizes). Nonetheless, $p - values$ for pairwise comparisons between 0 IL and 40, 50, 60, 70 IL are slightly higher than 0.1 ($0.124 \leq p - value \leq 0.125$) and can be accepted as representing a tendency of difference. Since the population in each group was small (3 rats), these results need to be handled with care and further tests might be conducted. Nevertheless, according to the previous results and since there was no significant difference between 40 IL and 50 IL, 40 IL should be considered as the smallest number of UV-B illuminations causing as little crusting as possible.

The comparative histological study allowed to conclude on which number of UV-B illumina-

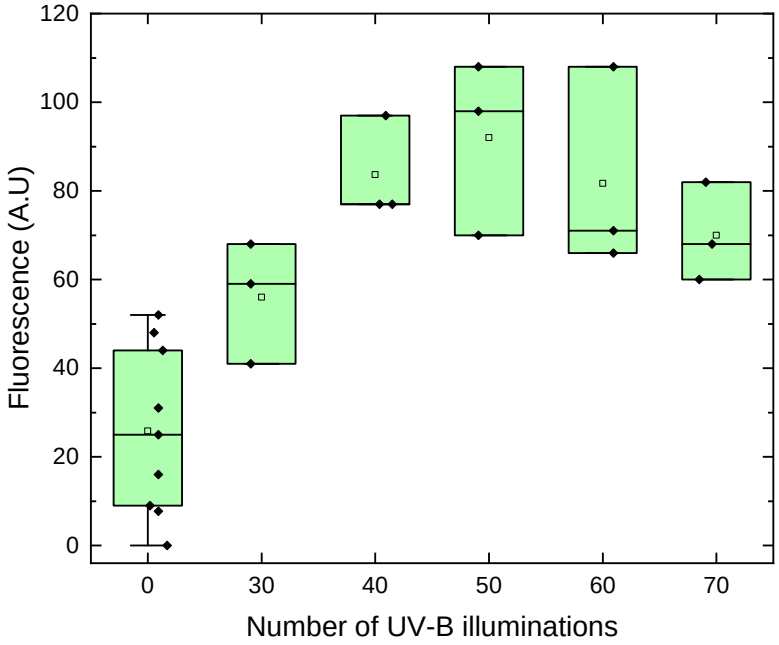

Figure 3: Monitoring graph of the evolution of skin lesions by fluorescence after application of Metvix® cream for 1 hour. The box charts at 60 IL and 70 IL should be taken with precaution since the presence of crusts might interfere with the quantification of fluorescence. The line within each box represents the median, while the lower and upper boundaries of the box indicate the first (25th percentile) and the third (75th percentile) quartiles, respectively. The empty square corresponds to the mean. Error bars (whiskers) represent the 1.5-fold interquartile range. (IL : UV-B illumination)

tions was necessary to induce skin lesions. Indeed, as seen in the annotated figure 5, there was a thickening of the epidermis even after 30 IL. At 30 IL, an acute response due to burns and repeated sunburns was noticeable but there was no sign of pre-cancerous cutaneous lesions. After 40 IL, an abnormal orientation of keratinocytes in the basal layer was observed. Moreover, the nuclei were not all round, there were triangular or squares ones. In some cases, the presence of nuclei in the upper layer (parakeratosis phenomenon) was observable. At 50, 60 or 70 IL, same observations as the one made at 40 IL can be done and in addition we found nuclei of any size (large or tiny). For the 60 and 70 IL cases, the skin biopsy was not realised on a large and deep crust which explained why the skin structure was always noticeable in figure 5. To conclude, it appeared that 40 UV-B illuminations allowed to induce pre-epitheliomatous keratosis that

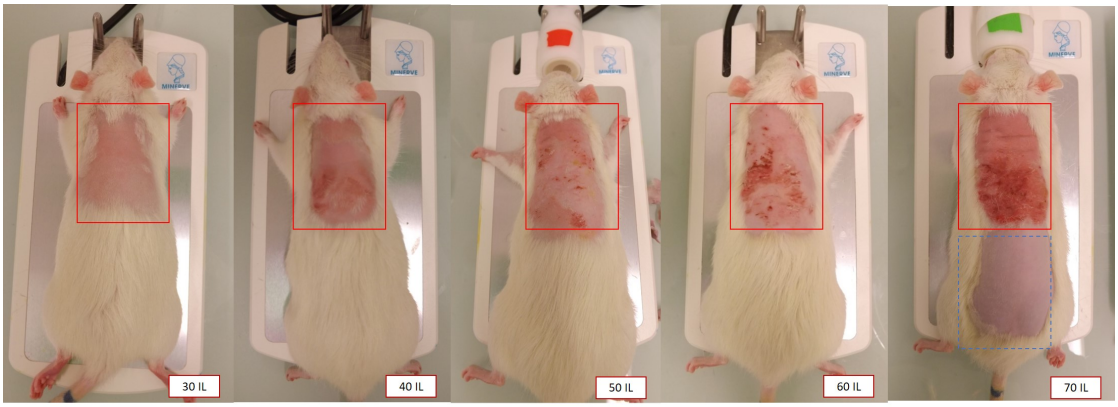

Figure 4: Photographs of UV-B-irradiated rat skin at indicated number of UV-B illuminations (IL). Red square corresponds to the skin exposed to UV-B and blue dotted square corresponds to the skin never exposed to UV-B.

extends to the appendages. The induction of skin lesions was therefore reached after 40 UV-B illuminations.

Regarding the literature, Pillon et al. studied the modelling of AKs in hairless mice chronically exposed to UV-B and the histological study showed disorganization of keratinocytes of the basal layer and a number of atypical nuclei which was characteristic of AKs. They obtained these AKs after 10 weeks of UV-B illumination, corresponding to 50 UV-B illuminations [28] which is congruent with our previous observations.

To conclude, the results obtained during the pharmacokinetics study and the exploitation of fluorescence levels concluded that 40 IL were enough to induce skin lesions and the results obtained with the histological study were consistent.

3.2.2. Validation of the animal model

The goal of the previous experimentations was to establish a protocol to induce cancerous lesions by exposing rats to different number of UV-B illuminations. In order to validate the model obtained on three rats, a larger study was performed on 40 rats. Working with a larger number of rats allowed to obtain fluorescence results that are less scattered, more reliable and more representative. The cream was applied for 30 or 60 minutes on rats undergoing 40 UV-B illuminations. PpIX fluorescence levels obtained were congruent with the previous test that included only 3 rats at 40 IL (Figure 3). The fluorescence levels are displayed in figure 6.

On the other hand, a Mann-Whitney statistical test on the results highlighted that the level of PpIX fluorescence after 60 minutes was superior to the one obtained after 30 minutes

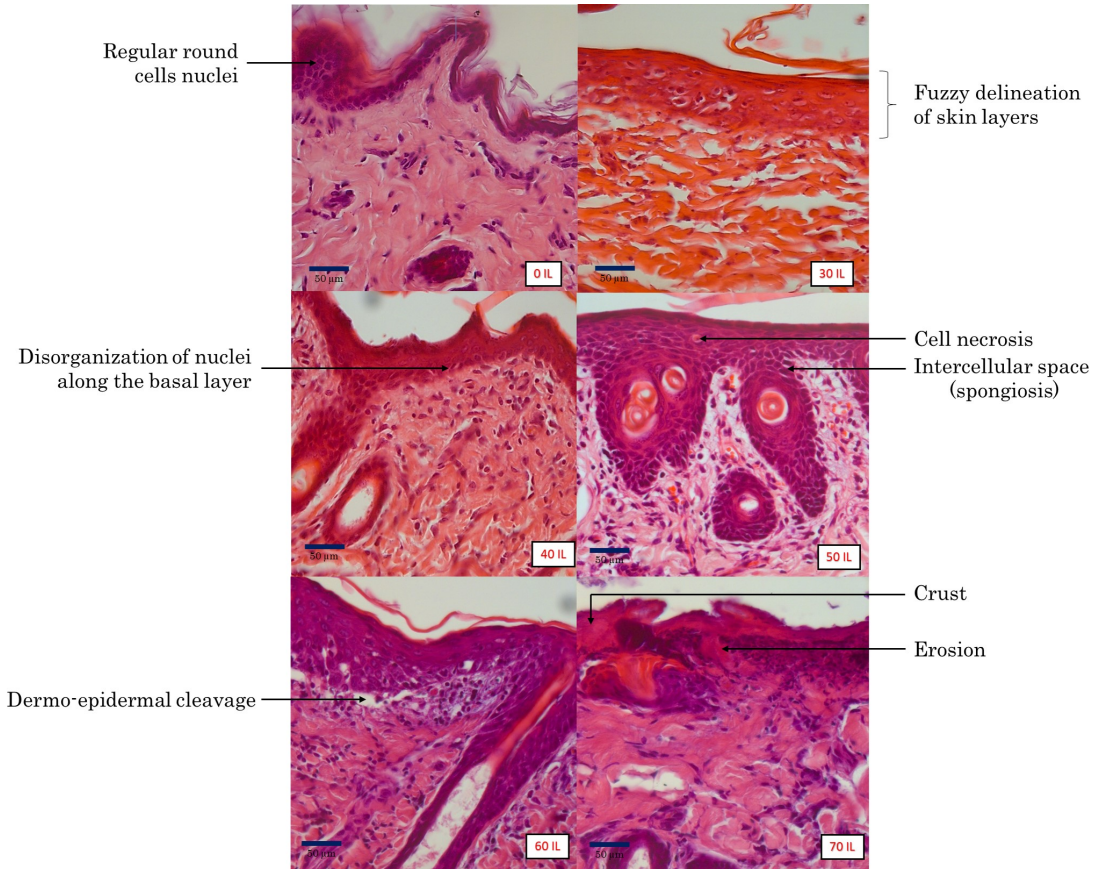

Figure 5: Comparative histology of skin rat after various UV-B illumination number. Scale bars represent 50 µm.

($p - value = 0.021$). This model allowed to evaluate the influence of the incubation time on the level of PpIX fluorescence obtained. As expected, the commercial cream application produced significant fluorescence levels and validated the model of precancerous lesions induced on rat skin on a larger rat sample. As rat skin is known to be closer to that of humans than to mice [16], this model could be useful in preclinical studies to assess the efficacy and penetration of novel molecules, or innovative drug delivery systems.

3.3. Testing of the MN-patch on the rat skin lesions model

3.3.1. Insertion and dissolution of the MN-patch in skin

The mechanical properties of the MN-patch were previously reported in [21]. As expected the MN-patch penetrated easily, without breakage in the injured rat skin since microholes on top of the skin were observed (figure 7.B). This was a first promising result since skin lesions have mechanical properties that are different from normal skin, being stiffer [29, 30]. Indeed, due to

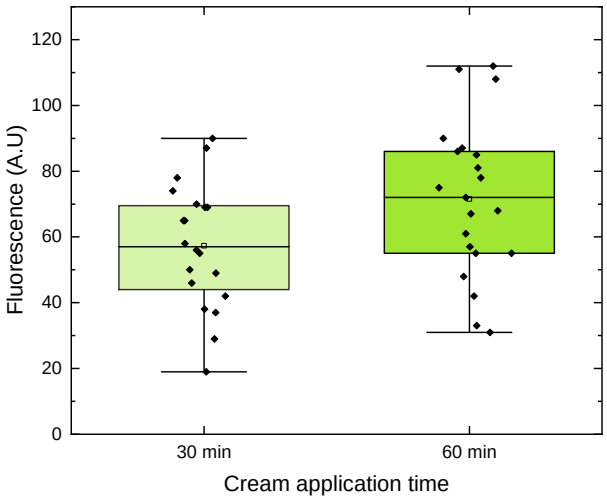

Figure 6: Skin surface fluorescence intensities from digital fluorescence photographies are shown in arbitrary unities (A.U) at two different times after cream application. The line within each box represents the median, while the lower and upper boundaries of the box indicate the first (25th percentile) and the third (75th percentile) quartiles, respectively. The empty square corresponds to the mean. Error bars (whiskers) represent the 1.5-fold interquartile range.

the thickening of the skin layers, the Young modulus tends to increase making the skin harder and potentially more difficult to perforate with MNs [29, 30]. On *ex vivo* healthy rat skin, after 30 minutes of MN-patch application only the needles tips started to dissolve and the MN-patch full dissolution was observed in one hour whereas *in vivo*, on rat suffering from skin lesions, a well initiated dissolution was observed in 30 minutes and the dissolution was completed in 1 hour for most of the animals (Figures 7.C and 7.D). Indeed, *in vivo*, temperature and humidity conditions are different from *ex vivo* parameters, which explains the difference in dissolution kinetics [31]. Nonetheless, the dissolution kinetics might also change from rat to human and Leone et al. in [31] point out that preclinical evaluation does not detract from the need to assess the dissolution of MNs in a clinical setting.

Although the dissolution was globally effective in figure 7.C (30 min), some MNs highlighted by purple arrows can still be observed on the left. On figure 7.D (60 min) the dissolution was more homogeneous despite a few MNs left in the up center of the image and also highlighted by arrows. Indeed, the elasticity and irregular surface topography of the skin is not conducive to a homogeneous application leading to a heterogeneous dissolution of the MN-patch. As already

suggested in previous studies [31–33], a MN applicator allowing a homogeneous pressure on the whole patch would lead to a better reproducibility of the piercing and a homogeneous dissolution.

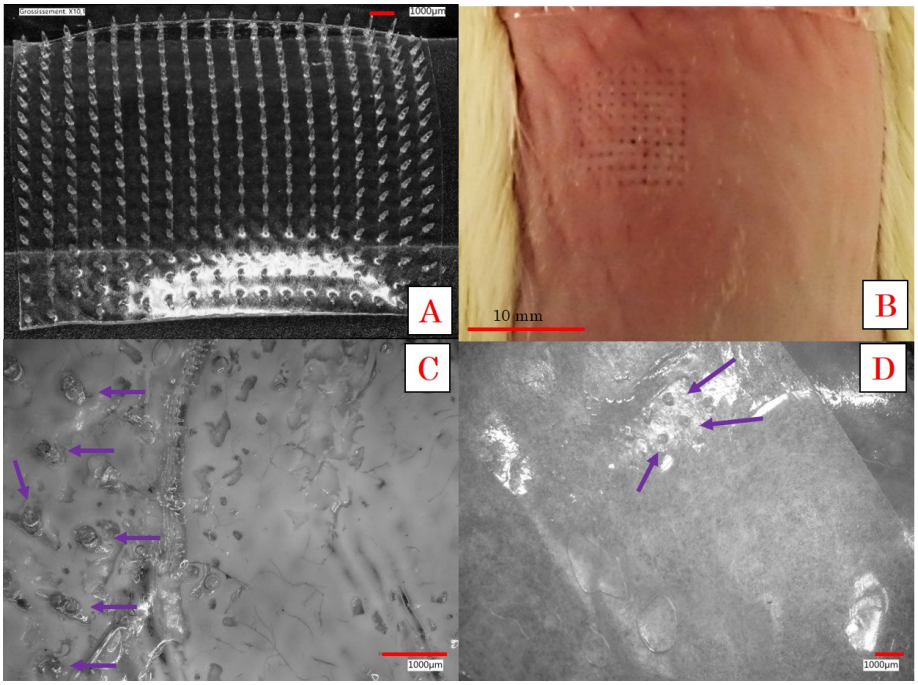

Figure 7: A : Top view observation of the MN-patch prior to insertion. B : Top view observation of rat skin after MN-patch removal and presence of microholes. C : Microscopic image of MN-patch after 30 minutes of application on the skin of a rat having received 40 UV-B illuminations : partial dissolution. D : Microscopic image of MN-patch after 60 minutes of application on the skin of a rat having received 40 UV-B illuminations : complete dissolution. Purple arrows show patch debris due to partial dissolution. (MN-patch : microneedles patch)

3.3.2. Top view observations of the PpIX fluorescence obtained with the MN-patch

A successful PDT treatment relies, *inter alia*, on a satisfactory level of PpIX in the tumour cells [6]. First, the ability of MN-patch to induce PpIX was visually evaluated on the rat skin lesions model validated in this study. When the MN-patch was applied on healthy rat skin, no fluorescence was noticeable, whereas when applied on damaged skin, PpIX fluorescence was observed (figure 8a). This observation was also reported by Zhu et al. in [14] who produced HA-based microneedles containing 5-ALA. The authors showed *in vitro* the transformation of 5-ALA to PpIX by observing a strong red fluorescence in the cells.

Besides, even if the MN-patch dissolution was not fully homogeneous, the overall fluorescence recorded was evenly distributed as shown in figure 8a and would allow a uniform PDT treatment

on the lesions having received the MN-patch [34, 35]. Indeed, Dijkstra et al. in [36] highlighted that when 5-ALA was topically applied on patients suffering from skin lesions, complete remission of tumour in certain areas was observed, but there was no response in other parts of the same lesion. The authors suspected that an unequal distribution of PpIX in the lesions may be the cause of this non-uniform clearance. Therefore, a uniform PpIX distribution is a clear advantage of the MN-patch.

Once the fluorescence was visually evaluated, the fluorescence levels were assessed and presented in figure 8b. This graph showed that the MN-patch induced a consequent level of PpIX as early as 30 minutes. Since PpIX is available, it may be supposed that a PDT session would be possible with this technology. Indeed, Zhu et al. in [14] and Zhao et al. in [13] who worked with dissolving MN made of HA and 5-ALA, did not check the PpIX fluorescence level observed *in vivo* on mice but they controlled the efficacy of their MNs in PDT. To evaluate the tumour inhibition rate, the authors applied a complete PDT treatment (application of the MNs and then illumination) and they showed that their MNs were significantly efficient compared to the control group that did not receive any treatment. As our MN-patch produced PpIX fluorescence, it would be expected to also obtain a positive PDT response. This skin lesions model on rats also showed, as already reported in [37], that PpIX fluorescence level depended on the incubation time. Indeed, a Mann-Whitney statistical test highlighted that the level of PpIX fluorescence after 1 hour was superior to the one obtained after 30 minutes ($p - value = 0.033$).

The rat skin lesion model was a good alternative to the mice one since it allowed to evaluate the penetration and dissolution of the MNs. It was also highlighted that the MN-patch was a suitable technology to induce PpIX on UV-B injured skin.

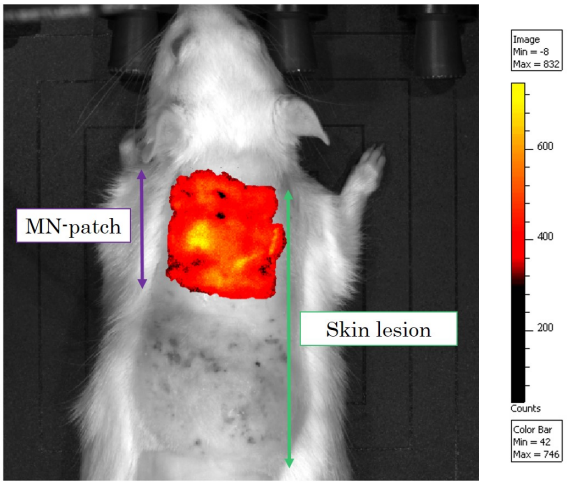

(a) Fluorescent IVIS image taken after 1 hour application of the MN-patch.

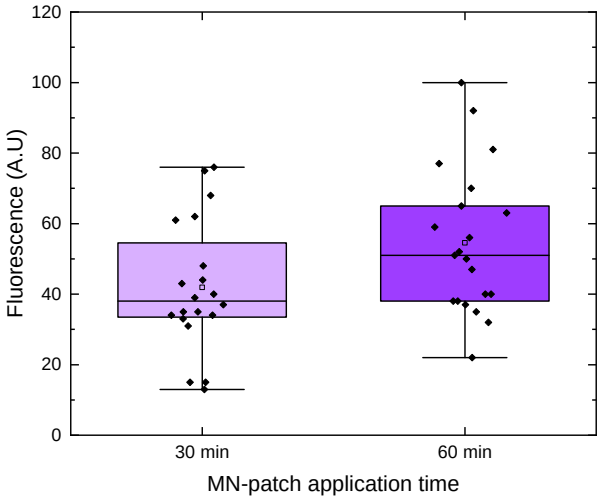

(b) Skin surface fluorescence levels from digital fluorescence photographies are shown in arbitrary unities (A.U) at two different times after MN-patch application. The line within each box represents the median, while the lower and upper boundaries of the box indicate the first (25th percentile) and the third (75th percentile) quartiles, respectively. The empty square corresponds to the mean. Error bars (whiskers) represent the 1.5-fold interquartile range.

Figure 8: Fluorescence image and data obtained after MN-patch application on skin lesion rat model. (MN-patch : microneedles patch)

4. Conclusion

This study aimed to developed a rat skin lesion model in order to evaluate the efficacy of penetration and dissolution of a MN-patch for PDT. Histological and pharmacokinetics studies demonstrated that 40 UV-B illuminations induced pre-epitheliomatous keratosis lesions on rat. Once the model was validated on a large sample of rats (n=40), the MN-patch that we developed was applied on the skin and has proven to dissolve within 1 hour and released 5-ALA leading to a homogeneous production of PpIX that might further induce a positive and uniform PDT treatment. As dissolving MNs are a burgeoning innovative technology for improving transdermal prodrug delivery, this model could be helpful for the scientific community who will want to test the MNs in a near-reality environment.

Acknowledgments

This project is supported by the European Union – European Regional Development Fund. These experiments would not have been possible without the authorization of Jean-Jacques Feige and Hervé Pointu to work in the IRIG animal facilities. The platform supported by GRAL, financed within the University Grenoble Alpes graduate school (Ecoles Universitaires de Recherche) CBH-EUR-GS (ANR-17-EURE-0003) is also acknowledged.

References

[1] J. C. Kennedy, S. L. Marcus, R. H. Pottier, Photodynamic therapy (PDT) and photodiagnosis (PD) using endogenous photosensitization induced by 5-aminolevulinic acid (ALA): Mechanisms and clinical results, Journal of clinical laser medicine & surgery 14 (1996) 289–304.

[2] A. Klein, P. Babilas, S. Karrer, M. Landthaler, R.-M. Szeimies, Photodynamic Therapy in Dermatology – an Update 2008, JDDG 6 (2008) 839–845. doi:10.1111/j.1610-0387.2008.06697.x.

[3] C. Morton, R.-M. Szeimies, N. Basset-Seguin, P. Calzavara-Pinton, Y. Gilaberte, M. Hædersdal, G. Hofbauer, R. Hunger, S. Karrer, S. Piaserico, C. Ulrich, A.-M. Wennberg, L. Braathen, European Dermatology Forum guidelines on topical photodynamic therapy 2019 Part 1: Treatment delivery and established indications – actinic keratoses, Bowen's disease and

basal cell carcinomas, Journal of the European Academy of Dermatology and Venereology 33 (2019) 2225–2238. doi:10.1111/jdv.16017.

[4] R. F. Donnelly, D. I. Morrow, P. A. McCarron, A. David Woolfson, A. Morrissey, P. Juzenas, A. Juzeniene, V. Iani, H. O. McCarthy, J. Moan, Microneedle arrays permit enhanced intradermal delivery of a preformed photosensitizer, Photochemistry and photobiology 85 (2009) 195–204.

[5] P. G. S. Rodrigues, P. F. Campos de Menezes, A. K. L. Fujita, A. Escobar, A. Barboza de Nardi, C. Kurachi, V. S. Bagnato, Assessment of ALA-induced PpIX production in porcine skin pretreated with microneedles, Journal of Biophotonics 8 (2015) 723–729. doi:10.1002/jbio.201400081.

[6] M. Champeau, S. Vignoud, L. Mortier, S. Mordon, Photodynamic therapy for skin cancer: How to enhance drug penetration?, Journal of Photochemistry and Photobiology B: Biology 197 (2019) 111544. doi:10.1016/j.jphotobiol.2019.111544.

[7] P. Mikolajewska, R. F. Donnelly, M. J. Garland, D. I. J. Morrow, T. R. R. Singh, V. Iani, J. Moan, A. Juzeniene, Microneedle Pre-treatment of Human Skin Improves 5-Aminolevulininc Acid (ALA)- and 5-Aminolevulinic Acid Methyl Ester (MAL)-Induced PpIX Production for Topical Photodynamic Therapy Without Increase in Pain or Erythema, Pharmaceutical Research 27 (2010) 2213–2220. doi:10.1007/s11095-010-0227-2.

[8] T. A. Petukhova, L. A. Hassoun, N. Foolad, M. Barath, R. K. Sivamani, Effect of Expedited Microneedle-Assisted Photodynamic Therapy for Field Treatment of Actinic Keratoses: A Randomized Clinical Trial, JAMA Dermatology 153 (2017) 637. doi:10.1001/jamadermatol.2017.0849.

[9] F. S. Iliescu, D. Dumitrescu-Ionescu, M. Petrescu, C. Iliescu, A review on transdermal drug delivery using microneedles: Current research and perspective, Ann. Acad. Rom. Sci 7 (2014) 7–34.

[10] R. F. Donnelly, D. I. J. Morrow, M. T. C. McCrudden, A. Z. Alkilani, E. M. Vicente-Pérez, C. O'Mahony, P. González-Vázquez, P. A. McCarron, A. D. Woolfson, Hydrogel-Forming and Dissolving Microneedles for Enhanced Delivery of Photosensitizers and Precursors, Photochemistry and Photobiology 90 (2014) 641–647. doi:10.1111/php.12209.

[11] R. F. Donnelly, D. I. Morrow, T. R. Singh, K. Migalska, P. A. McCarron, C. O'Mahony, A. D. Woolfson, Processing difficulties and instability of carbohydrate microneedle arrays, Drug Development and Industrial Pharmacy 35 (2009) 1242–1254. doi:10.1080/03639040902882280.

[12] M. B. Requena, Otimização da entrega de fármacos para tratamento de câncer de pele por terapia fotodinâmica, Doutorado em Física Aplicada, Universidade de São Paulo, São Carlos, 2020. doi:10.11606/T.76.2020.tde-07052020-165906.

[13] X. Zhao, X. Li, P. Zhang, J. Du, Y. Wang, Tip-loaded fast-dissolving microneedle patches for photodynamic therapy of subcutaneous tumor, Journal of Controlled Release 286 (2018) 201–209. doi:10.1016/j.jconrel.2018.07.038.

[14] J. Zhu, L. Dong, H. Du, J. Mao, Y. Xie, H. Wang, J. Lan, Y. Lou, Y. Fu, J. Wen, B. Jiang, Y. Li, J. Zhu, J. Tao, 5-Aminolevulinic Acid-Loaded Hyaluronic Acid Dissolving Microneedles for Effective Photodynamic Therapy of Superficial Tumors with Enhanced Long-Term Stability, Advanced Healthcare Materials 8 (2019) 1900896. doi:10.1002/adhm.201900896.

[15] H. Todo, Transdermal Permeation of Drugs in Various Animal Species, Pharmaceutics 9 (2017) 33. doi:10.3390/pharmaceutics9030033.

[16] E. C. Jung, H. I. Maibach, Animal models for percutaneous absorption: Animal models for percutaneous absorption, Journal of Applied Toxicology 35 (2015) 1–10. doi:10.1002/jat.3004.

[17] G. P. Pfeifer, A. Besaratinia, UV wavelength-dependent DNA damage and human nonmelanoma and melanoma skin cancer, Photochem. Photobiol. Sci. 11 (2012) 90–97. doi:10.1039/C1PP05144J.

[18] J. Ramos, J. Villa, A. Ruiz, R. Armstrong, J. Matta, UV dose determines key characteristics of nonmelanoma skin cancer, Cancer Epidemiology and Prevention Biomarkers 13 (2004) 2006–2011.

[19] R. P. Rastogi, Richa, A. Kumar, M. B. Tyagi, R. P. Sinha, Molecular Mechanisms of Ultraviolet Radiation-Induced DNA Damage and Repair, Journal of Nucleic Acids 2010 (2010) 1–32. doi:10.4061/2010/592980.

[20] H. Zhao, F. Traganos, Z. Darzynkiewicz, Kinetics of the UV-induced DNA damage response in relation to cell cycle phase. Correlation with DNA replication, Cytometry Part A (2009) n/a–n/a. doi:10.1002/cyto.a.20839.

[21] M. Champeau, D. Jary, L. Mortier, S. Mordon, S. Vignoud, A facile fabrication of dissolving microneedles containing 5-aminolevulinic acid, International Journal of Pharmaceutics 586 (2020) 119554. doi:10.1016/j.ijpharm.2020.119554.

[22] I. Chaillol, Mesure de l'exposition au rayonnement ultraviolet solaire pour les études épidémiologiques, Ph.D. thesis, Université Claude Bernard Lyon 1, 2011.

[23] C. J. Heckman, R. Chandler, J. D. Kloss, A. Benson, D. Rooney, T. Munshi, S. D. Darlow, C. Perlis, S. L. Manne, D. W. Oslin, Minimal Erythema Dose (MED) Testing, Journal of Visualized Experiments (2013). doi:10.3791/50175.

[24] H. Jeon, J. Kim, W. Kim, S. Lee, Effects of Oral Epigallocatechin Gallate Supplementation on the Minimal Erythema Dose and UV-Induced Skin Damage, Skin Pharmacology and Physiology 22 (2009) 137–141. doi:10.1159/000201562.

[25] G. Imokawa, K. Ishida, Biological Mechanisms Underlying the Ultraviolet Radiation-Induced Formation of Skin Wrinkling and Sagging I: Reduced Skin Elasticity, Highly Associated with Enhanced Dermal Elastase Activity, Triggers Wrinkling and Sagging, International Journal of Molecular Sciences 16 (2015) 7753–7775. doi:10.3390/ijms16047753.

[26] G. A. Krismayogi, I. D. Ratnayanti, N. M. Linawati, I. S. Wiryawan, I. W. Sugiritama, I. A. I. Wahyuniari, I. Nyoman Arijana, Purple Cabbage Extract Cream Effect on Erythema Score of Male Wistar Rats Back Skin Exposed to UV-B Radiation, Biomedical and Pharmacology Journal 11 (2018) 343–351. doi:10.13005/bpj/1378.

[27] C. Morton, R.-M. Szeimies, A. Sidoroff, L. Braathen, European guidelines for topical photodynamic therapy part 2: Emerging indications - field cancerization, photorejuvenation and inflammatory/infective dermatoses: European PDT guidelines, Journal of the European Academy of Dermatology and Venereology 27 (2013) 672–679. doi:10.1111/jdv.12026.

[28] A. Pillon, B. Gomes, I. Vandenberghe, V. Cartron, P. Cèbe, J.-C. Blanchet, V. Sibaud, N. Guilbaud, L. Audoly, L. Lamant, A. Kruczynski, Actinic keratosis modelling in mice: A translational study, PLOS ONE 12 (2017) e0179991. doi:10.1371/journal.pone.0179991.

[29] S. J. Kirkpatrick, R. K. Wang, D. D. Duncan, M. Kulesz-Martin, K. Lee, Imaging the mechanical stiffness of skin lesions by in vivo acousto-optical elastography, Optics Express 14 (2006) 9770. doi:10.1364/OE.14.009770.

[30] F. H. Silver, R. G. Shah, M. Richard, D. Benedetto, Comparative "virtual biopsies" of normal skin and skin lesions using vibrational optical coherence tomography, Skin Research and Technology 25 (2019) 743–749. doi:10.1111/srt.12712.

[31] M. Leone, J. Mönkäre, J. A. Bouwstra, G. Kersten, Dissolving Microneedle Patches for Dermal Vaccination, Pharmaceutical Research 34 (2017) 2223–2240. doi:10.1007/s11095-017-2223-2.

[32] A. Ripolin, J. Quinn, E. Larrañeta, E. M. Vicente-Perez, J. Barry, R. F. Donnelly, Successful application of large microneedle patches by human volunteers, International Journal of Pharmaceutics 521 (2017) 92–101. doi:10.1016/j.ijpharm.2017.02.011.

[33] T. R.R. Singh, N. J. Dunne, E. Cunningham, R. F. Donnelly, Review of Patents on Microneedle Applicators, Recent Patents on Drug Delivery & Formulation 5 (2011) 11–23. doi:10.2174/187221111794109484.

[34] W. D. Tope, A. Martin, J. M. Grevelink, J. C. Starr, J. L. Fewkes, T. J. Flotte, T. F. Deutsch, R. R. Anderson, Lack of selectivity of protoporphyrin IX fluorescence for basal cell carcinoma after topical application of 5-aminolevulinic acid: Implications for photodynamic treatment, Archives of Dermatological Research 287 (1995) 665–674. doi:10.1007/BF00371740.

[35] C. L. Campbell, C. T. A. Brown, K. Wood, H. Moseley, Modelling topical photodynamic therapy treatment including the continuous production of Protoporphyrin IX, Physics in Medicine and Biology 61 (2016) 7507–7521. doi:10.1088/0031-9155/61/21/7507.

[36] A. Dijkstra, I. Majoie, J. van Dongen, H. van Weelden, W. van Vloten, Photodynamic therapy with violet light and topical delta-aminolaevulinic acid in the treatment of actinic keratosis, Bowen's disease and basal cell carcinoma, Journal of the European Academy of Dermatology and Venereology 15 (2001) 550–554. doi:10.1046/j.1468-3083.2001.00333.x.

[37] M. Haedersdal, F. H. Sakamoto, W. A. Farinelli, A. G. Doukas, J. Tam, R. R. Anderson, Pretreatment with ablative fractional laser changes kinetics and biodistribution of topical 5-aminolevulinic acid (ALA) and methyl aminolevulinate (MAL): PRETREATMENT WITH

AFXL CHANGES OF ALA AND MAL, Lasers in Surgery and Medicine 46 (2014) 462–469. doi:10.1002/lsm.22259.

3.4 Supplementary informations

Some results have not been included in the article but allow to clarify and have a better understanding of the transdermal delivery of 5-ALA and are therefore presented hereinafter.

3.4.1 PY is not fluorescent

Fluorescence behaviour of PY purchased from Carbosynth Product has been checked with a microplate reader (TECAN) whose excitation wavelength has been set at 430 nm and emission wavelength has been set, in the scan mode, as varying from 550 nm to 850 nm. The results showed that no fluorescence was observed which confirmed that the fluorescence recorded by the IVIS system was only due to PpIX.

3.4.2 Bandage

During the preclinical investigation on rats, it was observed that the patch dissolution was not always uniform. Therefore, to address the problem, it was considered to perforate the occlusive Tegaderm film in order to drop a small amount of water on top to ensure full MN-patch dissolution. Perforation of the Tegaderm was performed by laser cutting (TROTEC Laser Speedy 400 Flexx) with the following set up: holes diameter of 360 µm and spaced 1100 µm apart (Figure 3.1).

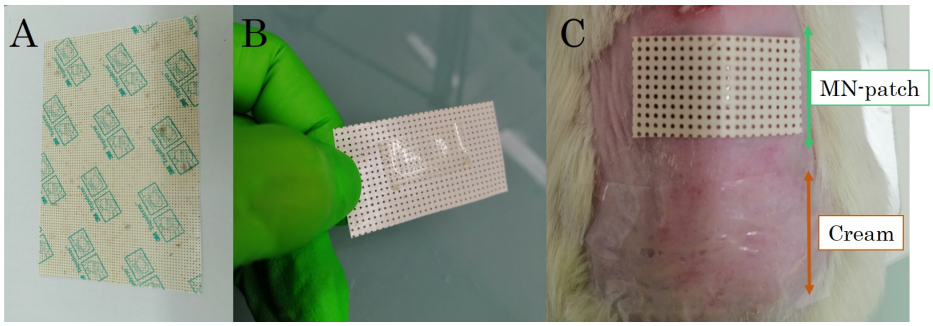

Figure 3.1 – A: Photography of the perforated Tegaderm bandage. B: MN-patch was stuck on the perforated Tegaderm. C: The device was applied on skin rat and a drop of water was deposited on top to ensure full dissolution.

3.4.3 Cross-section observations

The article in section 3.3 highlighted that microneedles were able to penetrate the skin, dissolved within one hour and produced a consequent fluorescence level on top of the skin. However, as microneedles were firstly designed to enhance the prodrug penetration in deep skin layers, the PpIX fluorescence distribution was also controlled in skin cross-section and compared to the fluorescence obtained with the cream. To observe the penetration of 5-ALA and its metabolization to PpIX, skin samples were embedded in OCT compound tissue freezing (TFM, M-M FRANCE). Tissue sections (10 µm thick) were cut and the slides were then observed under a microscope (Axio, ZEISS). The excitation filter was set at 434 nm with a bandwidth of 17 nm (MF-434-17, Thorlabs) and the emission filter was a colored glass long-pass filter with a cut-down wavelength at 560 nm (03FCG498, Melles Griot). The dichroic mirror was chosen with

a reflexion band between 415 and 470 nm and a transmission band between 490 and 720 nm (MD480, Thorlabs). Results obtained with skin lesion samples taken from rats treated according to the protocol described in section 3.3 are displayed in figure 3.2.

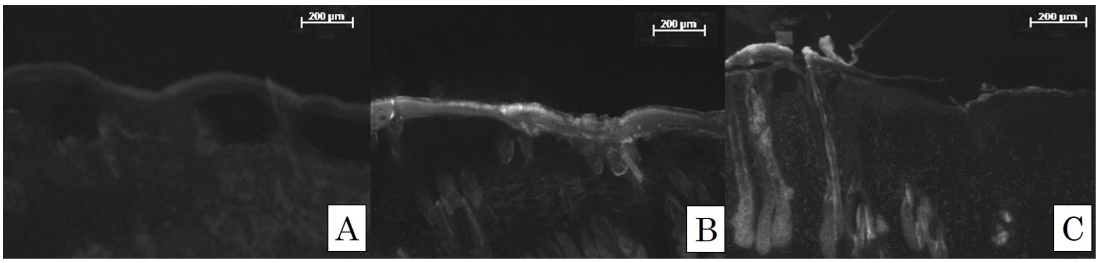

Figure 3.2 – Cross-sections of the skin of the same rat having received 40 UV-B illuminations (A), after 1 h of the cream application (B) and after 1 h of the MN-patch application (C).

Accumulation of PpIX in the upper layers of the skin (potentially in the SC) was clearly observed in figure 3.2.B. In microneedle-exposed skin (figure 3.2.C), the fluorescence seemed to extend deeper but by plotting the fluorescence profile no significant difference between both samples (cream and patch) was noticeable. Moreover, figure 3.2 underscored the limits of the animal model. Despite shaving, the hair follicles are still present (oval shapes) and produced fluorescence at the excitation and emission wavelengths chosen which interfered with the measurements.

3.5 Establishment of the depth penetration of 5-ALA through *ex vivo* skin

Due to fluorescence of other elements in the skin, it was difficult to observe the penetration of the prodrug and especially its metabolization to PpIX in deep skin layers only with only a fluorescence measurement. Therefore, to establish more precisely the MN benefit two others experiments were performed. The first one consisted of the use of a Time-of-Flight Secondary Ion Mass Spectrometry (ToF-SIMS) method in order to map the cross section 5-ALA profile penetration. The second approach was to study the *in vitro* transcutaneous passage of 5-ALA with the use of Franz diffusion cell apparatus.

3.5.1 Penetration of 5-ALA through *ex vivo* human skin

3.5.1.1 ToF-SIMS principle and method

ToF-SIMS described in figure 3.3 is a surface-sensitive analytical method that uses a pulsed ion beam in order to snatch molecules from the very outermost surface of the sample. The particles are removed from atomic monolayers on the surface (secondary ions). These particles (positive or negative) are then accelerated into a "flight tube" and their mass is determined by measuring the exact time at which they reach the detector [175].

3.5.1.2 ToF-SIMS experiment

MN-patch was applied on *ex vivo* human skin samples for 1 hour and were then prepared in a cross section geometry to image drug distribution. ToF-SIMS analysis was performed

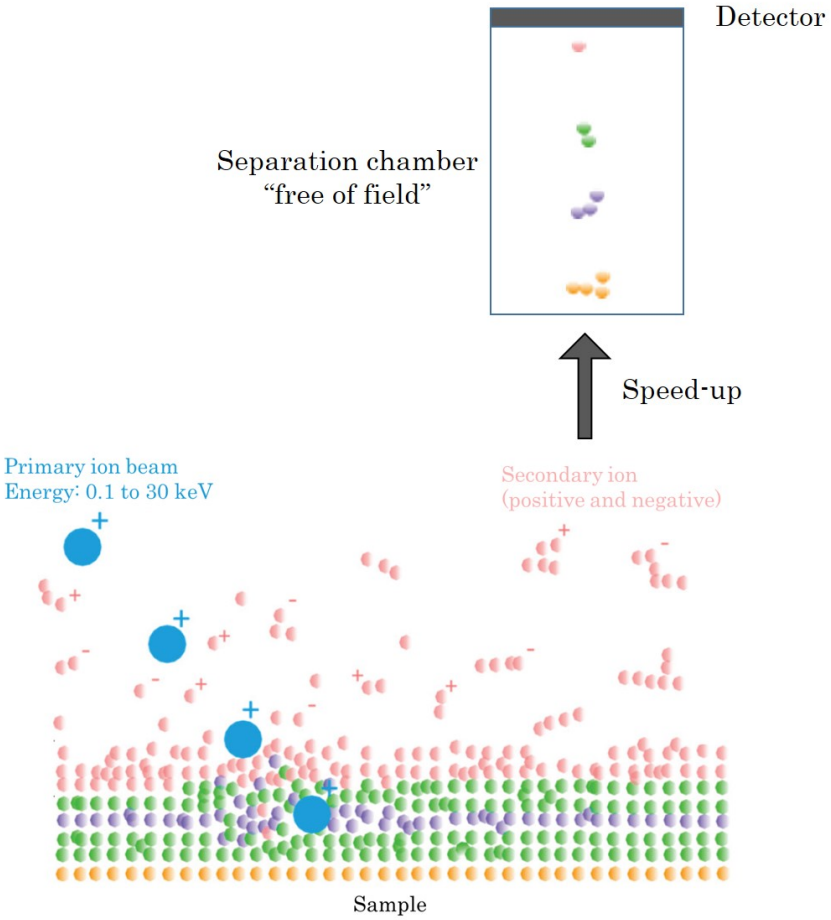

Figure 3.3 – Simplified view of the ToF-SIMS analysis after bombardment of a sample by an ion primary beam. Scheme adapted from [175].

using an ION-ToF ToF-SIMS 5 instrument with and analysis beam of Bi^{3+} at 15 keV in bunched mode. Images were acquired in both positive and negative polarity. Vacuum level was set at 5×10^{-7} mbar due to the hydrated samples degassing (the amount of tissue was minimized to reduce this effect).

3.5.1.3 Results, discussions and perspectives

The mapping in both positive and negative modes are displayed in figure 3.4 and highlighted that the signal of 5-ALA either at M/z 132 in positive polarity and or at M/z 130 in negative polarity were already present in the skin alone. These two signals corresponded respectively to the 5-ALA molecule ($M = 131\,g\,mol^{-1}$) plus a hydrogen atom or minus a hydrogen atom. Moreover, these characteristic peaks from the 5-ALA can also be found in the skin having been in contact with the MN-patch (that contains 5-ALA). On the whole human skin sample, of 500 µm thickness, the distribution was uniform and there was no gradient of 5-ALA over the whole thickness. This result seemed to indicate a diffusion with a sufficiently fast kinetics to

homogenize the concentration in the whole section. Nevertheless, with the cartography alone it was hard to say if the signal was higher in case of MN-patch application compared to the skin alone hence the intensities were normalized to the total ion intensity and were reported in table 3.2.

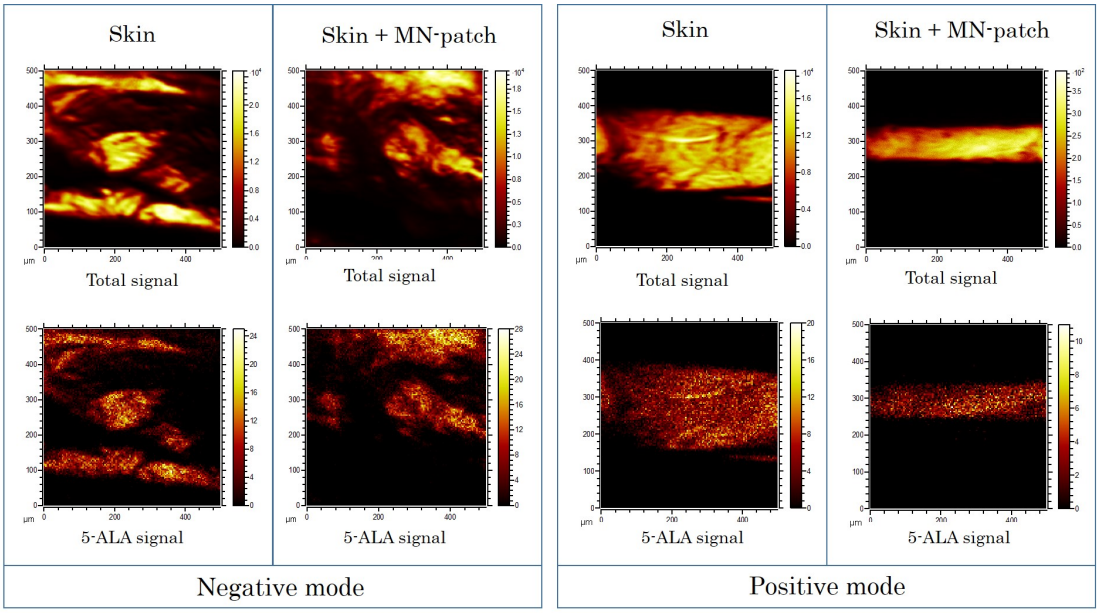

Figure 3.4 – Mapping images in both positive and negative modes of the skin alone and the skin having been in contact with the MN-patch. Total signals obtained are in the upper line and 5-ALA signal are displayed in the bottom line.

Samples	5-ALA signal in positive mode	5-ALA signal in negative mode
m/z	132.0608	129.9508
Skin	4.96×10^{-4}	4.14×10^{-4}
Skin + MN-patch	6.48×10^{-4}	7.29×10^{-4}

Table 3.2 – Intensities signal of 5-ALA normalized by the total ion intensity in positive and negative modes.

In order to establish if the 5-ALA quantity was superior after MN-patch application on human skin, the 5-ALA signal intensities, given in table 3.2, can be compared indicating that the MN deliver 1.3 to 1.8 fold compared to endogenous 5-ALA. ToF-SIMS is a very complex apparatus that could give numerous information. In our case we decided to only study the signal of the 5-ALA molecule plus or minus a hydrogen atom but it would also be possible to visualize signal intensity of molecule fragment such as C-NH_2 or C=O. This experiment was an exploratory work that confirmed the release of 5-ALA in deep but to go further we should:

- Work with a deeper cross-section human skin sample to observe the diffusion gradient of 5-ALA

- Use a 5-ALA isotope that has a higher molar mass for distinguishing more easily its characteristic signal among the skin signal
- Study other 5-ALA molecule fragments to evaluate if the tendency if the same as the one we observed
- Work with shorter application times (30 min or 45 min) to show the advantages of MN compared to patch without MN

Since the last 5 years, this technology has been widely used to study biological samples for example in 2017 to evaluate the penetration of fatty acids into *ex vivo* human skin [33] or in 2020 to examine the distribution of a beauty ingredient in the human skin [80]. Although our preliminary ToF-SIMS experiment was encouraging, it should be repeated and optimized in order to give precise results by a very innovative technique.

Acknowledgements This work has been realized with the support of Jean-Paul Barnes from the nano-characterization platform in CEA-Leti.

3.5.2 Penetration of 5-ALA through *ex vivo* rat skin

ToF-SIMS experiment provided information on the first 500 µm of human skin depth, therefore to evaluate deeper the profile penetration of 5-ALA, we worked with a deeper skin sample and use another approach with Franz cell apparatus.

3.5.2.1 Franz cell principle and method

The Franz cell apparatus from Proviskin (Besançon, France) consists of two primary chambers separated by a membrane which was in our case *ex vivo* rat skin retrieved from previous *in vivo* experiments. A schematic representation of the Franz cell apparatus is displayed in figure 3.5. The MN-patch ($MN_t - 20$) was applied on the *ex vivo* skin via the donor compartment. The receptor compartment contained water whose temperature was set at 33 °C according to the average skin temperature [155]. Usually, a precise amount of water contained in this bottom chamber is taken out at regular intervals for analysing the analyte (5-ALA). This method measures the analyte quantity that has gone through the skin sample. Nevertheless, most of the prodrug is often in the skin itself especially when the application time is only about one hour. Therefore, after 1 hour of MN-patch application, the *ex vivo* human skin was analysed layer by layer.

3.5.2.2 Extraction of 5-ALA from the different skin layers

The skin was removed from the Franz cell apparatus and cryoconserved in OCT compound tissue freezing (TFM, M-M FRANCE). A cryomicrotome (3050CM, Leica) was used to cut the cryoconserved skin from top to bottom in slices of 100 µm. Each slice was then dispersed in 1.0 mL of H_2O:acetonitrile (ACN) (90:10) and mixed for 4 h in order to be sure that all 5-ALA is well extracted by solubilisation. This solution was then filtered on 0.2 µm and analyzed to determine the amount of 5-ALA contained in it.

3.5.2.3 Dosage of 5-ALA by liquid chromatography analysis

^{1}H NMR was previously employed to determine 5-ALA quantity (see section 2.3) but because the amount expected with this experiment might be inferior to 1.0 mg mL^{-1}, a novel dosage method

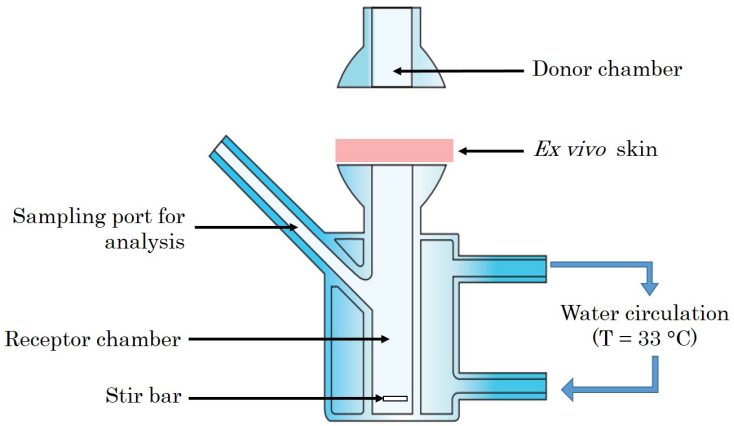

Figure 3.5 – Simplified schema of the Franz cell apparatus with the different compartments represented.

has been established using Ultra Performance Liquid Chromatography (UPLC) coupled with Evaporating Light Scattering detector (ELSD). Indeed, classical analytical methods to quantify 5-ALA often required a derivatization which meant that 5-ALA molecule underwent a number of different chemical reactions to make it fluorescent or UV-visible. Nonetheless, these techniques are often sources of error and when we tested them, we highlighted that the derivatized 5-ALA was not always stable in time making again new errors in quantification which justify the use of a new analytical method based on UPLC-ELSD detection.

For this reason, chromatographic analysis of the 5-ALA was performed using an Acquity UPLC H-Class system from Waters (Milford, USA) coupled with an Alltech 3300 ELSD from Grace (Columbia, USA). Quantification of the analyte was performed by hydrophilic interaction liquid chromatography (HILIC) using a CORTECS UPLC HILIC column (1.6 µm,150 × 2.1 mm, 90 Å, Waters). Separation was achieved using a gradient program with two solvents: 0.1 % TFA in water (phase A) and ACN (phase B). Chromatographic separation was carried out using as follow: t_{0min}:10 % of phase A and 90 % of phase B, t_{12min}: 50 % of phase A and 50 % of phase B. 10 µL of the sample to analyze was injected and the mobile phase flow rate was set at 0.3 mL min^{-1}. ELSD method was adapted from a previous study led by Armoškaitė et al. using HPLC-ELSD for the quantification of 5-ALA after penetration into human skin *ex vivo* [11]. Therefore ELSD evaporation temperature was set at 45 °C, nitrogen flow rate and gain were respectively fixed at 1.5 L min^{-1} and 16.

Calibration validation

Standard concentrations of 5-ALA were prepared from 10 µg mL^{-1} to 100 µg mL^{-1} in deionized water and the calibration curve (in red) is displayed in figure 3.6 and showed a polynomial relationship between concentration and ELSD responses which is linked to the type of detection [187, 11]. Therefore, a second-order polynomial was used as the fitting model (Equation 3.1) where X represents 5-ALA concentration in µg mL^{-1}, Y is the peak area and a, b and c are constants respectively equal to 139, 138 651 and −141 051. This model was considered as acceptable since the value of R^2 (coefficient of determination) was > 0.990.

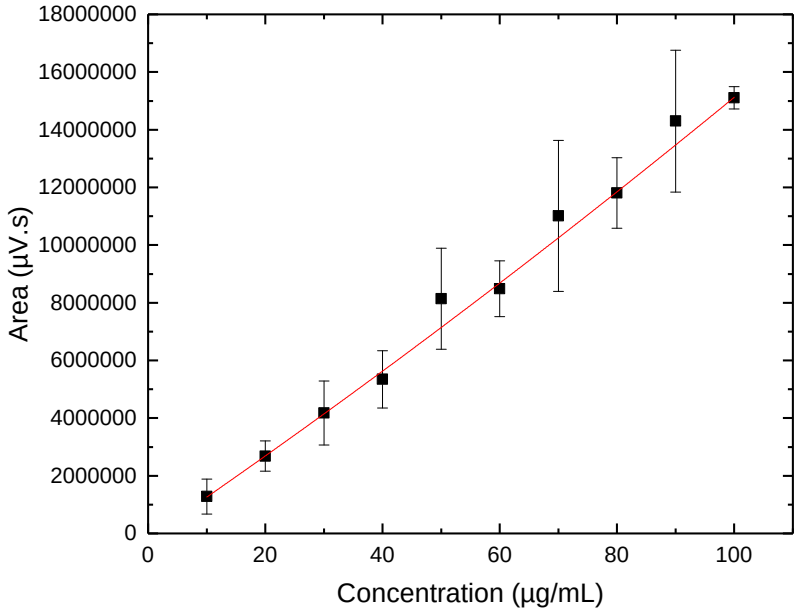

Figure 3.6 – Calibration curve obtained with UPLC-ELSD for quantification of 5-ALA. Results are presented as mean ± s.e.m.

$$Y = aX^2 + bX + c \tag{3.1}$$

3.5.2.4 Results, discussions and perspectives

Each slice of skin from the top to the bottom was analyzed with the UPLC-ELSD method, the signal response was measured and using the calibration curve, the concentration of 5-ALA in each slice was determined and the results are displayed in figure 3.7.

First of all, it was clear that from one sample to another there were fluctuations concerning the total amount of 5-ALA that reached 363 µg, 309 µg and 730 µg for samples 1, 2 and 3, respectively. One explanation of these differences may be due to the variable dissolution kinetics of the MN-patch that depended on the water content in the rat skin sample. Besides, the maximum penetration depth were also changing from one sample to another but the order of magnitude was the same with the maximum of 5-ALA released obtained respectively at 1500 µm, 1100 µm and 1500 µm for samples 1, 2 and 3. Since the MNs had a length of 750 µm and according to the previous results obtained in ToF-SIMS experiment we could expect that 5-ALA would be present up to 750 µm due to the dissolution of MNs. The presence of 5-ALA in depth superior to 750 µm was due to diffusion of the molecule through the skin layers. However, these results should be compared to fresh *ex vivo* rat skin since it was demonstrated that transdermal penetration of drugs might be increased with frozen skin [3]. On the other hand, the MN-patch applied to the rat skin sample contained a quantity of 5-ALA of ≈ 890 µg, therefore the total 5-ALA amounts collected after one hour in rat skin samples 1, 2 and 3 represented respectively

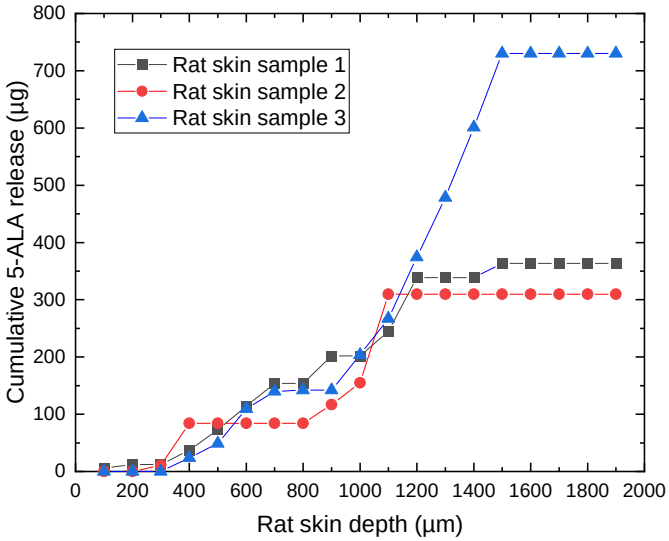

Figure 3.7 – Franz cell penetration profiles showing the cumulative concentration of 5-ALA in rat skin samples after 1 h of MN-patch application.

41 %, 35 % and 82 %. We are aware that this is a preliminary experiment and comparison with the Metvix® cream or a patch without MN would be interesting to really show the added value of the MNs. Nevertheless this experiment is encouraging and should be continued especially because this way of prodrug penetration quantification is getting often used. For example, Ahmadi et al. in [4] studied the penetration of 5-ALA through basal cell carcinoma and showed that after 4 h of cream application, depths of penetration of at least 2 mm from the lesion surface had been reached. Another example is Donnelly et al. in [42] who evaluated the delivery of a photosensitizer from MNs through porcine skin samples and revealed the dye presence up to 1.125 mm after 6 h of application.

To summarize, 5-ALA was quantified with a UPLC-ELSD detection which was a quite new analytical method. This method allowed to get an idea on the 5-ALA that had penetrated through the rat skin layers. In parallel and always with the idea to do not chemically modify the 5-ALA, ToF-SIMS also appeared as a new method to quantify 5-ALA through *ex vivo* human skin.

Conclusion

- A model of skin lesions on rats was developed by applying a total of 40 UV-B illuminations and validated by histology and pharmacokinetics studies.
- The $MN_t - 20$ patch was therefore tested on a realistic skin lesions model and proved that after a 1 hour application, the patch dissolved, released 5-ALA that further metabolized to PpIX. A significant amount of PpIX fluorescence level was recorded which indicated that a PDT session would be possible.
- The penetration of PpIX in depth was not really observable by fluorescence in cross-section since the hair follicles were auto-fluorescent and disturbed the amount of PpIX fluorescence recorded.
- ToF-SIMS was therefore used to better establish the penetration of 5-ALA in *ex vivo* healthy human skin and showed that the distribution was homogeneous from 0 to 500 µm in depth after 1 h of MN-patch-application.
- Cumulative 5-ALA penetration after Franz cell experiment highlighted that after 1 h of MN-patch-application, 5-ALA was present until 1100-1500 µm in depth in *ex vivo* rat skin. These results underlined that MN-patch would be a promising technology to treat deep skin lesions (such as nodular BCCs) that could extend to the interface epidermis/dermis. Nevertheless, these *in vitro* studies will have to be continued, in particular to study shorter times; to compare the MN-patch with cream or a patch without MN in order to definitely show the advantage of MNs.

Chapter 4

Coupling microneedles with light
Proposition of a proof of concept: PDT all-in-one

Outline of the current chapter

Introduction

- In this chapter, the motivation that led us to consider an all-in-one PDT system will be detailed.
- Then the choice of light source to be integrated in the embedded PDT device will be developed and its digital and electronic implementations will be presented.
- The 3D printing method chosen for coupling microneedles and light device will be specified.
- Initial characterizations that consisted of light diffusion uniformity, temperature control, wavelength and power measurements, and that were realized on the all-in-one PDT system comprising microneedles and light device will be described.
- An attempt to identify the regulatory positioning of the complete product in Europe will be reported.

4.1 Coupling light with microneedles

4.1.1 Clinical issues : background and purpose

The final goal of this thesis is to design an all-in-one device, composed on the one hand of dissolving microneedles that can perforate the *stratum corneum* and ensure the release of the 5-ALA in sufficient quantity; and on the other hand of an integrated light system. Indeed, the design and the preliminary tests of the microneedles were shown in chapters 2 and 3 and demonstrated that the release of 5-ALA was efficient in a short time. Nevertheless, to perform a PDT treatment, light is absolutely necessary and now, we would like to propose a full device that can allow a one-step PDT treatment.

As a reminder, the second step of a conventional PDT treatment is to irradiate the area with light at $\approx 635\,\text{nm}$ to activate the PpIX produced by 5-ALA metabolization during the heme synthesis. Typically, this step is performed after a long incubation time of 5-ALA (3 h) and requires the use of a high dose of light ($37\,\text{J}\,\text{cm}^{-2}$) to ensure good light diffusion through the different skin layers [177]. This treatment is generally tolerated but discomfort or pain is common during conventional PDT and in particular during light irradiation [115].

Ten years ago, there was no obvious evidence that pain was associated with light source, fluence rate, or light dose [196]. Nevertheless, in 2008, pain started to be correlated to another parameter that was the PpIX fluorescence amount in the treatment area and the first idea was to reduce the fluence rate from $68\,\text{mW}\,\text{cm}^{-2}$ to $34\,\text{mW}\,\text{cm}^{-2}$, which consequently decreased pain score from 8 to 6 [203]. Reducing the fluence rate resulted in prolonging the illumination, then the PpIX accumulated in the cells was not fully activated in a short time period and created a lower pain response due to lower inflammatory process and lower nerve endings stimulation [203]. Similarly, in 2011 Apalla et al. showed that the complete response rate was not depending on fluence rate but the pain felt by patients was less important when the fluence rate was set between 25-50 $\text{mW}\,\text{cm}^{-2}$ instead of $75\,\text{mW}\,\text{cm}^{-2}$ [10]. These studies showed that the pain felt during PDT is due to the important amount of PpIX accumulated in the cells during light activation. To overcome this problem, the first idea was to reduce the fluence rate to avoid a huge photochemical reaction in a short time period.

More recently in 2019, Vignion-Dewalle et al. compared the efficacy of 10 efficient protocols

for PDT of AKs and showed that, even with a lower light dose (either 10 or 12 J cm^{-2}), the three-month clearance rates were as good as those obtained with conventional PDT ($\approx$ 80 %) and the pain recorded was weaker [190, 112]. On the other hand, in 2020, it has also been shown that when the illumination was performed directly after prodrug application, the pain was lower since PpIX did not have time to diffuse through surrounding tissues containing sensory nerves [114]. Indeed, it is well known that when the illumination starts, the photons immediately activate all the PpIX, initiating the photochemical reactions inducing a painful nerve reaction due to the oxygen species that are known to cause mast cell degranulation leading to release of inflammatory mediators that stimulate sensory nerve endings [8, 115]. Therefore, reducing the accumulation of PpIX in the cells would reduce the level of oxygen species and allow a less painful PDT treatment. This accumulation of PpIX encountered is due in particular to the long incubation period required to allow prodrug diffusion in deep seated lesions. However, with the MN-patch that we have developed, this long incubation time of 3 hours would not be necessary and it would be appreciated to directly activate the PpIX produced.

On the other hand, to improve patient compliance, daylight PDT has started to be often used over the last decade and has been highlighted as painless. Indeed, exposure to natural daylight starts within 30 min after MAL application which is just after initial synthesis of PpIX and avoid diffusion of PpIX to deep tissues containing sensory nerves [117, 201].

Always with the idea to reduce pain, fractioned light approach has been investigated. This protocol consists of cycles of light irradiations and darkness and is known to increase the efficacy of PDT by allowing skin re-oxygenation during the dark phases [191]. In addition, a fractionation protocol (1 min of light, 2 min of darkness) has been shown to be superior in terms of tolerance and as effective as the conventional protocol [189]. In this study [189], the delivered dose was equal to 37 J cm^{-2} in order to be compared with the conventional protocol, but it would be possible to also work with a lower light dose since it has been recently demonstrated that 12 J cm^{-2} was as efficient as a light dose of 37 J cm^{-2} for AK treatment [112].

Therefore, the second objective of this project is to couple a light source to the microneedles array that would allow an efficient PDT treatment while limiting pain. For that reason, the illumination would start instantaneously to avoid PpIX accumulation. Moreover, the light dose should be drastically reduced to $\approx$ 12 J cm^{-2} since this dose has proven good efficiency and a lower pain sensation [190, 112]. A fractioned light approach may also be considered to improve patient compliance without impairing efficacy. Besides, the microneedles should conduct light into deeper areas of the skin, thus limiting the diffusion or absorption of light by the tissues of the superficial layers of the skin, which may also allow to reduce slightly the irradiance. In order to use the microneedles as a wave-guide, a transparent polymer is preferred and HA fulfil this criterion. Since the HA based MNs are shaped like the tip of a pencil, the tip facilitates insertion and the cylindrical base ensures a mechanical hold. Indeed, it is expected *in vivo* on human skin that the tip of the MNs will dissolve first and the cylindrical base would take longer to dissolve because it is more voluminous and made of more polymer. This cylindrical base would then be able to ensure the transmission of light into the deeper layers of the skin. Therefore, the use of other wavelength than the red one at 635 nm would also be considered[1].

In the future, this system will allow to develop an all-in-one device for PDT treatment which will be less painful, easy to use, portable, with a rapid processing in one single step. In the longer term, such a device should allow a simplification of use (lower qualified personnel), reduce fear of the needle for the patient, be faster and equally effective than conventional PDT.

[1] Red light is conventionally used because it can penetrate in the skin deeper than the green or blue one.

4.1.2 Light choice

4.1.2.1 Basic illumination protocols

To better understand the light choice made for the proof of concept that we developed, a rapid overview on the technologies previously used to allow good light diffusion through the skin is presented hereinafter.

In Europe, panel of LEDs or daylight are considered as approved protocols for photodynamic therapy for non melanoma skin cancers but many other protocols using irradiation by a variety of lights sources such as lasers, filtered intense pulsed light or discharge lamps (gas) have been also clinically efficient [116, 115].

In the 2000's, the rise around LED technology led researchers to use them as an incoherent light source for PDT [77]. Several LEDs were assembled as a panel and it was then articulated with the help of an arm and positioned where the light treatment needs to operate (Figure 4.1). Nowadays, the most used LED panel is the Aktilite® CL 128 that provides red light energy at a peak wavelength of 630 nm which corresponds to activation's peak for PpIX and the deepest penetration in the skin to treat both superficial lesions (actinic keratosis) and deeper lesions (basal cell carcinoma) [181]. Nevertheless, with this technology the spatial distribution of the light energy is not disclosed which is a problem to evaluate the delivered light dose [121]. In addition, the light power is also not adjustable and to reduce the energy the only solution is to move back the Aktilite® source. Therefore, it is not possible to illuminate a single area and that makes the system oversized in case of localized lesions such as BCCs extending no more that 9 square centimetres. Moreover, the system is not portable which forces the patient to stay in the hospital for the duration of the treatment that is generally long considering the 3 h drug incubation period and the 10 painful minutes of light illumination [190]. Otherwise, this light system is not suitable for fractionation protocol whereas it is a solution known to reduce pain as presented before.

Daylight PDT avoids the requirement for specific equipment and the treatment may be easily operated at home with the only constraint of applying sunscreen in order to prevent sunburn. Nevertheless, this treatment is difficult to justify considering that patients are suffering from skin cancer principally due to their previous sun exposure. Moreover, daylight PDT is indicated only for patients with grade I or II AKs. In addition, even if new applications such as smartphone dosimeter [106] to determine daylight irradiance has been developed, it stays often difficult to precisely know the light dose delivered due to weather conditions [117, 202].

LEDs panel or daylight PDT present several advantages but does not appear suitable for small and localized lesions. Therefore, LEDs panel has been miniaturized (Figure 4.2) and developed by Ambicare Health Ltd. This option, to wear a portable LED device, allows ambulatory PDT and reduces the need for hospital attendance. Its efficacy has been validated in different studies and in particular on superficial BCCs. The clearance rates were equivalent to those obtained with the Aktilite® lamp [67, 190]. Nevertheless, this Ambulight® source delivers a low irradiance light, about 5 mW cm^{-2}, which implies a long illumination time of 3 hours to deliver the required 75 J cm^{-2} [34]. Therefore, the system is directly fixed on the patient during all this time and usually causes thermal side effects [147].

Moreover and still to satisfy ambulatory PDT, others innovative lighting sources were developed. It firstly started with the use of organic light-emitting diodes (OLEDs) that were proposed as light-emitting bandages and were consequently flexible, with homogenous light distribution, wearable and lightweight. This technology was tested in 2009 for Bowen's disease or superficial BCC on 12 patients by Attili et al. and was efficient with a potential for more convenient home PDT but these results were not validated in larger studies [12]. Indeed, this method was later abandoned, mainly because it provided relatively low power density (between 3 and 5 mW cm^{-2})

[28, 185]. To overcome this irradiance problem, quantum dot light-emitting diodes (QLEDs) were recently developed. As OLEDs, they are still flexible, lightweight with uniform large area illumination but they have for specificity to have a narrow emission spectrum and high power density ($10\,mW\,cm^{-2} - 25\,mW\,cm^{-2}$) at clinically relevant deep red wavelengths [185, 28]. Nevertheless, to our knowledge this method has not yet been used in clinics and therefore this option would not be considered for our integrated light device.

Figure 4.1 – Lighting emitting device - LED panel (Aktilite®)

Figure 4.2 – Portable light emitting system Ambulight® used for PDT treatment.

4.1.2.2 Light emitting system chosen

According to the previous studies from the scientific literature and to the microneedles patch developed, it was clear that a wearable light emitting system was necessary. The last Ambulight® system is very close to the proof of concept that we want to realize except that it does not release the 5-ALA and at least two operations are needed to provide a PDT treatment (5-ALA application + light irradiation with the Ambulight® device). As the idea was to couple the microneedles

array with light, we were looking for a small LED panel with approximately the same dimensions as the patch[2] ($25 \times 25\,mm^2$). In particular, the LED panel must allow a red lighting (at $\approx 630\,nm$), not heat up, be powered with a small and light battery and be flexible. Therefore, Adafruit Dotstar High Density 8×8 grid (figure 4.3, left) has been chosen since it is characterized as the tiniest LED grid made by Adafruit, with 64 full Red Green Blue (RGB) color pixels in a surface of ($25.4 \times 25.4\,mm^2$). As it is a RGB pixels grid, the illumination is possible in red but also in green or blue and PpIX has also excitation peaks in the blue and in the green (see figure 1.5 in chapter 1), so it would be possible to illuminate the lesions with one of these colours. Besides, this little LEDs panel is monitored with a microcontroller which allow to set up light power, illumination time and also light wavelength (*It will be detailed in the following section 4.1.2.3*). For example, the LEDs might be set as red for 5 min, stopped for a few minutes to allow skin re-oxygenation, then re-illuminate in green for another 5 min etc. All the combinations are possible and offer a wide range of light treatment options. In addition, the Adafruit Dotstar is light and can be easily wearable ; at the moment it is powered by a rechargeable Lithium-polymer battery (RS PRO, 3.7 V,1.8 A h^{-1}, $53.5 \times 35 \times 10.4\,mm^3$). However, as the light emitting system is composed of several LEDs, it is expected that the system will heat up. Although, an increase in temperature might be beneficial since it allows for example blood vessels vasodilation and consequently better oxygenation, the skin temperature should not exceed 39 °C [113]. To avoid side effects such as burning of the skin, we plan to carry out cycles of irradiations and darkness (previously called fractional light irradiations) in order to cool down the Adafruit illumination device.

As mentioned in the previous paragraph, the lighting system we are developing should meet several criteria that have already been tested and that have proven to be as efficient while being better in terms of tolerability. In table 4.1, we have summarized the lighting set-up that we have planned to realize according to advances made in the light area in recent years.

Adafruit Dotstar LED fulfil most of the criteria except the flexibility parameter but as the work is still in progress we decided to continue with this light model. In the future, it would be interesting to design a printed circuit board (PCB) with precise dimensions and for example with a microLED in front of each microneedles since a PCB is generally flexible. Moreover, if further studies with QLEDs are released and if they highlight good clinical outcomes with acceptable tolerance, it would also be interesting to couple this lighting model with the MN-patch.

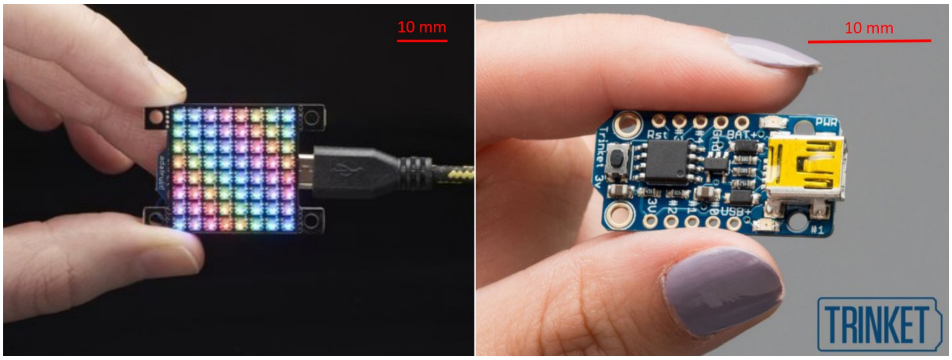

Figure 4.3 – Left: Light emitting system chosen: Adafruit Dotstar High Density 8×8 grid. Right: Arduino microcontroller: Adafruit Trinket.

[2]The MN patch is flexible and can be cut to reduce its surface.

Parameters	What will be done with the Adafruit system chosen	Tendency or what is recommended
Wavelength	Red light ($\approx 630\,nm$)	Red light allows PpIX excitation and penetrates in the deepest skin layers.
Fluence rate	$\approx 3.3\,mW\,cm^{-2}$	When the fluence rate decreases, the treatment was less painful.
Fractionation	2 min of illumination and 1 min of darkness	Fractioned light protocol increases the efficacy of PDT by allowing skin re-oxygenation during darkness and is better tolerated by patients.
Light dose	$\approx 12\,J\,cm^{-2}$	Doses around $12\,J\,cm^{-2}$ demonstrated good clinical results as the conventional one of $37\,J\,cm^{-2}$.
Time of treatment	Reducing the incubation time is controlled by the use of MNs. The illumination time including the darkness cycles will start directly after MN-patch application and last for 1h30.	The faster the treatment, the higher the patient's quality of life.
Temperature	Temperature should be kept at a maximum of 39 °C to avoid burning side-effects.	Increasing the temperature may increase 5-ALA uptake in deeper skin layers, conversion to PpIX and blood vessel vasodilatation.
Area	$25 \times 25\,mm^2$	As BCC is a localized lesion, a localized illumination is required.
Flexibility	The device is not flexible.	A system that adapts to the shape of the area to be treated allows to deliver the same light dose over the entire area.

Table 4.1 – Requirements specification for the light system developed in order to perform an efficient and tolerable PDT treatment.

4.1.2.3 Microcontroller and Arduino software to monitor Adafruit LED panel

A microcontroller is an integrated circuit that brings together the essential elements of a computer: processor, memories (read-only memory and random access memory), peripheral units and Input/Output interfaces. Microcontrollers are characterized by a higher degree of integration, lower power consumption, lower operating speed and lower cost compared to the general-purpose microprocessors used in personal computers. Compared to electronic systems based on microprocessors and other separate components, microcontrollers make it possible to reduce the size, power consumption and cost of products. Indeed, they are frequently used in embedded systems, such as automotive engine controllers, remote controls, office appliances, household appliances, toys, mobile phones etc. [13, 14].

A microcontroller can be for example programmed with Arduino, to send information from the computer code in C language to the Arduino microcontroller and finally to the specific circuit in order to execute the loaded commands. Arduino is an open-source platform used for constructing and programming of electronics. Its user friendly interface lead us to choose an Arduino microcontroller: Adafruit Trinket - Mini Microcontroller - 5V Logic which is very small ($2 \times 1\,cm^2$) and low cost (6.95 $ per unit) (figure 4.3, right).

The light system Adafruit Dotstar provides a library on its website that helps to code on Arduino and our programmed code is displayed in appendix A, on figure A.1. It was chosen to work only with red light, so the command "$uint32\_tred\_color = 0x00FF00$" was uploaded and launched in the setup with "$strip.fill(red\_color)$". The light intensity was set with the following command "$strip.setBrightness(\_d\_BRIGHTNESS)$". The brightness could go from 0 to 255 and in our case it was set as "176". Several tests were performed with a power-meter to adjust the received fluence rate at 176. The fractionation illumination time was uploaded in two loops: "TIME ON" and "TIME OFF". Once the system will have done all the necessary cycles (30) and after 1h30 the system will sleep down thanks to the third command "STOP".

Overall, this is an easy code, but as previously mentioned, other light combinations may be possible by slightly changing the Arduino code and by including different breaks or colors.

4.1.2.4 Electronic circuit

To better understand how the lighting of the Adafruit Dotstar is generated, the electronic circuit diagram of the assembly with the components representations is displayed in figure 4.4.

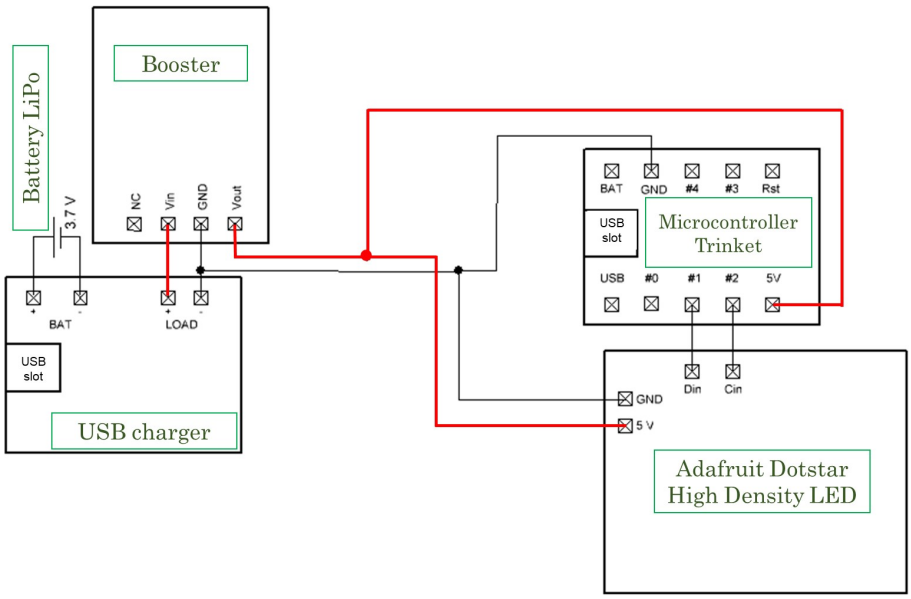

Figure 4.4 – Electronic diagram including all the components to produce the illumination light source.

To summarize, a rechargeable battery is associated to a booster regulator that can deliver a voltage of 5 V to power the microcontroller and the LED array as schematized by the red line on figure 4.4. Indeed, a booster, also called boost converter or step-up converter, is a direct

current(DC)-to-DC power converter that steps up voltage from its input to its output which allow us to use a 3.7 V battery, which is smaller than a 5 V battery ($53.5 \times 35.0 \times 10.4\,mm^3$ vs. $90.0 \times 63.0 \times 12.5\,mm^3$). This is a lithium-ion polymer battery (abbreviated as LiPo) chosen for its weight feature (36.0 g) since the final device should be wearable and consequently light. The LED Matrix is connected to the microcontroller via a serial peripheral interface which is a synchronous serial communication interface specification commonly used for short-distance communication in embedded systems. In this case, the connection is qualified as a "serial clock" as explained in the Trinket microcontroller user guide (https://docs.rs-online.com/d3ce/0900766b8153437f.pdf).

4.1.3 Assembling: 3D printing

Once the light system and all the electronics have been set up, it is now important to include it in a small box to create an embedded system and to couple it to the microneedles patch.

First of all, a box was designed in which the electronic set up (battery, USB charger, booster, microcontroller) was placed and organized (Figure 4.5). To elaborate this box, fused deposition modelling that is a 3D printing technique was used and was based on the deposition of successive layers of thermoplastic materials following their melting. The materials used was a copolymer (Amphora™ AM3300, Eastman Chemical Company) with the 3D printing machine ULTIMAKER 2+. The conception of the box was realized with computer-aided design software Solidworks and information were sent to the machine via the driving software ULTIMAKER CURA. A support, on which the box can be hold was produced with the same method.

Secondly, a plastic sheath was used to run the electrical cables that power the Adafruit Dotstar LED panel. The LED array was locked in a holder, also realized with the previous 3D printing method.

The last step was to couple the LEDs with the MN patch. Therefore, a double sticky layer was realized and added on top of the LEDs. It was composed of a modified PDMS with a Karstedt catalyst that sticks on the LED and also on the MN patch as displayed on figure 4.6.

A schematic representation generated with Solidworks software is introduced in figure 4.7a, and the real version including the MN patch is on figure 4.7b.

The embedded light device represented is re-usable after recharging the battery and disinfection with alcohol. It was essential since the printing time for all the elements was about 8 hours and we wanted to design an eco-friendly device that would not go to waste a single use.

Acknowledgements This work has been realized with the support of Olivier Menard (FABLAB, CEA Grenoble), Grégory Baert (OncoThaI) and Pascal Deleporte (OncoThaI).

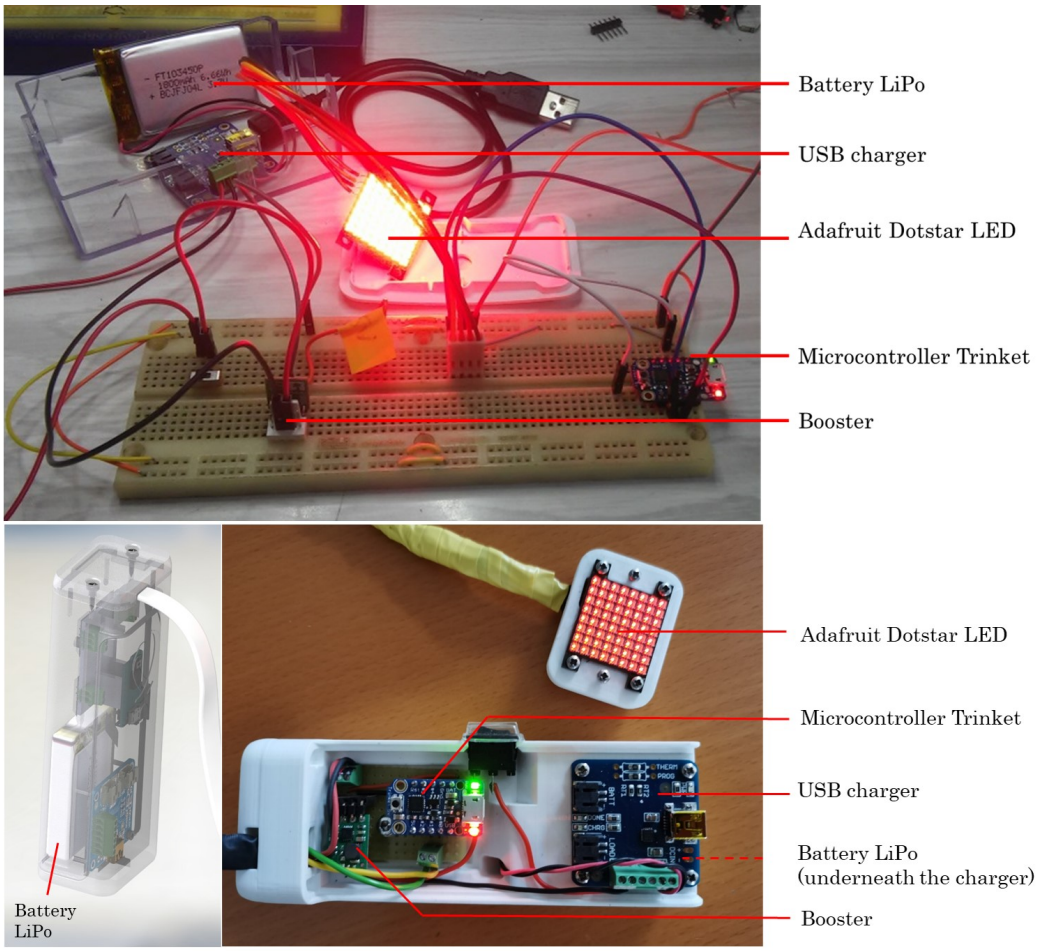

Figure 4.5 – UP: Photo of the disorganized electronic circuit extending on the bench-top. Down: Scheme of the electronic circuit included in the box, each component is well organized to avoid crowding and photo of the realisation.

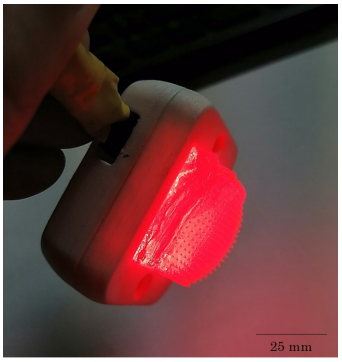

Figure 4.6 – Photo of the MN patch stuck to the LED array thanks to the double sticky layer realized with modified PDMS.

(a) Schematic representation of the embedded light device.

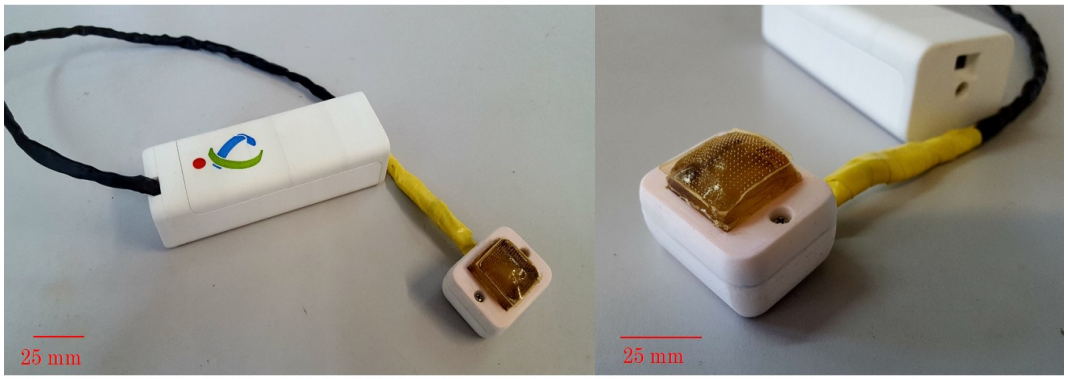

(b) Finished product including LED and MN patch.

Figure 4.7 – Comparison between expectation and reality.

4.1.4 Characterizations

All the characterizations were performed with the hereinabove developed device .

4.1.4.1 Wavelength

To precisely determine the wavelength of our system, a spectrophotometer (STS VIS, S06330) and its software (OceanView 2.0) were used and the results were displayed in figure 4.8.

The predominant wavelength of the Doststar LED panel was present at 631 nm whereas in the technical details of the product it was expected to be between 620 and 625 nm. Nonetheless, even if the double sticky layer or the MN-patch was added on top the Dotstar LED panel, there was no shifting of the wavelength which confirmed that the PpIX would be correctly activated for PDT session with our device. In the other hand, when the sticky layer (and the MN-patch) was added a decrease in intensity is noticeable in figure 4.8 which indicated a decrease in power that will be further explain in section 4.1.4.2.

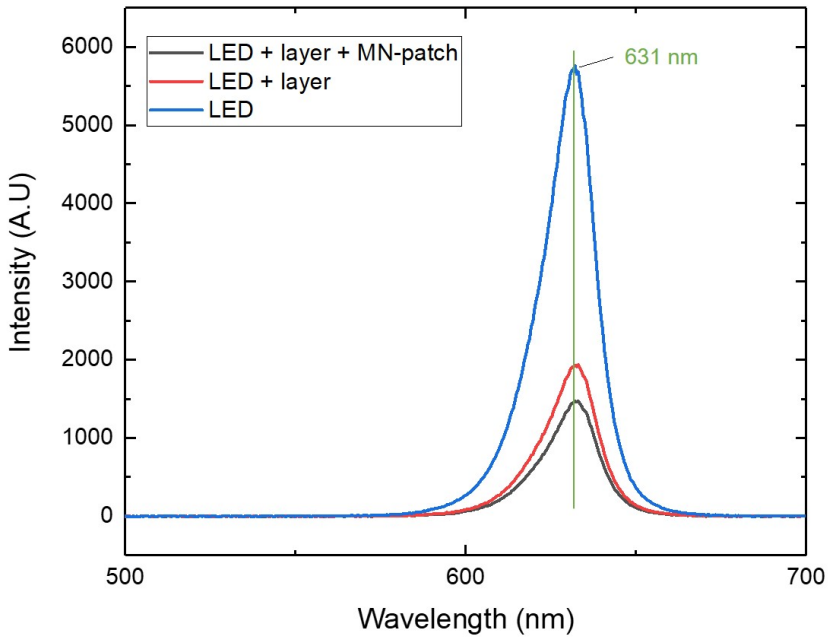

Figure 4.8 – Emission spectra in arbitrary unities (A.U) of the Dotstar LED panel (Blue), of the Dotstar LED panel covered with the double sticky layer (Red) and the whole developed device including MN-patch (Black). Green line represents the maximum obtained at 631 nm.

4.1.4.2 Power

As presented in the above table 4.1, a final power of approximately 3.3 mW cm^{-2} was required in order to deliver the needed light dose. With this irradiance, the effective illumination should

last for 60 min but with the fractionation chosen (2 min of light and1 min of darkness) the whole system will be in place for 90 min.

Since a double sticky layer was placed on top of the Adafruit Dotstar LED, the initial power of the Dotstar LEDs was set more intense than what wanted. Then the brightness was uploaded as 176 in the Arduino code. Indeed, as presented in table 4.2 the double sticky layer added to the LEDs tends to filter the light which was expected since it was composed of an opaque modified PDMS. When the MNs were added to the whole system, the light power decreased again and dropped to 2.91 mW cm^{-2}. This power is lower than the one really needed (3.3 mW cm^{-2}). Nevertheless, as the patch was supposed to dissolve over the time the light power received might become higher. To get an idea and according to the dissolution kinetics observed in vivo (see chapter 3), we supposed that from 0 to 30 min the patch was one-quarter dissolved, from 30 min to 60 min the patch was half dissolved and from 60 min to 90 min the patch was fully dissolved. By extension of the previous light powers reported in table 4.2 and according to the equations 4.1, we calculated the light powers from 0 to 30 min ($P_{0-30min}$), from 30 min to 60 min ($P_{30-60min}$) and from 60 min to 90 min ($P_{60-90min}$). Then the power resultant were respectively equal to 3.01 mW cm^{-2}, 3.22 mW cm^{-2} and 3.64 mW cm^{-2}. Due to the fractionation, the total light dose delivered was calculated with equation 4.2 where t_{eff} corresponds to the effective illumination time in seconds (20 min i.e 1200 sec) and was equal to 11.82×10^3 mJ cm^2. Obviously, these calculations are based on estimations like the dissolution kinetics that could change from one person to another and therefore modify the delivered dose. Nevertheless, it gave us an order of idea and highlighted that a dose of 12 J cm^{-2} could be easily delivered with our light system.

Dotstar LED (P_0)	Dotstar LED + double sticky layer (P_1)	Dotstar LED + double sticky layer + MN-patch (P_2)
5.74 ± 0.01mW cm^{-2}	3.64 ± 0.02mW cm^{-2}	2.81 ± 0.12mW cm^{-2}

Table 4.2 – Light power emitted by each element of the final embedded light device.

$$\begin{cases} P_{0-30min} = \frac{1}{4} \times P_1 + \frac{3}{4} \times P_2 \\ P_{30-60min} = \frac{1}{2} \times P_1 + \frac{1}{2} \times P_2 \\ P_{60-90min} = 1 \times P_1 \end{cases} \tag{4.1}$$

$$D_{tot} = P_{0-30min} \times t_{eff} + P_{30-60min} \times t_{eff} + P_{60-90min} \times t_{eff} \tag{4.2}$$

4.1.4.3 Light distribution

To identify the light uniformity obtained with the developed device, photographies of the Dotstar LEDs, then with the sticky layer and then plus the MN-patch were taken with a camera (Nikon, D5000) and were displayed in figure 4.9. Even without images' treatment, it was clear that the modified-PDMS sticky layer added tended to homogenize light diffusion (Figure 4.9.B) compared to the figure 4.9.A only representing the Dotstar LED panel. In 4.9.C, it appeared that the MN-patch also filtered light in some area but if a MN was in front of the LED there was a light re-concentration in the needle itself. To better visualize these first observations, a method based on computer tool was set up.

As it was noticeable on the photographies, a saturation of brightness was observed therefore we chose a lower exposure time for avoiding saturation on photographies and better study the

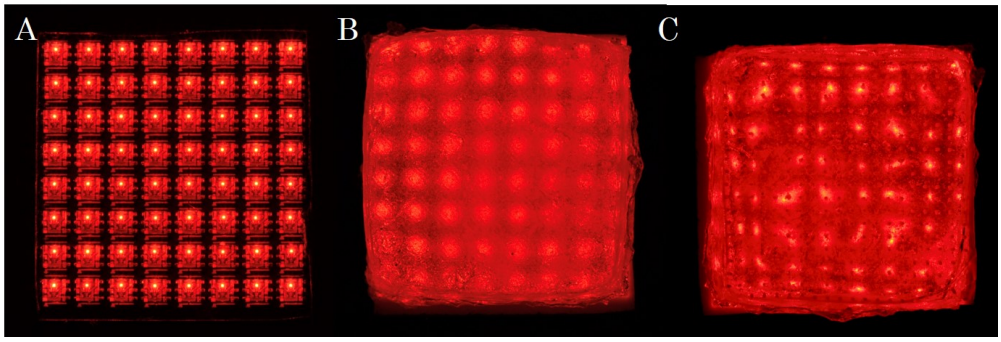

Figure 4.9 – Photographies of the Dotstar LED panel (A), of the Dotstar LED panel covered with the double sticky layer (B) and the whole developed device including MN-patch (C).

light uniformity. The exposure times were equal to 1.5 ms for the Dotstar LED panel and 20 ms for the Dotstar LED panel coupled with the sticky layer and with the MN-patch. Then a Matlab code was developed by OncoThai engineers to treat the photographies and consisting in the following steps :

- Uploading the photography (RGB, 1700 x 1700 pixels)
- Splitting the channels in order to only keep the Red component (Green and Blue channels did not emit signals)
- Averaging the image by creating a "new" pixel unit that will have a length of 0.2 mm[3] which will remove artefacts, reduce the size of images and allow a faster image treatment.
- Assigning to each "new" pixel its power value in mW cm^{-2}
- Plotting the profile

The results obtained are presented in figure 4.10. When the exposure time was reduced, the previous observations were more noticeable. Indeed, we clearly saw on photographies that the sticky layer filtered the Dostar light (4.10.B) and that the MN-patch re-concentrated the light in the needle (4.10.C). It was even more evident with the 2D-charts, since the sticky layer light profile (4.10.E) was lower in intensity than the the Dotstar light profile (4.10.C) and also more smooth i.e with less strong intensity peaks. Moreover on figure 4.10.F a more intense profile with well-defined intensities peaks were detectable compared to figure 4.10.E. Nonetheless, on figure 4.10.F, the z-axis corresponding to intensity was from 0 to 120 mW cm^{-2} and on figure 4.10.D z-axis was from 0 to 500 mW cm^{-2} which indicated that although MN-patch redistributed the light in the needle, it was not enough to obtain intensities of order of the Dotstar LED panel. To conclude, as long as the MNs will not be dissolved they could be used as wave-guide ton conduct light in deeper skin layers as presented in section 4.1.2.1. We are aware that this is a preliminary result and of course further studies should be conducted to study for example the light path in the needle cylinder to confirm that MNs are indeed a good way to conduct light in deeper skin layer. Solutions to improve depth of light penetration in tissue are a burgeoning research area. Recently and to answer this issue, fiber-optic microneedles were developed. They were designed to physically penetrate skin and were able to deliver light directly into the target area

[3] With the camera resolution the original pixel had a length of 0.0176 mm

below the skin [91, 65]. Nonetheless, they were mostly developed in silica materials, known to be not biocompatible. Therefore to replace silica materials, biocompatible (and biodegradable) polymers have been attractive candidates. Indeed, they have good mechanicals and optical properties and can be processed as implantable and resorbable light-guiding microneedles for long-term light delivery [127, 23]. Polythylene glycol (PEG) [29], polylactid-co-glycolic acid (PLGA) [127], polylactid acid (PLA) [127], agarose gel [70], polyurethane (PU) [207] have already been developed as micro-device to conduct light in deep layers of tissue and with our previous results HA could soon be part of the polymers optical waveguides.

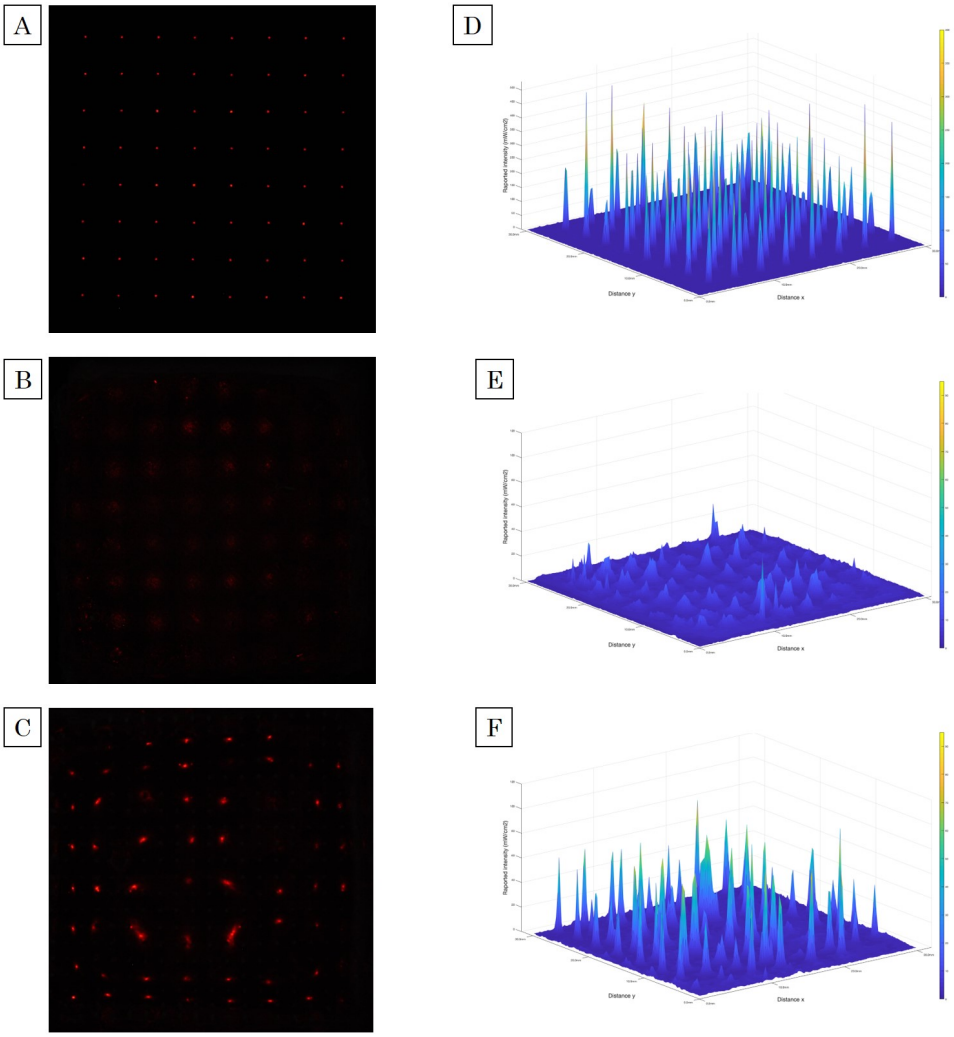

Figure 4.10 – A, B and C: Photographies uploading in Matlab program respectively corresponding to the Dotstar LED panel, plus the double sticky layer, plus the MN-patch. D, E, F: Intensity profiles in mW cm^{-2} plotted with Matlab for the Dotstar LED panel, plus the double sticky layer, plus the MN-patch.

4.1.4.4 Temperature

It is well known that LEDs have tendency to heat up due to the Joule effect, therefore we decided to check if the increase in temperature would be acceptable over the illumination time. We firstly monitored the increase in temperature of the device itself and the results are displayed in figure 4.11. Due to the implementation of the fractionation protocol, which consisted of turning off the LEDs every two minutes for one minute, the system temperature was lowered a little bit. This decrease in temperature is represented by dark arrows on the graph and allow a decrease of less than 1 °C. By modulating this fractionation (cut-off frequency and time off) it would be possible to optimize the temperature reached. However, the temperature attained by the device ($\approx 42\,°C$) was satisfactory since the final goal was to heat the skin to enhance metabolization of 5-ALA to PpIX.

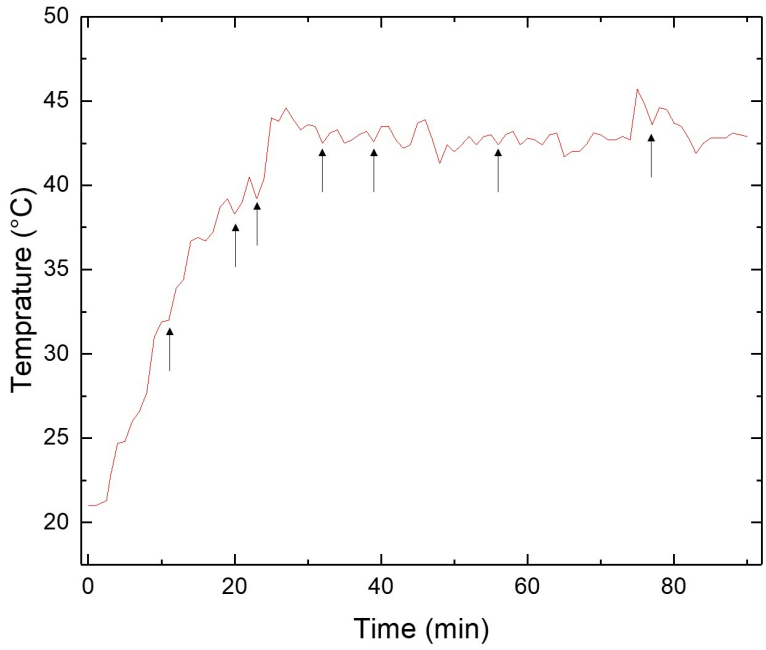

Figure 4.11 – Evolution of the temperature of the light emitting device during all the illumination procedure. Arrows represent the decrease in temperature when the device has the instruction to stop the illumination.

Secondly, we monitored the skin temperature when the light device was in contact with the forearm skin and the results are shown in figure 4.12. This experiment was performed on three different individuals and it seemed that the curve reached a plateau after 60 min with a mean temperature of 42.7 °C. In the scientific literature, it was recommanded not to exceed a temperature of 39 °C [113], nevertheless Wienert, Sick, and Mühlen in [204] showed that 43 °C is a temperature tolerated by human skin, without blood fluid restriction. Similarly, Leach, Peters, and Rossiter in [93] showed that exposition of 30 min with water at 45 °C had no effect. The experience feedback of the human testers after the 90 min illumination, was described as

a tolerated heat and no skin burn was observed. Therefore the temperature delivered by the device is not a problem and could even be beneficial to improve metabolization of 5-ALA to PpIX. However, if during clinical trials this temperature is considered as excessive or painful, it would be possible to lower it slightly by modifying the fractionation illumination.

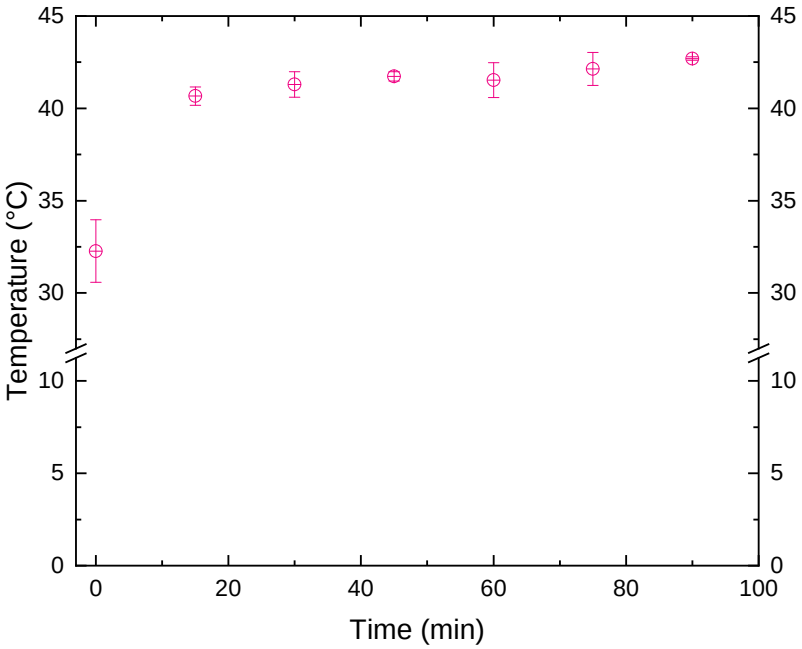

Figure 4.12 – Evolution of the (healthy human) skin temperature during all the illumination procedure. The light emitting device was removed each 15 minutes to measure the skin temperature. Results are presented as mean ± standard deviation (n=3).

To conclude, an Adafruit Dotstar LED matrix has been chosen due to its small size, wearable feature, and its ability to illuminate in red at a precise wavelength of 631 nm which is known to activate the PpIX. This light device was controlled with a microcontroller in which an Arduino code was implemented. This code consists of activating the light for two minutes, then turned it off for one minute in order to deliver a light dose of $12\,J\,cm^{-2}$ in 1h30. This illumination protocol enabled within reason to heat up which might increase 5-ALA metabolization to PpIX. The whole system was successfully coupled with the MN patch by means of 3D printing technology. The whole system is lightweight, easy to use with only an ON/OFF button, reusable and compact.

We are aware that only initial and essential characterizations were realized and in a near future further experimentations should be performed in order to evaluate the light's path in the cylinder of the MN or even the MN dissolution rate on human, or again the increase in temperature and impact on pain.

4.2 Regulation aspect

At the end of this PhD project, the device was well advanced and we already had strong evidences that our "all-in-one" concept for PDT is promising. Keeping in mind its clinical use, its industrialization and commercialization, it was necessary to precisely know the regulatory status of the device. Indeed, it exists several products containing 5-ALA such as Alafast® or Ameluz® but the first one is considered like a medical device class whereas the second one belongs to the medication class. Therefore to identify the regulatory positioning of our complete product (consisting of MN-patch containing 5-ALA and light device) in Europe, we worked with Voisin Consuting company that is accustomed to support life science companies and engages in communication with regulators.

This work provided information on the regulatory status and classification of the product allowing to know unambiguously the regulatory path to be followed, prior to the submission of the clinical evaluation protocol to the CPP (Committee for the Protection of Persons) and the ANSM (National Agency for the Safety of Medicines and Health Products). To study the regulatory positioning, the proof of concept was divided in two parts : the MN-patch and that is of single use and the light device that is reusable after disinfection. The regulatory classification of each will be studied in sections 4.2.0.1 and 4.2.0.2.

4.2.0.1 Classification of the MN-patch

The MN-patch contains two key elements that are the HA polymer allowing to process a microneedle form and the prodrug 5-ALA. It appeared that the principal mode of action of the MN-patch is **pharmacological** since it principally relies on the metabolization of 5-ALA in PpIX and its activation leading to the destruction of tumor cells. As for the microneedles, they are only an ancillary support to administer the active substance. As soon as the product has either a immunological or metabolic or pharmacological mode of action, the product is considered as a medication class that is why the MN-patch is classified as a medication. Therefore the MN-patch would require a marketing authorization and an opinion issued by a notified body. A notified body such as AFNOR or BSI might be asked for their opinion but the certification process is often long (> 6 months) and expensive (42-84 k€). Only a start-up or a pharmaceutical company might go for it by keeping in mind a future commercialization protected by a patent.

4.2.0.2 Classification of the light device

The main mode of action of the light product is the emission of light at the excitation wavelength of the PpIX. Therefore our light device should be considered as a medical device class IIa and requires a CE marking that could be delivered in 6 months.

In order to understand what kind of product was developed during this 3 years of PhD project and what the future has in store for it, a regulatory positioning was led and concluded that the MN-patch and the light device are respectively a medication and a medical device of class II a. At the time of the thesis is written only the French patent was deposit and waiting for the granting. The economic issue of our complete product is therefore restricted as soon as the patent will be limited to France.

Conclusion

- Different parameters such as the interval between drug application and illumination or light dose or fractionation are clinical issues known to reduce pain during PDT and will be considered for the design of our light device.
- Different light sources have been used for PDT purpose and LED appeared as a good choice for our application since they are wearable and not expensive.
- A microcontroller runs with a Arduino code allows to set up a precise illumination (fractionation, power controlled) for the LEDs chosen.
- All the electronics elements were organized in a small, wearable and easy to use box to produce an embedded light source.
- The embedded light source was further coupled to the MN-patch with the use of a home-made double sticky layer.
- Preliminary characterisations highlighted that the device we developed could be used in PDT since it delivered wavelength and power suitable.
- Due to the promising results of our proof of concept, we studied its regulatory status and it was concluded that the MN-patch and the light device were respectively of medication class and medical device IIa class.

Conclusion

The main purpose of this thesis work was to provide a new technology to enable the treatment of deep skin lesions with PDT. The principal objective was to propose a process that could enhance the prodrug penetration in deep skin layers. The second objective was to elaborate a light device that could deliver a lower dose of light than currently used and be coupled to the prodrug delivery system to generate an innovative all-in-one PDT concept.

An overview on the different chemical or physical methods to improve prodrug penetration before PDT treatment led us to choose microneedles (MNs) as a technology to answer the lack of prodrug penetration. Indeed, MNs have been already used as their solid forms in clinics and consisted in perforating the skin prior to the prodrug cream application to allow a better diffusion through the microchannels. Some difficulties were highlighted in clinics such as the fast closing of the microholes or infection risks. Therefore, we chose to develop dissolving MNs containing 5-ALA that could puncture the skin, maintain skin holes open and release the prodrug in depth during their dissolution. The constituent material of the MN-patch was the hyaluronic acid (HA) that is a polymer known for its water solubility, biocompatibility and biodegradability. MNs were designed according to the clinical indications, hence we manufactured two different needle lengths: 400 µm or 750 µm in order to reach lesions such as nodular BCCs that could extend to the deep epidermis. A "pencil-tip" design was defined to ensure a good mechanical strength due to the cylinder base and a good skin insertion due to the sharp tip. The MN length did not exceed 900 µm in order to be painless. The MN-patch has been elaborated by a soft process that does not require high temperature, organic solvents or noxious excipients that could be non-biocompatible, dangerous which make the prodrug unstable. Therefore, a solvent casting molding method was set up and consisted only on mixing HA with 5-ALA in water. Two different 5-ALA concentrations of 10 % and 33 % (w/w) were prepared for biological and chemical investigations and 5-ALA was stable in the MN-patch over 5 months.

Ex vivo tests on rat skin highlighted that the MNs had sufficient mechanical properties to pierce and penetrate the skin. Indeed, we also reported that the MNs did not bend or break at forces equal to the insertion force. The MN-patch was applied for different durations on the *ex vivo* rat skin and we observed that MNs were dissolved within 45 minutes of application. As the MN-patch dissolved, it could release 5-ALA and we therefore measured the delivered quantity and penetration depth of the 5-ALA in *ex vivo* rat skin. An experiment using cell Franz apparatus showed that 5-ALA reached deep skin layers since its presence was evidenced up to 1500 µm which means that after MN dissolution (MN length: 750 µm) 5-ALA also diffused through skin layers. The whole 5-ALA delivery in all the different skin layers could range from 35 % to 82 %. The difference in prodrug release might be explained by the fluctuations of dissolution that depend *inter alia* on the hydration of the *ex vivo* skin. Once, we confirmed that 5-ALA could be released with satisfactory quantities in the skin, the second major objective was to confirm if 5-ALA was always bioavailable to metabolize to PpIX to further initiate a PDT treatment.

In vivo experiments were implemented in order to check the production of PpIX. As PpIX is

preferentially accumulated in tumour cells, we decided to work on skin lesion to better study the presence of the photosensitizer. Nonetheless, skin lesions model only existed on mice and were not realistic. To assess the relevance of MNs, and especially to highlight their ability to perforate the SC, the rat skin which is known to be more representative of the human skin than the mice one was chosen in this study. Forty UV-B illuminations at 130 mJ cm^{-2} allowed to induce precancerous skin lesions that were validated by histology and pharmacokinetics studies. After one hour application on the rat skin lesions, the patch fully dissolved, released 5-ALA that further metabolized to PpIX. Indeed, a significant amount of PpIX fluorescence level was recorded which indicated that a PDT session would be possible with our developed 5-ALA loaded MN-patches.

The results obtained were encouraging and we decided to go further by coupling a small and wearable light device to the MN-patch in order to propose an all-in-one PDT concept. Indeed, pain during conventional PDT treatment was reported while the light illumination step was performed. Several parameters such as the long interval between drug application and illumination, or the light dose (75 J cm^{-2} in 10 min) are at the origin of pain because they create a huge photochemical reaction that stimulate sensory nerve endings. Therefore, we developed a light device composed of a panel of LEDs that could avoid these problems. First of all, we decided to control this light device with a code in which we implemented all the characteristics. The light wavelength was chosen in the red, at the peak of PpIX excitation, at 631 nm which also allow a deep light penetration in the skin. The light dose of 12 J cm^{-2} is delivered in one hour and half according to a fractionation model consisting in 2 min of illumination and 1 min of darkness to ensure the skin re-oxygenation. A temperature increase of the light device up to 42 °C was observed. Nevertheless when applied on human, after 1h30 the skin temperature did not exceed 42.7 °C due to heat transfer. An increase of temperature was also desired in order to enhance the metabolization of 5-ALA to PpIX. The device was well advanced and we already had strong evidences that our all-in-one concept for PDT was promising and we studied its regulatory status. It was concluded that the MN-patch and the light device were respectively of medication class and medical device IIa class.

To conclude, we managed to integrate 5-ALA in dissolving microneedles which allow to deliver in deep skin layers the prodrug conventionally used for PDT. It offers a new way for treatment of non melanoma skin cancers such as nodular BCC. This technology is also innovative due its coupling with a light device. This proof of concept was elaborated to treat non melanoma skin cancer but would be also useful for photorejuvenation or acne treatment with PDT as hyaluronic acid is commonly used for cosmetic purpose. Besides, this thesis opens up many other horizons since it is possible to integrate another drug or replace 5-ALA by another active molecule (for example imiquimod) as soon as the drug stay stable and MN keep strong mechanical properties. These modifications are conceivable but would require new physico-chemical characterizations before *in vivo* testing.

Bibliography

[1] P. Aggarwal and C.R. Johnston. "Geometrical Effects in Mechanical Characterizing of Microneedle for Biomedical Applications". en. In: *Sensors and Actuators B: Chemical* 102.2 (Sept. 2004), pp. 226–234. ISSN: 09254005. DOI: 10.1016/j.snb.2004.04.024.

[2] Patrizia Agostinis et al. "Photodynamic Therapy of Cancer: An Update". en. In: *CA: A Cancer Journal for Clinicians* 61.4 (July 2011), pp. 250–281. ISSN: 00079235. DOI: 10.3322/caac.20114.

[3] L. A. AHLSTROM, S. E. CROSS, and P. C. MILLS. "The Effects of Freezing Skin on Transdermal Drug Penetration Kinetics". In: *Veterinary pharmacology and therapeutics* (2007).

[4] Sharareh Ahmadi et al. "Evaluation of the Penetration of 5-Aminolevulinic Acid through Basal Cell Carcinoma: A Pilot Study". en. In: *Experimental Dermatology* 13.7 (July 2004), pp. 445–451. ISSN: 09066705, 16000625. DOI: 10.1111/j.0906-6705.2004.00181.x.

[5] Murad Alam and Desiree Ratner. "Cutaneous Squamous Cell Carcinoma". In: *N Engl J Med* (2001).

[6] Marine Amouroux. "Caractérisation de La Transformation Néoplasique de La Peau Par Spectroscopies Optiques Sur Fantôme de Mélanome et Carcinome Épidermoïde Murin Photo-Induit". PhD Thesis. Université Henri Poincaré-Nancy I, 2008.

[7] Sanjay Anand et al. "Biomodulatory Approaches to Photodynamic Therapy for Solid Tumors". en. In: *Cancer Letters* 326.1 (Dec. 2012), pp. 8–16. ISSN: 03043835. DOI: 10.1016/j.canlet.2012.07.026.

[8] Jennifer Maria Ang et al. "Photodynamic Therapy and Pain: A Systematic Review". en. In: *Photodiagnosis and Photodynamic Therapy* 19 (Sept. 2017), pp. 308–344. ISSN: 15721000. DOI: 10.1016/j.pdpdt.2017.07.002.

[9] Even Angell-Petersen et al. "Porphyrin Formation in Actinic Keratosis and Basal Cell Carcinoma after Topical Application of Methyl 5-Aminolevulinate". en. In: *Journal of Investigative Dermatology* 126.2 (Feb. 2006), pp. 265–271. ISSN: 0022202X. DOI: 10.1038/sj.jid.5700048.

[10] Zoi Apalla et al. "The Impact of Different Fluence Rates on Pain and Clinical Outcome in Patients with Actinic Keratoses Treated with Photodynamic Therapy: Impact of Different Fluence Rates on Pain and Clinical Outcome". en. In: *Photodermatology, Photoimmunology & Photomedicine* 27.4 (Aug. 2011), pp. 181–185. ISSN: 09054383. DOI: 10.1111/j.1600-0781.2011.00595.x.

[11] Vilma Armoškaitė et al. "Application of HPLC-ELSD for the Quantification of 5-Aminolevulinic Acid after Penetration into Human Skin Ex Vivo". en. In: *Analytical Letters* 46.5 (Mar. 2013), pp. 717–733. ISSN: 0003-2719, 1532-236X. DOI: 10.1080/00032719.2012.733898.

[12] S.K. Attili et al. “An Open Pilot Study of Ambulatory Photodynamic Therapy Using a Wearable Low-Irradiance Organic Light-Emitting Diode Light Source in the Treatment of Nonmelanoma Skin Cancer”. en. In: *British Journal of Dermatology* 161.1 (July 2009), pp. 170–173. ISSN: 00070963, 13652133. DOI: 10.1111/j.1365-2133.2009.09096.x.

[13] Yusuf Abdullahi Badamasi. “The Working Principle of an Arduino”. en. In: *2014 11th International Conference on Electronics, Computer and Computation (ICECCO)*. Abuja, Nigeria: IEEE, Sept. 2014, pp. 1–4. ISBN: 978-1-4799-4106-3 978-1-4799-4108-7. DOI: 10.1109/ICECCO.2014.6997578.

[14] Steven F. Barrett. “Arduino Microcontroller: Processing for Everyone! Second Edition”. en. In: *Synthesis Lectures on Digital Circuits and Systems* 7.2 (June 2012), pp. 1–371. ISSN: 1932-3166, 1932-3174. DOI: 10.2200/S00421ED1V01Y201205DCS038.

[15] N. Basset-Seguin. “La Photothérapie Dynamique En Dermatologie: Place Actuelle et Perspectives”. In: *Annales de Dermatologie et de Vénéréologie*. Vol. 133. Elsevier Masson, 2006, pp. 421–423.

[16] F. Bath-Hextall. “Interventions for Basal Cell Carcinoma of the Skin: Systematic Review”. en. In: *BMJ* 329.7468 (Sept. 2004), pp. 705–. ISSN: 0959-8138, 1468-5833. DOI: 10.1136/bmj.38219.515266.AE.

[17] Yann Berger. “Synthèse de Dérivés de l’acide 5-Aminolévulinique, Capable de Cibler Des Cellules Spécifiques, En Vue de Leur Utilisation En Thérapie Photodynamique”. PhD thesis. Université de Neuchâtel, 2002.

[18] Lasse R. Braathen et al. “Guidelines on the Use of Photodynamic Therapy for Nonmelanoma Skin Cancer: An International Consensus”. en. In: *Journal of the American Academy of Dermatology* 56.1 (Jan. 2007), pp. 125–143. ISSN: 01909622. DOI: 10.1016/j.jaad.2006.06.006.

[19] Stanley B. Brown, Elizabeth A. Brown, and Ian Walker. “The Present and Future Role of Photodynamic Therapy in Cancer Treatment”. In: *The lancet oncology* 5.8 (2004), pp. 497–508.

[20] S. Bystrova and R. Luttge. “Micromolding for Ceramic Microneedle Arrays”. en. In: *Microelectronic Engineering* 88.8 (Aug. 2011), pp. 1681–1684. ISSN: 01679317. DOI: 10.1016/j.mee.2010.12.067.

[21] P.G. Calzavara-Pinton et al. “Methylaminolaevulinate-Based Photodynamic Therapy of Bowen’s Disease and Squamous Cell Carcinoma”. en. In: *British Journal of Dermatology* 159.1 (July 2008), pp. 137–144. ISSN: 0007-0963, 1365-2133. DOI: 10.1111/j.1365-2133.2008.08593.x.

[22] Jaqueline Carneiro et al. “Development and Characterization of Hyaluronic Acid-Lysine Nanoparticles with Potential as Innovative Dermal Filling”. en. In: *Brazilian Journal of Pharmaceutical Sciences* 52.4 (Dec. 2016), pp. 645–651. ISSN: 1984-8250. DOI: 10.1590/s1984-82502016000400008.

[23] Christiane Carré et al. “Matériaux polymères pour la création de guides optiques”. French. In: vol. 35. Nov. 2013. ISBN: 978-2-918241-11-9.

[24] David S. Cassarino, Damian P. DeRienzo, and Ronald J. Barr. “Cutaneous Squamous Cell Carcinoma: A Comprehensive Clinicopathologic Classification”. In: *Journal of cutaneous pathology* 33.4 (2006), pp. 261–279.

[25] Ana P. Castano, Tatiana N. Demidova, and Michael R. Hamblin. "Mechanisms in Photodynamic Therapy: Part One—Photosensitizers, Photochemistry and Cellular Localization". en. In: *Photodiagnosis and Photodynamic Therapy* 1.4 (Dec. 2004), pp. 279–293. ISSN: 15721000. DOI: 10.1016/S1572-1000(05)00007-4.

[26] Buddhadev Paul Chaudhri et al. "A High Aspect Ratio SU-8 Fabrication Technique for Hollow Microneedles for Transdermal Drug Delivery and Blood Extraction". In: *Journal of Micromechanics and Microengineering* 20.6 (June 2010), p. 064006. ISSN: 0960-1317, 1361-6439. DOI: 10.1088/0960-1317/20/6/064006.

[27] Alvin I. Chen et al. "Multilayered Tissue Mimicking Skin and Vessel Phantoms with Tunable Mechanical, Optical, and Acoustic Properties". In: *Medical physics* 43.6Part1 (2016), pp. 3117–3131.

[28] Hao Chen et al. "Flexible Quantum Dot Light-emitting Devices for Targeted Photomedical Applications". en. In: (2018), p. 8.

[29] Myunghwan Choi et al. "Light-Guiding Hydrogels for Cell-Based Sensing and Optogenetic Synthesis in Vivo". en. In: *Nature Photonics* 7.12 (Dec. 2013), pp. 987–994. ISSN: 1749-4885, 1749-4893. DOI: 10.1038/nphoton.2013.278.

[30] Sun Young Choi et al. "Hyaluronic Acid Microneedle Patch for the Improvement of Crow's Feet Wrinkles". en. In: *Dermatologic Therapy* 30.6 (Nov. 2017), e12546. ISSN: 13960296. DOI: 10.1111/dth.12546.

[31] E. Christensen, C. Mørk, and E. Skogvoll. "High and Sustained Efficacy after Two Sessions of Topical 5-Aminolaevulinic Acid Photodynamic Therapy for Basal Cell Carcinoma: A Prospective, Clinical and Histological 10-Year Follow-up Study: Prospective 10-Year Follow-up Study of PDT in BCC". en. In: *British Journal of Dermatology* 166.6 (June 2012), pp. 1342–1348. ISSN: 00070963. DOI: 10.1111/j.1365-2133.2012.10878.x.

[32] E. S. M. Chu et al. "The Cytotoxic and Genotoxic Potential of 5-Aminolevulinic Acid on Lymphocytes: A Comet Assay Study". en. In: *Cancer Chemotherapy and Pharmacology* 58.3 (Sept. 2006), pp. 408–414. ISSN: 0344-5704, 1432-0843. DOI: 10.1007/s00280-005-0169-2.

[33] Vytis Čižinauskas et al. "Fatty Acids Penetration into Human Skin Ex Vivo : A TOF-SIMS Analysis Approach". en. In: *Biointerphases* 12.1 (Mar. 2017), p. 011003. ISSN: 1934-8630, 1559-4106. DOI: 10.1116/1.4977941.

[34] Cédric Cochrane et al. "New Design of Textile Light Diffusers for Photodynamic Therapy". en. In: *Materials Science and Engineering: C* 33.3 (Apr. 2013), pp. 1170–1175. ISSN: 09284931. DOI: 10.1016/j.msec.2012.12.007.

[35] Diana Cohen and Peter Lee. "Photodynamic Therapy for Non-Melanoma Skin Cancers". en. In: *Cancers* 8.10 (Oct. 2016), p. 90. ISSN: 2072-6694. DOI: 10.3390/cancers8100090.

[36] Michel Cormier et al. "Transdermal Delivery of Desmopressin Using a Coated Microneedle Array Patch System". en. In: *Journal of Controlled Release* 97.3 (July 2004), pp. 503–511. ISSN: 01683659. DOI: 10.1016/j.jconrel.2004.04.003.

[37] Shawn P. Davis, M. G. Allen, and M. R. Prausnitz. "The Mechanics of Microneedles". In: *Engineering in Medicine and Biology, 2002. 24th Annual Conference and the Annual Fall Meeting of the Biomedical Engineering Society EMBS/BMES Conference, 2002. Proceedings of the Second Joint*. Vol. 1. IEEE, 2002, pp. 498–499.

[38] Shawn P Davis et al. "Insertion of Microneedles into Skin: Measurement and Prediction of Insertion Force and Needle Fracture Force". en. In: *Journal of Biomechanics* 37.8 (Aug. 2004), pp. 1155–1163. ISSN: 00219290. DOI: 10.1016/j.jbiomech.2003.12.010.

[39] Koenraad De Boulle et al. “A Review of the Metabolism of 1,4-Butanediol Diglycidyl Ether-Crosslinked Hyaluronic Acid Dermal Fillers:” en. In: *Dermatologic Surgery* 39.12 (Dec. 2013), pp. 1758–1766. ISSN: 1076-0512. DOI: 10.1111/dsu.12301.

[40] Sabrina Alves de Oliveira et al. “Production and Characterization of Bacterial Cellulose Membranes with Hyaluronic Acid from Chicken Comb”. en. In: *International Journal of Biological Macromolecules* 97 (Apr. 2017), pp. 642–653. ISSN: 01418130. DOI: 10.1016/j.ijbiomac.2017.01.077.

[41] At Dijkstra et al. “Photodynamic Therapy with Violet Light and Topical Delta-Aminolaevulinic Acid in the Treatment of Actinic Keratosis, Bowen’s Disease and Basal Cell Carcinoma”. en. In: *Journal of the European Academy of Dermatology and Venereology* 15.6 (Nov. 2001), pp. 550–554. ISSN: 0926-9959, 1468-3083. DOI: 10.1046/j.1468-3083.2001.00333.x.

[42] Ryan F. Donnelly et al. “Microneedle-Mediated Intradermal Nanoparticle Delivery: Potential for Enhanced Local Administration of Hydrophobic Pre-Formed Photosensitisers”. en. In: *Photodiagnosis and Photodynamic Therapy* 7.4 (Dec. 2010), pp. 222–231. ISSN: 15721000. DOI: 10.1016/j.pdpdt.2010.09.001.

[43] Ryan F. Donnelly et al. “Processing Difficulties and Instability of Carbohydrate Microneedle Arrays”. en. In: *Drug Development and Industrial Pharmacy* 35.10 (Oct. 2009), pp. 1242–1254. ISSN: 0363-9045, 1520-5762. DOI: 10.1080/03639040902882280.

[44] Thomas J. Dougherty. “Photosensitizers: Therapy and Detection of Malignant Tumors”. In: *Photochemistry and Photobiology* 45.S1 (1987), pp. 879–889.

[45] Clément Dupont. “Photodynamic Therapies of High-Grade Gliomas: From Theory to Clinical Perspectives”. PhD thesis. Lille University, Nov. 2017.

[46] Clément Dupont et al. “A Novel Device for Intraoperative Photodynamic Therapy Dedicated to Glioblastoma Treatment”. en. In: *Future Oncology* 13.27 (Nov. 2017), pp. 2441–2454. ISSN: 1479-6694, 1744-8301. DOI: 10.2217/fon-2017-0261.

[47] Ervin H. Epstein. “Basal Cell Carcinomas: Attack of the Hedgehog”. In: *Nature Reviews Cancer* 8.10 (Oct. 2008), pp. 743–754. ISSN: 1474-175X, 1474-1768. DOI: 10.1038/nrc2503.

[48] Marica B. Ericson, Ann-Marie Wennberg, and Olle Larkö. “Review of Photodynamic Therapy in Actinic Keratosis and Basal Cell Carcinoma”. In: *Therapeutics and clinical risk management* 4.1 (2008), p. 1.

[49] J. R. E. Fraser, T. C. Laurent, and U. B. G. Laurent. “Hyaluronan: Its Nature, Distribution, Functions and Turnover”. In: *Journal of internal medicine* 242.1 (1997), pp. 27–33.

[50] J.R.E Fraser and T.C. Laurent. “Turnover and Metabolism of Hyaluronan”. In: *Ciba Foundation Symposium* (1989). DOI: 10.1002/9780470513774.ch4.

[51] Jürgen Fuchs and Jens Thiele. “The Role of Oxygen in Cutaneous Photodynamic Therapy”. In: *Free Radical Biology and Medicine* 24.5 (1998), pp. 835–847.

[52] Tanja Gabrecht. “Clinical Fluorescence Spectroscopy and Imaging for the Detection of Early Carcinoma by Autofluorescence Bronchoscopy and the Study of the Protoporphyrin IX Pharmacokinetics in the Endometrium”. In: (2006).

[53] H.J.G.E. Gardeniers et al. “Silicon Micromachined Hollow Microneedles for Transdermal Liquid Transport”. en. In: *Journal of Microelectromechanical Systems* 12.6 (Dec. 2003), pp. 855–862. ISSN: 1057-7157. DOI: 10.1109/JMEMS.2003.820293.

[54] M.J.P. Gerritsen et al. “Pretreatment to Enhance Protoporphyrin IX Accumulation in Photodynamic Therapy”. en. In: *Dermatology* 218.3 (2009), pp. 193–202. ISSN: 1018-8665, 1421-9832. DOI: 10.1159/000183753.

[55] Harvinder S. Gill and Mark R. Prausnitz. “Coated Microneedles for Transdermal Delivery”. en. In: *Journal of Controlled Release* 117.2 (Feb. 2007), pp. 227–237. ISSN: 01683659. DOI: 10.1016/j.jconrel.2006.10.017.

[56] Harvinder S. Gill and Mark R. Prausnitz. “Coating Formulations for Microneedles”. en. In: *Pharmaceutical Research* 24.7 (June 2007), pp. 1369–1380. ISSN: 0724-8741, 1573-904X. DOI: 10.1007/s11095-007-9286-4.

[57] Harvinder S. Gill and Mark R. Prausnitz. “Coating Formulations for Microneedles”. en. In: *Pharmaceutical Research* 24.7 (June 2007), pp. 1369–1380. ISSN: 0724-8741, 1573-904X. DOI: 10.1007/s11095-007-9286-4.

[58] Harvinder S. Gill et al. “Effect of Microneedle Design on Pain in Human Volunteers:” en. In: *The Clinical Journal of Pain* 24.7 (Sept. 2008), pp. 585–594. ISSN: 0749-8047. DOI: 10.1097/AJP.0b013e31816778f9.

[59] Geoffrey J. Gorse et al. “Intradermally-Administered Influenza Virus Vaccine Is Safe and Immunogenic in Healthy Adults 18–64 Years of Age”. en. In: *Vaccine* 31.19 (May 2013), pp. 2358–2365. ISSN: 0264410X. DOI: 10.1016/j.vaccine.2013.03.008.

[60] Melinda J. Griffiths et al. “Interference by Pigment in the Estimation of Microalgal Biomass Concentration by Optical Density”. en. In: *Journal of Microbiological Methods* 85.2 (May 2011), pp. 119–123. ISSN: 01677012. DOI: 10.1016/j.mimet.2011.02.005.

[61] Iman M.N. Hamdan et al. “Intradermal Delivery of a Near-Infrared Photosensitizer Using Dissolving Microneedle Arrays”. en. In: *Journal of Pharmaceutical Sciences* 107.9 (Sept. 2018), pp. 2439–2450. ISSN: 00223549. DOI: 10.1016/j.xphs.2018.05.017.

[62] Iltefat Hamzavi and Harvey Lui. “Using Light in Dermatology: An Update on Lasers, Ultraviolet Phototherapy, and Photodynamic Therapy”. en. In: *Dermatologic Clinics* 23.2 (Apr. 2005), pp. 199–207. ISSN: 07338635. DOI: 10.1016/j.det.2004.11.001.

[63] Sebastien Henry et al. “Microfabricated Microneedles: A Novel Approach to Transdermal Drug Delivery”. In: *Journal of pharmaceutical sciences* 87.8 (1998), pp. 922–925.

[64] Sachiko Hirobe et al. “Clinical Study and Stability Assessment of a Novel Transcutaneous Influenza Vaccination Using a Dissolving Microneedle Patch”. en. In: *Biomaterials* 57 (July 2015), pp. 50–58. ISSN: 01429612. DOI: 10.1016/j.biomaterials.2015.04.007.

[65] Robert L. Hood. “Fiber Optic Microneedles for Transdermal Light Delivery: Ex Vivo Porcine Skin Penetration Experiments”. en. In: *Journal of Biomechanical Engineering* 132.9 (Sept. 2010), p. 091014. ISSN: 0148-0731. DOI: 10.1115/1.4002192.

[66] M. Horn et al. “Topical Methyl Aminolaevulinate Photodynamic Therapy in Patients with Basal Cell Carcinoma Prone to Complications and Poor Cosmetic Outcome with Conventional Treatment”. In: *British Journal of Dermatology* 149.6 (2003), pp. 1242–1249.

[67] Sally Helen Ibbotson and James Ferguson. “Ambulatory Photodynamic Therapy Using Low Irradiance Inorganic Light-Emitting Diodes for the Treatment of Non-Melanoma Skin Cancer: An Open Study: Ambulatory Low Irradiance PDT for NMSC”. en. In: *Photodermatology, Photoimmunology & Photomedicine* 28.5 (Oct. 2012), pp. 235–239. ISSN: 09054383. DOI: 10.1111/j.1600-0781.2012.00681.x.

[68] Kevin Ita. “Transdermal Delivery of Drugs with Microneedles—Potential and Challenges”. en. In: *Pharmaceutics* 7.3 (June 2015), pp. 90–105. ISSN: 1999-4923. DOI: 10.3390/pharmaceutics7030090.

[69] Naoki Izawa et al. “Streptococcus Thermophilus Produces Exopolysaccharides Including Hyaluronic Acid”. en. In: *Journal of Bioscience and Bioengineering* 107.2 (Feb. 2009), pp. 119–123. ISSN: 13891723. DOI: 10.1016/j.jbiosc.2008.11.007.

[70] Aadhar Jain. “Optofluidic Devices For Biological And Energy Applications”. PhD thesis. Optofluidic Devices For Biological and Energy Applications, 2015.

[71] Amit K. Jain, Chang Hyun Lee, and Harvinder S. Gill. “5-Aminolevulinic Acid Coated Microneedles for Photodynamic Therapy of Skin Tumors”. en. In: *Journal of Controlled Release* 239 (Oct. 2016), pp. 72–81. ISSN: 01683659. DOI: 10.1016/j.jconrel.2016.08.015.

[72] Edward W. Jeffes et al. “Photodynamic Therapy of Actinic Keratosis with Topical 5-Aminolevulinic Acid: A Pilot Dose-Ranging Study”. In: *Archives of dermatology* 133.6 (1997), pp. 727–732.

[73] Hye-Rin Jeong et al. “Considerations in the Use of Microneedles: Pain, Convenience, Anxiety and Safety”. en. In: *Journal of Drug Targeting* 25.1 (Jan. 2017), pp. 29–40. ISSN: 1061-186X, 1029-2330. DOI: 10.1080/1061186X.2016.1200589.

[74] Jing Ji et al. “Microfabricated Silicon Microneedle Array for Transdermal Drug Delivery”. In: *Journal of Physics: Conference Series* 34 (Apr. 2006), pp. 1127–1131. ISSN: 1742-6588, 1742-6596. DOI: 10.1088/1742-6596/34/1/186.

[75] Jung-Hwan Park et al. “Tapered Conical Polymer Microneedles Fabricated Using an Integrated Lens Technique for Transdermal Drug Delivery”. In: *IEEE Transactions on Biomedical Engineering* 54.5 (May 2007), pp. 903–913. ISSN: 0018-9294, 1558-2531. DOI: 10.1109/TBME.2006.889173.

[76] Eui Chang Jung and Howard I. Maibach. “Animal Models for Percutaneous Absorption: Animal Models for Percutaneous Absorption”. en. In: *Journal of Applied Toxicology* 35.1 (Jan. 2015), pp. 1–10. ISSN: 0260437X. DOI: 10.1002/jat.3004.

[77] Asta Juzeniene et al. “Effectiveness of Different Light Sources for 5-Aminolevulinic Acid Photodynamic Therapy”. en. In: *Lasers in Medical Science* 19.3 (Dec. 2004), pp. 139–149. ISSN: 0268-8921, 1435-604X. DOI: 10.1007/s10103-004-0314-x.

[78] A. F. H. Kaplan. “An Analytical Model of Metal Cutting with a Laser Beam”. en. In: *Journal of Applied Physics* 79.5 (Mar. 1996), pp. 2198–2208. ISSN: 0021-8979, 1089-7550. DOI: 10.1063/1.361098.

[79] Shilpa Kaushik et al. “Lack of Pain Associated with Microfabricated Microneedles”. In: *Anesthesia & Analgesia* 92.2 (2001), pp. 502–504.

[80] Tomoko Kawashima et al. “Examination of Beauty Ingredient Distribution in the Human Skin by Time-of-Flight Secondary Ion Mass Spectrometry”. en. In: *Biointerphases* 15.3 (May 2020), p. 031013. ISSN: 1934-8630, 1559-4106. DOI: 10.1116/6.0000017.

[81] James C. Kennedy, Stuart L. Marcus, and Roy H. Pottier. “Photodynamic Therapy (PDT) and Photodiagnosis (PD) Using Endogenous Photosensitization Induced by 5-Aminolevulinic Acid (ALA): Mechanisms and Clinical Results”. In: *Journal of clinical laser medicine & surgery* 14.5 (1996), pp. 289–304.

[82] Janneke Kessels et al. “Two-Fold Illumination in Topical 5-Aminolevulinic Acid (ALA)-Mediated Photodynamic Therapy (PDT) for Superficial Basal Cell Carcinoma (sBCC): A Retrospective Case Series and Cohort Study”. en. In: *Journal of the American Academy of Dermatology* 74.5 (May 2016), pp. 899–906. ISSN: 01909622. DOI: 10.1016/j.jaad.2015.12.009.

[83] Kabseog Kim et al. “A Tapered Hollow Metallic Microneedle Array Using Backside Exposure of SU-8”. In: *Journal of Micromechanics and Microengineering* 14.4 (2004), p. 597.

[84] M. Kim et al. “Novel Cosmetic Patches for Wrinkle Improvement: Retinyl Retinoate- and Ascorbic Acid-Loaded Dissolving Microneedles”. en. In: *International Journal of Cosmetic Science* 36.3 (June 2014), pp. 207–212. ISSN: 01425463. DOI: 10.1111/ics.12115.

[85] MinYoung Kim, Bokyung Jung, and Jung-Hwan Park. “Hydrogel Swelling as a Trigger to Release Biodegradable Polymer Microneedles in Skin”. en. In: *Biomaterials* 33.2 (Jan. 2012), pp. 668–678. ISSN: 01429612. DOI: 10.1016/j.biomaterials.2011.09.074.

[86] Yeu-Chun Kim, Jung-Hwan Park, and Mark R. Prausnitz. “Microneedles for Drug and Vaccine Delivery”. en. In: *Advanced Drug Delivery Reviews* 64.14 (Nov. 2012), pp. 1547–1568. ISSN: 0169409X. DOI: 10.1016/j.addr.2012.04.005.

[87] Yujin Kim et al. “Fabrication and Characterization of Hyaluronic Acid Microneedles to Enhance Delivery of Magnesium Ascorbyl Phosphate into Skin”. en. In: *Biomedical Microdevices* 21.4 (Dec. 2019), p. 104. ISSN: 1387-2176, 1572-8781. DOI: 10.1007/s10544-019-0455-0.

[88] Annette Klein et al. “Photodynamic Therapy in Dermatology – an Update 2008”. en. In: *JDDG* 6.18 (Apr. 2008), pp. 839–845. ISSN: 1610-0379, 1610-0387. DOI: 10.1111/j.1610-0387.2008.06697.x.

[89] Jaspreet Singh Kochhar et al. “Effect of Microneedle Geometry and Supporting Substrate on Microneedle Array Penetration into Skin”. en. In: *Journal of Pharmaceutical Sciences* 102.11 (Nov. 2013), pp. 4100–4108. ISSN: 00223549. DOI: 10.1002/jps.23724.

[90] Mladen Korbelik. “Induction of Tumor Immunity by Photodynamic Therapy”. In: *Journal of clinical laser medicine & surgery* 14.5 (1996), pp. 329–334. DOI: 10.1089/clm.1996.14.329.

[91] Mehmet A. Kosoglu et al. “Fiberoptic Microneedles: Novel Optical Diffusers for Interstitial Delivery of Therapeutic Light”. en. In: *Lasers in Surgery and Medicine* 43.9 (Nov. 2011), pp. 914–920. ISSN: 01968092. DOI: 10.1002/lsm.21129.

[92] Dimitrios G. Koutsonanos et al. “Transdermal Influenza Immunization with Vaccine-Coated Microneedle Arrays”. en. In: *PLoS ONE* 4.3 (Mar. 2009). Ed. by Derya Unutmaz, e4773. ISSN: 1932-6203. DOI: 10.1371/journal.pone.0004773.

[93] E. H. Leach, R. A. Peters, and R. J. Rossiter. “EXPERIMENTAL THERMAL BURNS, ESPECIALLY THE MODERATE TEMPERATURE BURN”. en. In: *Quarterly Journal of Experimental Physiology and Cognate Medical Sciences* 32.1 (May 1943), pp. 67–86. ISSN: 00335541. DOI: 10.1113/expphysiol.1943.sp000875.

[94] Jeong W. Lee, Jung-Hwan Park, and Mark R. Prausnitz. “Dissolving Microneedles for Transdermal Drug Delivery”. en. In: *Biomaterials* 29.13 (May 2008), pp. 2113–2124. ISSN: 01429612. DOI: 10.1016/j.biomaterials.2007.12.048.

[95] Jeong Woo Lee et al. “Dissolving Microneedle Patch for Transdermal Delivery of Human Growth Hormone”. en. In: *Small* 7.4 (Feb. 2011), pp. 531–539. ISSN: 16136810. DOI: 10.1002/smll.201001091.

[96] Mara Leone et al. “Hyaluronan Molecular Weight: Effects on Dissolution Time of Dissolving Microneedles in the Skin and on Immunogenicity of Antigen”. en. In: *European Journal of Pharmaceutical Sciences* 146 (Apr. 2020), p. 105269. ISSN: 09280987. DOI: 10.1016/j.ejps.2020.105269.

[97] H. Lev-Tov et al. “Microneedle-Assisted Incubation during Aminolaevulinic Acid Photodynamic Therapy of Actinic Keratoses: A Randomized Controlled Evaluator-Blind Trial”. en. In: *British Journal of Dermatology* 176.2 (Feb. 2017), pp. 543–545. ISSN: 00070963. DOI: 10.1111/bjd.15116.

[98] Jintian Ling et al. “Effect of Honeybee Stinger and Its Microstructured Barbs on Insertion and Pull Force”. en. In: *Journal of the Mechanical Behavior of Biomedical Materials* 68 (Apr. 2017), pp. 173–179. ISSN: 17516161. DOI: 10.1016/j.jmbbm.2017.01.040.

[99] Shu Liu et al. “Transdermal Delivery of Relatively High Molecular Weight Drugs Using Novel Self-Dissolving Microneedle Arrays Fabricated from Hyaluronic Acid and Their Characteristics and Safety after Application to the Skin”. en. In: *European Journal of Pharmaceutics and Biopharmaceutics* 86.2 (Feb. 2014), pp. 267–276. ISSN: 09396411. DOI: 10.1016/j.ejpb.2013.10.001.

[100] Silvia Lucena et al. “Combined Treatments with Photodynamic Therapy for Non-Melanoma Skin Cancer”. en. In: *International Journal of Molecular Sciences* 16.11 (Oct. 2015), pp. 25912–25933. ISSN: 1422-0067. DOI: 10.3390/ijms161025912.

[101] Michael Luster et al. “Tumor Necrosis Factor and Toxicology”. In: *Critical reviews in toxicology* 29.5 (1999), pp. 491–511. DOI: 10.1080/10408449991349258.

[102] SuPing Lyu and Darrel Untereker. “Degradability of Polymers for Implantable Biomedical Devices”. en. In: *International Journal of Molecular Sciences* 10.12 (Sept. 2009), pp. 4033–4065. ISSN: 1422-0067. DOI: 10.3390/ijms10094033.

[103] Guojun Ma and Chengwei Wu. “Microneedle, Bio-Microneedle and Bio-Inspired Microneedle: A Review”. en. In: *Journal of Controlled Release* 251 (Apr. 2017), pp. 11–23. ISSN: 01683659. DOI: 10.1016/j.jconrel.2017.02.011.

[104] Wijaya Martanto et al. “Transdermal Delivery of Insulin Using Microneedles in Vivo”. In: *Pharmaceutical research* 21.6 (2004), pp. 947–952.

[105] Devin V. McAllister et al. “Microfabricated Needles for Transdermal Delivery of Macromolecules and Nanoparticles: Fabrication Methods and Transport Studies”. In: *Proceedings of the National Academy of Sciences* 100.24 (2003), pp. 13755–13760.

[106] L.J. McLellan et al. “Daylight Photodynamic Therapy: Patient Willingness to Undertake Home Treatment”. en. In: *British Journal of Dermatology* 181.4 (Oct. 2019), pp. 834–835. ISSN: 0007-0963, 1365-2133. DOI: 10.1111/bjd.17920.

[107] John A. Mikszta et al. “Protective Immunization against Inhalational Anthrax: A Comparison of Minimally Invasive Delivery Platforms”. In: *Journal of Infectious Diseases* 191.2 (2005), pp. 278–288.

[108] Takaya Miyano et al. “Sugar Micro Needles as Transdermic Drug Delivery System”. In: *Biomedical Microdevices* 7.3 (2005), pp. 185–188.

[109] Johan MOAN. *On the Diffusion Lenght of Singlet Oxygen in Cells and Tissues*. 1990.

[110] Juha Mönkäre et al. “IgG-Loaded Hyaluronan-Based Dissolving Microneedles for Intradermal Protein Delivery”. en. In: *Journal of Controlled Release* 218 (2015), pp. 53–62. ISSN: 01683659. DOI: 10.1016/j.jconrel.2015.10.002.

[111] Sang Jun Moon et al. “Fabrication of Microneedle Array Using LIGA and Hot Embossing Process”. en. In: *Microsystem Technologies* 11.4-5 (Apr. 2005), pp. 311–318. ISSN: 0946-7076, 1432-1858. DOI: 10.1007/s00542-004-0446-8.

[112] S. Mordon et al. “The Conventional Protocol vs. a Protocol Including Illumination with a Fabric-based Biophotonic Device (the Phosistos Protocol) in Photodynamic Therapy for Actinic Keratosis: A Randomized, Controlled, Noninferiority Clinical Study”. en. In: *British Journal of Dermatology* (Aug. 2019), bjd.18048. ISSN: 0007-0963, 1365-2133. DOI: 10.1111/bjd.18048.

[113] Serge Mordon. “A Commentary on the Role of Skin Temperature on the Effectiveness of ALA-PDT in Dermatology”. en. In: *Photodiagnosis and Photodynamic Therapy* 11.3 (Sept. 2014), pp. 416–419. ISSN: 15721000. DOI: 10.1016/j.pdpdt.2014.05.004.

[114] Serge Mordon. “Painless and Efficient ALA-PDT and MAL-PDT of Actinic Keratosis Can Be Achieved by Drastically Reducing the Drug-light Interval”. en. In: *Dermatologic Therapy* (Apr. 2020). ISSN: 1396-0296, 1529-8019. DOI: 10.1111/dth.13423.

[115] C.A. Morton et al. “European Dermatology Forum Guidelines on Topical Photodynamic Therapy 2019 Part 1: Treatment Delivery and Established Indications – Actinic Keratoses, Bowen’s Disease and Basal Cell Carcinomas”. en. In: *Journal of the European Academy of Dermatology and Venereology* 33.12 (Dec. 2019), pp. 2225–2238. ISSN: 0926-9959, 1468-3083. DOI: 10.1111/jdv.16017.

[116] C.A. Morton et al. “European Guidelines for Topical Photodynamic Therapy Part 1: Treatment Delivery and Current Indications - Actinic Keratoses, Bowen’s Disease, Basal Cell Carcinoma: European PDT Guidelines”. en. In: *Journal of the European Academy of Dermatology and Venereology* 27.5 (May 2013), pp. 536–544. ISSN: 09269959. DOI: 10.1111/jdv.12031.

[117] C.A. Morton et al. “Practical Approach to the Use of Daylight Photodynamic Therapy with Topical Methyl Aminolevulinate for Actinic Keratosis: A European Consensus”. en. In: *Journal of the European Academy of Dermatology and Venereology* 29.9 (Sept. 2015), pp. 1718–1723. ISSN: 09269959. DOI: 10.1111/jdv.12974.

[118] Colin Morton. *Photodynamic Therapy for Large or Multiple Patches of Bowen Disease and Basal Cell Carcinoma*. 2001.

[119] Colin Morton et al. “Comparison of Topical Methyl Aminolevulinate Photodynamic Therapy With Cryotherapy or Fluorouracil for Treatment of Squamous Cell Carcinoma In Situ: Results of a Multicenter Randomized Trial”. en. In: *Archives of Dermatology* 142.6 (June 2006). ISSN: 0003-987X. DOI: 10.1001/archderm.142.6.729.

[120] Colin Morton et al. “Comparison of Topical Methyl Aminolevulinate Photodynamic Therapy with Cryotherapy or Fluorouracil for Treatment of Squamous Cell Carcinoma in Situ: Results of a Multicenter Randomized Trial”. In: *Archives of dermatology* 142.6 (2006), pp. 729–735.

[121] Harry Moseley. “Light Distribution and Calibration of Commercial PDT LED Arrays”. en. In: *Photochemical & Photobiological Sciences* 4.11 (2005), p. 911. ISSN: 1474-905X, 1474-9092. DOI: 10.1039/b507325a.

[122] Ronald L. Moy. “Clinical Presentation of Actinic Keratoses and Squamous Cell Carcinoma”. In: *Journal of the American Academy of Dermatology* 42.1 (2000), S8–S10.

[123] John T. Mullen et al. “Invasive Squamous Cell Carcinoma of the Skin: Defining a High-Risk Group”. en. In: *Annals of Surgical Oncology* 13.7 (July 2006), pp. 902–909. ISSN: 1068-9265, 1534-4681. DOI: 10.1245/ASO.2006.07.022.

[124] M. A. Napier and N. M. Hadler. "Effect of Calcium on Structure and Function of a Hyaluronic Acid Matrix: Carbon-13 Nuclear Magnetic Resonance Analysis and the Diffusional Behavior of Small Solutes". en. In: *Proceedings of the National Academy of Sciences* 75.5 (May 1978), pp. 2261–2265. ISSN: 0027-8424, 1091-6490. DOI: 10.1073/pnas.75.5.2261.

[125] Atul Nayak and Diganta Bhusan Das. "Potential of Biodegradable Microneedles as a Transdermal Delivery Vehicle for Lidocaine". en. In: *Biotechnology Letters* 35.9 (Sept. 2013), pp. 1351–1363. ISSN: 0141-5492, 1573-6776. DOI: 10.1007/s10529-013-1217-3.

[126] J. Necas et al. "Hyaluronic Acid (Hyaluronan): A Review". en. In: *Veterinární Medicína* 53.No. 8 (Sept. 2008), pp. 397–411. ISSN: 03758427, 18059392. DOI: 10.17221/1930-VETMED.

[127] Sedat Nizamoglu et al. "Bioabsorbable Polymer Optical Waveguides for Deep-Tissue Photomedicine". In: *Nature Communications* 7 (Jan. 2016), p. 10374. ISSN: 2041-1723. DOI: 10.1038/ncomms10374.

[128] Ololade Olatunji, Diganta Bhusan Das, and Barrak Al-Qallaf. "Simulation Based Optimization of Microneedle Geometry to Improve Drug Permeability in Skin". In: (2009).

[129] Tomohiro Osaki et al. "Metformin Enhances the Cytotoxicity of 5-Aminolevulinic Acid-Mediated Photodynamic Therapy in Vitro". en. In: *Oncology Letters* 14.1 (July 2017), pp. 1049–1053. ISSN: 1792-1074, 1792-1082. DOI: 10.3892/ol.2017.6237.

[130] Emerson H. Padoveze et al. "Macrophage Subtypes in Recurrent Nodular Basal Cell Carcinoma after Mohs Micrographic Surgery". In: *International journal of dermatology* (2017).

[131] David M. Pariser et al. "Photodynamic Therapy with Topical Methyl Aminolevulinate for Actinic Keratosis: Results of a Prospective Randomized Multicenter Trial". en. In: *Journal of the American Academy of Dermatology* 48.2 (Feb. 2003), pp. 227–232. ISSN: 01909622. DOI: 10.1067/mjd.2003.49.

[132] Jung-Hwan Park, Mark G. Allen, and Mark R. Prausnitz. "Biodegradable Polymer Microneedles: Fabrication, Mechanics and Transdermal Drug Delivery". en. In: *Journal of Controlled Release* 104.1 (May 2005), pp. 51–66. ISSN: 01683659. DOI: 10.1016/j.jconrel.2005.02.002.

[133] Jung-Hwan Park, Mark G. Allen, and Mark R. Prausnitz. "Polymer Microneedles for Controlled-Release Drug Delivery". en. In: *Pharmaceutical Research* 23.5 (May 2006), pp. 1008–1019. ISSN: 0724-8741, 1573-904X. DOI: 10.1007/s11095-006-0028-9.

[134] Yonghun Park et al. "Fabrication and Characterization of Dissolving Microneedle Arrays for Improving Skin Permeability of Cosmetic Ingredients". en. In: *Journal of Industrial and Engineering Chemistry* 39 (July 2016), pp. 121–126. ISSN: 1226086X. DOI: 10.1016/j.jiec.2016.05.022.

[135] Qian Peng et al. "Selective Distribution of Porphyrins in Skin Thick Basal Cell Carcinoma after Topical Application of Methyl 5-Aminolevulinate". en. In: *Journal of Photochemistry and Photobiology B: Biology* 62.3 (Sept. 2001), pp. 140–145. ISSN: 10111344. DOI: 10.1016/S1011-1344(01)00173-7.

[136] F Pérennès et al. "Sharp Beveled Tip Hollow Microneedle Arrays Fabricated by LIGA and 3D Soft Lithography with Polyvinyl Alcohol". In: *Journal of Micromechanics and Microengineering* 16.3 (Mar. 2006), pp. 473–479. ISSN: 0960-1317, 1361-6439. DOI: 10.1088/0960-1317/16/3/001.

[137] Tatyana A. Petukhova et al. “Effect of Expedited Microneedle-Assisted Photodynamic Therapy for Field Treatment of Actinic Keratoses: A Randomized Clinical Trial”. en. In: *JAMA Dermatology* 153.7 (July 2017), p. 637. ISSN: 2168-6068. DOI: 10.1001/jamadermatol.2017.0849.

[138] Daniel Piacquadio et al. *Photodynamic Therapy with Aminolevulinic Acid Topical Solution and Visible Blue Light in the Treatment of Multiple Actinic Karatoses of the Face and Scalp*. 2004.

[139] Mark R Prausnitz. “Microneedles for Transdermal Drug Delivery”. en. In: *Advanced Drug Delivery Reviews* 56.5 (Mar. 2004), pp. 581–587. ISSN: 0169409X. DOI: 10.1016/j.addr.2003.10.023.

[140] Barrak Al-Qallaf and Diganta Bhusan Das. “Optimization of Square Microneedle Arrays for Increasing Drug Permeability in Skin”. en. In: *Chemical Engineering Science* 63.9 (May 2008), pp. 2523–2535. ISSN: 00092509. DOI: 10.1016/j.ces.2008.02.007.

[141] Barrak Al-Qallaf and Diganta Bhusan Das. “Optimizing Microneedle Arrays for Transdermal Drug Delivery: Extension to Non-Square Distribution of Microneedles”. en. In: *Journal of Drug Targeting* 17.2 (Jan. 2009), pp. 108–122. ISSN: 1061-186X, 1029-2330. DOI: 10.1080/10611860802472370.

[142] P J F Quaedvlieg et al. “Histopathological Characteristics of Metastasizing Squamous Cell Carcinoma of the Skin and Lips”. en. In: *Histopathology* 49.3 (Sept. 2006), pp. 256–264. ISSN: 0309-0167, 1365-2559. DOI: 10.1111/j.1365-2559.2006.02472.x.

[143] K Jagadeeswara Reddy and K T Karunakaran. “Purification and Characterization of Hyaluronic Acid Produced by Streptococcus Zooepidemicus Strain 3523-7”. en. In: (2013), p. 7.

[144] J J Rippey. “Why Classify Basal Cell Carcinomas?” en. In: (1998), p. 6.

[145] David JH Roberts and Fiona Cairnduff. “Photodynamic Therapy of Primary Skin Cancer: A Review”. In: *British journal of plastic surgery* 48.6 (1995), pp. 360–370.

[146] C.A. Robertson, D. Hawkins Evans, and H. Abrahamse. “Photodynamic Therapy (PDT): A Short Review on Cellular Mechanisms and Cancer Research Applications for PDT”. en. In: *Journal of Photochemistry and Photobiology B: Biology* 96.1 (July 2009), pp. 1–8. ISSN: 10111344. DOI: 10.1016/j.jphotobiol.2009.04.001.

[147] Gary S. Rogers and Samuel L. Hill. “LIGHT EMITTING SYSTEM FOR WOUND CARE”. US 2015/0335911 A1. 2015.

[148] Robert Rosen et al. “A New, Objective, Quantitative Scale for Measuring Local Skin Responses Following Topical Actinic Keratosis Therapy with Ingenol Mebutate”. en. In: *Dermatology and Therapy* 4.2 (Dec. 2014), pp. 207–219. ISSN: 2193-8210, 2190-9172. DOI: 10.1007/s13555-014-0059-9.

[149] J. Röwert-Huber et al. “Actinic Keratosis Is an Early in Situ Squamous Cell Carcinoma: A Proposal for Reclassification”. In: *British Journal of Dermatology* 156.s3 (2007), pp. 8–12.

[150] W. Mark Saltzman and Themis R. Kyriakides. “Cell Interactions with Polymers”. en. In: *Principles of Tissue Engineering*. Elsevier, 2014, pp. 385–406. ISBN: 978-0-12-398358-9. DOI: 10.1016/B978-0-12-398358-9.00020-3.

[151] A Samali, M Gorman, and T.G. Cotter. “Apoptosis - the Story so Far...” In: *Experentia* 52.10-11 (1996), pp. 933–941. ISSN: 1420-9071. DOI: 10.1007/BF01920101.

[152] Firas Sammoura et al. “Polymeric Microneedle Fabrication Using a Microinjection Molding Technique”. en. In: *Microsystem Technologies* 13.5-6 (Jan. 2007), pp. 517–522. ISSN: 0946-7076, 1432-1858. DOI: 10.1007/s00542-006-0204-1.

[153] Firas Sammoura et al. “Polymeric Microneedle Fabrication Using a Microinjection Molding Technique”. en. In: *Microsystem Technologies* 13.5-6 (Jan. 2007), pp. 517–522. ISSN: 0946-7076, 1432-1858. DOI: 10.1007/s00542-006-0204-1.

[154] Morgane Seon-Lutz. “Elaboration et Caractérisation de Matériaux Nanofibreux Fonctionnels à Base d’acide Hyaluronique et de Nanoparticules Lipidiques Pour Des Applications à Usage Biomédical”. PhD Thesis. Université de Strasbourg, 2019.

[155] Morgane Séon-Lutz et al. “Electrospinning in Water and in Situ Crosslinking of Hyaluronic Acid / Cyclodextrin Nanofibers: Towards Wound Dressing with Controlled Drug Release”. en. In: *Carbohydrate Polymers* 207 (Mar. 2019), pp. 276–287. ISSN: 01448617. DOI: 10.1016/j.carbpol.2018.11.085.

[156] Vivek Kumar Sharma and Amit Kumar. “Micro Machining-A Review”. In: *International Journal of Emerging Technology and Advanced Engineering* 4 (2014).

[157] Mitsuhiro Shikida et al. “Micromachined Pyramidal Shaped Biodegradable Microneedle and Its Skin Penetration Capability”. en. In: *Microsystem Technologies* 20.12 (Dec. 2014), pp. 2239–2245. ISSN: 0946-7076, 1432-1858. DOI: 10.1007/s00542-013-1924-7.

[158] M.C.F. Simões, J.J.S. Sousa, and A.A.C.C. Pais. “Skin Cancer and New Treatment Perspectives: A Review”. en. In: *Cancer Letters* 357.1 (Feb. 2015), pp. 8–42. ISSN: 03043835. DOI: 10.1016/j.canlet.2014.11.001.

[159] Raja K. Sivamani et al. “Clinical Microneedle Injection of Methyl Nicotinate: Stratum Corneum Penetration”. In: *Skin Research and Technology* 11.2 (2005), pp. 152–156.

[160] M. A. Smith and R. G. Schnellmann. “Calpains, Mitochondria, and Apoptosis”. en. In: *Cardiovascular Research* 96.1 (Oct. 2012), pp. 32–37. ISSN: 0008-6363. DOI: 10.1093/cvr/cvs163.

[161] A M Soler et al. “A Follow-up Study of Recurrence and Cosmesis in Completely Responding Superficial and Nodular Basal Cell Carcinomas Treated with Methyl 5-aminolaevulinate-based Photodynamic Therapy Alone and with Prior Curettage”. en. In: *British Journal of Dermatology* (2001), p. 5.

[162] A. M. Soler et al. “A Follow-up Study of Recurrence and Cosmesis in Completely Responding Superficial and Nodular Basal Cell Carcinomas Treated with Methyl 5-Aminolaevulinate-Based Photodynamic Therapy Alone and with Prior Curettage”. In: *British Journal of Dermatology* 145.3 (2001), pp. 467–471.

[163] J. Soriano et al. “Cell Death Mechanisms in Tumoral and Non-Tumoral Human Cell Lines Triggered by Photodynamic Treatments: Apoptosis, Necrosis and Parthanatos”. en. In: *Scientific Reports* 7.1 (Feb. 2017), p. 41340. ISSN: 2045-2322. DOI: 10.1038/srep41340.

[164] Rahul Srivastava et al. “Photodynamic Therapy Curbing the Uncontrolled Proliferations: An Orodental Perspective”. In: *Journal of Indian Academy of Oral Medicine and Radiology* 25 (2013), pp. 30–34. ISSN: 09751572. DOI: 10.5005/jp-journals-10011-1335.

[165] Robert Stern. “Hyaluronan Catabolism: A New Metabolic Pathway”. In: *European journal of cell biology* 83.7 (2004), pp. 317–325.

[166] Robert Stern et al. “The Many Ways to Cleave Hyaluronan”. en. In: *Biotechnology Advances* 25.6 (Nov. 2007), pp. 537–557. ISSN: 07349750. DOI: 10.1016/j.biotechadv.2007.07.001.

[167] B. Stoeber and D. Liepmann. "Arrays of Hollow Out-of-Plane Microneedles for Drug Delivery". In: *Journal of Microelectromechanical Systems* 14.3 (June 2005), pp. 472–479. ISSN: 1057-7157. DOI: 10.1109/JMEMS.2005.844843.

[168] Alexander Stratigos et al. "Diagnosis and Treatment of Invasive Squamous Cell Carcinoma of the Skin: European Consensus-Based Interdisciplinary Guideline". en. In: *European Journal of Cancer* 51.14 (Sept. 2015), pp. 1989–2007. ISSN: 09598049. DOI: 10.1016/j.ejca.2015.06.110.

[169] S. P. Sullivan, N. Murthy, and M. R. Prausnitz. "Minimally Invasive Protein Delivery with Rapidly Dissolving Polymer Microneedles". en. In: *Advanced Materials* 20.5 (Mar. 2008), pp. 933–938. ISSN: 09359648, 15214095. DOI: 10.1002/adma.200701205.

[170] Masato Suzuki et al. "Ultrafine Three-Dimensional (3D) Laser Lithographic Fabrication of Microneedle and Its Application to Painless Insertion and Blood Sampling Inspired by Mosquito". In: *Intelligent Robots and Systems (IROS), 2015 IEEE/RSJ International Conference On*. IEEE, 2015, pp. 2748–2753.

[171] Rm Szeimies et al. "A Clinical Study Comparing Methyl Aminolevulinate Photodynamic Therapy and Surgery in Small Superficial Basal Cell Carcinoma (8-20 Mm), with a 12-Month Follow-Up." en. In: *Journal of the European Academy of Dermatology and Venereology* 22.11 (Nov. 2008), pp. 1302–1311. ISSN: 09269959, 14683083. DOI: 10.1111/j.1468-3083.2008.02803.x.

[172] R.M. Szeimiesa et al. "Photodynamic Therapy Using Topical Methyl 5-Aminolevulinate Compared with Cryotherapy for Actinic Keratosis: A Prospective, Randomized Study". en. In: *Journal of the American Academy of Dermatology* 47.2 (Aug. 2002), pp. 258–262. ISSN: 01909622. DOI: 10.1067/mjd.2002.119649.

[173] Colin W. X. Tan et al. "Dissolving Triamcinolone-Embedded Microneedles for the Treatment of Keloids: A Single-Blinded Intra-Individual Controlled Clinical Trial". en. In: *Dermatology and Therapy* 9.3 (Sept. 2019), pp. 601–611. ISSN: 2193-8210, 2190-9172. DOI: 10.1007/s13555-019-00316-3.

[174] N.R. Telfer, G.B. Colver, and C.A. Morton. "Guidelines for the Management of Basal Cell Carcinoma". en. In: *British Journal of Dermatology* 159.1 (July 2008), pp. 35–48. ISSN: 0007-0963, 1365-2133. DOI: 10.1111/j.1365-2133.2008.08666.x.

[175] Tanguy Terlier. "Analyse par ToF-SIMS de matériaux organiques pour les applications en électronique organique". fr. In: (), p. 303.

[176] Hoa Le Thanh et al. "Low-Cost Fabrication of Hollow Microneedle Arrays Using CNC Machining and UV Lithography". en. In: *Journal of Microelectromechanical Systems* 24.5 (Oct. 2015), pp. 1583–1593. ISSN: 1057-7157, 1941-0158. DOI: 10.1109/JMEMS.2015.2424926.

[177] B.K. Todd et al. "Is There an Optimal Irradiation Dose for Photodynamic Therapy: 37 J Cm^2 or 75 J Cm^2?" en. In: *British Journal of Dermatology* 182.5 (May 2020), pp. 1287–1288. ISSN: 0007-0963, 1365-2133. DOI: 10.1111/bjd.18644.

[178] Hiroaki Todo. "Transdermal Permeation of Drugs in Various Animal Species". en. In: *Pharmaceutics* 9.4 (Sept. 2017), p. 33. ISSN: 1999-4923. DOI: 10.3390/pharmaceutics9030033.

[179] Y. Tokita and A. Okamoto. "Hydrolytic Degradation of Hyaluronic Acid". In: *Polymer Degradation and Stability* 48.2 (1995), pp. 269–273.

[180] Luís Torezan et al. “A Pilot Split-Face Study Comparing Conventional Methyl Aminolevulinate-Photodynamic Therapy (PDT) With Microneedling-Assisted PDT on Actinically Damaged Skin:” en. In: *Dermatologic Surgery* 39.8 (Aug. 2013), pp. 1197–1201. ISSN: 1076-0512. DOI: 10.1111/dsu.12233.

[181] Aktilite Trolleystand Ts. “Aktilite CL-128”. en. In: (), p. 2.

[182] Konstantinos Tsioris et al. “Fabrication of Silk Microneedles for Controlled-Release Drug Delivery”. en. In: *Advanced Functional Materials* 22.2 (Jan. 2012), pp. 330–335. ISSN: 1616301X. DOI: 10.1002/adfm.201102012.

[183] Tuan-Mazlelaa Tuan-Mahmood et al. “Microneedles for Intradermal and Transdermal Drug Delivery”. en. In: *European Journal of Pharmaceutical Sciences* 50.5 (Dec. 2013), pp. 623–637. ISSN: 09280987. DOI: 10.1016/j.ejps.2013.05.005.

[184] Martina Ulrich et al. “Actinic Keratoses: Non-Invasive Diagnosis for Field Cancerisation”. In: *British Journal of Dermatology* 156 (2007), pp. 13–17.

[185] Manuel Triana Valencia et al. “Quantum Dot Light-Emitting Diodes as Light Sources in Photomedicine: Photodynamic Therapy and Photobiomodulation”. en. In: *Journal of Physics: Materials* (May 2020). ISSN: 2515-7639. DOI: 10.1088/2515-7639/ab95e8.

[186] Koen van der Maaden, Wim Jiskoot, and Joke Bouwstra. “Microneedle Technologies for (Trans)Dermal Drug and Vaccine Delivery”. en. In: *Journal of Controlled Release* 161.2 (July 2012), pp. 645–655. ISSN: 01683659. DOI: 10.1016/j.jconrel.2012.01.042.

[187] Mathieu Varache, Mathieu Ciancone, and Anne-Claude Couffin. “Development and Validation of a Novel UPLC-ELSD Method for the Assessment of Lipid Composition of Nanomedicine Formulation”. en. In: *International Journal of Pharmaceutics* 566 (July 2019), pp. 11–23. ISSN: 03785173. DOI: 10.1016/j.ijpharm.2019.05.038.

[188] C. Vicentini et al. “Photodynamic Therapy for Actinic Keratosis of the Forehead and Scalp with the Aktilite CL 128: Is There a Cut-off Value for PpIX-Weighted Irradiance for Effective Treatment?” en. In: *Photodermatology, Photoimmunology & Photomedicine* (Feb. 2019). ISSN: 09054383. DOI: 10.1111/phpp.12457.

[189] C. Vicentini et al. “Photodynamic Therapy for Actinic Keratosis of the Forehead and Scalp: A Randomized, Controlled, Phase II Clinical Study Evaluating the Noninferiority of a New Protocol Involving Irradiation with a Light-Emitting, Fabric-Based Device (the Flexitheralight p”. en. In: *British Journal of Dermatology* (Jan. 2019). ISSN: 00070963. DOI: 10.1111/bjd.17350.

[190] Anne Sophie Vignion-Dewalle et al. “Comparison of 10 Efficient Protocols for Photodynamic Therapy of Actinic Keratosis: How Relevant Are Effective Light Dose and Local Damage in Predicting the Complete Response Rat at 3 Months ?” In: *Lasers in Surgery and Medicine* (2018).

[191] Anne-Sophie Vignion-Dewalle et al. “Red Light Photodynamic Therapy for Actinic Keratosis Using 37 J/Cm2: Fractionated Irradiation with 12.3 mW/Cm2 after 30 Minutes Incubation Time Compared to Standard Continuous Irradiation with 75 mW/Cm2 after 3 Hours Incubation Time Using a Mathematical m: RED LIGHT PHOTODYNAMIC THERAPY FOR ACTINIC KERATOSIS”. en. In: *Lasers in Surgery and Medicine* 49.7 (Sept. 2017), pp. 686–697. ISSN: 01968092. DOI: 10.1002/lsm.22665.

[192] Anne-Sophie Vignion-Dewalle et al. "Red Light Photodynamic Therapy for Actinic Keratosis Using 37 J/Cm2: Fractionated Irradiation with 12.3 mW/Cm2 after 30 Minutes Incubation Time Compared to Standard Continuous Irradiation with 75 mW/Cm2 after 3 Hours Incubation Time Using a Mathematical m: RED LIGHT PHOTODYNAMIC THERAPY FOR ACTINIC KERATOSIS". en. In: *Lasers in Surgery and Medicine* 49.7 (Sept. 2017), pp. 686–697. ISSN: 01968092. DOI: 10.1002/lsm.22665.

[193] K B Vinayakumar et al. "A Hollow Stainless Steel Microneedle Array to Deliver Insulin to a Diabetic Rat". In: *Journal of Micromechanics and Microengineering* 26.6 (June 2016), p. 065013. ISSN: 0960-1317, 1361-6439. DOI: 10.1088/0960-1317/26/6/065013.

[194] C. Vinciullo et al. "Photodynamic Therapy with Topical Methyl Aminolaevulinate for 'difficult-to-Treat' Basal Cell Carcinoma". en. In: *British Journal of Dermatology* 152.4 (Apr. 2005), pp. 765–772. ISSN: 0007-0963, 1365-2133. DOI: 10.1111/j.1365-2133.2005.06484.x.

[195] Qingqing Wang et al. "Investigation on Fabrication Process of Dissolving Microneedle Arrays to Improve Effective Needle Drug Distribution". en. In: *European Journal of Pharmaceutical Sciences* 66 (Jan. 2015), pp. 148–156. ISSN: 09280987. DOI: 10.1016/j.ejps.2014.09.011.

[196] Christine B. Warren et al. "Pain Associated with Aminolevulinic Acid-Photodynamic Therapy of Skin Disease". en. In: *Journal of the American Academy of Dermatology* 61.6 (Dec. 2009), pp. 1033–1043. ISSN: 01909622. DOI: 10.1016/j.jaad.2009.03.048.

[197] Li Wei-Ze et al. "Super-Short Solid Silicon Microneedles for Transdermal Drug Delivery Applications". en. In: *International Journal of Pharmaceutics* 389.1-2 (Apr. 2010), pp. 122–129. ISSN: 03785173. DOI: 10.1016/j.ijpharm.2010.01.024.

[198] R.N. Werner et al. "The Natural History of Actinic Keratosis: A Systematic Review". en. In: *British Journal of Dermatology* 169.3 (Sept. 2013), pp. 502–518. ISSN: 00070963. DOI: 10.1111/bjd.12420.

[199] Annet Westers-Attema et al. "Photodynamic Therapy in Bowen's Disease: Influence of Histological Features and Clinical Characteristics on Its Success". en. In: *Dermatology* 230.1 (2015), pp. 55–61. ISSN: 1018-8665, 1421-9832. DOI: 10.1159/000366500.

[200] Jim R. White. "Polymer Ageing: Physics, Chemistry or Engineering? Time to Reflect". en. In: *Comptes Rendus Chimie* 9.11-12 (Nov. 2006), pp. 1396–1408. ISSN: 16310748. DOI: 10.1016/j.crci.2006.07.008.

[201] S. R. Wiegell et al. "Continuous Activation of PpIX by Daylight Is as Effective as and Less Painful than Conventional Photodynamic Therapy for Actinic Keratoses; a Randomized, Controlled, Single-Blinded Study". In: *British Journal of Dermatology* 158.4 (2008), pp. 740–746.

[202] S.R. Wiegell et al. "Daylight Photodynamic Therapy for Actinic Keratosis: An International Consensus: International Society for Photodynamic Therapy in Dermatology". en. In: *Journal of the European Academy of Dermatology and Venereology* 26.6 (June 2012), pp. 673–679. ISSN: 09269959. DOI: 10.1111/j.1468-3083.2011.04386.x.

[203] S.R. Wiegell et al. "Pain during Photodynamic Therapy Is Associated with Protoporphyrin IX Fluorescence and Fluence Rate". en. In: *British Journal of Dermatology* 158.4 (Apr. 2008), pp. 727–733. ISSN: 0007-0963, 1365-2133. DOI: 10.1111/j.1365-2133.2008.08451.x.

[204] V Wienert, H Sick, and J zur Mühlen. "Local Thermal Stress Tolerance of Human Skin". In: *Anasth Intensivther Notfallmed* . (1983), pp. 88–90.

[205] N. Wilke et al. “Process Optimization and Characterization of Silicon Microneedles Fabricated by Wet Etch Technology”. en. In: *Microelectronics Journal* 36.7 (July 2005), pp. 650–656. ISSN: 00262692. DOI: 10.1016/j.mejo.2005.04.044.

[206] N. Wilke et al. “Silicon Microneedle Electrode Array with Temperature Monitoring for Electroporation”. en. In: *Sensors and Actuators A: Physical* 123-124 (Sept. 2005), pp. 319–325. ISSN: 09244247. DOI: 10.1016/j.sna.2005.05.017.

[207] Thomas S. Wilson et al. *Shape Memory Polymer Therapeutic Devices for Stroke*. Tech. rep. Lawrence Livermore National Laboratory (LLNL), Livermore, CA, 2005.

[208] James T. Wolter and Ross M. Kedl. “Delivery of Immune Response Modifier Compounds”. 8961477. Feb. 2015.

[209] C. S. M. Wong, R. C. Strange, and J. T. Lear. “Basal Cell Carcinoma”. In: *BMJ: British Medical Journal* 327.7418 (2003), p. 794.

[210] Yanhai Xi et al. “Dual Targeting Curcumin Loaded Alendronate-Hyaluronan- Octadecanoic Acid Micelles for Improving Osteosarcoma Therapy”. en. In: *International Journal of Nanomedicine* Volume 14 (Aug. 2019), pp. 6425–6437. ISSN: 1178-2013. DOI: 10.2147/IJN.S211981.

[211] Jing Yao et al. “Enhanced and Sustained Topical Ocular Delivery of Cyclosporine A in Thermosensitive Hyaluronic Acid-Based in Situ Forming Microgels”. en. In: *International Journal of Nanomedicine* (Sept. 2013), p. 3587. ISSN: 1178-2013. DOI: 10.2147/IJN.S47665.

[212] Iris Zalaudek et al. “Morphologic Grading and Treatment of Facial Actinic Keratosis”. en. In: *Clinics in Dermatology* 32.1 (Jan. 2014), pp. 80–87. ISSN: 0738081X. DOI: 10.1016/j.clindermatol.2013.05.028.

[213] N Zeitouni. “Photodynamic Therapy for Nonmelanoma Skin cancersCurrent Review and Update”. en. In: *Molecular Immunology* 39.17-18 (July 2003), pp. 1133–1136. ISSN: 01615890. DOI: 10.1016/S0161-5890(03)00083-X.

[214] Ying Zhang et al. “Development of Lidocaine-Coated Microneedle Product for Rapid, Safe, and Prolonged Local Analgesic Action”. en. In: *Pharmaceutical Research* 29.1 (Jan. 2012), pp. 170–177. ISSN: 0724-8741, 1573-904X. DOI: 10.1007/s11095-011-0524-4.

[215] Xiao Zhao et al. “Tip-Loaded Fast-Dissolving Microneedle Patches for Photodynamic Therapy of Subcutaneous Tumor”. en. In: *Journal of Controlled Release* 286 (Sept. 2018), pp. 201–209. ISSN: 01683659. DOI: 10.1016/j.jconrel.2018.07.038.

[216] Cui-Ping Zhou et al. “Transdermal Delivery of Insulin Using Microneedle Rollers in Vivo”. en. In: *International Journal of Pharmaceutics* 392.1-2 (June 2010), pp. 127–133. ISSN: 03785173. DOI: 10.1016/j.ijpharm.2010.03.041.

[217] Jinjin Zhu et al. “5-Aminolevulinic Acid-Loaded Hyaluronic Acid Dissolving Microneedles for Effective Photodynamic Therapy of Superficial Tumors with Enhanced Long-Term Stability”. en. In: *Advanced Healthcare Materials* 8.22 (Nov. 2019), p. 1900896. ISSN: 2192-2640, 2192-2659. DOI: 10.1002/adhm.201900896.

[218] Zhuangzhi Zhu et al. “Rapidly Dissolvable Microneedle Patches for Transdermal Delivery of Exenatide”. en. In: *Pharmaceutical Research* 31.12 (Dec. 2014), pp. 3348–3360. ISSN: 0724-8741, 1573-904X. DOI: 10.1007/s11095-014-1424-1.

[219] S Zwiebel and E Baron. “PDT in Squamous Cell Carcinoma of the Skin”. In: *Journal on dermatology and sexual transmitted diseases.* (2011).

Appendix A

Arduino code

```
LED_adafruit | Arduino 1.8.10
Fichier  Édition  Croquis  Outils  Aide
LED_adafruit

#include <Adafruit_DotStar.h> // Load the characteristic library of the LED matrix Adafruit Dotstar

// Because conditional #includes don't work w/Arduino sketches...
//#include <SPI.h>          // COMMENT OUT THIS LINE FOR GEMMA OR TRINKET
#include <avr/power.h>  // ENABLE THIS LINE FOR GEMMA OR TRINKET
#include <avr/sleep.h>  // pour set_sleep_mode

// The "define" command allow to define the variables
#define _d_NUMPIXELS 64  // Number of LEDs in strip
#define _d_BRIGHTNESS 176  // Luminosité des LEDs à utiliser

// Here's how to control the LEDs from any two pins:
#define _d_DATAPIN    1
#define _d_CLOCKPIN   2
Adafruit_DotStar strip(_d_NUMPIXELS, _d_DATAPIN, _d_CLOCKPIN, DOTSTAR_RGB); \\Variables

//"""
//    MICROCONTROLLER INITIALISATION
//"""
void setup()
{
  // Test si Trinket 16 MHz plutôt que 8 MHz
  #if defined(__AVR_ATtiny85__) && (F_CPU == 16000000L)
    clock_prescale_set(clock_div_1);  // Enable 16 MHz on Trinket
  #endif

  strip.begin();  // Init. pins en sortie
  strip.clear();
}

void sleep()
{

    GIMSK |= _BV(PCIE);                     // Enable Pin Change Interrupts
    PCMSK |= _BV(PCINT0);                   // Use PB0 as interrupt pin 0
    ADCSRA &= ~_BV(ADEN);                   // ADC off
    set_sleep_mode(SLEEP_MODE_PWR_DOWN);    // replaces above statement

    sleep_enable();                         // Sets the Sleep Enable bit in the MCUCR Register (SE BIT)
    sei();                                  // Enable interrupts
    sleep_cpu();                            // sleep

    cli();                                  // Disable interrupts
    PCMSK &= ~_BV(PCINT0);                  // Turn off PB0 as interrupt pin
    sleep_disable();                        // Clear SE bit
    ADCSRA |= _BV(ADEN);                    // ADC on

    sei();                                  // Enable interrupts
}


//"""
//    MAIN PROGRAM
//"""

const uint32_t red_color = 0x0000FF;   // Command written in hexadecimal instead of binary to load the red (RGB)
const uint32_t green_color = 0x00FF00; // This is an example to show that it is also possible to work with green

const unsigned long timeOn = 120000L;  // Fractional time ON (in ms)
const unsigned long timeOff = 60000L;  // Fractional time OFF (in ms)
const unsigned long time8hutdown = 5400000L;  // Full time of illumination (1H30 = 5400 seconds)
unsigned long previousMillis = 0;  // Primeval time

void loop()
{
  strip.setBrightness(_d_BRIGHTNESS);  // Adjust the brightness (0:minimum, 255:maximum)
  strip.fill(red_color); // LED in red color
  strip.show();  // Refresh

  // 1. TEMPS ON : WAIT FOR TWO MINUTES
  while (true)
  {
    if ( (unsigned long)(millis() - previousMillis) >= timeOn)
    {
      previousMillis = millis();
      break;
    }
  }
  // ================

  strip.clear();  // LED matrix in dark : 0 / black / off
  strip.show();  // Refresh

  // 2. TEMPS OFF : WAIT FOR ONE MINUTE
  while (true)
  {
    if ( (unsigned long)(millis() - previousMillis) >= timeOff)
    {
      previousMillis = millis();
      break;
    }
  }
  // ================

  // 3. "STOP" OF THE SYSTEM AFTER 1h30
  if ( (unsigned long)millis() >= time8hutdown)
  {
    sleep();
    while (true)
    {
      delay(5);  // pour alléger le processeur...
    }
  }
}
                                                                                                    END
```

Figure A.1 – C program on Arduino platform to control the system driving the Trinket microcontroller and the Adafruit LED array. For better understanding, comments were added after the double slash (//).

Appendix B

Demonstrator

In order to present easily this technology to potential companies, a demonstrator including a video and a quick manipulation of the device will take place in the CEA Hauts de France showroom as displayed in figure B.1. This demonstrator has been set up with the help of Axone Design and the script of the video motion is displayed in the following page.

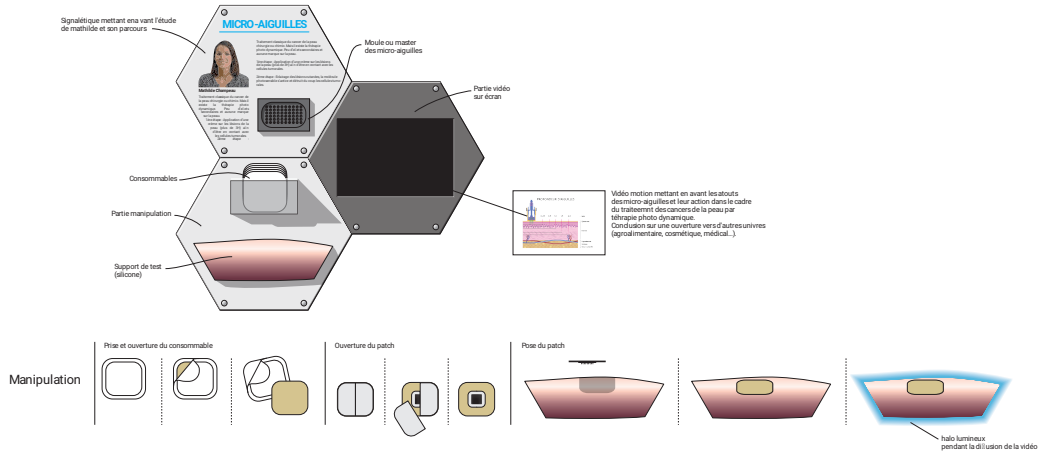

Figure B.1 – Demonstrator design on three panels.

STORYBOARD MOTION PATCH MICRO-AIGUILLES

Le motion commence sur le visage d'une femme qui porte un patch

La question « comment le patch à micro aiguilles améliore les soins du cancer de la peau? » apparait par glissement sur la gauche du personnage. Les bandes roses apparaissent chacune à une vitesse puis le texte se cale dessus.

La question disparait en sortant de l'ecran par la gauche

Un zoom sur le patch débute . Un texte indique qu'il s'agit du patch et des fleches «clignotent» autour.

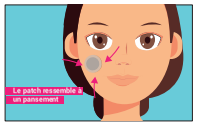

Le zoom s'accentue et on apercoit les points des microaiguilles. On peut ajouter un chiffre pour se rendre compte du nombre d'aiguilles présentes sur le patch

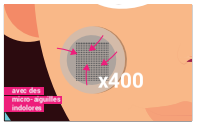

f o n d u

On zoom et on entre dans les couches de la peau

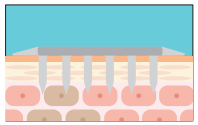

Le cadrage se fait sur les couches de l'épiderme et leur nom apparaissent

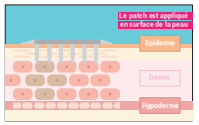

deux lignes apparaissent pour signifier à quelle profondeur se situent les aiguilles

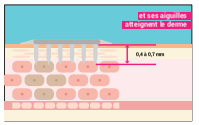

Puis on cible les cellules tumorales en rendant plus clair le reste de l'image

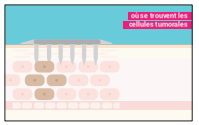

les couleurs reviennent et on cible le patch

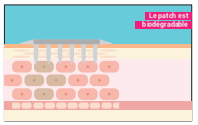

Une bulle de «zoom» apparait pour expliquer la composition des micro aiguilles. Les molécules seront en mouvement dans l'aiguille

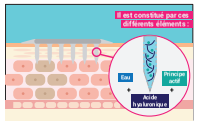

Les leds apparaissent, leur longueur d'onde est précisée

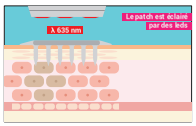

Les leds s'allument et un chrono apparait

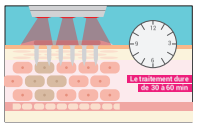

Le temps défile

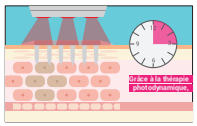

Le patch se dissoud au fur et à mesure en libérant le principe actif

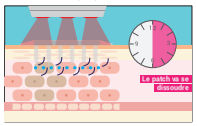

les aiguilles se dissolvent au fur et à mesure en libérant le principe actif

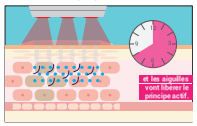

Le principe actif se concentre autour des cellules tumorales

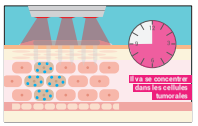

Les cellules tumorales rétrécissent

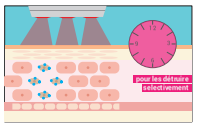

puis disparaissent. la lumière s'éteint.

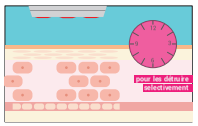

Transition vers l'explication de la méthode employée

Le tube apparait et la creme se répand sur la peau

le chrono apparait et fait 3 tour de cadrans pour montrer les 3H de pose.

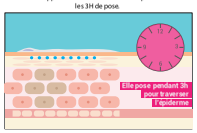

Le principe actif se libère et n'atteint pas les lésions profondes

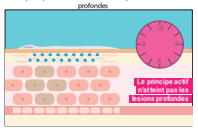

puis la lumière apparait et s'allume. Le chrono repart pour 10 min

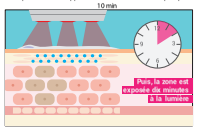

le principe actif se concentre dans la seule cellule qu'il peut attendre

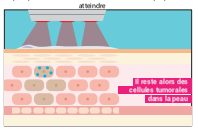

La cellule rétrecie et disparait

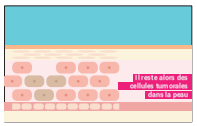

Transition vers un fond uni

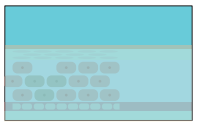

LES AVANTAGES DU PATCH. le patch est au centre

il s'anime, bouge sur la droite et les infos apparaissent

Le patch revient au centre

Le patch retrecit et des bulles apparaissent (petite et taille augmente en arrivant au premier plan)

Le patch retrecit et des bulles apparaissent (petite et taille augmente en arrivant au premier plan)

les bulles disparaissent , le patch s'agrandit

ecran de fin

Appendix C

Communications

Outline of the current chapter

C.1 Articles published in peer-reviewed journals

- **M. Champeau**, S. Vignoud, L. Mortier, et S. Mordon, « Photodynamic therapy for skin cancer: How to enhance drug penetration? », *Journal of Photochemistry and Photobiology B: Biology*, vol. 197, p. 111544, août 2019, doi: 10.1016/j.jphotobiol.2019.111544.
- **M. Champeau**, D.Jary, L. Mortier, S. Mordon et S.Vignoud, « A facile fabrication of dissolving microneedles containing 5-aminolevulinic acid », *International Journal of Pharmaceutics*, vol. 586, p. 119554, août 2020, doi: 10.1016/j.ijpharm.2020.119554.
- submitted in the International Journal of Pharmacetics: **M. Champeau**, D.Jary, A-S. Vignion-Dewalle, Serge Mordon, E. Martin de Lassallec, Séverine Vignoud, Laurent Mortier, « Introduction of a model of skin lesions on rats and testing of dissolving microneedles containing 5-aminolevulinic acid.

C.2 International conferences

- **M. Champeau**, S. Vignoud, D.Jary, L. Mortier, et S. Mordon, « Photodynamic therapy for skin cancers: how to enhance 5-ALA penetration with dissolving microneedles?», *SPIE, IPA, 17th international photodynamic association world congress*, 28 June - 4 July 2019, Cambridge, Massachusetts, United States. Poster Presentation
- **M. Champeau**, S. Vignoud, D.Jary, L. Mortier, et S. Mordon, « PDT for skin cancers: how to enhance 5-ALA penetration with polymeric dissolving microneedles?», *EUROPDT*,

European Society for Photodynamic Therapy in Dermatology, 28-29 February 2020, Seville, Spain. Oral Presentation. (*Award for the second best oral communication.*)

- M. Champeau, D.Jary, S. Mordon L. Mortier, et S. Vignoud, « PDT FOR SKIN CANCERS: HOW TO ENHANCE 5-ALA PENETRATION WITH POLYMERIC DISSOLVING MICRONEEDLES?», *World Biomaterials Congress*, rescheduled 11-16 December 2020 , Glasgow, Scotland. Oral Presentation.

C.3 Patent

DEPOSIT FR - DD19654, June 2020, M. Champeau, D.Jary, S. Mordon L. Mortier, et S. Vignoud, "Dispositif de type patch à appliquer sur la peau d'un être vivant"

C.4 Popularization of science

- Pré-sélection régionale Ma Thèse en 180 secondes, mars 2018, Région Hauts de France
- Finale régionale Ma Thèse en 180 secondes, mai 2018, Région Hauts de France (https://www.youtube.com/watch?v=DVb6hhGyvwg)
- PhD generation saison 1, Leti Com (https://www.youtube.com/watch?v=AYmyCxIa0wg)

Contents

Dissolving microneedles for an optimal transdermal delivery of an active principle used in photodynamic therapy: Development and proof of concept.

Abstract

Non-melanoma skin cancers are on the rise with 2 to 3 million people diagnosed each year and are sometimes treated by local ablation therapy. To avoid this surgery, photodynamic therapy (PDT) appears as an advantageous treatment. Currently used in clinics, PDT consists of applying a cream containing a photosensitive precursor to the damaged skin, which, then metabolizes and under light excitation induces cell death. However, this technique is not fully effective if the skin lesion extends into the deep skin layers. To improve the therapeutic treatment of this type of skin cancer, a patch with dissolving microneedles (MNs) was develop to reach the deep layers of lesions that are difficult to treat. Hyaluronic acid, known for its biocompatibility, solubility and biodegradability, was chosen as the constituent material, and mixed with the 5-aminolevulinic acid (photosensitive precursor, 5-ALA). To ensure the best penetration without causing pain by touching the nerve endings, an optimal "pencil-tip" design was defined with MNs length going from 400 to 750 µm. A simple and robust manufacturing process called solvent casting molding method, has been set up which is an asset for potential industrialization. In absence of realistic skin lesions model, we chose to establish one on rats skin by applying daily UV-B doses. Histology and pharmacokinetic studies validated the presence of precancerous skin lesions and the MN-patch *in vivo* efficiency was therefore tested. After one hour application on the injured rat skin, the MN-patch dissolved and released the 5-ALA that further metabolized to protoporphyrin IX (PpIX). A significant level of PpIX fluorescence was recorded suggesting that after light excitation, a PDT session could be effective. In parallel, to reduce pain felt during PDT treatment, a light device with suitable optical and thermal properties was conceived and coupled to the MN-patch. The idea would be to start the illumination directly after MN-patch application in order to avoid a painful photochemical reaction. This wearable and easy to use system purpose a all-in-one PDT processing which fulfills the criterion of patient compliance, better efficiency and speed of treatment.

Keywords: photodynamic therapy, dissolving microneedles, 5-aminolevulinic acid, transdermal drug delivery, skin cancer, hyaluronic acid

---

Microaiguilles solubles pour la délivrance transdermique optimale d'un principe actif utilisé en thérapie photodynamique : Mise au point et preuve de concept.

Résumé

Les cancers de la peau de type non mélanome constituent un enjeu sanitaire majeur : l'OMS en dénombre 2 à 3 millions par an. Pour les traiter, il faut parfois recourir à une résection chirurgicale localisée. Pour éviter ce geste, la thérapie photodynamique (PDT) est un traitement alternatif intéressant. Actuellement utilisée en clinique, la PDT consiste à appliquer sur la peau lésée une crème contenant un précurseur photosensible qui après métabolisation et sous excitation lumineuse induit la mort cellulaire. Néanmoins, cette technique atteint ses limites thérapeutiques lorsque la crème ne pénètre pas dans les couches lésées et profondes de la peau. Pour améliorer la délivrance de la PDT, un patch de microaiguilles (MAs) soluble dont la longueur des MAs peut être comprise entre 400 à 750 µm a été développé permettant ainsi d'atteindre l'interface épiderme/derme sans induire de douleur. L'acide hyaluronique, polymère connu pour sa biocompatibilité, solubilité et biodégradabilité, a été choisi comme matériau constitutif du patch et a été mélangé avec l'acide aminolévunique (précurseur photosensible, 5-ALA). Un procédé de fabrication simple et robuste dit de moulage a été mis en place dans une perspective de potentielle industrialisation. Du fait de l'absence d'un modèle réaliste de lésions cutanées, nous avons choisi d'en développer un sur des rats en leur appliquant des doses d'UV-B quotidiennes. Ce modèle a été validé par des études d'histologie et de pharmacocinétique et a permis de tester l'efficacité du patch *in vivo*. Lorsque le patch a été appliqué sur les lésions précancéreuses, il s'est dissous en 1 heure, a libéré le 5-ALA qui s'est ensuite métabolisé en protoporphyrin IX (PpIX). Un taux significatif de fluorescence dû à la PpIX a été recueilli et montre qu'après excitation lumineuse, un traitement PDT pourrait être efficace. Aussi, afin de réduire la douleur ressentie pendant une session PDT, l'illumination commencerait juste après l'application du patch pour éviter l'accumulation de PpIX et *a fortiori* une réaction photochimique douloureuse. De ce fait, un système lumineux dont nous avons contrôlé les propriétés optiques, thermiques et temporelles a été couplé au patch de MAs. Ce système portatif et simple d'utilisation pourrait proposer un traitement PDT tout-en-un qui répond aux critères de rapidité, d'efficacité de traitement et de confort du patient.

Mots clés : thérapie photodynamique, microaiguilles solubles, acide 5-aminolévulinique, délivrance transdermique, cancer de la peau, acide hyaluronique